Differential vertical shortening in timber-concrete high-rise structures

(Pilon, et al., 2017)

Differential vertical shortening in timber-concrete high-rise structures

Master thesis report

by

Okke Willebrands

Faculty of Civil Engineering & Geoscience
Building Engineering

Delft University of Technology

November 2017

Graduation committee:
Prof.dr.ir. J.W.G. vd Kuilen
Dr.ir. G.J.P. Ravenshorst
Dr.ir. K.C. Terwel
Ir. P. Lagendijk

I Preface

This thesis contains the documentation of a research on differential vertical shortening in timber-concrete high-rise structures. This thesis serves as a completion of the master's degree in Building Engineering at the faculty of Civil Engineering an Geosciences, Delft University of Technology. The research has been performed at the Delft University of Technology.

I first encountered timber in high-rise buildings when participated in the multidisciplinary project 'MEGA' at the TU Delft, faculty of architecture. With my project team, we designed a high-rise that made use of timber floors. The use of this floor type helped us to reduce the carbon footprint, reduce the weight of the building structure, reduce crane time and integrate installation systems. The design gave so much gratification that I decided to stick to the hybrid building subject for my master thesis.

For conducting my research I would like to express my gratitude to Jan-Willem van de Kuilen for chairing my graduation committee, his great enthusiasm and sharing of knowledge in the field of high-rise and timber engineering. I would like to thank Geert Ravenshorst for the many times we spoke on lots of subjects in this research. He also gave me the freedom to finding my way in and to my research topic. On the other hand, he also pushed me threw the last bit of my material studies. For structuring my research and report I would like to thank Karel Terwel. The meetings with Karel Terwel helped me a lot in setting clear goals and research questions. Last but not least I would like to thanks Paul Lagendijk for his critical view and great interest on the topic. Our meetings helped me a lot in gaining knowledge in concrete and analysing the building structure that I studied in this research.

Delft, November 2017
O.A.P. Willebrands

II Abstract

Background
Differential vertical shortening (DVS) is the relative vertical shortening between two adjacent vertical load bearing elements. DVS originates because axial loading conditions on- and the design of adjacent vertical load bearing elements are different. Due to these differences, the reaction of the adjacent vertical structural elements expressed as length change can be different.

The aim of this thesis is to research differential vertical shortening effects in high-rise buildings that use a concrete core as a lateral stability system and a timber pendulum structure as a gravitational system. The Tallwood House in Brock Commons is a perfect example of such a structural system where the engineers have considered the shortening effects which will be reviewed in this research. Furthermore, this research will look for measures in the design and implementation phase that have influence on the magnitude of differential vertical shortening deformations.

Problem
In the Tallwood House project the problem was only tackled on basis of the individual column shortening and the effect it would have on vertical mechanical systems. A clear understanding of the relative difference between core and column shortening (DVS) and the effect it can have on secondary building systems is lacking. The determination of criteria on which the DVS deformations are assessed in the Brock Commons building, are based on the deformation capacity of the vertical mechanical systems, which does not necessarily relate to the DVS deformations. A more methodological approach is necessary for the prediction of DVS deformations and the determination of criteria regarding DVS deformations.

Research question
The sub question have the aim to reach to a more general and methodological approach in predicting DVS deformations and determining criteria for DVS deformations.

> *"What are the criteria on which differential vertical shortening deformations in the building structure should be assessed in order to guarantee the functional performance of the building during its service life?"*
>
> *"How can differential vertical shortening deformations be quantified for a timber-concrete high-rise structure?"*

After answering the sub-questions that relate to the criteria on DVS deformations and the quantification of DVS deformations, a research can be conducted to the influence of some input variables for the design and construction process to answer the main question of this research:

> *"What are effective measures which can be applied in the design and construction phase to mitigate the differential vertical shortening during the service life of high-rise buildings that uses a timber gravitational load bearing system with stabilizing concrete cores?''*

Work approach/method
Problem areas where DVS deformations can have a negative effect on secondary building structures are researched. A general approach for the determination of criteria for DVS deformations is elaborated, based on principles for vertical deformation criteria that are described by the Eurocode.

The response mechanism of axially loaded concrete load bearing elements and axially loaded timber load bearing elements on external influences is researched qualitative by a literature study. The CEB-fip 2010 strain model is used to predict deformations in concrete. For timber, the strength class system is used according to Eurocode 5 to determine the elastic strains. The creep and shrinkage strains in timber are determined by experimental results that are found in a literature study.

The influence of the building process on DVS deformations is researched by a literature study. Staged construction analysis provides the possibility to simulate the sequential loading in a building process and to distinguish the DVS-deformations that can affect secondary building elements (post-DVS deformations) from the total-DVS deformations.

A case study on the Tallwood House at Brock commons in Vancouver is conducted to provide a basic geometric model in which DVS deformations can be predicted in which all previous research in this thesis serves as input properties of the model. From this basic model, variables in the design and building process are altered to conduct a sensitivity analysis of these variables. The building height expressed in number of floors, column cross section and the building speed of finishings in a building are taken as the analysed variables.

Conclusions

Increasing the column cross section can be an effective measure to decrease post- and total-DVS deformations due to elastic and creep strains. The effectiveness decreases with the increase of the column cross section because shrinkage strains are not affected. The post-DVS deformations can be decreased by postponing the building process of secondary structural elements in the construction schedule. The effectiveness decreases with increasing building duration because DVS-deformations due to loads of the finishes itself are not affected. Total-DVS deformations are not affected. Compensation has effect on the total difference in vertical position between the floor supports. The vertical translational movement is not prevented. This means that post-DVS deformations cannot be influenced by compensation.

Table of contents

1 Introduction

Differential shortening in high-rise building structures is a well described phenomenon by various literature articles. Differential shortening originates because axial loading conditions on- and the design of adjacent vertical load bearing elements are different. Due to these differences, the reaction of the adjacent vertical structural elements expressed as length change can be different (Matar & Faschan, 2017; Choi, Kim, Kim, & Park, 2013; Park H. , 2003; Park, Choi, & Park, 2013).

In the design of high-rise building structures, two main force transfers should be dealt with to obtain a sustainable building structure. Vertical structural load bearing elements are subjected to gravitational loads that emanate from the floor structures and that will accumulate when the amount of floors increase. Lateral loads that originates from wind or seismic activity should also be transferred from floor to floor, through the load bearing elements to the base of the building.

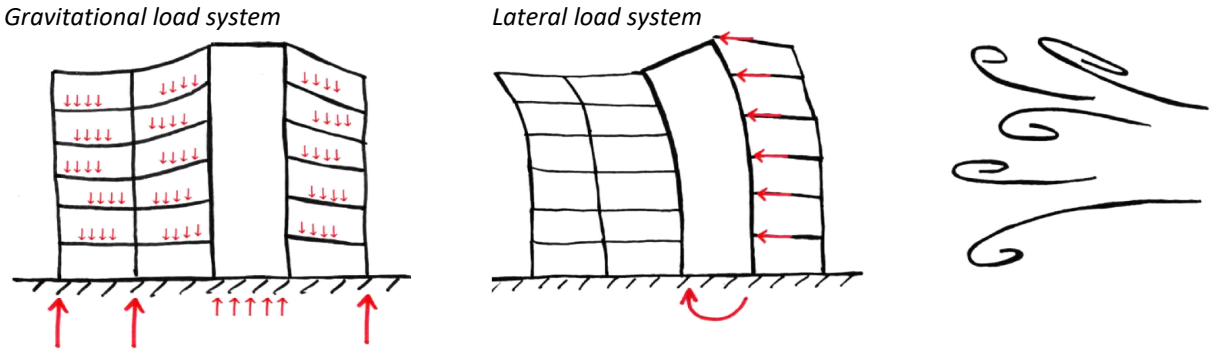

figure 1-1: Seperation between gravitational and lateral load system.

In a high-rise structure design the lateral load system and the gravitational load system can be separated by using a concrete core structure with a pendulum skeleton structure. The advantage of such a system is that the concrete core can house all vertical transport systems such as elevators, fire stairs and vertical ducting while the rest of the building can be kept flexible and fairly simple in it structural design with hinged connections. A consequence is that the vertical load bearing elements are designed for totally different load utilizations, which can lead to differential length change in their respond to gravitational loads.

1.1 Aim

The introduction describes the phenomenon of differential vertical shortening and its cause of origin in a nutshell. The phenomenon is already present in our ‘conventional’ way of building high-rise structures fully in concrete or concrete and steel. Recent developments for timber high-rise structures shows that there is a trend of increasing building height with the use of timber as a structural material (CTBUH, 2017). In 2009 the ‘Stadthaus’ apartment building in London was completely built out of wood with cross laminated timber panels to a height of 9 stories. The eight storey LCT One building in Austria uses a concrete core and timber column structure and was finished in 2012 (Tahan, 2013). ‘Treet’ in Bergen, Norway managed to reach 14 stories in the end of 2015. In Vancouver, the ‘Brock Commons’ apartment building of 18 stories which uses a concrete core and timber skeleton structure is just finished (Pilon, Utimati, & Jin, 2016). Plans for a 24 storey building in Vienna, called ‘Hoho Wien’, will use a concrete core with mass timber columns from which construction will start in 2017 (Groot, 2016). The latter two building projects and the LCT One building make us of a concrete core with a pendulum timber column structure.

As explained in the first paragraph of the introduction, separation of the gravitational and lateral load system allows that the vertical loading conditions on adjacent load bearing elements can differ, leading to differential vertical length change between both systems. Using for both systems a different structural material by using a concrete core and a timber skeleton structure, the structural properties of both systems are also differentiated

which can further increase or decrease the differential vertical shortening deformations. The aim of this thesis is to research differential vertical shortening effects in high-rise buildings that use a concrete core as a lateral stability system and a timber pendulum structure as a gravitational system. Furthermore, this research will look for measures in the design and implementation phase that have influence on the magnitude of differential vertical shortening.

A good example of a building that uses the in this research considered structural system, is the Tallwood House in Brock Commons, Vancouver. The designers and engineers of the project considered the problem of axial shortening of the timber columns. "*The main concern surrounding these shortening effects is the impact the deformations can have on the vertical mechanical services and the elevation tolerances between the wood superstructure and the stiff concrete cores*" (Fast, Gafner, Jackson, & Li, 2016, p. 5). The engineers provided results on the axial column shortening when left unmitigated. The strategy for mitigating the effects was to place a package of shim plates at three strategic levels and correct half of the expected axial column shortening deformations to avoid overcompensation. "*The concrete cores are installed prior to the timber superstructure and do not support significant gravity load other than their self-weight. Therefore, it is likely that the small amount of creep and elastic axial shortening will have taken place before the timber is installed, and could therefore be ignored"* (Fast, Gafner, Jackson, & Li, 2016, p. 6).

figure 1-2: Overview of the Brock Commons structural system. Left: Concrete platform and cores. Right: Timber pendulum structure (Fast, Gafner, Jackson, & Li, 2016).

1.2 Problem statement

The problem statement has taken shape on the basis of how the engineers handled the topic of differential vertical shortening in the case study. The first quotation in the last paragraph of the previous chapter relates to the problem that might occur due to differential vertical shortening:

"*The main concern surrounding these shortening effects is the impact the deformations can have on the vertical mechanical services and the elevation tolerances between the wood superstructure and the stiff concrete cores*" (Fast, Gafner, Jackson, & Li, 2016, p. 5).

In this quotation there is only referred to vertical mechanical systems, but not to other secondary building systems. The impact the deformations can have on the secondary building systems is of interest, but also if all deformations can have an impact on the secondary building systems and how much deformations can be allowed. Criteria on which the DVS deformations should be assessed should be determined for assurance of quality and functional performance of the building structure and secondary building elements.

The mitigations strategy was based on the predicted axial column shortening. Differential vertical shortening deformations would be the difference in vertical deformations between the concrete core and the timber column structure. According to the engineers, elastic and creep deformations in the concrete core can be neglected, but shrinkage in the concrete cores remains unmentioned.

"*The concrete cores are installed prior to the timber superstructure and do not support significant gravity load other than their self-weight. Therefore, it is likely that the small amount of creep and elastic axial shortening will have taken place before the timber is installed, and could therefore be ignored"* (Fast, Gafner, Jackson, & Li, 2016, p. 6).

The method how differential vertical shortening deformations between the concrete cores and the timber pendulum structure should be quantified is of interest. How deformations develop in both materials and how these deformations in both the concrete cores and the timber pendulum structure relate to each other is key for the prediction of differential vertical shortening in the total building structure.

The previous discussion and problem statement relates to mapping differential vertical shortening in a building structure similar to that of the Tallwood House in Brock Commons. A more methodological approach is necessary for the prediction of DVS deformations and the determination of criteria regarding DVS deformations. The final interest is the influence of several continues factors in the structural design and building process of a high-rise structure with concrete cores and a timber pendulum structure.

1.2.1 Main research question and sub questions

From the problem statement that is explicated in the previous chapter, sub questions are drawn up:

"What are the criteria on which differential vertical shortening deformations in the building structure should be assessed in order to guarantee the functional performance of the building during its service life?"

"How can differential vertical shortening deformations be quantified for a timber-concrete high-rise structure?"

"What is the response mechanism of axially loaded concrete load bearing elements and axially loaded timber load bearing elements on external influences?"

"What factors in the design and construction phase have influence on the magnitude of differential vertical shortening?"

After answering the sub-questions that relate to the criteria on DVS deformations and the quantification of DVS deformations, a research can be conducted to the influence of some input variables for the design and construction process to answer the main question of this research:

"What are effective measures which can be applied in the design and construction phase to mitigate the differential vertical shortening during the service life of high-rise buildings that uses a timber gravitational load bearing system with stabilizing concrete cores?''

1.2.2 Demarcation of the subject

This thesis will focus on high-rise buildings that make use of a timber gravitational load system with a stabilizing concrete core system for lateral loads. Within this building system the response mechanism of both materials will be researched as a basis for further study. This further study will look into technical design measures of the structure and influences of the building process on differential vertical shortening in the upper structure.

Additional vertical deformations, as shown in figure 1-3, that influence the differential deformations due to wind load or foundation settlements are shortly and qualitatively addressed, but will not be elaborated in detail.

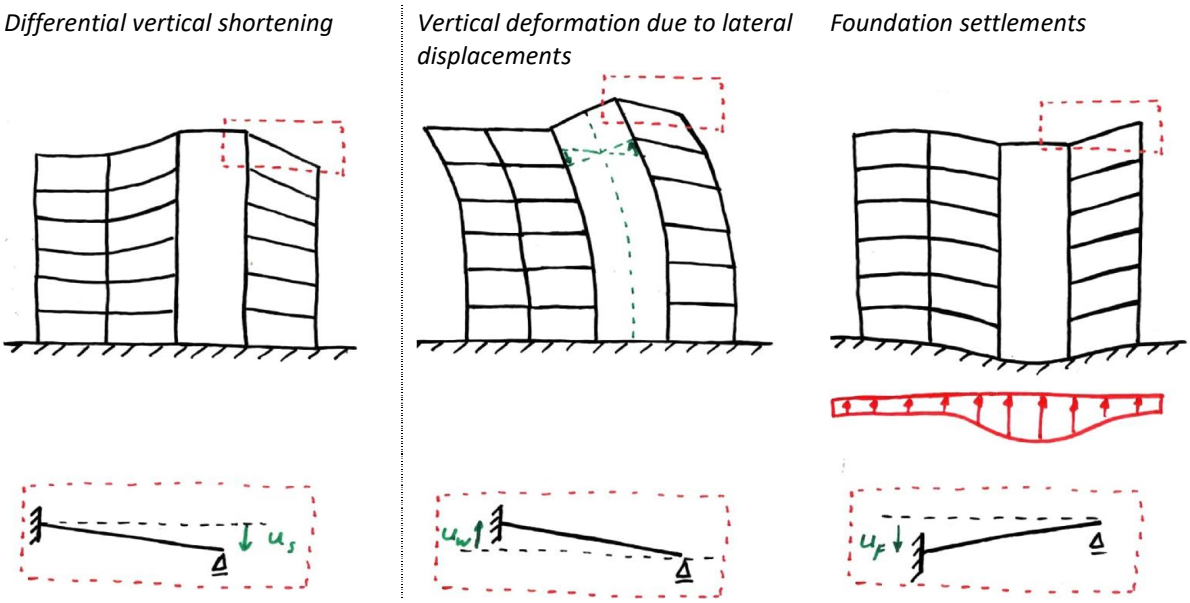

figure 1-3: Differential vertical shortening in the upper structure and other vertical deformations.

1.3 Research method

In figure 1-4 the sub-questions are formulated and clustered under different levels. The first part will further map the problem and has the aim to formulate criteria for differential vertical shortening deformations. The second part will focus on quantifying differential vertical shortening. This is subdivided in research to the material response mechanisms of both timber and concrete on loading and environmental conditions and the influencing factors on the structural level and building process. The third part is a parametric study for the analysis on the influence of several factors. Conclusions can be made from the results and will give an answer to the research question.

Main question

"What are effective measures which can be applied in the design and construction phase to mitigate the differential vertical shortening during the service life of high-rise buildings that uses a timber gravitational load bearing system with stabilizing concrete cores?''

Further study on the problem and criteria

"What are the criteria on which differential vertical shortening deformations in the building structure should be assessed in order to guarantee the functional performance of the building during its service life?"

Study on secondary building systems	-	Criteria to maintain quality and functional performance in the service life	-	Building systems specifications - Eurocode requirements

Quantification of differential vertical shortening

"How can differential vertical shortening deformations be quantified for a timber concrete high-rise structure?"

"What is the response mechanism of axially loaded concrete load bearing elements and axially loaded timber load bearing elements on external influences?"

Material study	-	Influencing factors on micro and macro level	-	Qualitative literature study
Material study	-	Mean and deviation values in practice	-	Analysis on experimental studies

"What factors in the design and construction phase have influence on the magnitude of differential vertical shortening?"

Case study	-	Study on Brock Commons as a starting point for a software model	-	Literature study Software model

Parametric study

Application and exploration of theory

Parametric study	-	Several parameter will be altered to study their effect on differential vertical shortening	-	Parametric analysis

Conclusions and recommendations

"What are effective measures which can be applied in the design and construction phase to control the differential vertical shortening during the service life of high-rise buildings that uses a timber gravitational load bearing system with stabilizing concrete cores?''

Concluding and recommending

Feedback to main research question and sub questions

figure 1-4: Research overview and methodology.

1.3.1 Thesis outline

The research outline will be implemented in chapters that will form the structure of this thesis. A quick description is given of the chapter content and the goals that each chapter serves.

1. *Introduction*

   Describes the background of the research. The problem is described by the example of 'Brock Commons'. Goals and the research question follow from the problem description.

2. *Effects of DVS on secondary building elements*

   The effect of differential vertical displacements of the load bearing structure on other building systems is explained. Next to that, the resilience of these other building systems on movement of the main load bearing structure is explained. Finally, criteria are determined from Eurocode principles on which differential vertical shortening deformations can be assessed.

3. *Straining in timber in concrete*

   Explains theoretically the elastic, shrinkage and creep behaviour of timber and concrete. It will give an insight in the response mechanism of both materials on internal and external influencing factors.

4. *Quantification of the material strains*

   The strain models from the CEB-fip 2010 model are adopted to quantify the elastic, creep and shrinkage strains in concrete. This model will be the reference document of the revised EN 1992-1-1 that will be published in 2020 (Walraven & Bigaj-van Vliet, 2016).
   The strength class system from Eurocode 5 will be adopted to quantify the elastic strains in timber. Shrinkage and creep in timber are quantified by the analysis of several shrinkage and creep experimental results that are found in literature, because the Eurocode 5 is not found to be sufficient for the prediction of these strains.
   Finally, all strain predictions in timber and concrete are treated as equally as possible, by determining mean strain values and deviations on these values in a 90-percent confidence interval.

5. *Building execution*

   The influence of several factors in the building process on differential vertical shortening deformations are discussed. The building process is explained by the presentation of sequential loading. The influence of the building method on the staged construction analysis is explained. Furthermore, compensation methods are elaborated and the general result of these methods is explained.

6. *Case study: Tallwood House at Brock Commons*

   The structural design of the Tallwood House at Brock Commons is mapped. It will function as a basis for the variable study of chapter 0.

7. *Sensitivity/variable study on DVS deformations*

   In this chapter the variables that influence differential shortening deformations will be explored by a variable study. The goal is to explore the variables which can be used by the engineer to manipulate the differential shortening in a timber concrete hybrid high-rise.

8. *Conclusions*

The effectiveness of influencing factors that are explored are judged. Also the applicability of these factors in a design or building process will be judged in order to determine if they can be used as a measure.

2 Effect of DVS on secondary building elements

Differential column shortening causes that slabs and beams will deflect from their original intended position and slope. These deflections can induce forces in non-structural systems like partition walls, façades, cladding and mechanical systems with cracks and failure as a consequence. Next to the influence on adjacent non-structural elements, the differential column shortening can also induce additional stresses or severe deformations in the structure itself that influence the appearance and safety of the loadbearing structure.

This chapter will elaborate the effect of differential vertical shortening on the execution of other building systems and the loadbearing structure itself according to the subdivision of table 1.

Finishing structures	Façades and cladding Partition walls
Technical	HVAC systems Sewerage and drainage systems
Structural	SLS requirements ULS additional stresses

table 1: Subdivision of affected areas due to column differential vertical deformations.

2.1 Finishing structures

With the occurrence of excessive deformations in the structural system, forces could be introduced in non-structural space separating elements which can cause failure of façades and partition walls. Because partition wall systems and facades span from floor to floor, the column shortening δL, that is in general most severe at the base of the building, can cause crushing of these intermediate elements when these are not properly designed for deformations. At higher levels in the building, the partition walls can be subjected to shearing due to differential shortening between adjacent vertical load bearing elements.

When there is accounted for enough deformation capacity in the connection details, the deformation of the main load bearing system should not cause any problem regarding damage to partition walls and façades.

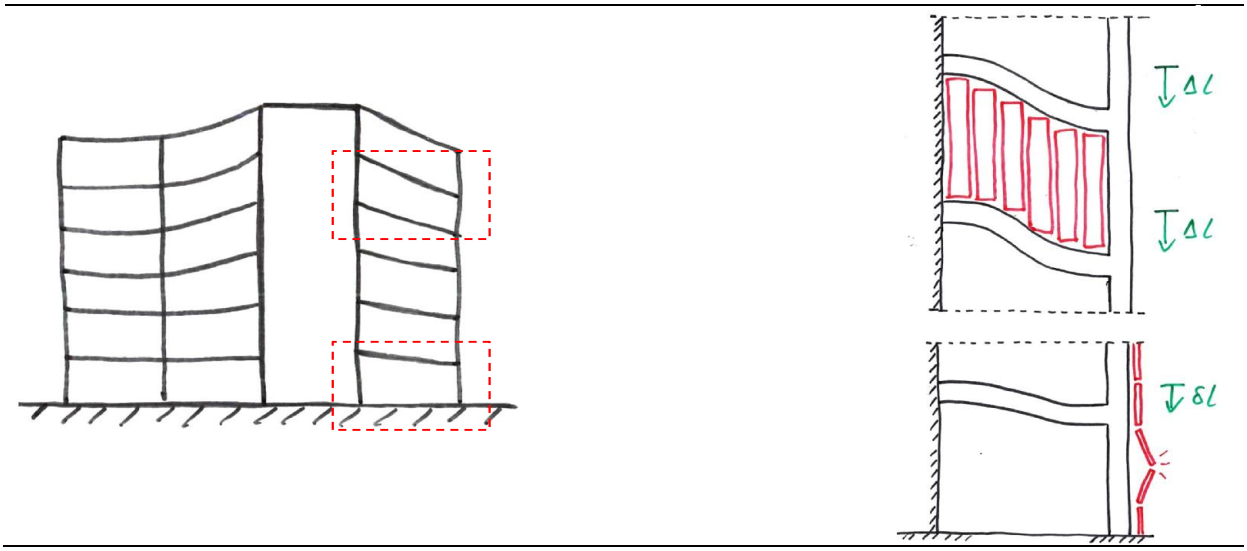

figure 2-1: Possible problem areas for architectural elements when considering (differential) vertical shortening.

2.1.1 Façades

In modern building design it is common that the main load bearing structure supports the façade structure and the façade is shielding the internal building structure from outside weather conditions, sound and unwanted intruders. Next to functional characteristics the façade also gives the building its architectural appearance (Poot, 2013). The development of the separation of the load bearing and shielding functions originates from the neoclassical era. Before this period, buildings where mostly constructed from massive load bearing walls that comprised all functions (Knaack, Klein, Bilow, & Auer, 2014).

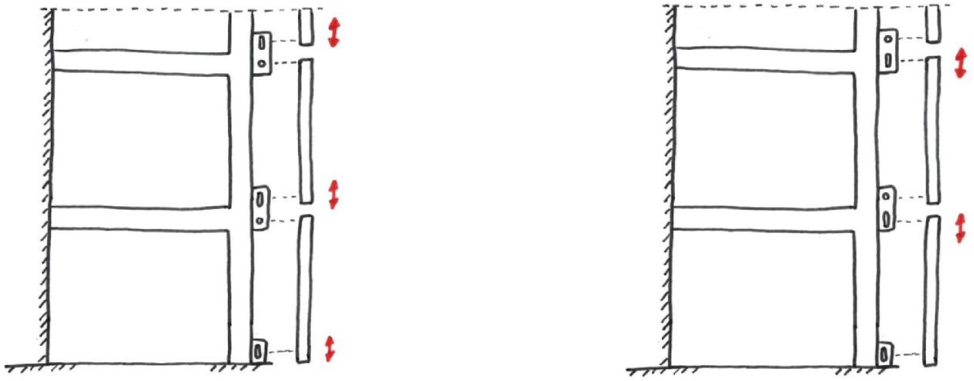

figure 2-2: Hanging and standing secondary façade structure.

Due to the separation of functions, the façade elements are not designed any more to be a part of the main load path of the structure. With today's principles the façade is in the most extreme case designed as a secondary structure that transfers dead weight loads and wind loads to the main load bearing structure. In a multi storey building, the secondary structure usually spans from floor to floor and provides a load bearing structure for infills such as windows and cladding. A distinction is made between standing post beam systems and hanging systems that are also called curtain wall systems from which the principles are shown in figure 2-2. Both systems have in common that one support is unrestrained in vertical direction so that vertical deformation capacity is provided for vertical deformations in the façade itself or vertical deformations of the main load bearing structure.

In the design of the horizontal dilatation between vertical adjacent façade elements one must be aware of the several deformations that can occur in the façade and the main loadbearing structure after the façade is installed. Next to column shortening, thermal expansion of the façade and deflection of the floor edge beam are common and relevant deformities in multi-storey buildings. To place deformations due to column shortening in perspective, some quantities of these deformities are elaborated in figure 2-3. When considering a building where the outside perimeter contributes to the lateral stability system in for instance an outrigger or façade tube system, vertical column shortening due to wind loads may be expected. This is not further elaborated because this research is limited to pendulum column structures with a core for lateral stability.

Column shortening (b_c)

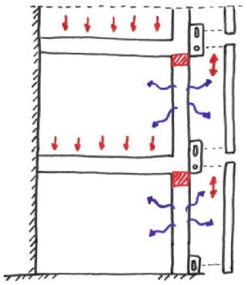

(per floor)
4mm (Burj Dubai)

Linear thermal expansion (b_t)

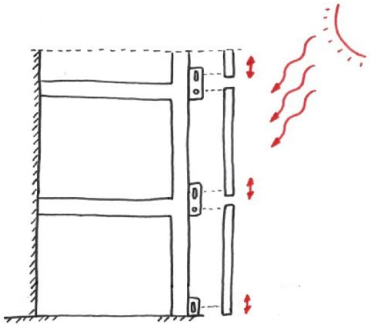

(ΔT = 50 °C)
−0,6 to +0,6 mm (Timber parallel)
−2,3 to +2,3 mm (Concrete)
−4,3 to +4,3 mm (Aluminium)
−1,0 to +1,0 mm (Glass)
−1,3 to +1,3 mm (Brick)

Edge beam deflection (b_b)

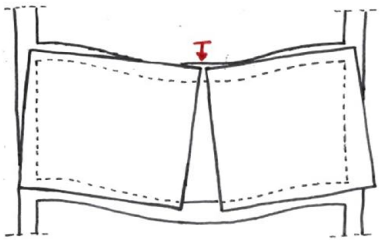

($w_2 + w_3 = L_{rep}/500$)
8mm ($L_{rep} = 4\ meters$)
16mm ($L_{rep} = 8\ meters$)

figure 2-3: Thermal facade expansion and main structure deformations.

The deformations that occur in the façade itself are mainly due to thermal expansion. The amount of thermal expansion is dependent on the material that is used. Values that are given in figure 2-3 are based on one floor to floor height of 3600mm and a temperature change of 50 °C.

The maximum allowable edge beam deflection is the deflection that occurs after the installation of the façade elements. Initial permanent deflections will occur before and during installation and the adjustment of the elements eliminate these deflections. The edge beam deflection that will affect the after assembly movement in the façade will be due to long-term deformations from permanent and quasi permanent loads w_2 and live loads w_3, from which the sum is allowed to be $L_{rep}/500$ according to the Eurocode (chapter 2.3.1 page 29).

For the Burj Dubai tower design, the column shortening due to elastic, creep and shrinkage deformations was compensated on beforehand per floor for the typical lower floors by increasing the floor to floor height by 4mm (Baker, Korista, Novak, Pawlikowski, & Young, 2007). An individual column shortening at the base of 4mm is a significant amount. However, when placing it into perspective of other deformations due to thermal expansion and edge beam deflections it does not seem to be a fundamental problem. Nevertheless, it should be accounted for in the total deformations that occur between vertical adjacent façade elements for the design of horizontal dilatations. In the design of horizontal dilatations the various deformities of figure 2-3 should be superimposed to determine the minimal deformation capacity of the horizontal dilatation.

The façade systems that are used can be categorized into stick systems or unit systems (Knaack, Klein, Bilow, & Auer, 2014). The first is characterized by many separated parts that are assembled on site. The latter is prefabricated in a factory and installed as big units.

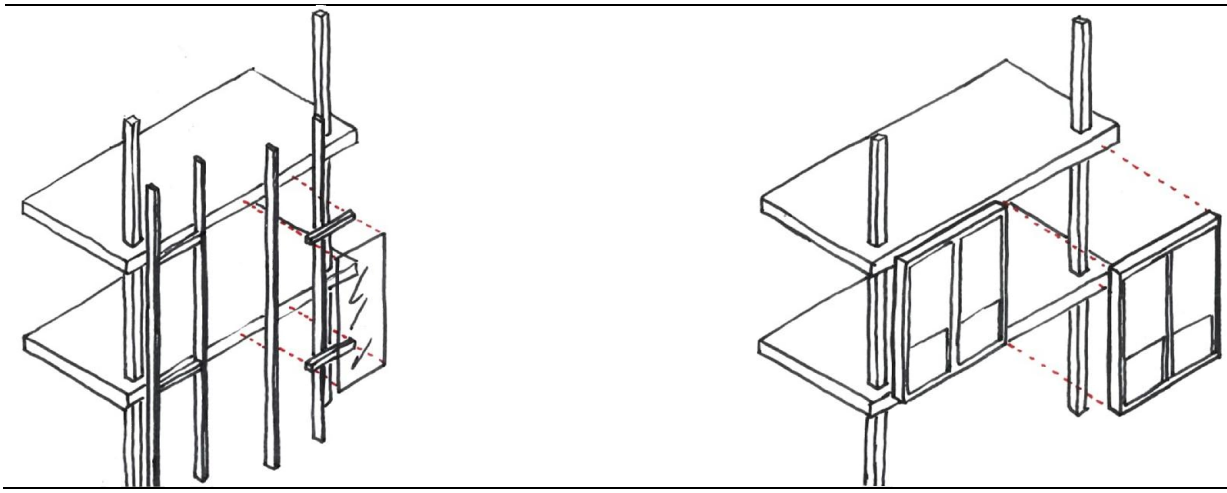

figure 2-4: Stick system versus unit system.

The stick system is assembled on site which makes it easy to correct size deviations (Knaack, Klein, Bilow, & Auer, 2014). During assembly the minimum dilatation width for the deformation capacity should be assured.

Due to the high prefabrication rate of the unit system, there is little room for on-site adaptions to accommodate for size deviations and deformations. Special attention is needed in the design of connecting details and dilatations to provide enough tolerance space for pre-assembly size deviations and to assure that there is still a minimum of space left to provide capacity for after-assembly deformations. In figure 2-6 a horizontal dilatation detail for the façade is shown. Grooves are applied that provide vertical tolerance and movement space for the sealants (Knaack, Klein, Bilow, & Auer, 2014).

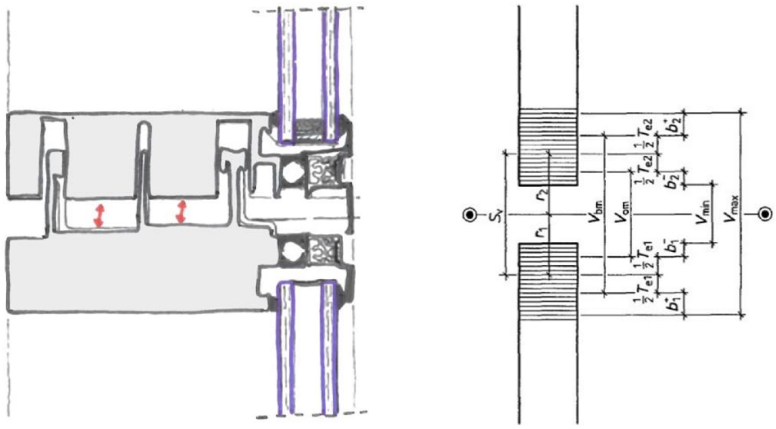

S_v: Target size of the dilatation
V_{min}: Lower boundary size
b^-: Deformation capacity
T: Total positional tolerance
V_{max}: Upper boundary size

figure 2-5: Unit system façade detail with deformation capacity (NSC, 2013) and determining factors for the dilatation size (NPR 3685, 1995).

Next to dilatation space for after assembly deformations, tolerance space is required between adjacent elements to cover size deviations that occur before assembly. These size deviation originate from manufacturing deviations, outlining deviation and adjustment deviations which are treated as stochastic variables. The first is more predominant in the unit system due to the high level of prefabrication. The latter two deviations are much more easily corrected in the stick system during assembly. The vertical tolerances for a one storey high prefabricated façade element are shown in table 2. These tolerances originate from Eurocode requirements and manufacturer information from which more information can be found in appendix F starting on page 160. It is assumed that the façade elements span one floor height of 3600mm.

Tolerance (assuming 3600mm floor to floor height)		**Timber façade**	**Concrete façade**
Manufacturing	T_i	±3mm (6mm)	±10mm (20mm)
Outlining	T_u	±5mm (10mm)	±5mm (10mm)
Adjustment	T_s	±5mm (10mm)	±5mm (10mm)
Total positional	$T_e = \sqrt{T_i + T_u + T_s}$	±8mm (16mm)	±12mm (24mm)

table 2: Tolerances for prefabricated façade elements.

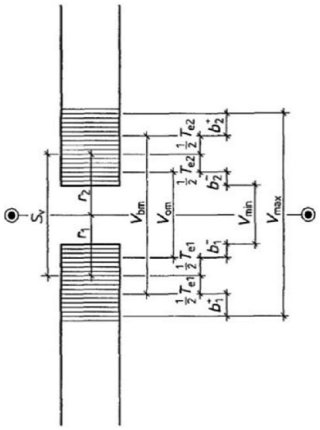

$b^- = b_c + b_t + b_b =$ 17 mm
$T_e = \sqrt{T_i + T_u + T_s} =$ 16 mm
$V_{min} =$ 5 mm
$S_v = b^- + T_e + V_{min} =$ 38 mm
$V_{max} = S_v + T_e + b_t =$ 55 mm

figure 2-6: Unit system façade detail with deformation capacity (NSC, 2013) and determining factors for the dilatation size (NPR 3685, 1995).

Column shortening can have a relevant share in the total deformation capacity that is needed in façade dilatations and should be accounted for in the design. However, it does not seem to be the predominant factor in the total required dimensions of a dilatation detail when considering deformation capacity for other phenomena and tolerance space for manufacturing, outlining and adjustment.

2.1.2 Partition walls

A partition wall is usually a non-load bearing wall that can function as a separation wall for visibility, acoustics or fire. The walls are mostly situated between the floor and ceiling and can be made of timber, metal, gypsum board, concrete, bricks or glass. This chapter will not consider the heavy weight materials like concrete or brick because this would not be a suitable option for a partition wall in a high rise building.

Because partition walls are not designed as a load bearing element, it is desirable that the main load bearing structure can deform within certain limits without inducing loads in the partition walls. A commonly used system for partition walls is the metal stud wall system. This lightweight system can be installed in several varieties with different specifications, regarding fire proofing and sound insulation (Saint-Gobain Gyproc, 2011). The wall system is connected to the main structure at the floor and ceiling. A wall with a standard upper end connection detail can take up deformations until 10mm. When high deformations due to elastic, creep and shrinkage strains are expected, the design of the connection detail can take up higher deformations until 30mm by a sliding upper end detail. These upper end details are shown in figure 2-7.

Standard upper end connection:

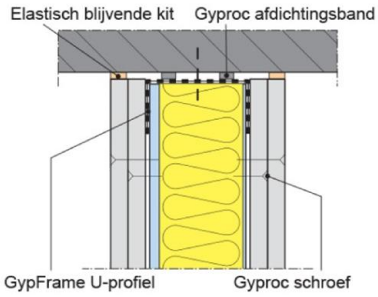

$\leq 10mm$

Sliding upper end connection:

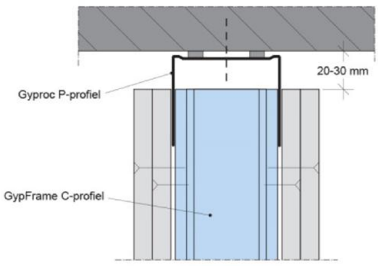

$\leq 30mm$

Fire proof sliding upper end connection:

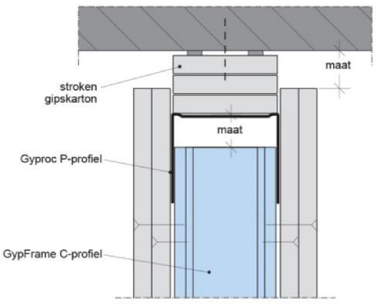

$Custom$

figure 2-7: Upper end connection detail of metal stud partition wall (Saint-Gobain Gyproc, 2011).

Glass partition walls that are commonly used in office spaces have an upper end detail that is designed according to the same principle as a metal stud wall. The detail ensures that the upper floor can move freely and that floor vibrations will not propagate through the glass partition wall. The glass wall is assembled from several glass panes over the length of the wall which gives the wall some in plane shearing capacity (figure 2-1).

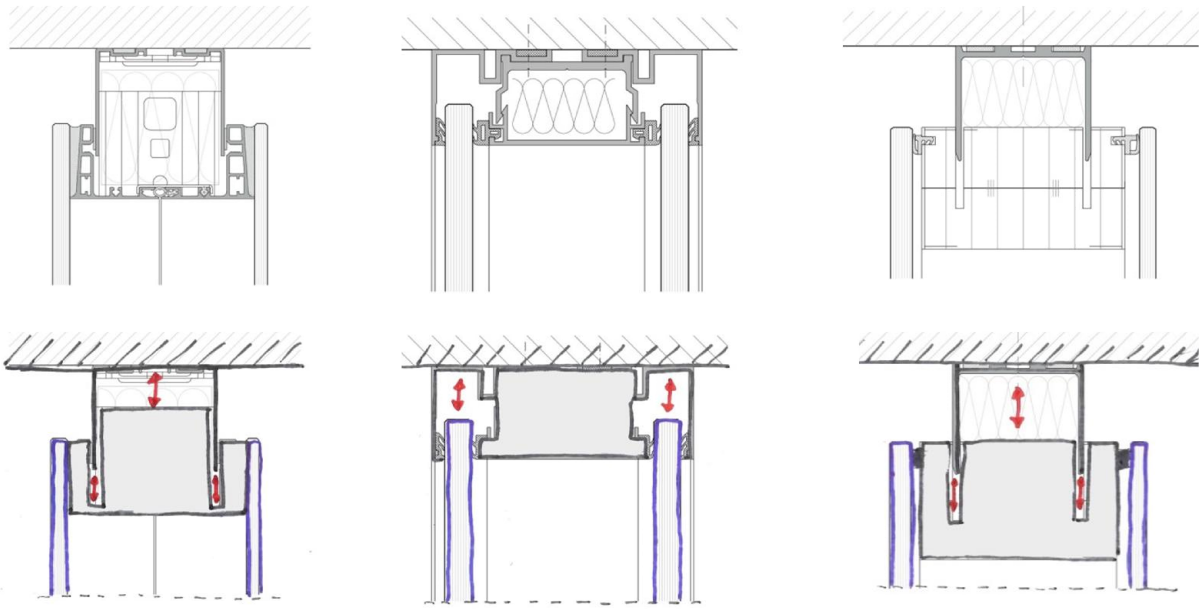

figure 2-8: Upper end connection detail of glass partition wall (Strähle Raum-systeme Gmbh).

From this study to partition walls it can be concluded that deformation capacity for floor deformations and column shortening is provided by standardized partition wall products. These standardized product can take deformations up to 30 mm into account. However, when more excessive deformations may occur it does not seem to be an invincible obstacle to customize the upper end detail to attain more deformation capacity. Because of the probable high repetition factor of partition walls in a high-rise building, such a customized detail can still be an economically sound solution.

2.2 Technical systems

With the occurrence of excessive deformations in the structural system, forces could be introduced in the ducts of climate, water and sewerage systems which could cause damage to these ducts. For vertical ducts, the problem occurs mostly in lower parts of the building where floor to floor shortening δL is most severe due to the highest gravitational loads. For horizontal ducts, it is most likely that the problem occurs at the higher floors of the building where the differential shortening is more severe due to the cumulative effect. Due to this differential shortening, the horizontal ducts can be subjected to bending and shearing.

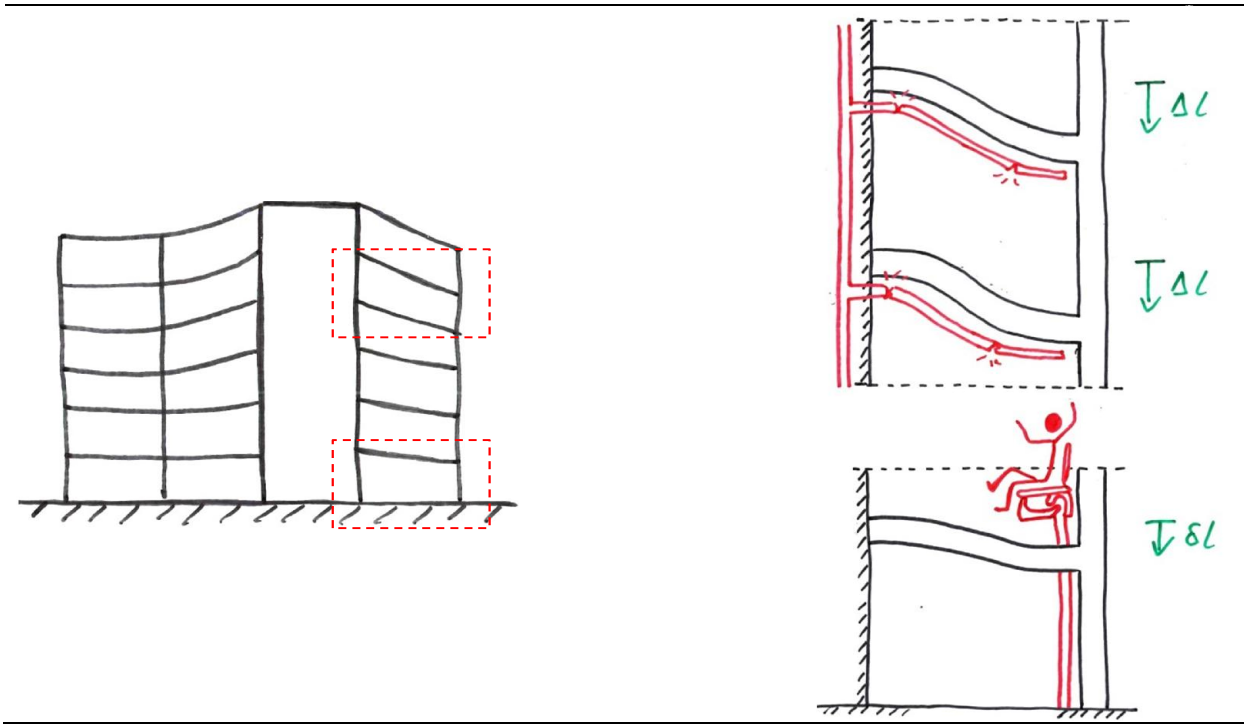

figure 2-9: Possible problem areas for technical systems when considering (differential) vertical shortening.

When there is accounted for enough deformation space in detailing connectors at transitions from floor to floor or vertical to horizontal pipes, the deformation of the main load bearing system should not cause any problem regarding damage to ducts.

2.2.1 HVAC systems

The ventilation and air handling infrastructure in a building is often made of steel ducts with a round or rectangular section that are mounted by suspension brackets to structural walls and floors for vertical and horizontal ventilation ducts respectively. When deformations occur due to bending or compression, forces can be introduced due to the rigidity of these steel ducts.

Rigid expansion sockets:

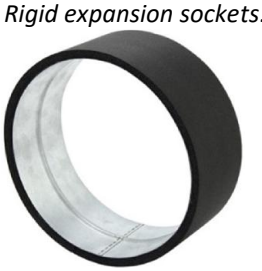

Flexible and semi-flexible ventilation hoses:

figure 2-10: Fittings for ventilation systems (Ventilatieshop.com B.V., 2012).

In the HVAC industry there is a variety of connectors that can provide deformation capacity to the ventilation system. Connector sleeves can provide deformation capacity in the axial direction of ventilation ducts and flexible transitional pieces can provide deformation capacity in bending and shearing. With proper detailing the limits of deformation capacity can be raised to the level that is desired. The condition is that the location where problems may rise should be mapped.

2.2.2 Water and supply ducts

The water and heating ducts are often subjected to high temperatures which cause thermal expansion in the system. The thermal expansion requires measures that ensure that the ducts can move freely to prevent the introduction of stresses that can cause damage to the system.
The variations in length can be captured by axial compensators or dilatation loops. Angular variations or misalignment can be captured by flexible hoses. These components are depicted in figure 2-11. The position of attachment points also determines if the duct has freedom to move. Attachments at corner points cause a restraint in the axial direction for one of the adjacent ducts of that corner.
These measures, that are mainly intended to provide deformation capacity for thermal expansion, also provide deformation capacity for movements that are caused by differential vertical shortening. It is assumed that with proper detailing the deformation capacity of water and supply ducts can be more than enough to capture the movements due to differential vertical shortening.

Rigid axial compensation measures: *Flexible and semi-flexible water hoses:*

figure 2-11: Fittings for supply ducts (fvb ffc constructiv, 2000). Right: Expansion joint in sprinkler system of Brock Commons where the system exits the core (The University of British Columbia's Centre for Interative Research on Sustainabilty and Forestry and Innovation Management, 2017).

2.2.3 Sewerage and drainage systems

The sewerage and drainage systems in a high-rise consists of vertical and horizontal oriented piping. Due to column shortening, loads can be induced in vertical downpipes if not designed for vertical deformations. Due to differential shortening, loads can be induced in horizontal piping due to bending and shearing of the pipes.

The Dutch covenant for high-rise buildings mentions some typical problems that appear for downpipes in high-rise buildings. These are problems are mainly caused by vertical velocity of waste, pressure differences and thermal expansion. With conventional downpipes problems can occur where horizontal branches meet the vertical downpipe. In practice it is assumed that the conventional norms for downpipes are applicable for building till a height of 50 meters (NTA 4614-6, 2012).

For high-rise buildings the Sovent system is applied with an aerator fitting to ensure that waste velocity is decreased by an offset chamber. This prevents that the waste reaches its terminal velocity thus eliminating back pressure (Sovent, 2005). The aerator fitting is required at each floor at the connection with horizontal branches. Each aerator fitting is installed with an expansion socket on each floor to accommodate for expansion and movement of the vertical pipes. When expansion sockets are consistently applied in down pipes of high-rise buildings it may be assumed that the down pipes have sufficient axial deformation capacity and will not be a limiting factor for the vertical displacements of the load bearing structure.

Also flexible sewerage coupling pieces are available in the ducting industry. These coupling pieces can provide angular deformation capacity and are useful on places where misalignment between ducting may occur.

Rigid axial compensation measures:

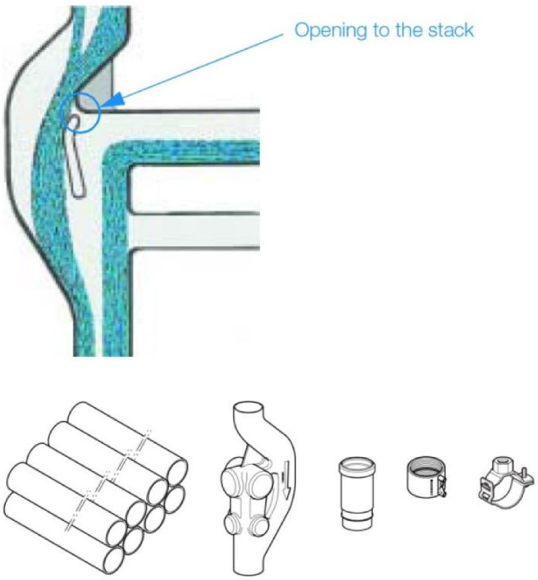

Flexible and semi-flexible water hoses:

figure 2-12: Sovent drainage and sewerage system (Geberit, 2004). Flexible sewerage coupling piece (Akatherm BV, 2017).

2.3 Structural factors

The EN1990 sets principles for the safety, usability and durability for the design of building structures. The basic principle for safety states that the building structure should resist all loads and influences during the whole service life of the building. The structure should comply with the specified usability demands over the whole service life to guarantee quality. Limit states are drafted that are associated with design situations to test safety, usability and durability. (NEN-EN 1990, 2011)

The limit states that are related to functioning of the structure with normal use, comfort of people or the appearance of the building are subdivided as serviceability limit states (SLS). Serviceability limit states should be tested to the standards which relate to deformations that affect the appearance, the comfort and the functioning of the structure and can cause damage to finishing's and non-structural elements.

The limit states that are related to the safety of the building structure and the people who use the building are subdivided as ultimate limit states (ULS). Ultimate limit states that should be tested are loss of stability of the structure, failure due to excessive deformations including supports and foundations, and failure due to time dependent effects.

2.3.1 SLS requirements

The serviceability limit states (SLS) are the limit states that are related to the functioning of the structure in normal use, the comfort of people and the appearance of the structure. The Eurocode describes that the checking of serviceability limit states should be based on standards that relate to deformations, vibrations and damage that have a negative effect on the appearance, durability and functioning of the structure (NEN-EN 1990, 2011, p. 30).

This research will concentrate on the checking of serviceability limit states to standards that are related to vertical deformations. These vertical deformations may affect the appearance of the structure, can cause discomfort for users or can cause damage to secondary structures or service systems that are discussed in the previous chapters. As the Eurocode notes, the SLS requirements are mostly determined for every project independently (NEN-EN 1990, 2011, p. 30). It also states that the SLS requirements should be determined for

every project and agreed upon with the client with the note that these requirements can be prescribed by the national annex (NEN-EN 1990, 2011, p. 56). In some cases, the demands on vertical deformations can be of little importance dependent on the use of the space above or below the considered space. It can also be the case that part of the deformations are masked by the finishing of the structure. These deformations do not have to be included in stated demands regarding aesthetics.

According to the Eurocode, the checking of limit states should be conducted for all possible design situations and all possible loadcases (NEN-EN 1990, 2011, p. 31). In the analysis of vertical deformations of floor slabs and floor supports, other deformation phenomena besides differential vertical shortening should be accounted for. Lateral displacements due wind or seismic loads can cause rotation in the concrete core which may result in vertical deformations of floor supports that are attached to the core. Foundation settlements can cause vertical deformations as is shown in figure 2-13. Next to the vertical deformation of floor supports, the floor will also deflect in the middle of the span. One should consider the combination of all deformations in order to fulfil the serviceability state requirements. “The column shortening due to gravity loads and shrinkage should be superimposed with other effects and limitations established on the combined movement” (Fintel, Ghosh, & Iyengar, 1987, p. 22).

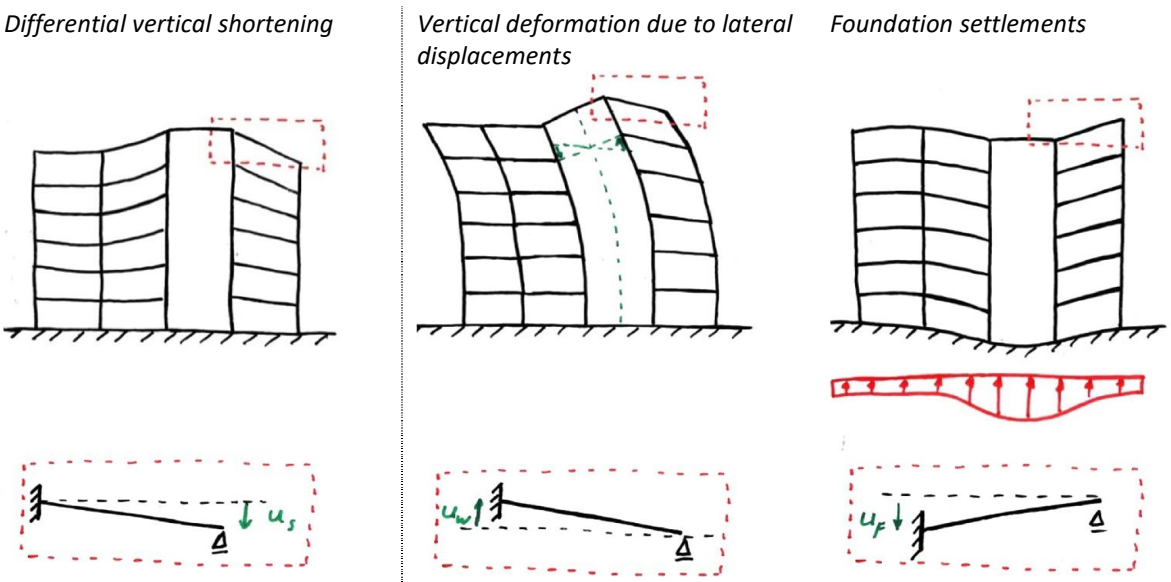

figure 2-13: Differential vertical shortening in the upper structure and other vertical deformations.

The deformations due to possible foundation settlements are assumed to be opposite to deformations due to DVS because most mass of the building will be in the stabilizing core as shown in figure 2-13. For this reason, these deformations are further left out of consideration in this research and it is assumed that the foundation has infinite stiffness which implies that only the deformations whose origin occurs in the upper structure are considered.

figure 2-14: Governing location for SLS requirements.

When the differential vertical deformation between two floor supports of two adjacent vertical members is larger than the mid span deflection, it is assumed that the deflection at mid span is not governing as shown in figure 2-14.

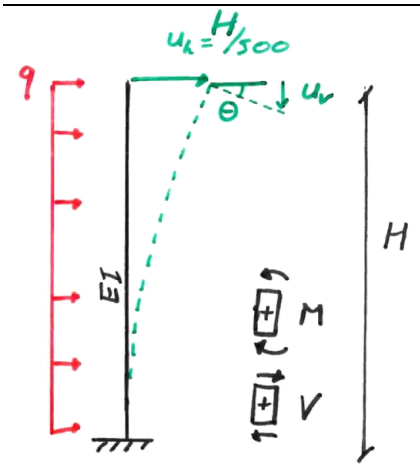

figure 2-15: Lateral displacement requirement for the core with the corresponding maximum rotation

For a general approach, the vertical deformations of floor supports due to lateral displacements can be based on the horizontal displacement limit over the total building height that is given by the Dutch National annex of the Eurocode as $u_h \leq H/500$, with H being the building height (NEN-EN 1990-1-1/NB, 2011, p. 15). From this limit a maximum core rotation can be derived analytically. When assuming small rotations, the vertical displacement of the floor supports at the core due to lateral displacement can be approximated by the product of the rotation and half the core width. The outcome of this procedure, which is elaborated in appendix G on page 166, provides a fixed maximum core rotation that corresponds to the ratio $u_h \leq H/500$ of $u_h' = 0{,}00267$ that is independent of the building height H.

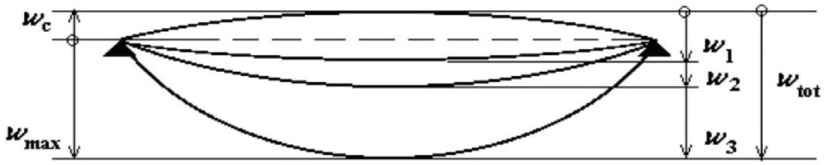

w_c	Applied camber of the unloaded structural element.
w_1	Initial short term deformation due to permanent loads.
w_2	Long-term deformations due to permanent and quasi permanent loads.
w_3	Additional deformations due to live loads that are determined by short-term characteristics.
w_{tot}	Total deformation of w_1, w_2 and w_3.
w_{max}	Total deformation considering the camber.

$w_2 + w_3 \leq \frac{l_{rep}}{500}$:	For floors that support crack sensitive partition walls.
$w_2 + w_3 \leq \frac{3\, l_{rep}}{1000}$:	For floors that are intensively used.
$w_{max} \leq \frac{l_{rep}}{250}$:	For floors and roofs with aesthetic value.

figure 2-16: Vertical deformations (NEN-EN 1990-1-1/NB, 2011).

A direct limit on vertical deformations of floor supports is not provided by the Eurocode. However, these deformations can be derived from requirements that are provided by the Eurocode for the mid span deflections of a simply supported beam or end deflections of a cantilevered beam as is shown in figure 2-17.

From these requirements a sag to span ratio can be derived that is presented in figure 2-17 that can be used as a basic principle for vertical deformation requirements.

$$l_{rep} = l$$

$$w_{2+3} = \frac{3 \cdot l_{rep}}{1000} \rightarrow \theta_{2+3} = \frac{w_{2+3}}{l/2} = \frac{6}{1000}$$

$$w_{max} = \frac{4 \cdot l_{rep}}{1000} \rightarrow \theta_{max} = \frac{w_{max}}{l/2} = \frac{8}{1000}$$

$$l_{rep} = 2l$$

$$w_{2+3} = \frac{3 \cdot l_{rep}}{1000} \rightarrow \theta_{2+3} = \frac{w_{2+3}}{l} = \frac{6}{1000}$$

$$w_{max} = \frac{4 \cdot l_{rep}}{1000} \rightarrow \theta_{max} = \frac{w_{max}}{l} = \frac{8}{1000}$$

figure 2-17: Basic principle of deformation requirements.

The Eurocode mentions that when considering the functioning of non-constructive elements such as partition walls, façades or technical systems, the deformations that occur due to permanent and variable loading after realisation (post-deformations) of the considered element(s) should be taken into account (NEN-EN 1990, 2011, p. 57). To meet this requirement, the total DVS deformations should be subdivided into pre- and post-DVS deformations for which the distinction is made according to a particular moment in time at which finishing elements or technical systems are installed at a particular floor instead of making a subdivision between elastic and time dependent deformations. On the one hand, the finishings and installations can be placed at a lower floor in the building when the upper structure is still under construction so elastic deformations are still added afterwards. On the other hand, time dependent deformations can already develop before placing these finishings and installations because the main load bearing structure is build several floors before placement of finishings and installations. The Dutch national annex of the Eurocode states that it may be presumed that these requirements on these post-deformations are met if one adheres the requirements that are given in figure 2-16.

Despite this presumption of the Dutch national annex, the post-deformations will still be distinguished from the total deformations in this research in order to make it possible to study possible influences on post- and total differential vertical shortening deformations. The post-DVS deformations $\Delta L_{post-DVS}$ will be assessed to θ_{2+3} or w_{2+3} and the total-DVS deformations $\Delta L_{total-DVS}$ to θ_{max}or w_{max}. The SLS-requirement is dependent of the floor span as is shown in figure 2-18. Because the DVS deformations will be superimposed with the vertical deformations due to lateral displacements of the building, the SLS requirement regarding only DVS deformations is also dependent of the core width.

$$\Delta L_{post-DVS} \leq \theta_{2+3} \cdot l - u_v \qquad \theta_{2+3} = 6/1000$$

$$\Delta L_{total-DVS} \leq \theta_{max} \cdot l - u_v \qquad \theta_{max} = 8/1000$$

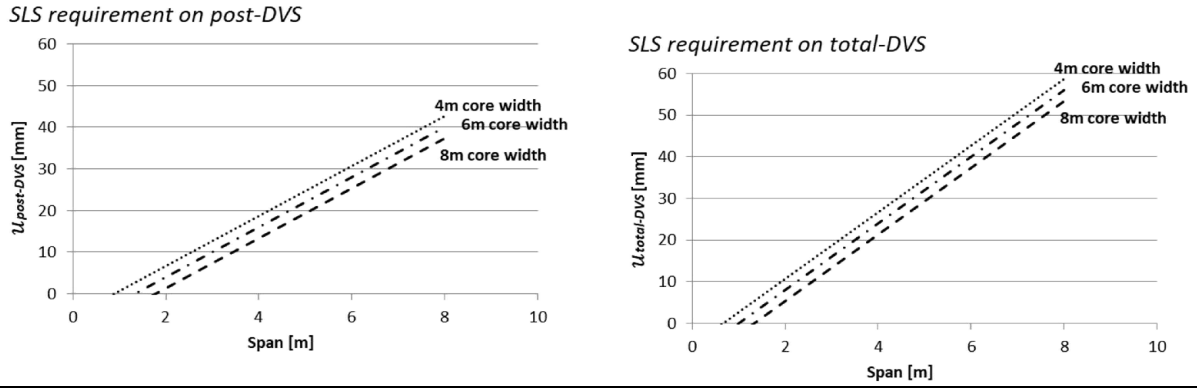

figure 2-18: Serviceability limit state requirement for post- and total-DVS deformations.

2.3.2 ULS requirements

Differential shortening of vertical load bearing elements of high-rise buildings can cause additional stresses in horizontal floor structures and vertical load bearing structures due to the resisting capacity of these structural elements against unequal support settlements. Axial forces in vertical load bearing elements can be transferred from the more shortened to the less shortened elements which implies a load redistribution over the building plan and a restraining effect on differential vertical shortening (Kim H.-S. , 2013; Fintel, Ghosh, & Iyengar, 1987).

Three main mechanical schemes of a horizontal element with a certain stiffness are shown in figure 2-19. Force redistribution is possible due to the stiffness and boundary conditions of the horizontal beam or floor element. The first situation does not provide resistance to unequal support settlements, which also means that no additional forces will occur in the horizontal element. The second situation provides resistance to unequal support settlements due to the bending stiffness and the clamped right end of the beam. The third situation causes the most force redistribution because both beam ends are clamped. The figure shows the most extreme situations where the beam ends are fully hinged or fully clamped. It is most likely that reality is somewhere in between these situations.

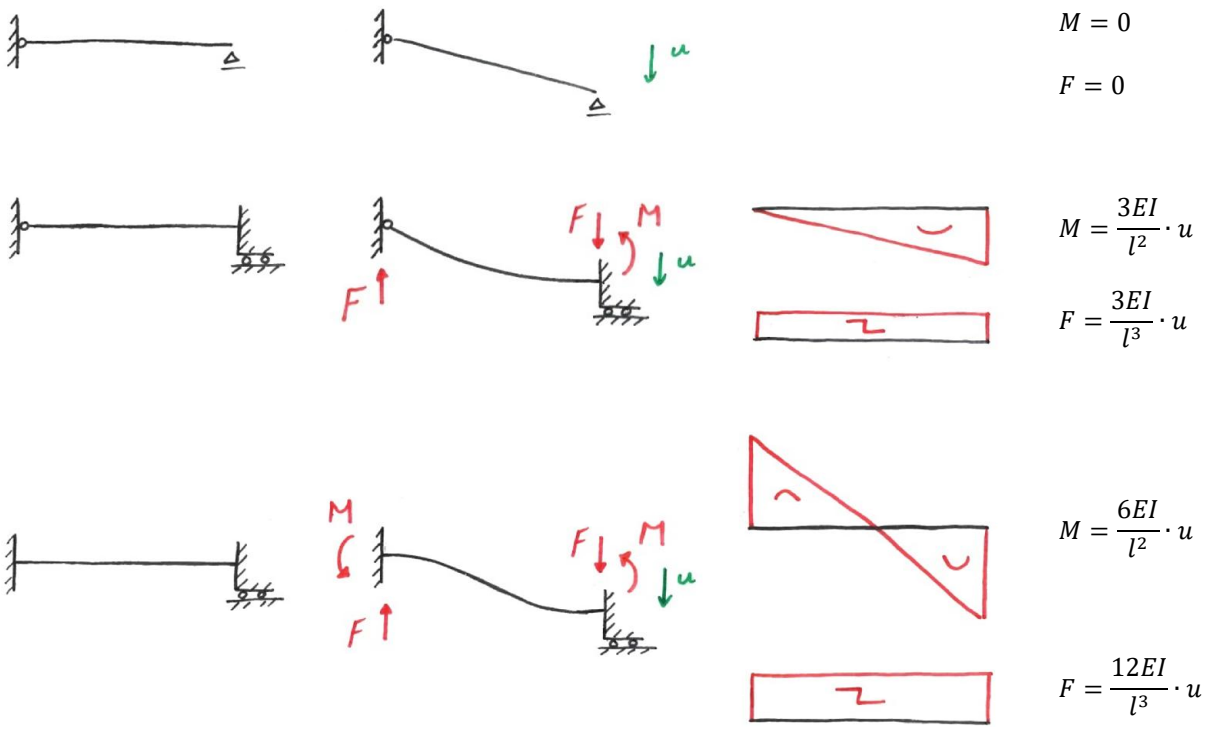

figure 2-19: Basic beam or floor span mechanics.

The main mechanical schemes for beam or slab elements reacting on a support settlement are explained by figure 2-19. It shows a situations with infinite rigidity on the beam ends though this idealised situation is impossible in practise. Even when beam end connections have infinite rigidity, the flexibility of adjacent members will facilitate rotational movement.

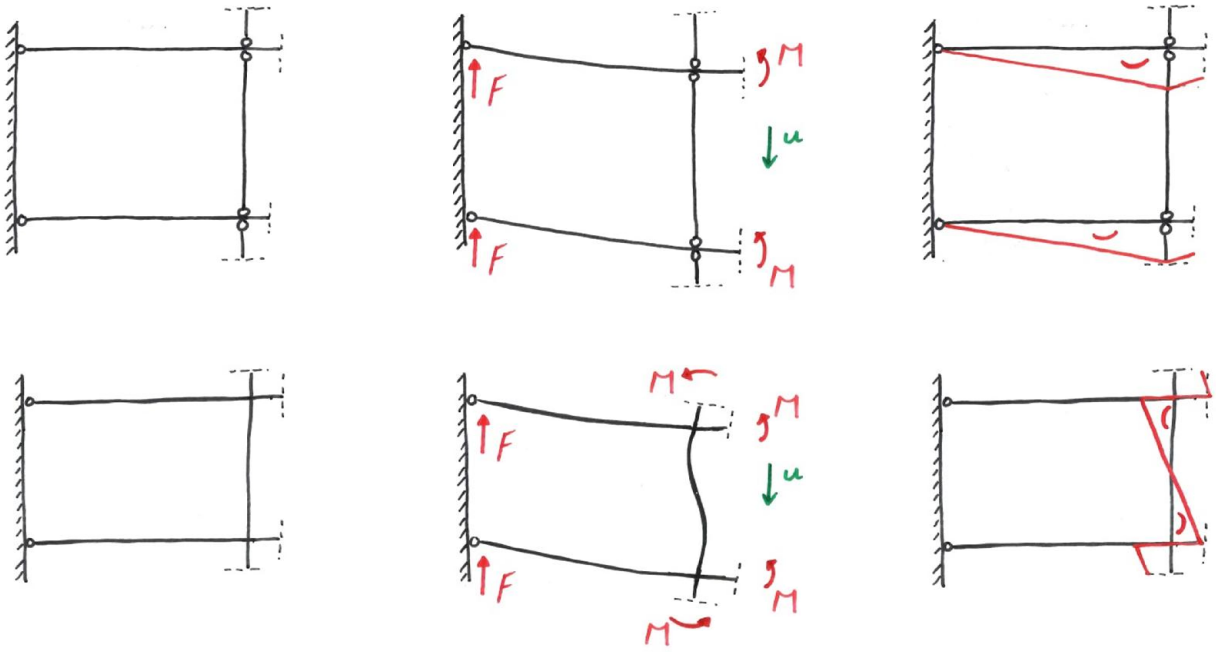

figure 2-20: Mechanical system in relation to adjacent members.

An instantaneous support settlement Δ of a floor slab due to elastic strains will cause instantaneous stresses in this beam or slab due to the bending moment and shear force. When the floor slab is prone to creep, relaxation will occur which causes that the bending moment and shear force will gradually decrease with time. Curve A in figure 2-21 shows the development of the bending moment in a floor slab when it is prone to creep and loaded with an instantaneous support settlement. In reality the support settlement will not be instantaneous, but will develop gradually with time because loads are applied gradually in the building process and creep and shrinkage in the supporting columns will also develop gradually. This causes that the bending moment in the slabs will increase gradually and that relaxation will start from the moment that the first loads are applied. Curve B of figure 2-21 shows the bending moment development with a gradual increasing support settlement for a floor slab that is prone to creep (Fintel, Ghosh, & Iyengar, 1987).

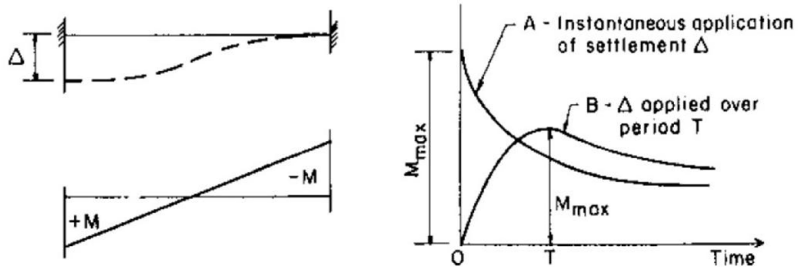

figure 2-21: Dependence of internal beam stresses to settlement rate (Fintel, Ghosh, & Iyengar, 1987).

It can be expected that additional stresses in structural members due to differential support settlements are lower when these members are prone to creep and relaxation behaviour. The stress in these members will reach its maximum after some time due to gradual settlements. After the maximum is reached, the stresses can decrease due to the relaxation behaviour of these members. This means that the restraining effect on the support settlements will also diminish over time.

2.4 Evaluation

The areas where vertical differential shortening could cause any problems to the safety, usability and durability of the structure are considered in this chapter. The individual floor to floor column shortening is not a predominant issue when compared to the total of other deformations, such as thermal expansion of the façade and floor edge deflections, or size deviations. However, built-in tolerance space in connection details for technical systems, façades and partition walls should account for all mentioned movements including the individual floor to floor column shortening.

Differential vertical shortening (DVS) deformations at the higher floors of the building can be a predominant issue due to the cumulative effect. Architectural and technical building systems can be designed with deformation capacity to accommodate for DVS, but may still be affected by deformations in the load bearing structure that occur after placement of these systems. Fixed limitations on these deformation capacities are not found by literature study and product specifications. However, the Eurocode does provide standards on maximum vertical deformations based on the ratio between span and deformation of horizontal structural members. It also specifically states that when considering structural elements that can affect non-structural elements, the deformations that can occur after assembly of these non-structural elements should be taken into account (NEN-EN 1990, 2011).

To perform an accurate analysis on DVS deformations, the part of the DVS deformations that may affect secondary building elements should be distinguished from the total-DVS deformations. Further in this research these are the so-called post-DVS deformations, which are the DVS deformations that occur after placement of secondary building systems. In this manner, the serviceability limit states can be assessed conform the Eurocode 0 prescriptions of clause 3.4(3a) (NEN-EN 1990, 2011, p. 30). The comfort of the building users regarding deformations can be guaranteed by assessing the total-DVS deformations against criteria that relate to the appearance of the structure and by assessing the post-DVS deformations against criteria that relate to damage of secondary building elements.

According to clause A1.4.2(2) of Eurocode 0, the serviceability limit state criteria should be determined for each individual building project and should be agreed with the client (NEN-EN 1990, 2011, p. 56). For this research the criteria that are elaborated in figure 2-17 will be used as criteria for the total- and post-DVS deformations as formulated by equation 1.

$u_{post-,DVS} + u_{lateral}$	$\leq \theta_{2+3} \cdot l$	$\theta_{2+3} = \frac{6}{1000}$	*Related to damage on secondary building elements*
$u_{total,DVS} + u_{lateral}$	$\leq \theta_{max} \cdot l$	$\theta_{max} = \frac{8}{1000}$	*Related to the appearance of the structure.*

equation 1: Serviceability limit state requirement for DVS deformations.

The ultimate limit state is also of importance in the structural analysis of high-rise buildings, because the DVS deformations can cause additional stresses in the structure due to load redistributions. Nevertheless, in the case study and variable study further on in this thesis, only the serviceability limit state will be considered.

3 Straining in timber and concrete

3.1 Response mechanism of timber and concrete

The materials timber and concrete show some similarities in their response to loads and climate conditions. Both materials show linear viscoelastic behaviour for sufficiently low stresses. This means that the response to loads has elastic characteristics and viscous characteristics. Finally, the Boltzmann superposition principle can be applied on both material models when dealing with load increments. This chapter explains the fundamentals of an ideal linear viscoelastic material which can be the case for both concrete and timber.

3.1.1 Linear elastic behaviour

Both concrete and timber can be modelled as linear elastic for short term loads that are sufficiently low relative to the ultimate strength of the material. The elastic strains are related to the stress through the Young's modulus. A material with a full linear elastic character will deform linearly related to the applied load. When the load is removed, the material will deform back to its original shape. The elastic character of an axially loaded piece of material can be modelled as a spring element with a stiffness that is equal to the product of the Young's modulus and the cross section according to Hooke's law and that is loaded by a force F.

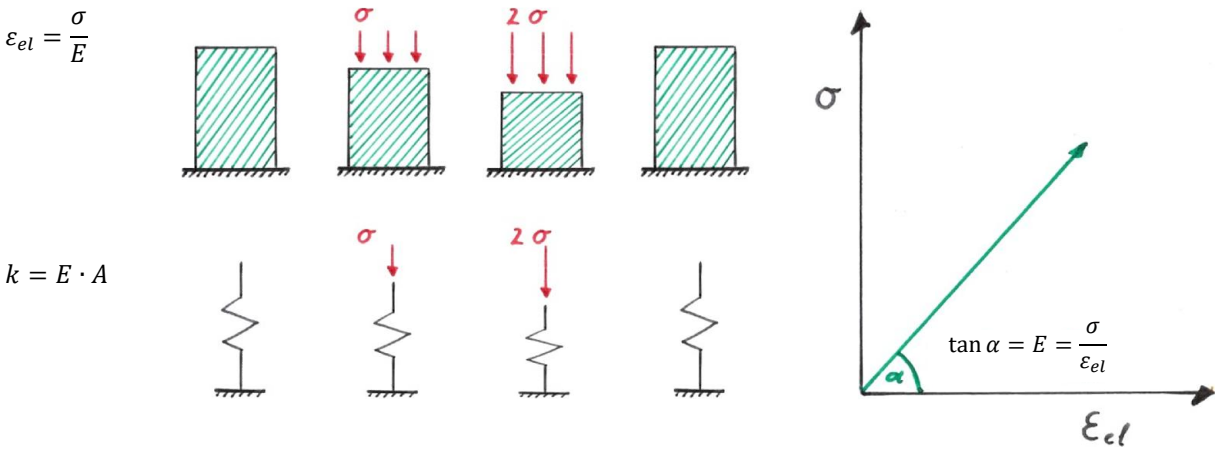

figure 3-1: A linear elastic material modelled as a spring element according to Hooke's law.

A pure linear elastic material obeys the superposition principle. The superposition principle indicates how the response mechanism can be determined for multiple loadings. "In physics and systems theory, the superposition principle, also known as superposition property, states that, for all linear systems, the net response at a given place and time caused by two or more stimuli is the sum of the responses that would have been caused by each stimulus individually" (Wikipedia, 2017). The principle is limited to linear material behaviour and structures that undergo small deformations only, so the geometry can be assumed linear. In the basic superposition principle, time is not considered and the order in which force A or B of figure 3-2 are applied is not of influence.

Additivity

$Input\ (\Delta\sigma_1)$ $\rightarrow Response\ (\Delta\varepsilon_1)$
$Input\ (\Delta\sigma_2)$ $\rightarrow Response\ (\Delta\varepsilon_2)$

$Input\ (\Delta\sigma_1 + \Delta\sigma_2)$ $\rightarrow Response\ (\Delta\varepsilon_1 + \Delta\varepsilon_2)$

Homogeneity

$Input\ (\Delta\sigma_1)$ $\rightarrow Response\ (\Delta\varepsilon_1)$

$Input\ (2\Delta\sigma_1)$ $\rightarrow 2 \cdot Input\ (\Delta\sigma_1)$

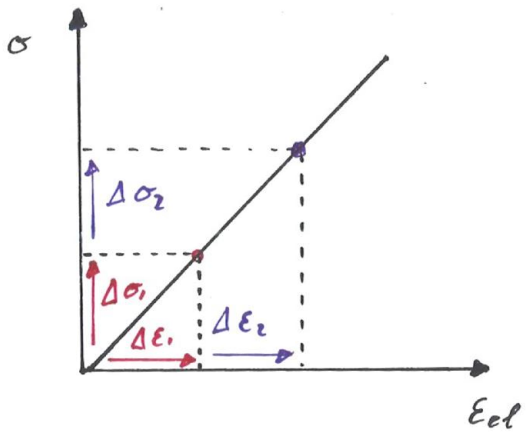

figure 3-2: Superposition principle.

3.1.2 Viscous behaviour

After the initial deformation, that is caused by a load, both timber and concrete will show viscous deformations. In the case of sustained loading, creep deformations will develop over time that are partly elastic and partly viscous.

A material with a full viscous character will deform linear with time when a constant stress is applied. The material will not recover to its original shape when the load is removed, but will stop deforming further. Materials with a low viscosity, like water, have a low resistance to shear flow. Materials with high viscosity, like maple syrup, have a higher resistance to shear flow. The viscous character of a material can be modelled as a viscous damper according to Newton's law. This describes that the speed in which a viscous material (fluid) will deform is linear dependent to the applied stress on the material and the viscosity (shear resistance) of the material (Vincent, 2012).

$$d\varepsilon = \frac{\sigma}{\eta} \cdot dt$$

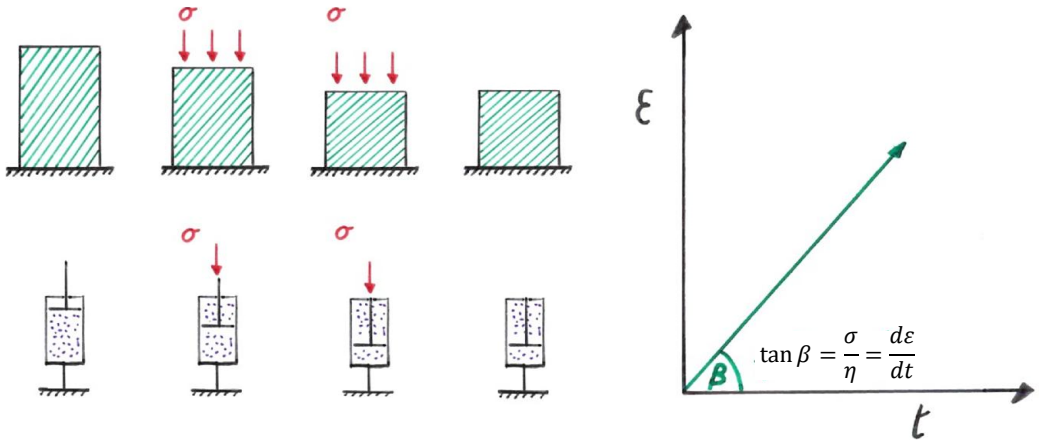

figure 3-3: Viscous deformation according to Newton's law.

Viscosity should not be confused with plasticity. An ideal viscous material acts like a fluid in which a shear rate will develop for every shear stress that is applied, no matter how small this stress will be. This means that an ideal viscous fluid has no strength.

3.1.3 Linear viscoelastic response mechanism

Concrete and timber are non-linear viscoelastic. However, when stresses are sufficiently low the non-linearity is so small that both materials can be assumed as linear viscoelastic for this study. The pure linear viscoelastic behaviour is a combination of the elastic and viscous material characteristics. The response behaviour to a certain stress in time is shown in figure 3-4. On t_1 the material is loaded and deforms elastically right away. The creep strain will develop over time from t_1 to t_2 with a decreasing rate. When the stress is removed at t_2 the material will deform back elastically with the same amount of the initial elastic strain on t_1. Also the creep strain that developed from t_1 to t_2 will recover fully or partly over time after the load is removed from t_2 to t_3 with a decreasing rate.

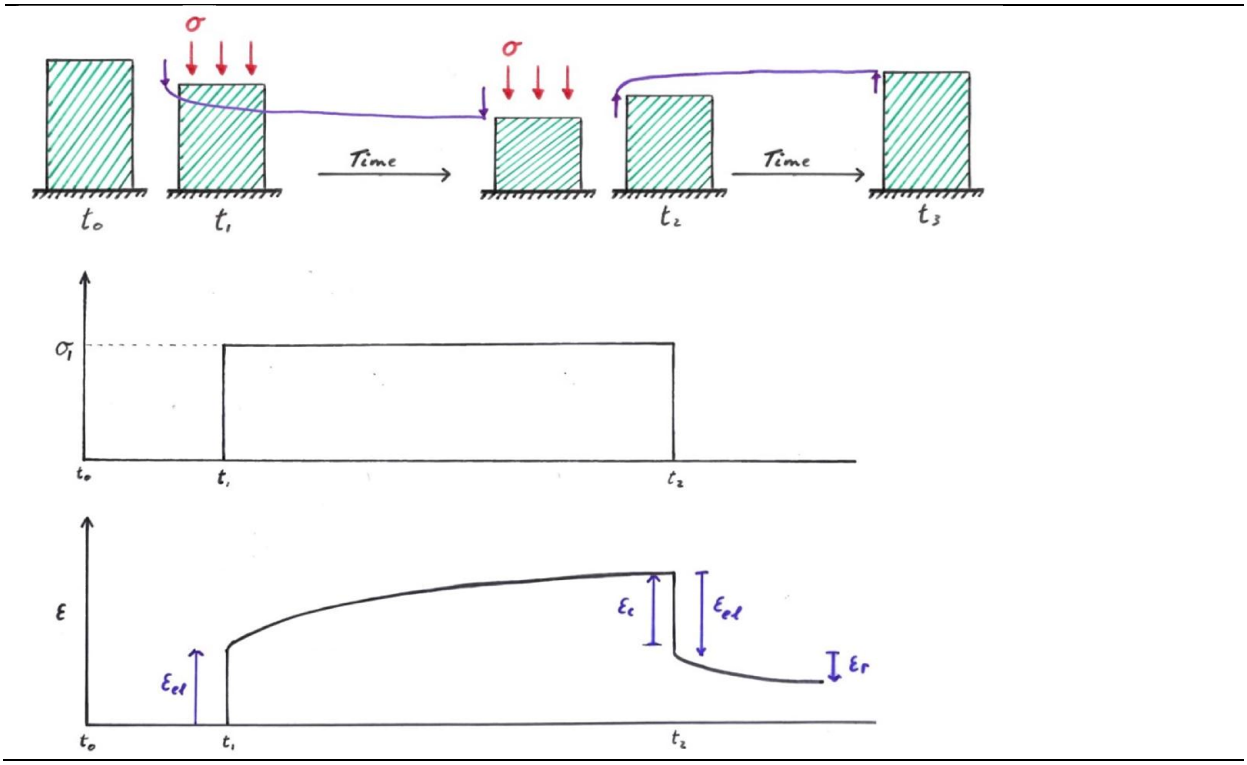

figure 3-4: Viscoelastic behaviour.

3.1.4 Boltzmann superposition principle

The Boltzmann superposition principle refers to the response of a linear viscoelastic material regarding the creep behaviour due to several load increments. The principle states that the creep behaviour in a specimen is dependent of the entire loading history on that specimen and that the response to each individual load increment is independent. This means that the total response is the sum of all individual responses for each individual load increment, but dependent of time (Young & Lovell, 2011).

The creep response can be described by the time dependent creep compliance $J(t)$ which relates the creep strain linearly to the applied stress. Because of the time dependence of the creep compliance, the moment at which the response is observed and the moment at which loads are applied influence the observed response.

Both timber and concrete can be considered as linear viscoelastic materials when stresses are sufficiently low. This means that the creep strain for several load increments of both materials can be described according to the Boltzmann superposition principle when stresses are sufficiently low.

$$\varepsilon(t) = J(t) \cdot \sigma \qquad \varepsilon_n(t) = J(t - \tau_n) \cdot \Delta\sigma_n$$

$$\varepsilon(t) = \varepsilon_1(t) + \varepsilon_2(t) + \cdots$$
$$\varepsilon(t) = J(t - \tau_1) \cdot \Delta\sigma_1 + J(t - \tau_2) \cdot \Delta\sigma_2 + \cdots$$

$$\varepsilon(t) = \sum_{n=0}^{n} J(t - \tau_n) \cdot \Delta\sigma_n$$

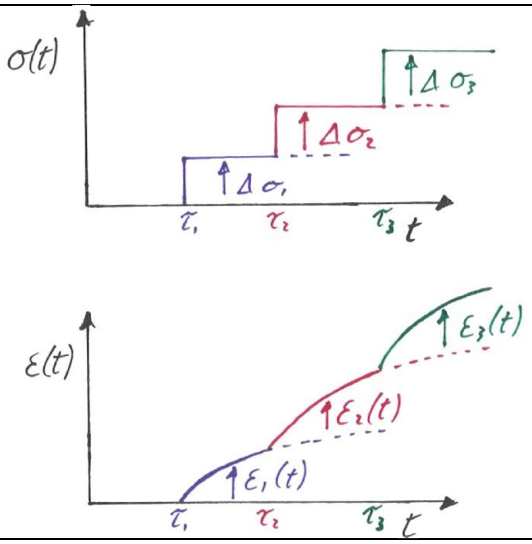

figure 3-5: Boltzmann superposition principle.

3.1.5 Shrinkage & swelling

Next to the stress related deformations, timber and concrete both show shrinkage behaviour. Shrinkage or swelling strain is the strain that is observed in the absence of an external mechanical load. The shrinkage strain develops due to influences of the environmental conditions or the curing process of a material. For concrete the shrinkage behaviour is part of the curing process, where the water and cement ingredients have a bigger volume than the concrete product. Timber shrinks or swells due to its hygroscopic character (Hoffmeyer P. , 1995).

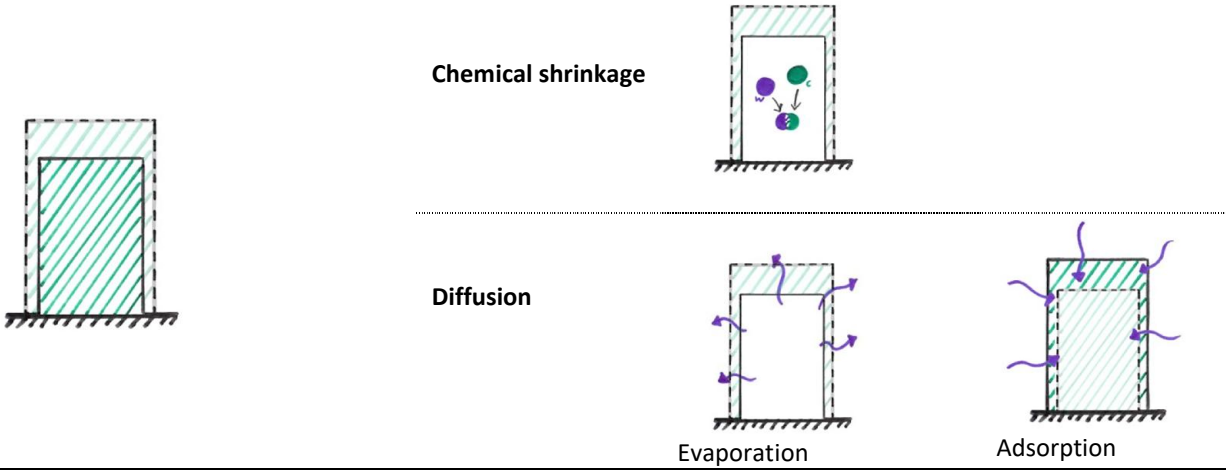

figure 3-6: Different types of shrinkage.

3.1.6 Evaluation

This chapter discussed the response mechanism that belongs to a linear viscoelastic material. This mechanism can be observed in both timber and concrete. In the following chapters the materials will be discussed separately to explain how internal and external variables influence the linear viscoelastic response mechanism. The total strain in both for a linear viscoelastic material can be subdivided into the elastic (initial) strain, the creep strain and the shrinkage/swelling strain.

$$\varepsilon_{tot}(t) = \varepsilon_{el}(t) + \varepsilon_c(t) + \varepsilon_{sh}(t)$$

Each type of strain will be discussed separately.

3.2 Deformations in concrete

The elastic, creep and shrinkage strain in concrete are dependent of many factors that are related to either internal factors (material properties and concrete quality), as external factors (relative humidity, temperature and loads).
The different types of strains in concrete and their influencing factors will be explicated qualitatively on material level.

3.2.1 Elastic strain

The elastic strain is dependent on the stress level and the magnitude of the modulus of elasticity. In figure 3-7 a schematic elastic stress strain relation of concrete is given. The actual elastic behaviour of concrete is non-linear which implies that the modulus of elasticity cannot be considered as a constant value when quantifying the strain for every stress condition. For practical reasons, the stress strain relation is often simplified to a linear relation with a constant Young's modulus. There are several approaches for the determination of a constant Young's modulus:

Secant modulus: The secant Modulus corresponds to the stress strain ratio at a stress of 40% of the ultimate strength ($0{,}4 \cdot f_{cm}$) of the concrete for short-term loading. This is called the average modulus of elasticity and suits very well for linear approximation. The secant modulus is formulated by the Eurocode and is dependant of the mean compressive strength. The elastic stress strain relation with the secant modulus will be:

$$\varepsilon_{el}(t) = \frac{\sigma(t)}{E_{cm}} \qquad \text{With:} \qquad E_{cm} = 22 \cdot 10^3 \cdot \left(\frac{f_{cm}}{10}\right)^{0,3}$$

f_{cm}: Ultimate strength in [N/mm^2]

equation 2: Linear elastic strain with secant modulus.

Initial tangent modulus: This is the Young's modulus at the origin of the stress strain relationship. This value for the Young's modulus is true for very small and short-term loads. This value is used in the Eurocode to describe the creep strain and is derived from the secant modulus according to equation 3:

$$\varepsilon_{el}(t) = \frac{\sigma(t)}{E_c} \qquad \text{With:} \qquad E_c = 1{,}05 \cdot E_{cm}$$

equation 3: Linear elastic strain with initial tangent modulus.

Tangent modulus: This is the Young's modulus that corresponds to an infinite small stress increment starting from a certain initial stress and describes the non-linear stress strain relation of concrete.

The initial (short-term) elastic strain can be simplified by linearization as described above, but one should be aware of the value of the Young's modulus that should be in accordance with the stress level that is applied. In chapter 4.1.1 the quantity of the stress level relative to the ultimate strength is further elaborated.

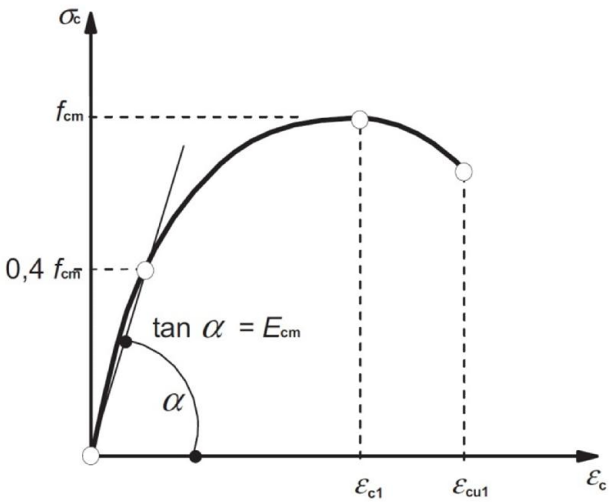

figure 3-7: Schematic stress-strain relationship for structural calculations (NEN-EN 1992-1-1, 2011, p. section 3.1.5).

In NEN-EN 1992 a simplified stress-strain diagram is given (figure 3-8). This relation is used for calculation of cross sections in the ultimate limit state, but is unsuitable and not intended for the calculation of deformations. The Modulus of Elasticity can be derived from these diagrams, but will result in a global value that partly accounts for long-term deformations. The values that are given in figure 3-8 are true for strength classes until C50/60. High-strength concrete classes are more brittle, which means that the beginning plastic deformation strain ε_{c2} and ε_{c3} will be higher and the failure strain ε_{cu2} and ε_{cu3} will be lower (Braam & Lagendijk, 2011).

$\varepsilon_{c2} \quad = 2‰$ $\qquad$ $\varepsilon_{c3} \quad = 1.75‰$

$\varepsilon_{cu2} \quad = 3.5‰$ $\qquad$ $\varepsilon_{cu3} \quad = 3.5‰$

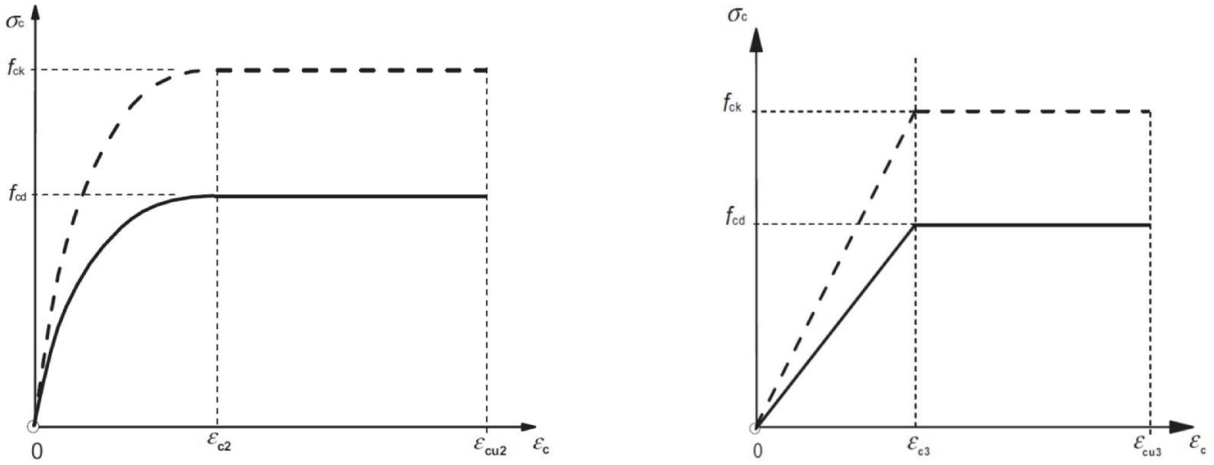

figure 3-8: Simplified stress strain diagram for calculations in ULS (NEN-EN 1992-1-1, 2011, p. section 3.1.6).

In practice a linear relation is often used with a Young's modulus that is equal to the secant modulus E_{cm} for stresses until 40% of the mean compressive strength. Just as the strength, the stiffness of the concrete will develop during the curing process. This development of the Young's modulus with time can be an important factor when a building process is subjected to high building speeds. The material properties that are established in the concrete strength classes correspond with the properties at 28 days after pouring. The concrete is normally set after 1 day, but has no real strength or stiffness. After a week the hydration process is far from complete, but considerable strength and stiffness is reached. At 28 days after pouring, the concrete has reached 80% of its final strength and stiffness (Braam & Lagendijk, 2011). The development of the concrete strength and stiffness are related to each other and dependent of the hydration process. The biggest influencing factor of the speed of the hydration process, and by that the strength and stiffness development, is

the temperature. A higher temperature causes an accelerated development of strength and stiffness, but has a negative influence on the end strength and stiffness (BetonPrisma, 1996). The development of the mean compressive strength and stiffness is described by Eurocode 2. The quantification of the stiffness development is further elaborated in chapter 4.1.1 on page 63.

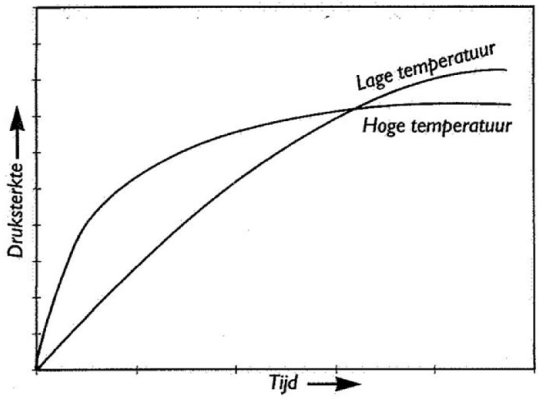

figure 3-9: Influence of temperature on strength development (BetonPrisma, 1996).

3.2.2 Shrinkage strain

The shrinkage strain develops during the curing process of the concrete and is the amount of strain that develops without the influence of external stresses. Because of the independency of stress, the shrinkage strain is not expressed as a function of the Young's modulus. Shrinkage occurs in the cement paste of the concrete. Because of the presence of aggregate, the shrinkage in the cement paste is restrained and causes development of local tension stresses in the cement paste and compression stresses in the aggregate. The aggregate reduces the overall shrinkage strain (Illston, Dinwoodie, & Smith, 1979). In the past, only one type of shrinkage was considered in the building codes. The shrinkage was only ascribed to the evaporation of water molecules from the concrete to the environment. With today's knowledge, also the autogenous (chemical) shrinkage is included in the codes (AEneas, 2012).

Autogenous shrinkage is the part of shrinkage that is not influenced by the environmental conditions, but is caused by the hydration of the cement. The reaction product has a smaller volume than sum of the volume of the individual ingredients water and cement. This volume decrease is also called chemical shrinkage or hydration shrinkage.
The autogenous or chemical shrinkage can be fully measurable on the outside of the concrete or can develop internally, which is not visible on the outside. The first occurs when the concrete is still wet and does not have any resistance to the chemical shrinkage. This is fully measurable on the outside. The latter occurs when the concrete has hardened and is still shrinking. The hardened concrete is restraining the chemical shrinkage and the volume reduction is occurring internally in the concrete which creates pores. This part of shrinkage is not measurable. In the full autogenous shrinkage process concrete is both fluid and hardened so there will be a visible volume reduction and a formation of internal pores.
High strength concretes have a low water cement factor which causes a more dense cement matrix with smaller pores. This has the result that more water is used for the chemical process and less water will evaporate due to the restrained diffusion process (AEneas, 2012).

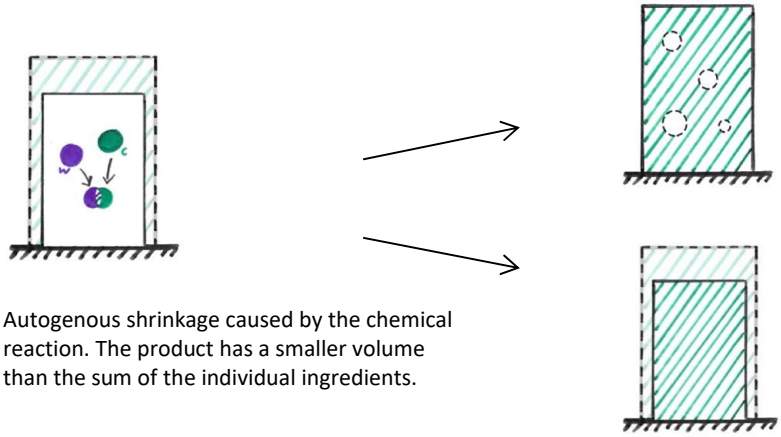

figure 3-10: Autogenous shrinkage and its observational forms.

Drying shrinkage is the result of desorption of water molecules from the concrete to the environment. With a low relative humidity of the environment and a higher water cement ratio in the concrete element, there is a large difference in moisture content between the concrete element and the environment which causes a faster diffusion process with a higher end value.
The drying shrinkage is most present at the perimeter of a concrete element where the diffusion to the environment takes place. This causes that the drying shrinkage is not constant over the cross section of a concrete element, but causes a shrinkage gradient. A smaller volume to surface ratio of the concrete element causes that there is a relatively large perimeter which causes a high rate of diffusion.
The transport of water molecules in the diffusion process takes place through the pores of the concrete. When concrete has a more dense structure, which is the case for higher strength concretes, there is a higher resistance on this transport so the diffusion process will slow down (AEneas, 2012).

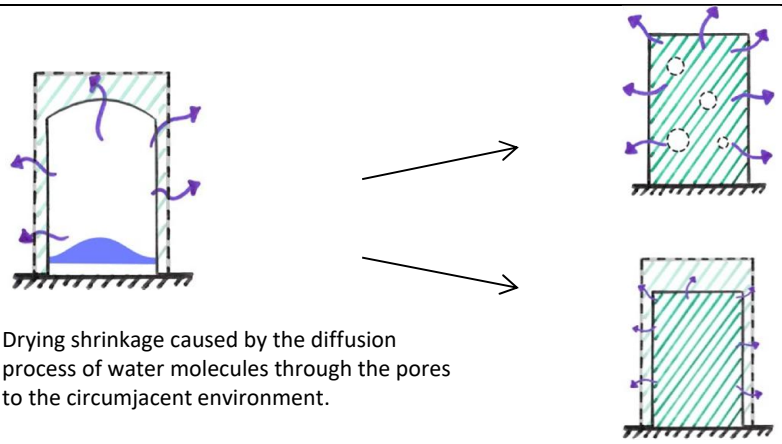

figure 3-11: Drying shrinkage and its relation to autogenous shrinkage.

Both types of shrinkage can be separated when monitoring the mass of the considered specimen. Autogenous shrinkage develops without the loss of mass, while drying shrinkage is associated with the loss of water due to evaporation, so there is a loss of mass (AEneas, 2012). The phenomena of autogenous and drying shrinkage related to the loss of mass are depicted in figure 3-12.

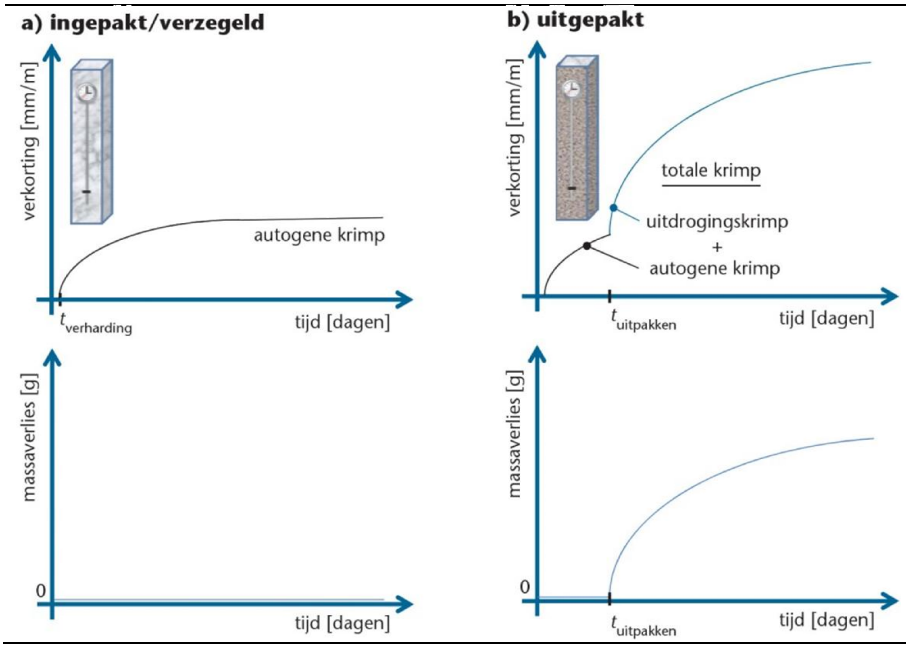

figure 3-12: Autogenous versus drying shrinkage related to the loss of mass (AEneas, 2012).

Since 2011 the distinction of autogenous shrinkage and drying shrinkage is made in Eurocode 2. Drying shrinkage is described as the migration of water through the concrete and autogenous shrinkage develops during the curing process of the concrete (NEN-EN 1992-1-1, 2011). The quantitative formulation of drying and autogenous shrinkage according to EC2 will be further elaborated in chapter 4.1.2 on page 66. The factors that are influencing the total shrinkage behaviour are explicated in table 3.

Time dependencies	Time	t
	Age at end of curing	t_s
Strength	Mean strength	f_{ctm}
Structural element	Notional size	h_0
Environmental conditions	Relative Humidity	RH
	Temperature	T
Concrete mix properties	Cement type	N, R, S

table 3: Variables influencing concrete shrinkage.

3.2.3 Creep strain

“Creep represents the increase of the deformation with time, under a constant applied action” (Andriamitantsoa, 1995). The creep strain in concrete is expressed as a dimensionless factor of the initial elastic strain and is therefore automatically related to the stress level and the initial tangent modulus (Vereniging Nederlandse Cementindustrie, 1990). This is the Young’s modulus at the origin of the stress strain diagram as explained in chapter 3.2.1 on page 41.

$$\varepsilon_{cc} = \varphi(t, t_0) \cdot \frac{\sigma_c(t)}{E_c}$$ With: E_c: The initial tangent modulus

equation 4: Creep strain relation in concrete.

It is very difficult to find an explanation on what exactly happens during the creep process in the concrete material. Several explaining mechanisms can be found in literature which will be explained shortly (Illston, Dinwoodie, & Smith, 1979; Bažant, 2001). Whether the creep process is caused by one of these mechanisms or a combination of them is not of further importance for this research, but acts as background information for a better understanding of creep.

Moisture diffusion Due to capillary stresses chemically unbound water molecules will not evaporate from the concrete specimen to the environment. An induced load on the specimen causes a disturbance in the internal stresses which causes moisture to rearrange internally in the concrete. Unloading reverses the process, which explains the reversible part of creep.
During the movement of moisture some water molecules encounter unbound cement molecules and link together. It seems that the stress stimulates moisture diffusion which then again stimulates further curing with autogenous shrinkage due to an induced load as a consequence. It is also conceivable that when water molecules move due to internal stresses, some of them escape from the concrete specimen, which is analogue to drying shrinkage except that it is induced by a mechanical load (Illston, Dinwoodie, & Smith, 1979; Bažant, 2001).

Structural adjustment Due to the heterogeneous character of concrete, concentrated stresses will develop under an applied load. The concrete will consolidate on places where concentrated stresses occur. Particles will rearrange to empty pores by sliding over one another under the action of shear stresses. The process causes a decrease in volume and rupture and reconnection of primary bonds. Moisture movement and temperature changes influence the molecular pattern. The mechanism explains irreversible creep, but it does not clarify the reversible part (Illston, Dinwoodie, & Smith, 1979; Bažant, 2001).

Delayed elastic strain Delayed elastic strain is caused by redistribution of stresses between the creeping cement and the aggregate. During the creep process of the cement, inert material like aggregate will take over stresses and will deform elastically. The inert material actually reduces the creep strain of the concrete (Illston, Dinwoodie, & Smith, 1979; Bažant, 2001).

Micro cracking For high stresses it is quite possible that micro cracks occur in the cement and between the cement and the aggregate. It causes local losses of strength and small failures in the material. During the drying process the moisture gradient provokes stress levels that causes micro cracking (Illston, Dinwoodie, & Smith, 1979; Bažant, 2001).

There is a distinction in basic creep and drying creep. Basic creep is the creep that occurs in a sealed of loaded concrete specimen that cannot interact with the circumjacent environment. Drying creep is the additional creep deformation that is measured when a loaded concrete specimen is able to interact with the circumjacent environment by diffusion.

Basic creep is caused by internal movement of moisture due to pressure differences within the pores that are provoked by the load. During this internal movement, water molecules encounter cement molecules and bond chemically. This is actually the same phenomenon as autogenous shrinkage, but only occurs with an inducement of a long-term load.
Another factor of basic creep is the internal damage in the material. For high stresses above 50 % of the compressive strength value, the internal damage due to micro cracking plays a more important role in the total creep behaviour (Vereniging Nederlandse Cementindustrie, 1990). The Eurocode gives a threshold at 45% of the compressive strength. Above this threshold creep should be considered as non-linear.

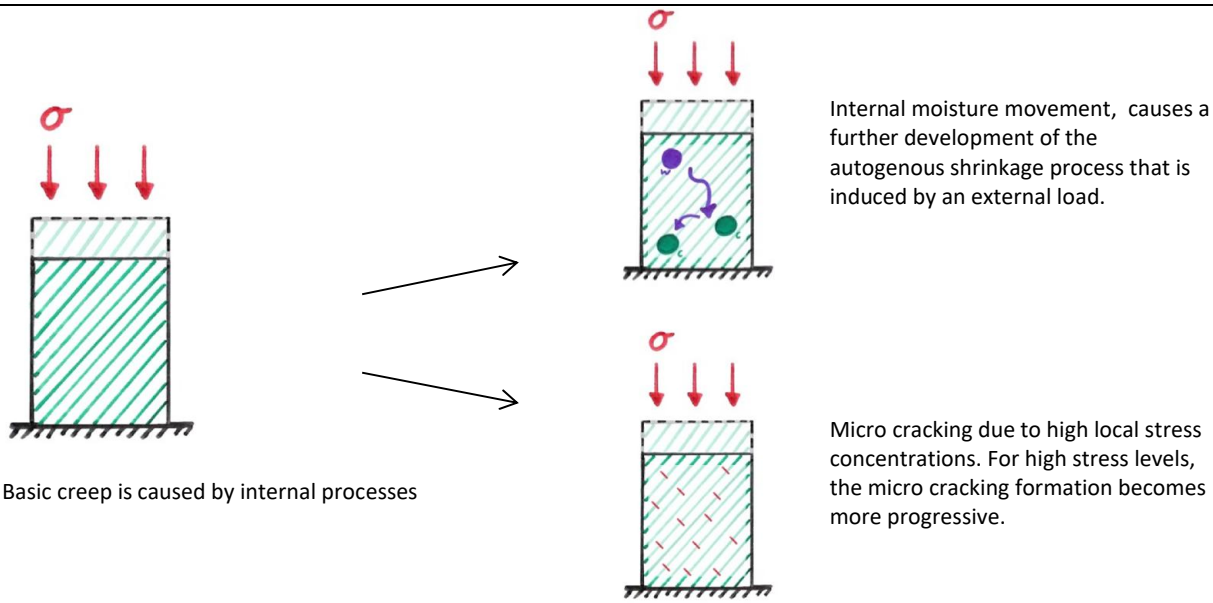

figure 3-13: Basic creep and its observational forms.

Drying creep is caused by movement of moisture to the environment which is induced by an external load. This is same phenomenon as with drying shrinkage, but then induced by an external load. A low relative humidity increases the difference between the moisture content of the concrete specimen and the environment. Together with a long-term stress this causes an over pressure in the concrete pores which accelerates and increases the diffusion process and results in a higher creep value (Vereniging Nederlandse Cementindustrie, 1990).

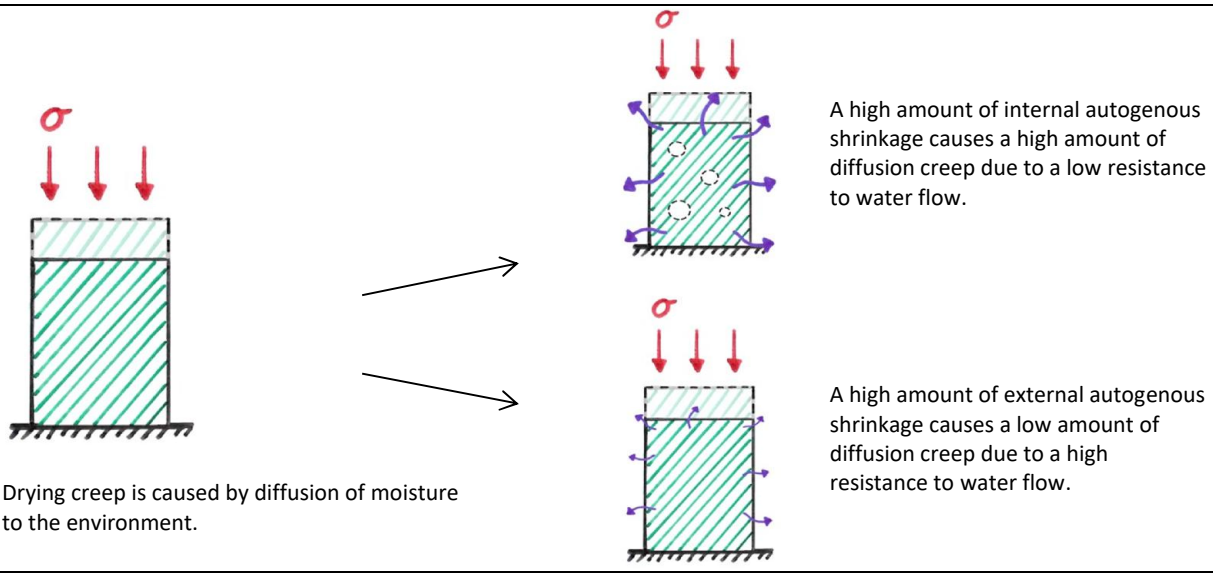

figure 3-14: Drying creep and its relation to autogenous shrinkage.

A higher concrete strength class is associated with a lower water cement factor. This causes less porosity and therefore a low permeability with a slower diffusion process as a consequence. Due to this consequence it can be said that the creep factor decreases with higher concrete classes. The Young's modulus is positively affected by a higher concrete strength and therefore causes a lower creep strain, so a double profit can be achieved on the creep strain when choosing for a higher concrete class.

The time at which a load is applied is significant for the amount of creep that will occur. A creep deformation that is related to a load increment at a later moment in time will be less severe than the creep deformation

that is related to an earlier load increment due to further development in the curing process of the concrete. Still the Boltzmann superposition principle that is explained in chapter 3.1.4 holds if the total stress in the concrete is sufficiently low and the creep behaviour can be considered linear. For concrete the creep compliance function will not be only dependent of time but also of the time moment t_0 at which the load is applied. A substitution of equation 4 on page 45 will result in the following:

$$\varepsilon_{cc}(t) = \sum_{n=0}^{n} J(t-\tau_n, t_0) \cdot \Delta\sigma_n \qquad \text{With:} \quad J(t-\tau_n, t_0) = \frac{\varphi(t,t_0)}{E_c}$$

equation 5: Creep strain in concrete according to Boltzmann superposition principle.

The different influencing factors on the concrete creep behaviour are described by Eurocode 2. A more detailed description of the EC2 creep model will be given in chapter 4.1. Variables that influence the creep behaviour and that are included in the EC2 model are given in table 4.

Time dependencies	Time	t
	Time on which load is applied	t_0
	Duration of loading	$\sigma_c(t)$
Load	Stress level	$\sigma_c(t)$
Strength	Mean strength	f_{ctm}
Structural element	Notional size	h_0
Environmental conditions	Relative Humidity	RH
	Temperature	T
	Curing conditions	
Concrete mix properties	Cement type	N, R, S

table 4: Variables influencing creep

3.3 Influence factors on concrete element level

The short- and long-term deformations of the concrete material are influenced by factors that are related to the way a structural element is designed or executed. The element shape and size, the length in which the deformations are considered and the amount of reinforcement bars affect the elastic, shrinkage and creep strain. This chapter explains these influences.

3.3.1 Shape and size

The element shape and size can be taken together as the notional size. The notional size is twice the ratio between the cross sections surface and its perimeter. For wall or shell elements this results in a notional size that is equal to the thickness of the element when the edges are neglected. The notional size of circular sections will be equal to the radius.

The shrinkage and creep process in a large structural element (big volume and relatively small outer surface) will take longer and will have a smaller end value (Walraven & Braam, 2015). This is because there is relatively less contact with the ambient air and water molecules encounter more resistance in their passage through the element. The notional size is a variable for concrete shrinkage and creep deformations in the material model of the Eurocode and is expressed according to the following formula:

$$h_0 = \frac{2A_c}{u}$$

A_c: The cross section surface in mm^2.
u: The perimeter of the cross section.

Wall or slab

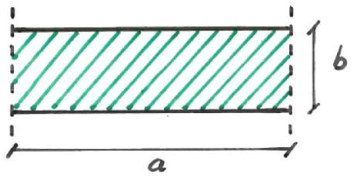

$u = 2 \cdot a$
$A_c = a \cdot b$
$h_0 = \frac{2 \cdot (a \cdot b)}{2 \cdot a} = b$

Circular column

$u = 2 \cdot \pi \cdot r$
$A_c = \pi \cdot r^2$
$h_0 = \frac{2 \cdot (\pi \cdot r^2)}{2 \cdot \pi \cdot r} = r$

Rectangular column

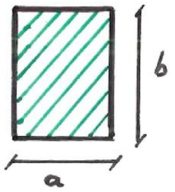

$u = 2 \cdot (a + b)$
$A_c = a \cdot b$
$h_0 = \frac{2 \cdot (a \cdot b)}{2 \cdot (a+b)} = \frac{a \cdot b}{(a+b)}$

figure 3-15: Notional size of basic shapes.

3.3.2 Reinforcement

When a reinforced column or wall element is axially deformed, the reinforcement restrains the deformation that would occur in that same, but unreinforced column or wall element. This means that for every deformation of the concrete, whether it is induced by a load or differentiation in moisture content, there will be an internal force redistribution between the steel reinforcement bars and the concrete. For expansion and contraction by temperature differences this is not the case, because the reinforcement bars are directly and independently of the concrete affected by the temperature change.
The first picture in figure 3-16 is an undeformed reinforced concrete element. The second picture shows an applied deformation on the concrete that is not bonded to the reinforcement so the concrete is not restrained and can deform freely. The third picture shows the situation where there is bonding between the steel and the concrete. The steel pulls up the concrete with a force $-\Delta N_s$ while the concrete pulls down the steel with the same amount of force but reverted ΔN_c to attain equilibrium. This will reduce the strain in the reinforced concrete element with a factor δ_{red}. This factor is dependent of the cross sectional surface ratio and the stiffness ratio of the applied steel and concrete. The reduction factor is elaborated in figure 3-16.

The elastic, load induced deformation is reduced by a factor δ_{red}. The shrinkage deformation is reduced by a factor δ_{red}. And the creep deformation, that is already a factor of the reduced elastic deformation, is reduced by a factor δ_{red}. The reduction factor affects the creep deformation in a reinforced concrete element twice relative to an unreinforced concrete element because creep is a factor of the elastic strain.

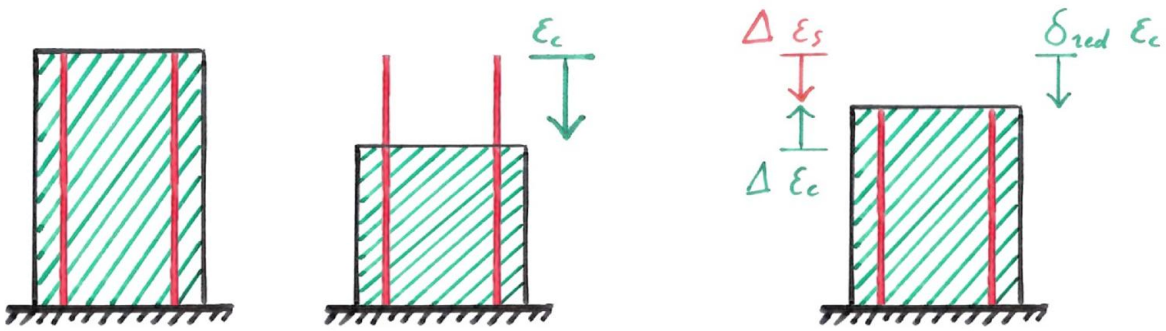

$\Delta N_c = -\Delta N_s$ Because of force equilibrium: $N = N_c(t) + N_s(t)$

$\Delta\varepsilon_c \cdot E_c \cdot A_c = -\Delta\varepsilon_s \cdot E_s \cdot A_s$

$\Delta\varepsilon_c = -\Delta\varepsilon_s \cdot \frac{E_s \cdot A_s}{E_c \cdot A_c}$ With: $\varepsilon_c = \Delta\varepsilon_s - \Delta\varepsilon_c$;

$\Delta\varepsilon_s - \varepsilon_c = -\Delta\varepsilon_s \cdot \rho_e \cdot \alpha_e$ With: $\alpha_e = \frac{A_s}{A_c}$; $\rho_e = \frac{E_s}{E_c}$

$\Delta\varepsilon_s \cdot (1 + \rho_e\alpha_e) = \varepsilon_c$ With: $\Delta\varepsilon_s = \delta_{red} \cdot \varepsilon_c$

$\delta_{red} \cdot \varepsilon_c = \frac{\varepsilon_c}{1+\rho_e\alpha_e}$

$\delta_{red} = \frac{1}{1+\rho_e\alpha_e}$

figure 3-16: Reinforcement reduction factor δ_{red}.

3.4 Deformations in Timber

The elastic, creep, shrinkage and swelling strain in timber are dependent of many factors that are related to either internal factors (material properties and timber quality), as external factors (relative humidity, temperature and loads).
In this chapter the different types of strains in timber and their influencing factors will be explicated qualitatively on material level.

3.4.1 Elastic strain

Linear elastic behaviour is observed in timber for average values of stress and non-linearity occurs for high levels of stress (Van der Put, 1989). As explained for concrete, also the stress strain relation for timber is non-linear. A schematic representation of the stress strain relationship of wood is given in figure 3-17. In tension wood can be considered as a material behaving linear with brittle failure. Wood shows plastic behaviour under high compressive stresses. However, wood can be considered as a linear elastic material when stresses are sufficiently low. A linear stress strain relation is considered to be suitable for wood behaviour until approximately a 40% stress level of the short-term characteristic strength (Toratti, 1992; Holzer, Loferski, & Dillard, 1989). In a linear stress strain relation the stiffness can be represented by a constant Young's modulus or modulus of elasticity which is a stress strain ratio. The modulus of elasticity (MoE) is a mechanical property of timber that varies per wood species, but also from tree to tree and within a tree due to anatomical and environmental factors.

Parallel

$$\varepsilon_{el} = \frac{\sigma_0}{E_{0,mean}}$$

Perpendicular

$$\varepsilon_{el} = \frac{\sigma_{90}}{E_{90,mean}}$$

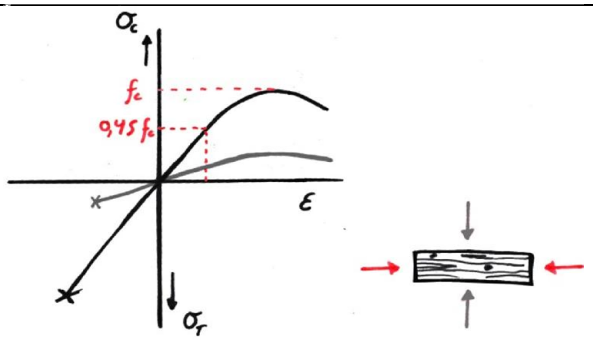

figure 3-17: Schematic stress-strain relationship of wood. Based on (Buchanan, 1990).

Anatomic factors

Because wood is an anisotropic material, the stiffness changes with the orientation relatively to the grain. Three main directions are distinguished in Longitudinal, Tangential and Radial direction. The stiffness in longitudinal direction is in general a factor 20 to 40 of the transverse to the grain stiffness. The high stiffness in the longitudinal direction is due to the dominant S2 layer in the cell wall. This layer consists of microfibrils that are almost axially or longitudinal oriented and are supported by the smaller S1 and S3 layer to prevent buckling when loaded in compression (Hoffmeyer P. , 1995; Ross, 2010).

Grain deviations can occur as a result of a helix grown tree. The cells orientation can grow in a spiral around the pit of the tree stem. Due to these deviations the grain will be loaded in an angle in which the stiffness decreases. Grain deviations for high quality timber are accepted in the order 1 to 10 (Hoffmeyer P. , 1995).

Knots in a timber board are originated from the embedment's of branches in the main stem. The knots cause discontinuities in the wood material and change of fibre direction around the knots which affects the stiffness of a timber element (Ross, 2010).

The density of timber is an important characteristic from which the mechanical properties can be derived. Part of the volume of wood is occupied by pores and cell cavities. The density of the wood is dependent on the proportion of pores and actual wood material. The dry density at 0% moisture content ρ_0 of structural softwood timber is in general in the range of 300 to 550 kg/m^3. The density of the cell wall ρ_c can be considered as constant with a value of around 1500 kg/m^3. So the differences in densities are dependent of the

porosity of the timber material. Higher strength and stiffness can be reached when the proportion of actual wood material increases, thus density increases. Therefore, the timber strength classes are directly related to certain density limits. Moisture content (MC) influences the density of a considered timber specimen. For engineering purposes the dry density is determined at a MC of 12% (Hoffmeyer P. , 1995; Ross, 2010; Ritter, 1990).

Juvenile wood is the inner part of the tree stem, usually the first 5 to 20 growth rings, that develops in the first years of growth. The strength and stiffness properties of juvenile wood are lower than the mature wood due to thin-walled tracheids in which the microfibrils direction is inclined (Ritter, 1990; Hoffmeyer P. , 1995).

Environmental factors

A higher moisture content affects the mechanical properties negatively. Partly it can be explained by the swelling of the cell wall, which causes that less cell wall material is available per unit area. This phenomenon is only a small part that affects the mechanical properties. The weakening of hydrogen bonds that holds the cell wall together is of bigger influence on the mechanical properties. Around 12% MC a differentiation in MC of 1% causes a differentiation in the modulus of elasticity of 1,5% and 3-4% respectively for parallel and perpendicular to the grain direction (Hoffmeyer P. , 1995; Gerhards, 1980).

The modulus of elasticity will decrease with 6% on average when the temperature rises from 20°C to 50°C and will increase with 11% when the temperature decreases from 20°C to -50°C (Gerhards, 1980). Temperatures above 55 °C have a much bigger influence because this value is known as the temperature at which lignin alters its structure and hemicellulose will soften (Morlier & Palka, 1994).

Anatomic factors (Macro level)

Anisotropy

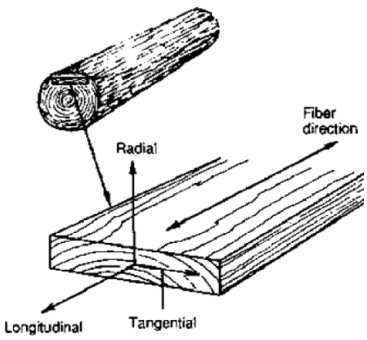

Grain deviations

Knots

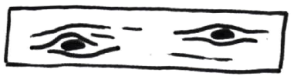

Juvenile & mature wood

Reaction wood

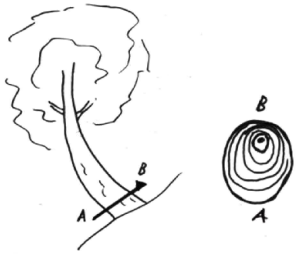

Environmental factors

Relative humidity

Temperature

figure 3-18: Influencing factors on mechanical properties. Top left: (Ritter, 1990).

The mechanical properties of wood show high variation from tree to tree, but also within a tree stem itself due to the anatomical and environmental factors that are depicted in figure 3-18. The variations between sawn timber elements are even greater than for round wood that is made of a full tree stem, because imperfections have much more impact on a smaller element and fibres can be interrupted in the cutting process (Glos, 1995).

For engineering purposes the characteristic strength values are used that are determined from the 5^{th} percentile value of a population. It is desirable that the total population of sawn timber is graded, so sawn timber pieces can be categorized in groups. Each group has its sorting criteria and mechanical design values assigned to it that are determined from testing samples representing a particular group that is called strength class. This strength class system ensures that high quality and low quality timber are sorted out in strength classes, so the total produced timber population can be utilized in an economical manner with a high reliability for engineering purposes (Glos, 1995; Ritter, 1990).

Within a certain strength class, the modulus of elasticity can still deviate from the mean value that is specified for this strength class because wood has a natural variability . Chapter 4.2.1 gives more information about the quantified values of the Young's modulus and how is dealt with deviations.

3.4.2 Creep strain

"Creep represents the increase of the deformation with time, under a constant applied action" (Andriamitantsoa, 1995). Just as in concrete, the creep strain in timber is expressed as a dimensionless factor of the initial elastic strain and is therefore automatically related to the stress level and the Young's modulus of the material as shown in equation 6. This creep factor develops over time and can therefore be expressed as a time dependent factor.

$$\varepsilon_{cc} = \varphi(t) \cdot \frac{\sigma(t)}{E_{mean}}$$

With: E_{mean}: The mean modulus of elasticity

equation 6: Creep strain relation in timber.

The creep behaviour in parallel to the grain loaded timber can be explained by the slip plane formation mechanism that is explained in several papers (Hoffmeyer P. , 1993; Hoffmeyer & Davidson, 1989).

Slip plane formation

A slip plane is a zone in which the axially orientated microfibrils in the S2 layer of the cell wall re-orientate due to buckling that is caused by an induced load. The formation of slip planes is considered as progressive failure of the material which starts when stresses exceed 50% of the short-term compressive strength. This is the amount of stress from which the stress strain relation starts to be non-linear.
The development of slip planes is linear related to the creep strain. When wood is subjected to moisture content variations the development of slip planes tend to increase. On the one hand this is caused by the weakening of the junction between the microfibrils due to the breaking of hydrogen bonds. This causes that slip planes can develop at lower stresses. On the other hand the moisture content variations cause shrinkage and swelling which can induce internal stresses so local stress concentrations appear that exceed the 50% threshold (Hoffmeyer P. , 1993).

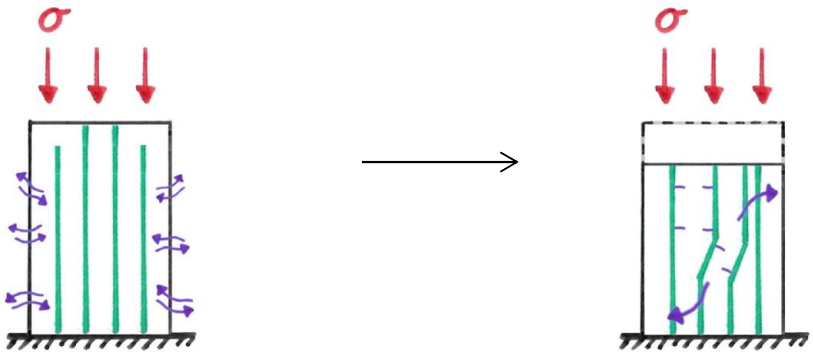

figure 3-19: Slip plane formation in pure creep.

In literature about creep behaviour in timber a distinction is made between pure creep and mechano-sorptive creep. These two forms of creep are observationally distinguished.

Pure creep is the strain that is observed with a decreasing rate during a longer period of time after the initial strain by loading under constant environmental conditions (Toratti, 1992). This means that pure creep is the creep that is observed when the moisture content in the wood stays constant. Generally it has been concluded that pure creep increases when the level of constant moisture content increases, but the study of Toratti does not acknowledge this relation, because previous studies are contradictory.
The constant moisture content in the wood does not mean that there is no flow of water molecules in the wood or to or from the circumjacent environment. It does mean that there is equilibrium between inward and outward flow. However, there will not occur any shrinkage or swelling because the moisture content stays constant so the pure creep form is little to not induced by internal stress concentrations, the internal and equilibrium flow can still affect and weaken the hydrogen bonds and cause slip plane formation.

Mechano-sorptive creep strain is the additional strain that is observed when a loaded specimen is subjected to variations in atmospheric humidity, so the specimen undergoes variations in its moisture content. This means that there is a high rate of flow of water molecules in the wood, but the wood is also subjected to shrinkage and swelling due to a non-constant moisture content gradient over the cross section. The slip planes will appear on the one hand by weakening of the material by breaking of hydrogen bonds and on the other hand by high local stress concentrations that are induced by shrinkage and swelling.

During moisture content cycling the creep strain decreases during absorption and increases during desorption. The slip plane formation theory explains this behaviour by shrinking and swelling of the already buckled microfibrils. Due to shrinkage of the microfibrils in a desorption stage, the slip planes have room to incline their slip plane angle, which causes more deformation. In a absorption stage the microfibrils swell and cause a declination of the angle which causes a deformation recovery. This mechanism is depicted in figure 3-20 and explains the fluctuating creep behaviour when exposed to fluctuating moisture content.

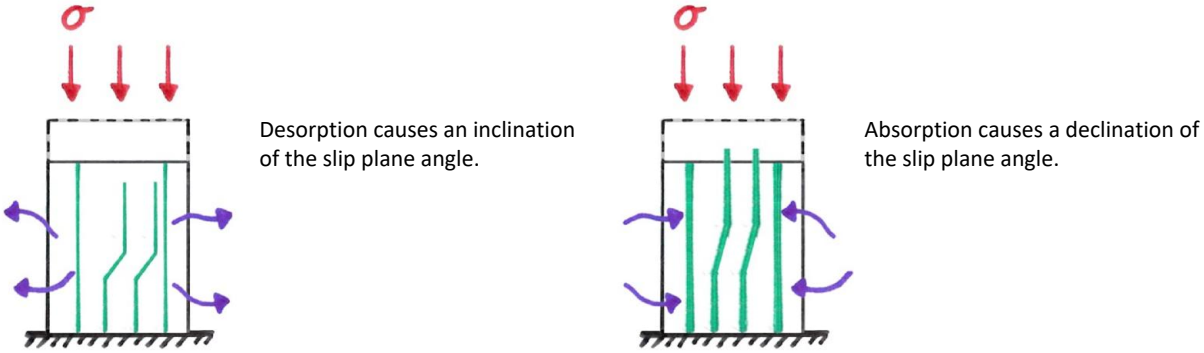

figure 3-20: Effect of desorption and absorption on deformations in slip planes.

The moment on which a load is applied with respect to time does not have influence, like in concrete, on the amplitude of the creep compliance. This is because there is no curing process involved like in concrete. The moment in which the load is applied with respect to the moisture content is of great influence. Timber that is loaded in wet condition and dries under this constant sustained load is highly susceptible to creep. (Andriamitantsoa, 1995).

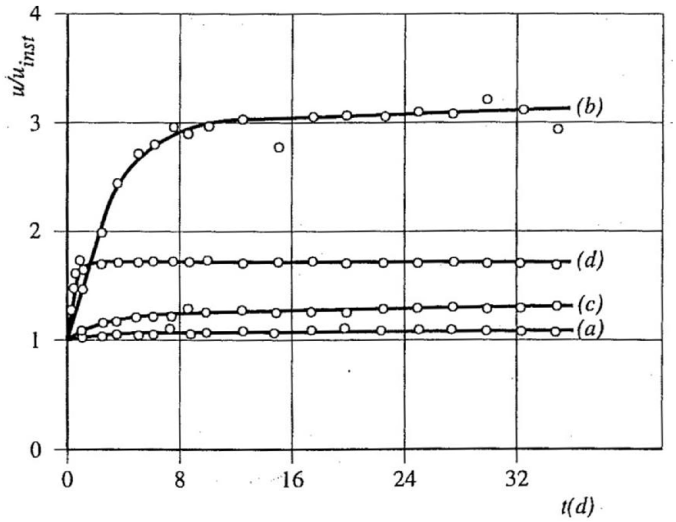

a) Green timber kept green.
b) Green timber drying to 12% moisture content.
c) Timber kept at 12% moisture content.
d) Timber initially at 12% moisture content allowed to absorb moisture.

Wood: Alpine ash.
Load: 24% of average short term strength.
T = 25 °C

figure 3-21: Relative deformation-time curves for beams at different moisture conditions (Andriamitantsoa, 1995).

Other parameters that have influence on the slip plane formation are temperature and the amount of stress. Above 55 °C hemicellulose softens and lignin alters its structure. Temperature variations under 50°C have a negligible effect (Andriamitantsoa, 1995). However the relation between creep and temperature is a very complex behaviour, it can be assumed that temperatures corresponding to an indoor climate barely have an influence on the creep development. A high long-term stress level relative to the short-term strength of the timber element can cause progressive damage due to excessive formation of slip planes. This can lead to an unstable creep curve as shown in figure 3-22.

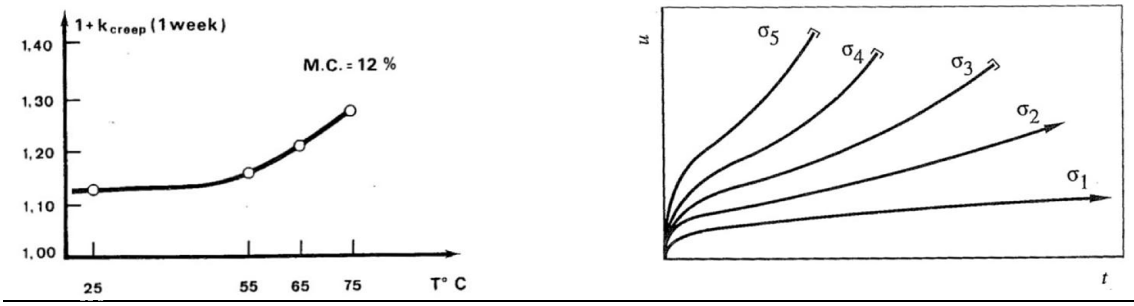

figure 3-22: Left: Creep versus temperature for spruce in bending at constant MC (Morlier & Palka, 1994). Right: Stability of creep curve at different stress levels. $\sigma_1 < \sigma_2 < \sigma_3 < \sigma_4 < \sigma_5$. (Andriamitantsoa, 1995).

It can be concluded that creep is caused by material failure on micro level due to the formation of slip planes which can be described as buckling of the microfibrils. Buckling of the microfibrils can be caused by excessive stress or weakening of the material. The material weakens due to hydrogen bond breaking. This causes that the microfibrils can lose stability, buckle and form a slip plane. Pure creep occurs when the moisture content is stable so there is only little moisture flow. Mechano-sorptive creep occurs when the moisture content is fluctuating which causes a higher moisture flow, thus more bond breaking and weakening of the material. During these moisture cycles higher local internal stresses can occur due to shrinkage and swelling of the material which can cause slip plane formation. The variables that are of considerable influence are summarized in table 5. Chapter 4.2.2 explains how the creep strain will be quantified.

Time	Time Duration of load	t $\sigma_c(t)$
Load	Stress level	$\sigma_c(t)$
Moisture content	MC	ω

	Change of MC	$\Delta\omega$
Structural element	Notional size	h_0
Environmental conditions	Relative Humidity	RH

table 5: Variables influencing wood creep.

3.4.3 Shrinkage/swelling strain

In absence of external stresses, timber can undergo dimensional changes due to the adsorption or desorption of moisture from or to the environment. Due to the hygroscopic character of wood a timber element will adsorb or desorb water vapour in such a way that equilibrium is reached with the relative humidity of the environment so that inward or outward diffusion of moisture are equal. When exposed to a high relative humidity the adsorption of water vapour by the cell walls continues until the fibre saturation point is reached. This point corresponds to a moisture content of about 27-30% for most softwoods. Below this point the change of moisture content is accompanied with change in mechanical properties and also with change in volume. Above this point the cell walls are saturated and the moisture content change will take place in the cell cavities which does not affect the mechanical properties nor the volume.

The relation between the relative humidity and the moisture content is slightly different for adsorbing and desorbing water vapour. Both show an S-shaped isotherm, but with an offset relative to one another. This means that there is a delay of the desorbing process after adsorbing and vice versa. The equilibrium has to be disturbed with a certain threshold value before desorption will start after an adsorption process. This is the hysteretic character of the shrinkage and swelling behaviour as depicted in figure 3-23. This is beneficial for engineering purposes, because small relative humidity fluctuations will not affect the moisture content (Hoffmeyer P. , 1995).

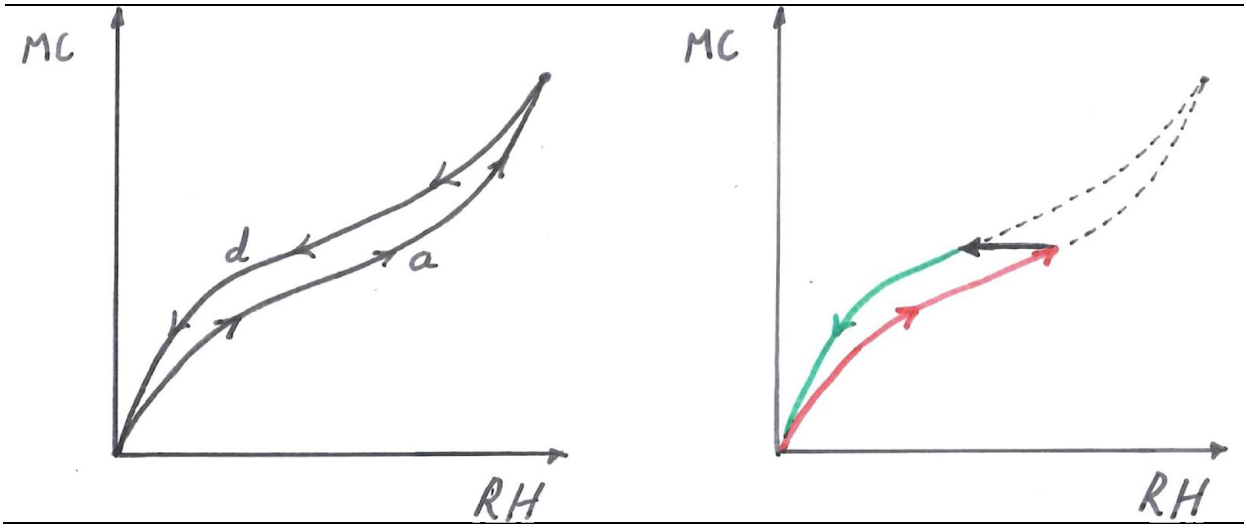

figure 3-23: Hysteretic behaviour.

Direction relative to grain	Parallel Perpendicular	β_0 β_{90}
Moisture content	Change of MC	$\Delta\omega$
Structural element	Notional size	h_0
Environmental conditions	Relative Humidity	RH

table 6: Variables influencing wood shrinkage/swelling.

3.5 Influence factors on timber element level

The short- and long-term deformations of the timber material are influenced by factors that are related to the way a structural element is designed or executed. The element shape and size and the way a timber structural element is engineered affect the elastic, shrinkage and creep strain.

3.5.1 Shape and size

A bigger size of the structural element causes a bigger volume to surface ratio which slows down the diffusion process of water vapour with the ambient air. The slower diffusion process weakens the fluctuations of moisture content, caused by fluctuations of the relative humidity of the ambient air, which is evident in figure 3-24. The smaller differentiation of moisture content due to a bigger element size will have a direct influence on the shrinkage and swelling behaviour. Also the mechano-sorptive part of creep is influenced by fluctuations in moisture content. It can be expected that the mechano-sorptive creep behaviour for bigger element sizes or elements that are conducted with a surface coating is less present.

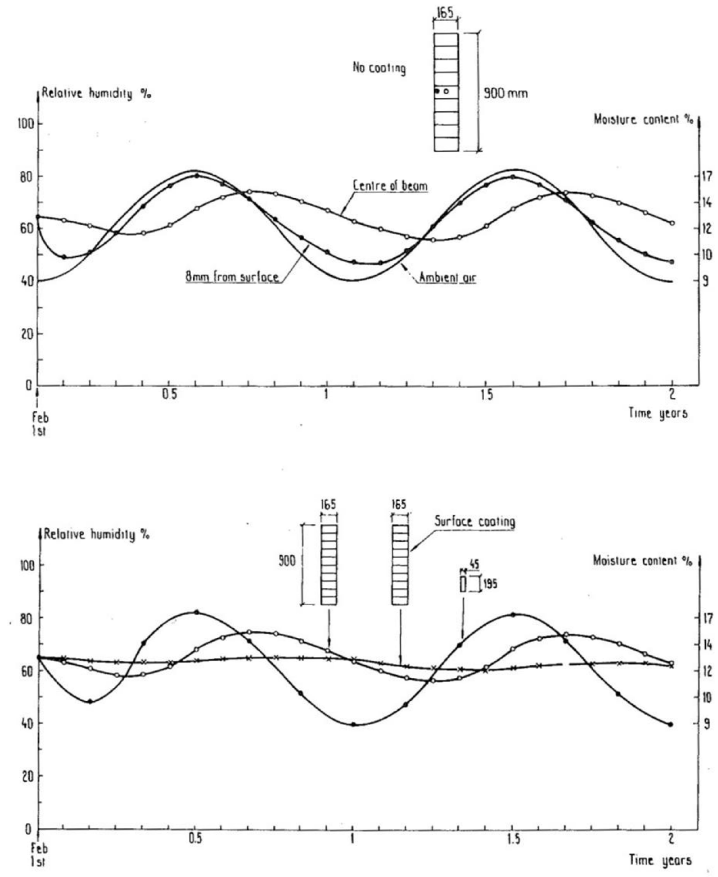

figure 3-24: Variation of MC in a section of a glulam beam section exposed to climate typical for southern Scandinavia (Thelandersson, 1994).

3.5.2 Engineered timber

Wood can be turned in to a timber product in several ways. Common engineered timber products are sawn timber, glue laminated timber, cross laminated timber, laminated veneer lumber and particle/fibre boards. Reasons for engineering wood in a certain timber product are to attain flexibility in shape and size, homogenize the structural properties, attain isotropic behaviour in two plane directions or optimization of a structural element by composing it out of smaller pieces with the most suitable wood properties. Some examples of linear load bearing products are Parallel Strand Lumber (PSL) or Glue Laminated Timber (GLT). Two-dimensional load bearing products are Oriented Strand Board (OSB), Laminated Veneer Lumber (LVL) or Cross

Laminated Timber (CLT) (Brandner, 2013). This chapter explains the commonly used timber products and the advantage of engineering wood in these timber products.

Parallel Strand Lumber (PSL) 	Was launched as a commercial proprietary product in 1986 under the trade name Parallam® PSL. Parallel strand lumber is composed of long veneer strands that are bonded by an adhesive under heat and pressure. This technique minimizes grain deviations and distributes knots uniformly.
Glue Laminated Timber (GLT) 	Glue laminated timber elements are made of timber lamellas with a thickness that is generally around 20mm. The crosscut sides of the lamellas are connected by finger or scarf joints. The lamellas are glued and stacked on top of each other to form large structural members. Glue laminated timber has a high degree of shape, size and composition freedom. During the drying process the lamellas can be clamped in a curved shape to form curved beams. Laminating smaller pieces of sawn timber, that are limited in size, makes it possible to produce members in any size needed. This technique gives the possibility to combine low and high strength grade lamellas and use them in low and high stress zones respectively to maximise the strength to cost ratio. Knots are not distributed as uniformly as PSL does, but are broken down to smaller imperfections that are scattered over a the element. This results in a more homogenized element.
Laminated Veneer Lumber (LVL) 	Laminated veneer Lumber is made according to the same principle as GLT, but it is made from wood veneer sheets that are peeled of a log, instead of sawn timber lamellas. The LVL product can be produced with the grain angle of all veneer sheets oriented in the same direction or a cross wise lay-up. The first gives the member high uniaxial strength which is suitable for columns or beams. The latter gives the member a high two dimensional in plane strength and stiffness, which is suitable for shear wall or floor elements. The cross wise lay-up also restrains the shrinkage behaviour in both in plane directions.
Cross Laminated Timber (CLT) 	CLT products are made, comparable to GLT, of timber boards that are finger jointed and glued on top of each other. Where GLT is composed unidirectional, CLT is primarily made in a cross wise lay-up. This makes it suitable to use as a shear wall or a floor slab element. This cross wise lay-up will restrain shrinkage behaviour in both in-plane directions.

table 7: Description of several engineered timber products. Pictures are attained from (StructureCraft).

When a homogenous glue laminated timber element is manufactured with strength class GL28h according to the European standard, it should be composed out of sawn timber laminations of strength class T18 (NEN-EN 14080, 2013). When plotting the normal distribution of the stiffness of both strength classes that is retrieved from $E_{0,mean}$ and $E_{0,05}$, it can be seen in figure 3-25 that the mean value increases a small amount. What is more relevant is that the plot is narrowed around the mean value, which indicates a smaller variability in the

considered strength class. The smaller variability is caused by the homogenisation of the physical material properties. The small increase of the mean value can be attributed to the load sharing effect.

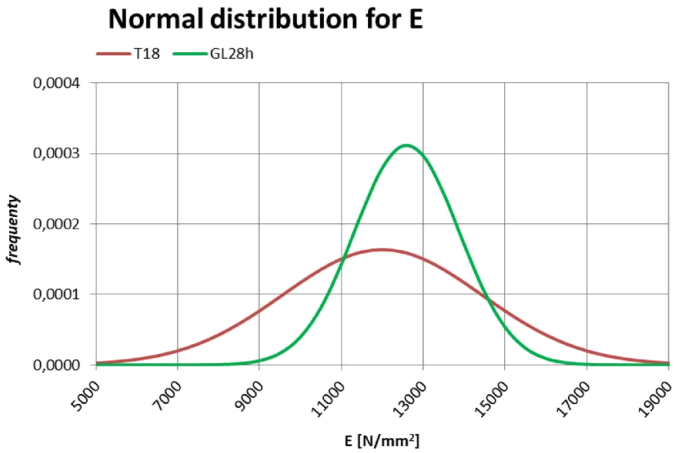

T18

$E_{0,mean}$	$= 12000$	N/mm^2
$E_{0,05}$	$= 8000$	N/mm^2
σ	$= 2432$	N/mm^2

GL28h

$E_{0,mean}$	$= 12600$	N/mm^2
$E_{0,05}$	$= 10500$	N/mm^2
σ	$= 1277$	N/mm^2

figure 3-25: Normal distribution of stiffness from glue laminated member and individual laminations.

Both linear as two-dimensional engineered timber products are subjected to a homogenisation of the physical material properties relative to sawn timber products and experiences a load sharing effect. This homogenisation causes a smaller variability in mechanical properties which can be explained by the dispersion or elimination of material defects. The load sharing effect of the laminations causes that a higher strength can be attained in an engineered timber element. Where a single lamination would fail, the adjacent laminations take over the load when they are combined. Although the mean strength values are only slightly increased in engineered timber products, the 5th percentile characteristic strength values will increase much more by the smaller variability of homogenized timber products (Lam & Prion, 2003; Colling, 1995).

The characteristic strength, that is used by engineers for ultimate limit state calculations, is defined as the 5th percentile strength. This means that it is expected that not more than 5% of all specimens will fail if this value is kept as the ultimate limit. Making a more reliable timber building product by engineering it in for instance GLT, means that the 5th percentile value will get closer to the average or mean value. This gives the possibility to use higher characteristic values with the same level of confidence, which results in a more economical material use that is exploited more efficiently.

3.6 Evaluation

This chapter has evaluated the influencing factors on material and element level for the elastic, shrinkage and creep strains in a qualitative manner. All three strain types are evaluated. Points of attention are formulated for the quantitative determination of the strain models that will be elaborated in chapter 0.

3.6.1 Elastic strain

Both wood and concrete have a non-linear stress strain relation only for compressive stresses. However, for both materials the stress strain relation for stresses up to around 40% to 45% of the short-term strength can be considered linear. To determine how to deal with the initial elastic response mechanism, it is important that the maximum occurring characteristic stress relative to the characteristic strength of both materials is assessed.

In timber the elastic strain is mostly dependent on anatomical factors. The material defects cause that there is a high variation in the elastic properties. The timber strength class system ensures that this variance is controlled through visual strength grading or machine strength grading. The variance within a used strength class is useful to know for reliability purposes.

Concrete is manufactured at different qualities and strengths. It is of importance that also for the estimation of concrete elastic deformations, the stiffness of the different strength classes is known.

3.6.2 Creep strain

The creep behaviour for both concrete and wood tends to be unstable for higher stresses. For both materials the relation between the creep factor and the initial strain is linear up to long-term stresses around 40% to 45% of the short-term characteristic compressive strength. As earlier mentioned, below this threshold both materials can be considered as linear viscoelastic.

Concrete creep is influenced by the curing process. This means that a low relative humidity causes a high concrete creep value. The creep factor is higher for loads applied earlier after pouring, because of the curing process. This means that the time of loading is an important factor. The Boltzmann superposition principle is still valid, but the time of loading t_0 is an additional variable for the creep compliance $J(t, t_0)$.

The amplitude of the creep factor for wood is not dependent of the time of loading because there is no curing process involved. The creep factor for wood is mostly influenced by fluctuations of the relative humidity, due to breaking and remaking of hydrogen bonds.

3.6.3 Shrinkage strain

Concrete shrinkage is caused by the curing process of the concrete due to hydration (autogenous) and evaporation (drying). This shrinkage property ensures that the shrinkage deformation in concrete is an irreversible deformation. Because concrete is an isotropic material it shows the same shrinkage behaviour in all directions. However, reinforcing the concrete will affect the shrinkage strain because of internal stress redistribution of a structural element between the steel and the concrete. It is of importance to know the amount of shrinkage of a structural element that is caused by the concrete material.

Due to the hygroscopic property of wood, the shrinkage and swelling fluctuation will go along with the relative humidity fluctuation of the environment. This means that the shrinkage/swelling deformation is reversible. For the engineer it is important to know that the moisture content in the timber structural elements can be higher at the moment of construction due to outside environmental conditions and that the moisture content will decrease in inside heated conditions. Next to the shrinkage coefficient in the three main directions relative to the grain it is also important to know what the maximum moisture content might be at the time of construction and the minimum moisture content during the service life of the building.

4 Quantification of the material strains

The goal of this chapter is to formulate the material models that will be used to quantify the actual deformations that can cause differential vertical shortening. The models will be elaborated for better understanding and to verify their performance. The material models will be implemented in ETABS, which is a structural software package for building analysis that is developed by CSI America. This software package will be used to model differential vertical shortening.

For the prediction of concrete strains, the CEB-fib 2010 model is used. This will be the reference document for the revised Eurocode 2 that is planned to be published in 2020 (Walraven & Bigaj-van Vliet, 2016). This model is already implemented in ETABS and will be elaborated in 4.1.

For the prediction of timber strains, there is no preprogramed model available in ETABS. There is the possibility to create a manual material model for timber in ETABS. How the timber elastic, shrinkage and creep strains are modelled is explained in chapter 4.2.

4.1 Quantification of concrete strains

The CEB-fip 2010 model will be adopted in this research to model the concrete strains. The older CEB-fip 1990 model has developed into the most important reference document of the current Eurocode EN 1992-1-1. The CEB-fip 2010 model will be the reference document of the revised EN 1992-1-1 that will be published in 2020 (Walraven & Bigaj-van Vliet, 2016). The model represents all the influencing factors quantitatively on the elastic, shrinkage and creep strains of concrete that are explained qualitatively in chapter 3.2 and 3.3.
This chapter will elaborate the CEB-fip 2010 material model for each strain type and how it is dealt with in this research. The total strain $\varepsilon_c(t)$ at time t, of a concrete member uniaxial loaded at time t_0 with a constant stress $\sigma_c(t_0)$ may be expressed as the superposition of the individual elastic, shrinkage, creep and thermal strain.

$$\varepsilon_c(t) = \varepsilon_{c,el}(t) + \varepsilon_{c,c}(t) + \varepsilon_{c,s}(t) + \varepsilon_{c,T}(t)$$

$\varepsilon_{c,el}(t)$: The initial elastic strain at the application of a load.
$\varepsilon_{c,s}(t)$: The shrinkage strain at time t.
$\varepsilon_{c,c}(t)$: The creep strain at time t.
$\varepsilon_{c,T}(t)$: The thermal strain at time t. This type of strain is not considered in this research.

equation 7: The total strain of a uniaxial loaded concrete member.

It is assumed that the serviceability stress range in the concrete material will never exceed 45% of the characteristic compressive strength f_{ck} or 40% of the mean compressive strength f_{cm}. The serviceability stress range for concrete is elaborated in appendix E. Because this research is focussed on an indoor loadbearing structure of a high-rise it is assumed that temperatures in the structure will stay constant and therefore the thermal strain will not be considered.

4.1.1 Elasticity

The analysis of elastic deformations in uniaxial loaded concrete members can be approximated by a linear formulation with the use of the secant modulus. This approximation is an idealised linear relation that corresponds with a compressive stress that is equal to 40% of the mean compressive strength. In reality, the full stress strain relation of concrete is non-linear as is depicted in figure 4-1. Because it is assumed that the serviceability stress range will never exceed $0{,}4f_{cm}$, the initial elastic deformations are determined according to the linear relation of figure 4-1 with use of the secant modulus.

The Eurocode 2 and the CEB-fip 2010 model have a slightly different approach in the formulation of the concrete stiffness. The CEB-fip model gives lower values for both the tangent modulus E_c and the secant modulus E_{cm} (NEN-EN 1992-1-1, 2011; CEB-fib, 2012). In figure 4-1 a comparison is made between both models. The CEB-fip model is used for the calculation of the elastic deformations.

	EC2	**CEB-fib 2010**
Tangent modulus E_c	$= 1{,}05 \cdot E_{cm}$	$= 21{,}5 \cdot 10^3 \cdot \left(\frac{f_{cm}}{10}\right)^{\frac{1}{3}}$
Secant modulus E_{cm}	$= 22 \cdot 10^3 \cdot \left(\frac{f_{cm}}{10}\right)^{0{,}3}$	$= \alpha_i \cdot E_c$ With: $\alpha_i = 0{,}8 + 0{,}2 \cdot \frac{f_{cm}}{88} \leq 1{,}0$

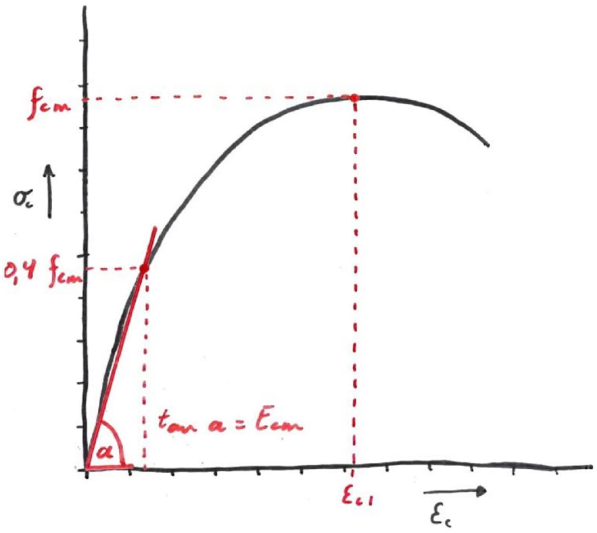

$$\varepsilon_{c,el} = \frac{\sigma}{E_{cm}}$$

	C20/25	**C30/37**	**C40/50**	**C50/60**
E_{cm} *(EC2)*	$30 \cdot 10^3$	$32{,}8 \cdot 10^3$	$35{,}2 \cdot 10^3$	$37{,}3 \cdot 10^3$
E_{cm} *(CEB-fib 2010)*	$26{,}2 \cdot 10^3$	$29{,}7 \cdot 10^3$	$33 \cdot 10^3$	$36 \cdot 10^3$

figure 4-1: Comparison of the EC2 and CEB-fib 2010 model for the determination of the secant modulus.

The development of the concrete stiffness is expressed as the secant modulus $E_{cm}(t)$ dependent of time. The stiffness is assumed to be a 100% developed relative to the value E_{cm} at an age of 28 days after pouring. After 28 days the stiffness will keep on developing as can be seen in figure 4-2.

Cement can be produced as normal (N) or rapid (R) curing product that is indicated in the cement name. The various cement types that can be produced are subdivided in a rapid (R), normal (N) and slow (S) cement class. One should be aware of how these letters are used. It can be confusing, because a cement with normal strength development N can be posted under cement class R or vice versa in the Eurocode as can be seen in the formulation of '*s*' in figure 4-2.

As can be seen in the right graph of figure 4-2, the actual stiffness develops quite fast and within a week the slowest curing cement class already has reached 70% of the stiffness at 28 days. Because cast in place concrete will be loaded after the scaffolding and formwork is removed, which is assumed to be a week, and prefabricated concrete already has sufficient age, the stiffness will be sufficiently developed. In the case that a load is applied on a vertical loadbearing element that has not yet its full developed stiffness, this load would be only a fraction of the total load for which the element is designed because of the relatively slowly increasing load due to the building sequence. For these reasons it is assumed that the influence of the stiffness development on deformations of vertical load bearing elements will be negligibly small. For the reason the stiffness development is not considered in the quantification of vertical shortening deformations.

$$E_{cm}(t) = \left(\beta_{cc}(t)\right)^{0,5} \cdot E_{cm}$$

E_{cm}: Concrete stiffness at 28days after pouring that corresponds to stresses of 0,4f_{cm}.

$$\beta_{cc}(t) = \frac{f_{cm}(t)}{f_{cm}} = e^{s\cdot\left(1-\left(\frac{28}{t}\right)^{0,5}\right)}$$

Coefficient that is dependent of the concrete age in days. With:

$$s = \begin{cases} 0,2 & Cement\ class\ R\text{:}\ \ CEM\ 42.5\ R; CEM\ 52.5\ N\ en\ CEM\ 52.5\ R \\ 0,25 & Cement\ class\ N\text{:}\ \ CEM\ 32.5\ R; CEM\ 42.5\ N \\ 0,38 & Cement\ class\ S\text{:}\ \ CEM\ 32.5\ N \end{cases}$$

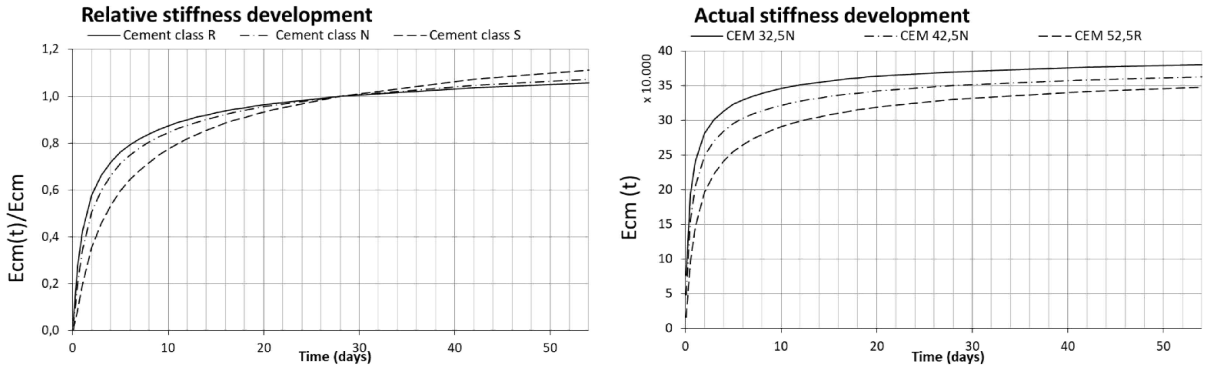

figure 4-2: Concrete relative stiffness development (left), concrete actual stiffness development (right) according to CEB-fip 2010.

It is likely that the in-situ concrete strength and stiffness deviate from the intended concrete strength and stiffness from the chosen concrete strength class during the design process of a structure. The concrete strength class system provides a mean compressive strength value f_{cm}, which is the average compressive strength in this concrete strength class. In the ultimate limit state, the engineer is required to use the characteristic strength value f_{ck}, which is the 5th percentile value. "This value may be derived from strength tests by the criterion that 5% of all possible strength measurements for the specified concrete is expected to fall below the value of f_{ck}" (CEB-fib, 2012). This mean and 5th percentile value can be used to elaborate a normal distribution for the strength of a certain concrete strength class as shown in the left graph of figure 4-3. Because strength and stiffness are related to one another by equation 2 of chapter 3.2.1, a normal distribution for the stiffness can be elaborated analogue to the normal distribution for the strength. This gives the possibility to determine a certain bandwidth for the stiffness of the concrete of a particular strength class with a certain probability. Because of the linear stress strain relation of figure 4-1 this bandwidth is directly applicable on the elastic deformations. The lower limit will be derived from the 5th percentile strength value. The upper limit will be the 95th percentile value, which is the mirrored value of the 5th percentile value around the mean/average value. These limits provide a 90% confidence area.

$$E_{cm} = 22 \cdot 10^3 \cdot \left(\frac{f_{cm}}{10}\right)^{0,3}$$

$$E_{ck} = 22 \cdot 10^3 \cdot \left(\frac{f_{ck}}{10}\right)^{0,3}$$

	f_{cm}	f_{ck}	E_{cm}	E_{ck}	σ_{90} (Deviation 90% area)
C20/25	28	20	30000	27100	±9,6%
C30/37	38	30	32800	30600	±6,8%
C35/45	43	35	34100	32000	±6%
C45/55	53	45	36300	34500	±4,8%

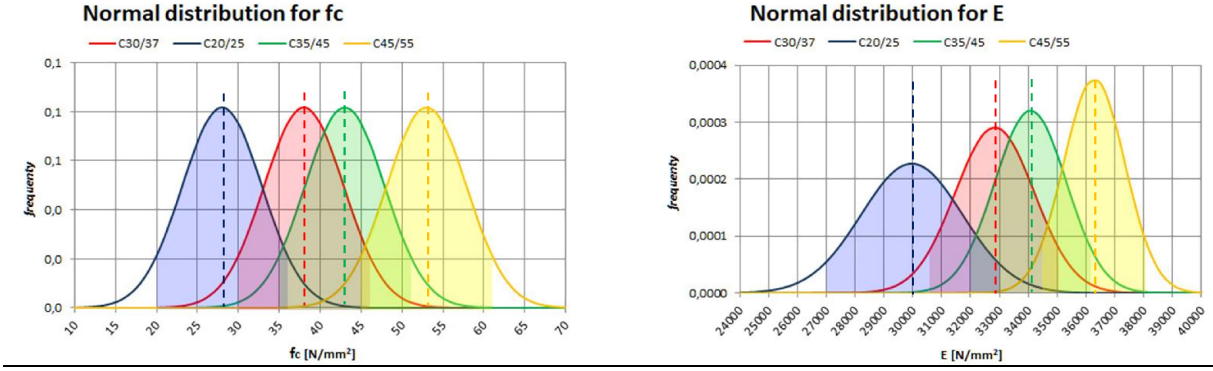

figure 4-3: Normal distribution concrete for strength and stiffness of concrete strength classes.

As a summary of the discussion about the quantification of elastic deformations in concrete, the following statements can be made when modelling the elastic strain in concrete:

Elastic displacements will be modelled linear by use of the secant modulus.	$\varepsilon_{c,el}(t) = \frac{\sigma(t)}{E_{cm}}$	
The course of stiffness development is not considered in the model, because effects would be negligibly small.	$E_{cm}(t) = E_{cm}$	
For the possible stiffness deviation, thus elastic deformation deviation, the 90% confidence area of the stiffness normal distribution according to figure 4-3 is considered.	$E_{cm,min} = 0{,}90 \cdot E_{cm}$ $E_{cm,max} = 1{,}10 \cdot E_{cm}$	(Depending on strength class).

table 8: Assumptions for modelling elastic strain in concrete.

4.1.2 Shrinkage

As explained in chapter 3.2.2, the shrinkage strain consists of autogenous shrinkage that develops due to the hydration process of water and cement, and drying shrinkage that develops due to the diffusion process of moisture to the environment. Since 2011 a distinction between autogenous and drying shrinkage is made in EC2 (NEN-EN 1992-1-1, 2011). The CEB-fip Model Code 2010 formulates the total shrinkage strain with the same distinction (CEB-fib, 2012). The total shrinkage strain for both models is described according to equation 8.

$$\varepsilon_{cs}(t) = \varepsilon_{cds}(t) + \varepsilon_{cas}(t)$$

$\varepsilon_{cd}(t)$: Concrete drying shrinkage strain.
$\varepsilon_{ca}(t)$: Concrete autogenous shrinkage strain.

equation 8: Total shrinkage strain according to EN 1992-1-1 and CEB-fib 2010.

The CEB-fip Model Code 2010 predicts greater shrinkage values when compared to the EC2 model. The model can be applied in a relative humidity of 40 to 100% with a temperature between 5°C and 30°C. The conditions for an indoor timber structure of a consequence class 3 high-rise meet these requirements, so the CEB-fip model 2010 is assumed to be very suitable for this research.

In complementation to the EC2 model, the CEB-fip 2010 model also provides a mean coefficient of variation for the predicted shrinkage function $\varepsilon_{cs}(t, t_s)$ that has been estimated on the basis of a computerized data bank (CEB-fib, 2012). When a normal distribution is assumed, a 5th and 95th percentile value can be found, which can provide a 90% confidence area for predicted shrinkage strain. The values and normal distribution for the shrinkage strain are depicted in figure 4-4. According to these values the shrinkage strain can deviate $\pm 58\%$ for a 90% confidence area.

$$\varepsilon_{cs,mean} = 1{,}0 \cdot \varepsilon_{cs}(t, t_s)$$
$$\varepsilon_{cs0{,}05} = 0{,}42 \cdot \varepsilon_{cs}(t, t_s)$$
$$\varepsilon_{cs0{,}95} = 1{,}58 \cdot \varepsilon_{cs}(t, t_s)$$

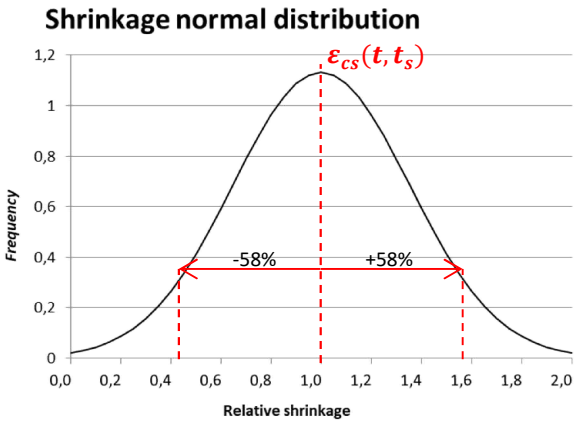

figure 4-4: Normal distribution for shrinkage strain according to CEB-fip 2010 with 90% confidence interval.

The shrinkage strain prediction of both the EC2 model and the CEB-fip 2010 model are plotted against time in a graph which is shown in figure 4-5. The 5th and 95th percentile value of the CEB-fip 2010 model are also plotted in this graph. Here one can see that the difference with the EC2 model is negligibly small when considering the 90% confidence area. In this research the CEB-fip 2010 model will be adopted with the 90% confidence area.

Parameters

h_0	$= 150$	mm
RH	$= 50$	%
f_{cm}	$= 38$	N/mm^2
t_s	$= 5$	days

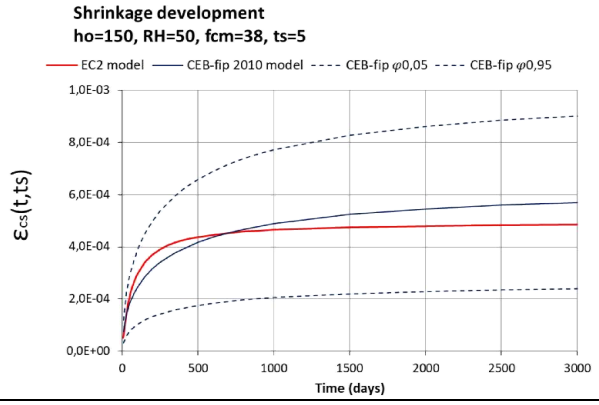

figure 4-5: Shrinkage EC2 model (red), Shrinkage CEB-fip 2010 model (blue).

The CEB-fip 2010 shrinkage function is a summation of an autogenous shrinkage function $\varepsilon_{cas}(t)$ and a drying shrinkage function $\varepsilon_{cds}(t, t_s)$ which are both shown in equation 9. A full description of the shrinkage strain function of the CEB-fip model 2010 is elaborated in appendix A.1.
The autogenous shrinkage function is only dependent of time t and concrete mean compressive strength f_{cm}. However, the function implies that the autogenous strain depends on the concrete strength, it actually depends on the water to cement ratio. The mean concrete strength serves as a substitute parameter (CEB-fib, 2012).
The drying shrinkage function is highly dependent on the relative humidity of the environment and the notional size of the considered concrete element. Again the concrete mean compressive strength f_{cm} serves as a substitute parameter. Higher strength concrete classes tend to have a higher density and are less porous which decreases the diffusion rate of water vapour through the concrete.

$\varepsilon_{cas}(t) = \varepsilon_{cas0}(f_{cm}) \cdot \beta_{as}(t)$	$\varepsilon_{cas0}(f_{cm})$: Notional autogenous shrinkage coefficient. $\beta_{as}(t)$ Autogenous shrinkage time function.
$\varepsilon_{cds}(t, t_s) = \varepsilon_{cds0}(f_{cm}) \cdot \beta_{RH}(RH) \cdot \beta_{ds}(t - t_s)$	$\varepsilon_{cds0}(f_{cm})$: Notional drying shrinkage coefficient. $\beta_{RH}(RH)$: Relative humidity coefficient. $\beta_{ds}(t - t_s)$: Drying shrinkage time function.

equation 9: Autogenous and drying shrinkage function according to the CEB-fip 2010 model.

As a summary of the discussion about the quantification of shrinkage deformations in concrete, the following statements can be made when modelling the shrinkage strain in concrete:

The concrete shrinkage will be modelled according to the CEB-fip 2010 model.	$\varepsilon_{cs}(t) = \varepsilon_{cas}(t) + \varepsilon_{cds}(t, t_s)$
The model assumes a relative humidity (RH) of 50% as an input parameter.	$RH = 50\%$
For the possible shrinkage strain deviation, thus deviation on shrinkage deformation, the 90% confidence area of the shrinkage normal distribution according to figure 4-4 is considered.	$\varepsilon_{cs,mean}$ = 1,0 φ $\varepsilon_{cs,0,05}$ = 0,42 φ $\varepsilon_{cs,0,95}$ = 1,58 φ

table 9: Assumptions for modelling shrinkage deformations according to the CEB-fip 2010 model.

4.1.3 Creep

According to Eurocode 2 the creep strain is a factor of the initial elastic strain that is formulated with the initial tangent modulus and caused by quasi-permanent loads. This linear relation can be used when the concrete is subjected to compressive stresses due to quasi-permanent loads that are below 45% of the mean compressive strength f_{cm}. If stresses are higher than this threshold, the creep factor will be substituted by a non-linear creep coefficient that is formulated in equation 10. The creep model of EC2 does not distinguish basic and drying creep.

$\varepsilon_{cc}(t) = \varphi(t, t_0) \cdot \frac{\sigma_c}{E_c}$	Linear creep strain for $\sigma_c \leq 0{,}45 f_{cm}$
$\varepsilon_{cc}(t) = \varphi(t, t_0) \cdot e^{1{,}5 \cdot \left(\frac{\sigma_c}{f_{ck}(t_0)} - 0{,}45\right)} \cdot \frac{\sigma_c}{E_c}$	Non-linear creep strain for $\sigma_c > 0{,}45 f_{cm}$

equation 10: Linear and non-linear creep strain according to EC2 (NEN-EN 1992-1-1, 2011).

The CEB-fip Model Code 2010 is similar to the creep model of EC2, but is more extensive with a distinction of basic and drying creep. The model can be applied within a range of service stresses that are lower than 40% of the mean compressive strength f_{cm}, is valid for ordinary structural concrete ($20\text{MPa} \leq f_{cm} \leq 120\text{MPa}$) and in a relative humidity of 40 to 100% with a temperature between 5°C and 30°C. The creep strain is a factor of the initial elastic strain that is formulated with the secant modulus (CEB-fib, 2012). The conditions for an indoor concrete structure of a consequence class 3 high-rise meets these requirements, so the CEB-fip model 2010 is assumed to be very suitable for this research.

$$\varepsilon_{cc}(t) = \varphi(t,t_0) \cdot \frac{\sigma_c}{E_{cm}} \qquad \text{Linear creep strain for } \sigma_c \leq 0{,}40 f_{cm}$$

$$\varphi(t,t_0) = \varphi_{bc}(t,t_0) + \varphi_{dc}(t,t_0)$$

equation 11: Linear creep strain according to CEB-fip model 2010.

The model also provides a mean coefficient of variation for the predicted creep function. When a normal distribution is assumed, a 5th and 95th percentile value can be found, which can provide a 90% confidence area for the creep factor. The values and normal distribution for the creep factor are depicted in figure 4-6. These values are based on a computerized data bank of laboratory test results (CEB-fib, 2012). According to these values the creep factor can deviate $\pm 41\%$ in a 90% confidence interval.

$$\varphi_{mean} = 1{,}0 \cdot \varphi(t,t_0)$$
$$\varphi_{0{,}05} = 0{,}59 \cdot \varphi(t,t_0)$$
$$\varphi_{0{,}95} = 1{,}41 \cdot \varphi(t,t_0)$$

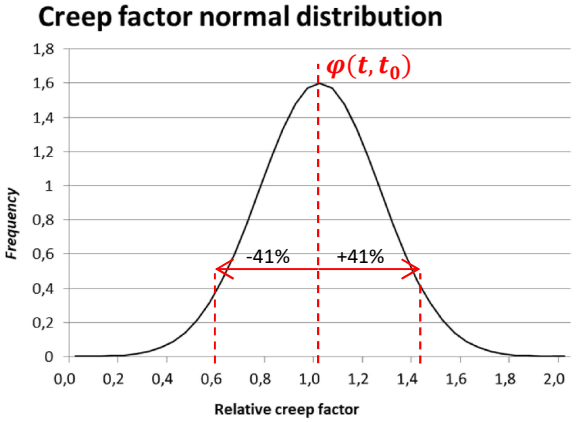

figure 4-6: Normal distribution for creep factor according to CEB-fip 2010 with 90% confidence interval.

The creep factor of both the EC2 model and the CEB-fip 2010 model are plotted against time in a graph which is shown in figure 4-7. The 5th and 95th percentile value of the CEB-fip 2010 model is also plotted in this graph. Here one can see that the difference with the EC2 model is negligibly small when considering the 90% confidence area. In this research the CEB-fip 2010 model will be adopted with the 90% confidence area.

Parameters

h_0	$= 150$	mm
RH	$= 50$	%
f_{cm}	$= 38$	N/mm^2
t_0	$= 10$	days

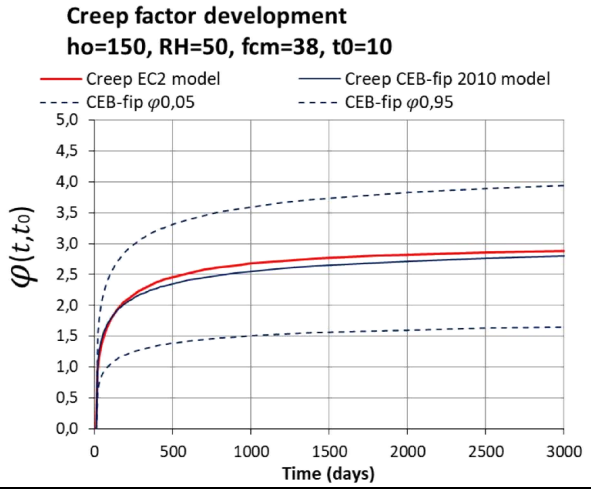

figure 4-7: Creep EC2 model (red), Creep CEB-fip 2010 model (blue).

The CEB-fip 2010 creep factor is a summation of a basic creep function $\varphi_{bc}(t, t_0)$ and a drying creep function $\varphi_{dc}(t, t_0)$ which are both shown in equation 12. A full description of the creep function of the CEB-fip model 2010 is elaborated in appendix A.2.
The basic creep function is only dependent of time, time of loading, the concrete mean strength and curing temperature. These are internal factors that influence the creep behaviour.
The drying creep function is highly dependent on the relative humidity of the environment and the notional size of the considered concrete element. Also time of loading and concrete strength are of influence on the drying creep behaviour. The drying creep function is mainly dependent on factors that influence the diffusion of water vapour between the considered concrete element and circumjacent environment.

$$\varphi_{bc}(t, t_0) = \beta_{bc}(t, t_0) \cdot \beta_{bc}(f_{cm})$$

$\beta_{bc}(t, t_0)$: Time dependent basic creep coefficient.
$\beta_{bc}(f_{cm})$: Strength dependent basic creep factor.

$$\varphi_{dc}(t, t_0) = \beta_{dc}(t, t_0) \cdot \beta_{dc}(f_{cm}) \cdot \beta_{dc}(t_0) \cdot \beta(RH)$$

$\beta_{dc}(t, t_0)$: Time dependent drying creep coefficient.
$\beta_{dc}(f_{cm})$: Strength dependent drying creep factor.
$\beta_{dc}(t_0)$: Factor dependent on time of loading.
$\beta(RH)$: Factor dependent of relative humidity.

equation 12: Basic and drying creep function according to CEB-fip 2010.

As a summary of the discussion about the quantification of creep deformations in concrete, the following statements can be made when modelling the creep strain in concrete:

The creep strain will be computed linear.	$\varepsilon_{cc}(t) = \varphi(t, t_0) \cdot \frac{\sigma_c}{E_{cm}}$
The model assumes a relative humidity (RH) of 50% as an input parameter.	$RH = 50\%$
For the possible creep factor deviation, thus deviation on creep deformation, the 90% confidence area of the creep normal distribution according to figure 4-6 is used.	φ_{mean} = 1,0 φ $\varphi_{0,05}$ = 0,59 φ $\varphi_{0,95}$ = 1,41 φ

table 10: Assumptions for modelling creep deformations according to the CEB-fip 2010 model.

4.1.4 Computation method for concrete creep

Due to the hydration process of concrete, the creep factor in concrete tends to decrease when the age of the concrete at loading is in a later moment of time during the curing process. For a single stress increment, a single creep factor function is determined with only one time of loading parameter t_0 that corresponds to the moment at which the single stress increment is applied. The creep strain for one stress increment can be simply determined by a creep factor function that is dependent of static parameters and time t:

$$\Delta\varepsilon_{cc}(t) = \frac{\Delta\sigma(t)}{E_c} \cdot \varphi(t, t_0)$$

When a series of stress increments is applied at different time moments, the creep strain is determined by a creep factor function $\varphi(t, t_i)$ that differs for every stress increment because of the moment at which the load is applied that is represented by t_i. The Boltzmann superposition principle is still valid, but the independence of each loading step is not only caused by time t, but also by the time of loading t_i. The determination of the creep strain can be formulated by the given function in figure 4-8.

Because of the time dependence and the dependence of the moment at which loads are applied on the creep factor, the response will propagate over time and is dependent of the loading order and history. The net response is still the sum of all individual responses with a fixed time of loading moment. This means that load increments cannot be alternated or moved over the time axis without influencing the creep response.

$$\varepsilon_{cc}(t) = \frac{1}{E_c} \cdot \sum_{i=0}^{n} \Delta\sigma_i(t) \cdot \varphi(t, t_i)$$

With:

t: Time

t_i: Time of loading corresponding to the stress increment $\Delta\sigma_i(t)$.

E_c: The concretes modulus of elasticity.

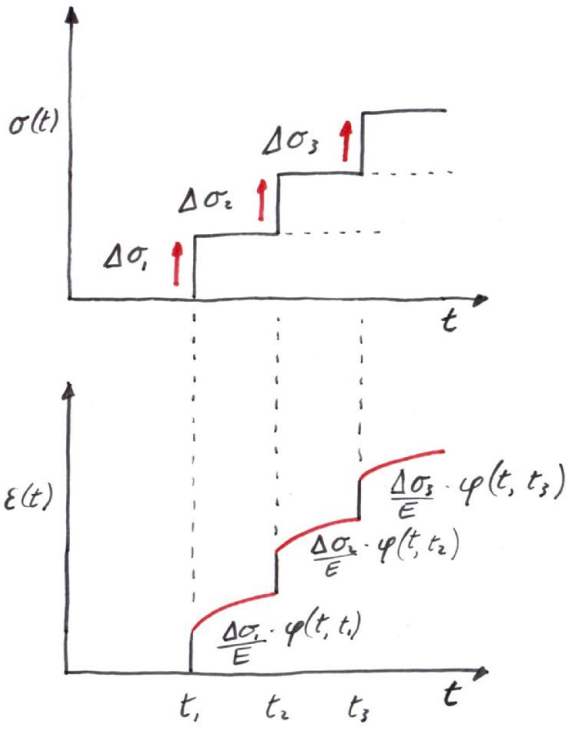

figure 4-8: Formulation of the creep strain according to Boltzmann's superposition principle.

The formulation in figure 4-8 will provide accurate predictions when the following conditions are met (Bazant, 1989):

- Stresses are within the service stress range, which is approximately from 0 to 40% of the strength.
- There is only an increment of stresses and not a decrement of stresses.
- There is no significant change in moisture content distribution.
- There is no large sudden stress increase long after the initial loading.

Stresses are within the service stress range as is elaborated in appendix E. When considering quasi-permanent loads that affect the creep strain, the stresses in the gravitational system are assumed to increase gradually during construction as the building is built floor by floor. This also states that there will be no large sudden stress increases long after the initial loading. Finally, the relative humidity in an indoor heated environment of a high rise building is relatively stable, so it is assumed that there is no significant change in moisture content distribution in the load bearing members.

Assuming these argumentations it can be concluded that the Boltzmann superposition principle is valid and may provide accurate predictions.

4.2 Quantification of timber strains

The material model for timber of Eurocode 5 will be adopted in this research. The EC5 model describes how to quantify elastic and creep deformations, but also has a number of shortcomings when compared to the EC2 material model of concrete.
This chapter will elaborate the EC5 material model for each strain type and how it is dealt with in this research.

4.2.1 Elasticity

The elastic strain can be assumed linear related to the applied stress in the corresponding direction relative to the wood grain when stresses are sufficiently low. In reality, the full stress strain relation is linear for tension, but shows non-linearity in compression as is depicted in figure 4-9. Because the serviceability stresses are determined to not exceed 45% of the characteristic strength (0,45f_{ck}), it is assumed that a linear approach of the elastic deformations is a good representation of reality.

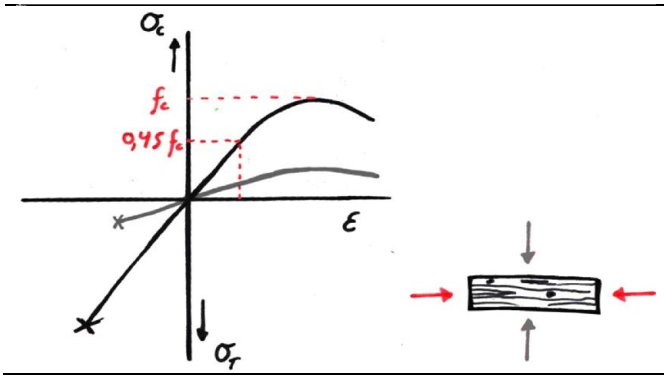

figure 4-9: Stress strain relation diagram for parallel and perpendicular loaded wood. Based on (Buchanan, 1990).

Timber has a far greater stiffness when loaded parallel to the grain instead of perpendicular to the grain and shows a ratio of approximately 16 to 1 respectively (Hoffmeyer P. , 1995). The mean modulus of elasticity parallel and perpendicular to the grain are indicated with $E_{0,mean}$ and $E_{90,mean}$. This chapter will elaborate the initial elastic strains for parallel to the grain loading, thus the parallel to the grain stiffness expressed as $E_{0,mean}$.

$$\varepsilon_{0,el}(t) = \frac{\sigma_0(t)}{E_{0,mean}}$$

The mean modulus of elasticity of a certain timber strength class is the expected average that is retrieved from tests of a series of samples that represent this strength class. It is highly unlikely that the deformations that will occur in practice are exactly the same as the theoretical deformations when using the mean modulus of elasticity. It is more useful to provide a certain bandwidth in which deformations can deviate from the mean value with a certain probability. When using the 5th and 95th percentile value for the modulus of elasticity one can say with a 90% confidence that the deformations will stay within this range. This range or bandwidth is given in figure 4-10 for several glue laminated timber strength classes and compared to the sawn timber

strength classes from which they are composed of. The elastic deformations that will occur are directly related to the modulus of elasticity so the 90% confidence area for the deformations can be considered as the same, depending on the strength class that is used. From this figure it can be observed that sawn timber has a relatively high coefficient of variation of 33% with a 90% confidence interval. GLT shows a lower coefficient of variation of 17% with the same 90% confidence interval.

	$E_{0,mean}$	$E_{0,05}$	$E_{0,95}$	σ_{90} (90% confidence area)
T16	11500	7700	15300	±33,0%
T18	12000	8000	16000	±33,3%
T24	13500	9000	18000	±33,3%
GL26h (T16)	12100	10100	14100	±16,5%
GL28h (T18)	12600	10500	14700	±16,7%
GL32h (T24)	14200	11800	16600	±16,9%

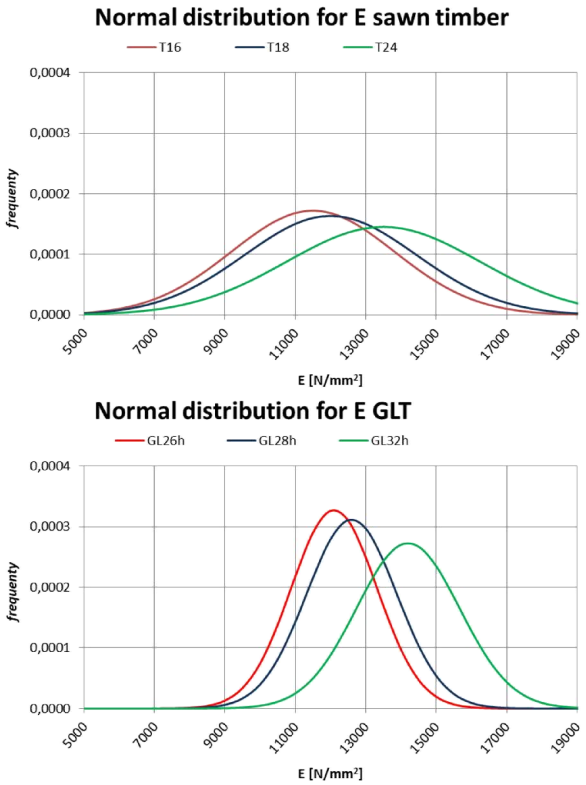

figure 4-10: Determination of 90% inaccuracy area of sawn timber and glue laminated timber E-modulus parallel to the grain for several strength classes.

As a summary of the discussion about the quantification of elastic deformations in timber, the following statements can be made when modelling the elastic strain in timber:

Elastic strains will be modelled linear by use of the mean modulus of elasticity $E_{0,mean}$ for parallel to the grain orientation and $E_{90,mean}$ for perpendicular to the grain orientation.	$\varepsilon_{t,0,el}(t) = \frac{\sigma_0(t)}{E_{0,mean}}$ $\varepsilon_{t,90,el}(t) = \frac{\sigma_{90}(t)}{E_{90,mean}}$
For the possible stiffness deviation, thus elastic deformation deviation, the 90% confidence area of the stiffness normal distribution according to figure 4-10 is considered.	For GLT: $E_{05} = 0{,}83 \cdot E_{mean}$ $E_{95} = 1{,}17 \cdot E_{mean}$

table 11: Assumptions for modelling elastic strain in timber.

4.2.2 Creep

According Eurocode 5 the creep strain is a factor of the elastic strain that is caused by quasi-permanent loads. This factor is expressed as a constant k_{def} that predicts the creep strain after 50 years of time. This deformation factor should be chosen on the basis of the climate class in which the timber is situated and the type of engineered timber that is used. The description of the climate classes are elaborated in table 12. The

environmental influencing factors like relative humidity RH and temperature are embedded in these climate classes. Some of the deformation factor values are shown in table 13 and should be chosen accordingly.

Climate class 1	The moisture content corresponds to a temperature of 20 degrees and a relative humidity that exceeds 65% for only a few weeks in a year.	For most softwoods the moisture content will not exceed 12%
Climate class 2	The moisture content corresponds to a temperature of 20 degrees and a relative humidity that exceeds 85% for only a few weeks in a year.	For most softwoods the moisture content will not exceed 20%
Climate class 3	The moisture content will exceed the moisture content that corresponds to climate class 2.	

table 12: Climate class description according to EC5.

To calculate the creep strain or creep deformation, the k_{def} factor is used as a multiplication factor over the instantaneous deformations due to permanent and quasi-permanent loads. This corresponds to the application of the creep compliance as in equation 6 on page 54 where t=50 years. Eurocode 5 does not consider the development of the creep strain related to time.

	Climate class		
	1	*2*	*3*
Sawn timber	0.6	0.8	2.0
Glue laminated timber	0.6	0.8	2.0
Plywood	0.8	1.0	2.5

table 13: Deformation factor k_{def} for different climate classes and engineered timber products (NEN-EN 1995-1-1, 2011).

$u_{c,G} = u_{inst,G} \cdot k_{def}$	Long-term deformations for permanent loads.
$u_{c,Q1} = u_{inst,Q1} \cdot \Psi_2 \cdot k_{def}$	Long-term deformations for quasi-permanent loads.

equation 13: Calculation of additional long-term deformations according to Eurocode 5 (NEN-EN 1995-1-1, 2011).

For a verification of the creep deformation factor and the propagation of the creep factor over time, a literature study is conducted on several experimental studies that considered creep behaviour over a 4 year time period in sawn and glue laminated timber (GLT) specimens. Three experimental creep studies that were conducted in climate class 1 conditions, are elaborated and compared to one another (Gowda, Kortesmaa, & Ranta-Maunus, 1996; Aratake, Morita, & Arima, 2011; Abdul-Wahab, Taylor, Price, & Pope, 1998). The mean creep curves and standard error of these experiments are shown in figure 4-11.

From the graph it can be seen that the results of Gowda and Abdul-Wahab are similar and show a creep factor of 0,6 after 4 years of constant loading already. The results of Aratake are much lower. It is very unlikely that this difference is caused by chance variability because the mean curve differs significantly with respect to the standard error. It is possible that the significantly lower results of Aratake are due to the fact that the specimens were composite glue laminated timber beams that used low graded timber for the inner lamellas and high graded Douglas fir with a high Young's modulus for the outer lamellas. Because it was a bending test, the outer lamellas would have the highest contribution to the experimental results.

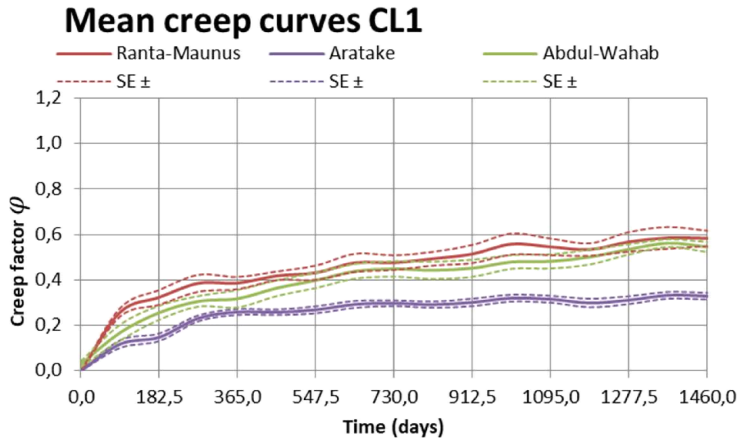

Gowda, Kortesmaa and Ranta-Maunus:
n=8

Abdul-Wahab, et al:
n=12

Aratake, Morita and Arima:
n=8

figure 4-11: Mean creep curves for several experimental researches with their Standard Error.

In further analysis the results of Gowda and Abdul-Wahab are taken together in a meta-analysis for the determination of an overall mean creep curve and standard deviation (figure 4-12). The mean creep curve was curve fitted and extrapolated to 50 years. Based on the experimental results of Gowda, Kortesmaa, Ranta-Maunus and Abdul-Wahab, et al, a 90% confidence interval is determined with a range of $\pm 37\%$ from the mean creep value $\varphi(t)$. A more comprehensive elaboration on the considered experimental studies for the determination of the creep behaviour can be found in appendix D starting from page 150.

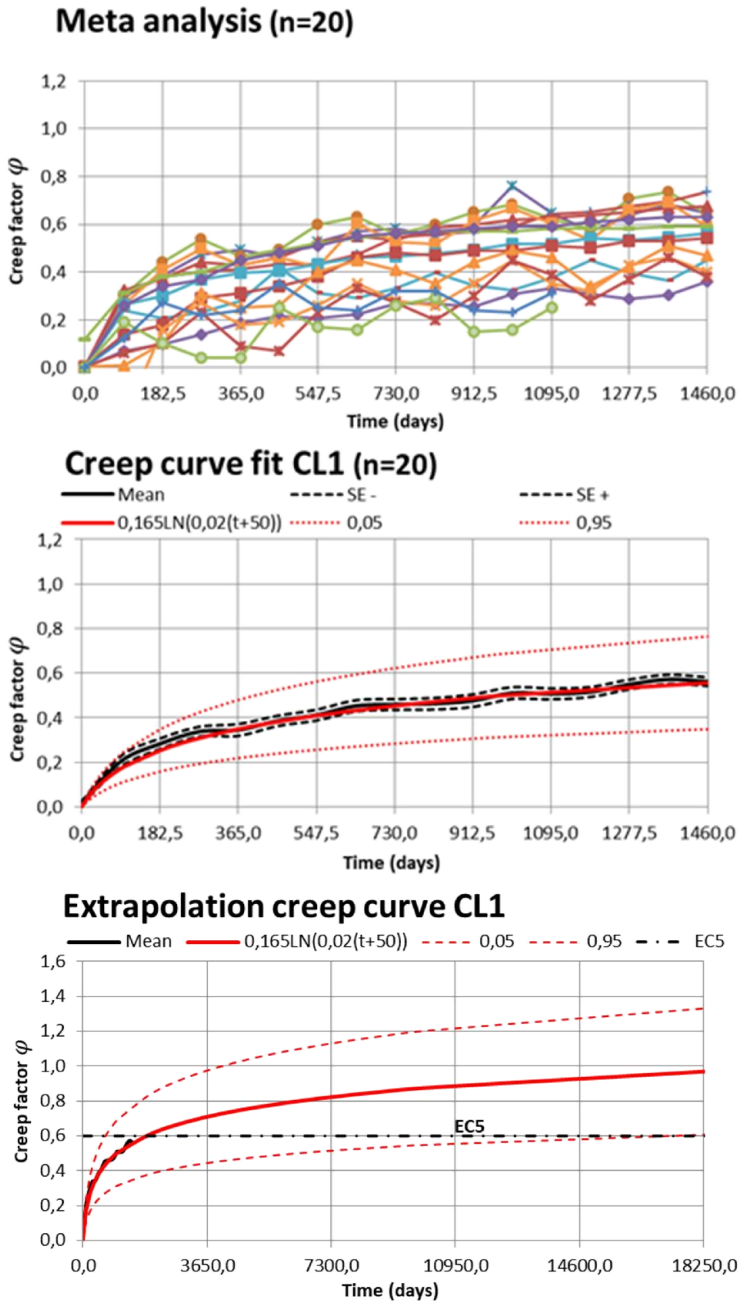

Gowda, et al. + Abdul-Wahab, et al:
n=20
(Sawn timber and GLT specimens)

$\varphi(t) = a \cdot \ln(1 + b \cdot t)$
with:
$a = 0{,}165$
$b = 0{,}02$

$\varphi_{0,05} = 0{,}63 \cdot \varphi(t)$

$\varphi_{0,05} = 1{,}37 \cdot \varphi(t)$

figure 4-12: Mean creep curves and curve fit extrapolation from meta-analysis.

It can be established that the Eurocode does not provide a suitable approach for determining creep over time as this is a static creep factor. When compared to the creep factor established from the analysis of creep experiments, the Eurocode creep factor of 0,6 is already reached at 5 years. When extrapolating the curve fit of the experimental results, it is expected that the mean creep factor will be 0,97 at 50 years with a 90-percent confidence interval spanning from 0,61 to 1,33.

From the analysis results it can be concluded that the Eurocode underestimates the creep factor when considering a 50 year service life. For this reason the creep curve that is established in appendix D is judged to be more reliable as it also provides a 90-percent confidence interval. This creep curve may only be used for the modelling of the creep strain for timber in climate class 1 that is loaded parallel to the grain in the service stress range.

The creep strain will be computed linear.	$\varepsilon_{cc}(t) = \varphi(t, t_0) \cdot \frac{\sigma_c}{E_{cm}}$
The time dependent creep factor will be based on experimental result from Gowda et al and Abdul-Wahab et al by a curve fitting function.	$\varphi(t) \quad = 0{,}165 \ln\left(0{,}02 \cdot \left(t + \frac{1}{0{,}02}\right)\right)$
For the possible creep factor deviation, thus deviation on creep deformation, the 90% confidence area of the creep normal distribution according to figure 4-12 is used.	$\varphi_{0,05} \quad = 0{,}63\ \varphi$ $\varphi_{0,95} \quad = 1{,}37\ \varphi$

table 14: Assumptions for modelling creep deformations for timber that is loaded parallel to the grain in the service stress range in climate class 1.

4.2.3 Shrinkage/swelling

The amount of shrinkage or swelling of a structural element is dependent of the amount of change in moisture content and the considered material axis relative to the grain. Due to the hygroscopic character of timber, the moisture content of timber will vary in order to reach equilibrium with the relative humidity of the environment.

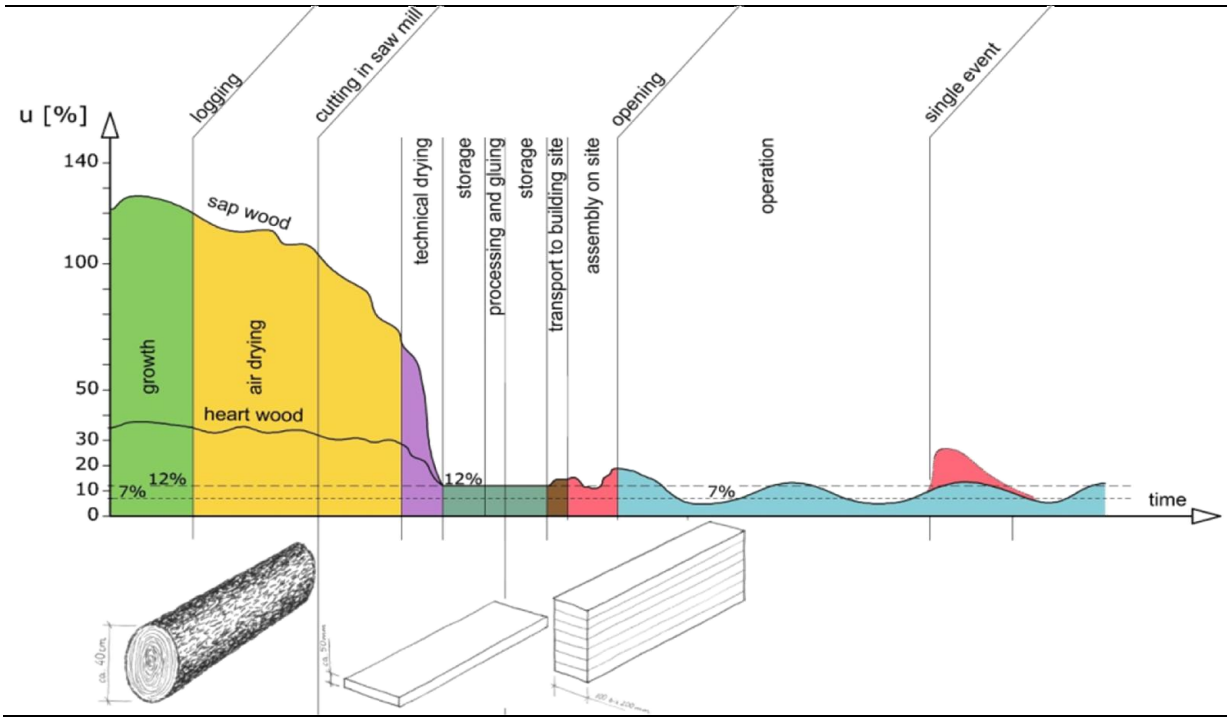

figure 4-13: Indication of moisture content in wood from logging to in service conditions (Dietsch, Gamper, Merk, & Winter, 2015).

Eurocode 5: Design of Timber Structures, states that timber structural elements should not be subjected to unnecessary heavier weather conditions during transport and construction than the in service environmental conditions. It is also mentioned that the timber structural elements should be dried to a moisture content that corresponds to the climate conditions in the finished structure (NEN-EN 1995-1-1, 2011).

Despite the measures that can be taken to protect timber from heavier weather conditions during transport, shrinkage should still be expected because the moisture content may rise due to the exposing of timber structural elements to high relative humidities during construction. Due to heating of the building, the indoor relative humidity thus the moisture content of the timber will decrease to an equilibrium moisture content in service.

In this chapter the amount of shrinkage strain and the development over time is assessed as good as possible by determining the expected moisture content of a timber structural element at construction and the regression of moisture content over time by analysis of conducted field measurement by (Serrano, 2009; Dietsch, Gamper, Merk, & Winter, 2015). The longitudinal shrinkage coefficient α_l is determined by analysis of experimental research and verified by literature.

Higher moisture content value

The moisture content value at the time of installation of timber structural elements is of interest, because afterward moisture content change can cause shrinkage or swelling in these elements causing the total structure to deform. In the production process of glue laminated timber and cross laminated timber elements the moisture content is controlled around a moisture content of 12% (Stora Enso; Hasslacher Norica Timber, 2016). As indicated in figure 4-13 the moisture content can increase from leaving the factory to the building site because of outside weather conditions. On basis of the analysis on a conducted experiment by (Franke, Franke, Schiere, & Müller, 2016) that can be found in appendix B.1 on page 139, and assuming that there is consciously dealt with protecting the structural elements against harsh weather conditions, it is assumed that the average moisture content increase is not more than 3%, when considering mass timber elements. This would imply that the higher moisture content value has a maximum of 15%.

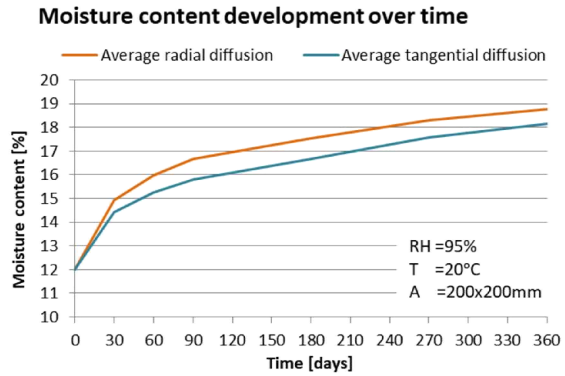

figure 4-14: Estimation of moisture content increase after leaving the factory when only radial or tangential diffusion is possible. Based on (Franke, Franke, Schiere, & Müller, 2016).

Lower moisture content value

Field measurements conducted by (Dietsch, Gamper, Merk, & Winter, 2015) show that the equilibrium moisture content can reach values of 8%-10%. These values where measured in heated indoor climates in Germany with constant temperatures of 20°C and a relative humidity of 40%-50%. Table 4-2 of the Wood handbook shows similar equilibrium moisture content values of 7,7%-9,2% at a temperature of 21,1°C and a relative humidity between 40%-50% (Ross, 2010).

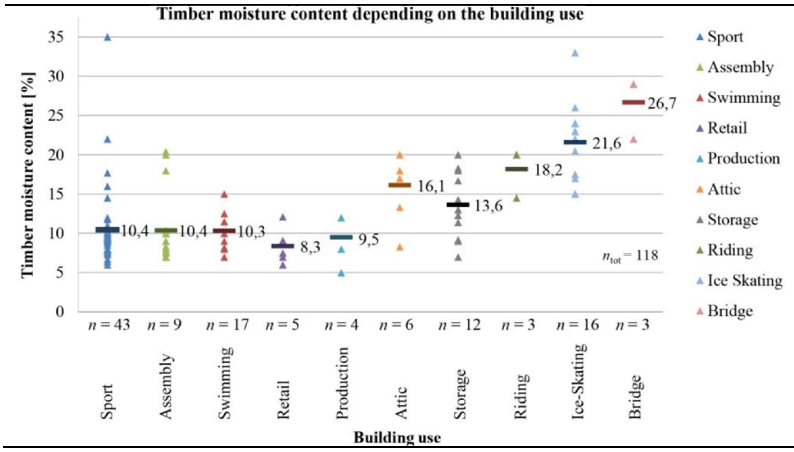

figure 4-15: Timber moisture content field measurements categorized by building use (Dietsch, Gamper, Merk, & Winter, 2015).

For a high-rise timber building for use of housing or office space, it is assumed that temperature and relative humidity are relatively constant and the earlier mentioned values from literature are representative. A lower moisture content value of 8% is assumed for a constantly heated indoor climate.

Moisture content regression

After installation of timber structural elements, the building structure will be closed by placing the façade elements. In further occupation, the relative humidity will decrease due to heating of the building, with a decrease of the average moisture content of the structure as a result.

From the upper and lower moisture content value and the analysis on the regression of moisture content in appendix B.2 on page 141 for structural elements after placement, an estimate of a possible trend curve is drawn up for the average moisture content over the total cross section of a structural element. The graph is shown in figure 4-16 and will be used to predict the development of shrinkage strain.

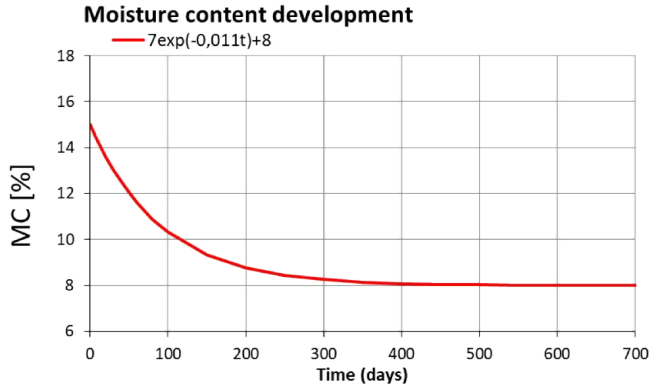

$$MC(t) = \Delta MC \cdot e^{-0{,}011 \cdot t} + MC_{lower}$$

$$\Delta MC = MC_{upper} - MC_{lower}$$

$$MC_{upper} = 15\%$$

$$MC_{lower} = 8\%$$

figure 4-16:Estimate of moisture content regression after placement in the total structure.

Shrinkage coefficient

Several longitudinal shrinkage experiments are studied and analysed in appendix C. A normal distribution has been drawn up from the mean longitudinal shrinkage coefficient values and standard deviations of the several experiments. The total mean longitudinal shrinkage coefficient $\beta_{0,mean}$ that is determined by the analysis corresponds to the longitudinal shrinkage coefficient $\beta_{0,mean} = 0{,}01$ that is found in literature in a range of 5-20% moisture content (Hoffmeyer P. , 1995).

n=12

Mean:		*0,011*
Standard deviation:		*0,0052*
$k_s(12) = \frac{6{,}8 \cdot 12 + 6}{3{,}7 \cdot 12 - 3} = 2{,}1$		
$\beta_{0,05}$:	$\mu - k_s \cdot SD$	*0,001*
$\beta_{0,95}$:	$\mu + k_s \cdot SD$	*0,021*

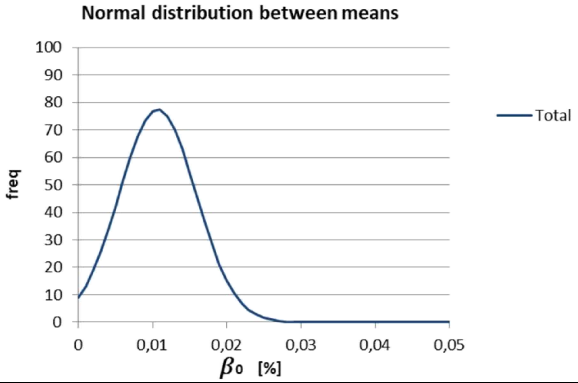

figure 4-17: Normal distribution retrieved from shrinkage experiment of Johansson (Johansson, 2003).

The variation in the longitudinal shrinkage coefficient is quite high because the tested specimens were relatively small, which makes the influence of a material defect on a specimen relatively large causing high variability within a sample. For this reason the results of Johansson are taken to determine the variance as the specimens from these results represent full size structural elements.

The mean shrinkage coefficient for the longitudinal direction is used for the estimation of longitudinal shrinkage strain in timber. A linear relation between longitudinal shrinkage strain and average moisture content is possible with the mean longitudinal shrinkage coefficient when the moisture content is in the range of 5-20% (Hoffmeyer P. , 1995, p. 12). The relation is shown in equation 14.

$$h_2 = h_1[1 + \frac{\beta_0}{100}(|\omega_2 - \omega_1|)] \qquad \beta_0 = 0{,}011 \quad \text{(spruce, pine, fir, larch, poplar, oak).}$$

$$\Delta\varepsilon = \frac{\beta_0}{100}(|\omega_2 - \omega_1|)$$

equation 14: Relation between length and moisture content (Hoffmeyer P. , 1995, p. 12).

Based on the estimate on average moisture content regression, the mean shrinkage strain can be determined by equation 14. The estimate of shrinkage strain development is shown in figure 4-18. The deviations on the shrinkage strain are based on the deviations of the shrinkage coefficient that is established on findings from appendix C. These values will be used to model shrinkage deformations over time.

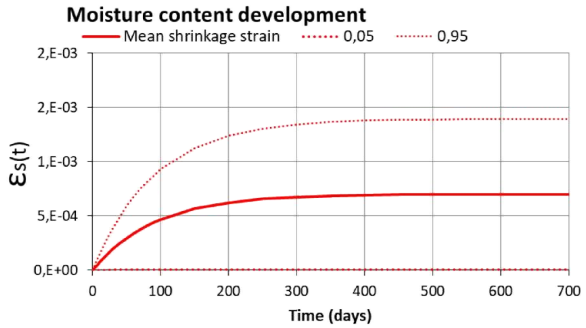

$$MC(t) = 7 \cdot e^{-0{,}011 \cdot t} + 8$$

$$\varepsilon_{sh}(t) = \frac{\beta_0}{100} \cdot MC(t)$$

$$\varepsilon_{sh,05}(t) = 0{,}01 \cdot \varepsilon_{sh}(t)$$
$$\varepsilon_{sh,95}(t) = 1{,}99 \cdot \varepsilon_{sh}(t)$$

figure 4-18: Determination of shrinkage strain development by curve fitting.

4.3 Deviations

In this chapter it is determined how to quantify the elastic, shrinkage and creep strain. Next to the mean value, also the possible deviation for each strain in the 90% confidence interval is determined. This subchapter gives an explanation how these deviation are used and how these evolve over the building height.

When considering one column and the deformations that are induced in this column, the deviations that might occur within the 90% confidence interval are easily determined by the specified 5th and 95th percentile values in the previous chapters. It is assumed that these values may be applied on full structural elements. When stacking multiple full sized structural column elements in a building, it is highly unlikely that the deformation for every column will deviate with the same 'high' relative amount. The probability that the properties of the total column will deviate with that same 'high' relative amount as found in the previous chapters underneath a particular floor will decrease when considering floors at higher levels.

When considering the columns in a building design where the columns are stacked per floor, the possible relative deviation on the calculated column shortening is for each individual column the same, assuming that the properties of all columns are the same. When looking at the possible deviation of the calculated floor deformation on the nth level with n columns underneath, the possible deviations should be added up analogue to the summation of n identical, independent stochastic variables to maintain the 90% inaccuracy area on the normal distribution. This results in a decrease of relative deviation when considering floor deformations at a higher level when maintaining the same confidence interval. An example is shown in figure 4-19 on how the relative deviations decrease when considering the deformations on higher floors due to column shortening.

Deformation deviation on the n[th] floor:

$$\sigma_{90,n} = \frac{\sqrt{n \cdot \sigma_{90}^2}}{n}$$

Example for the 10[th] floor with glue laminated columns GL26h

$$\sigma_{90,10} = \frac{\sqrt{10 \cdot 16{,}5^2}}{10} = \pm 5{,}2\%$$

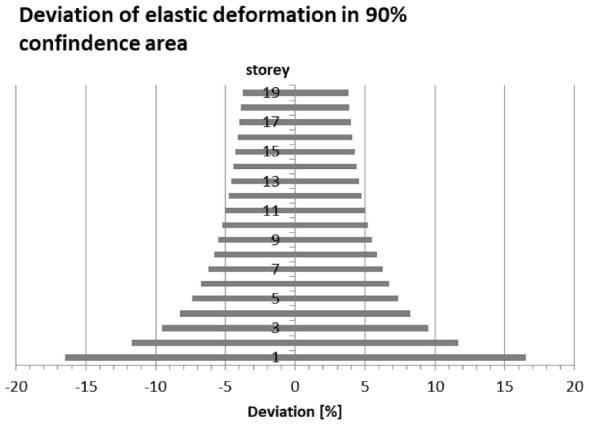

figure 4-19: Deformation deviation on the nth floor.

The mean value of the several strain predictions that are formulated throughout this chapter will be used in calculating deformations due to differential vertical shortening. These mean values of the deformations will be post processed by the deviations that are found according to this chapter.

5 Building execution

This chapter explains how vertical load bearing elements are loaded after placement on their final position and how the deformed shape of the already built structure influences the still to build structure. Loadings that occur before placement due to hoisting during prefabrication, transport and positioning on the building site are not elaborated because these are short-term loads that are not present in the element when being part of the total structure.

5.1 Load increments

The building speed of the upper load bearing structure of a high-rise building can be expressed in time per constructed floor. This value can be taken as a constant during the building process of a high-rise upper structure to simplify the building process model. The load in the base columns of the building can be plotted as a step function that is dependent of time in which the time interval for each load increment is equal to this building speed.

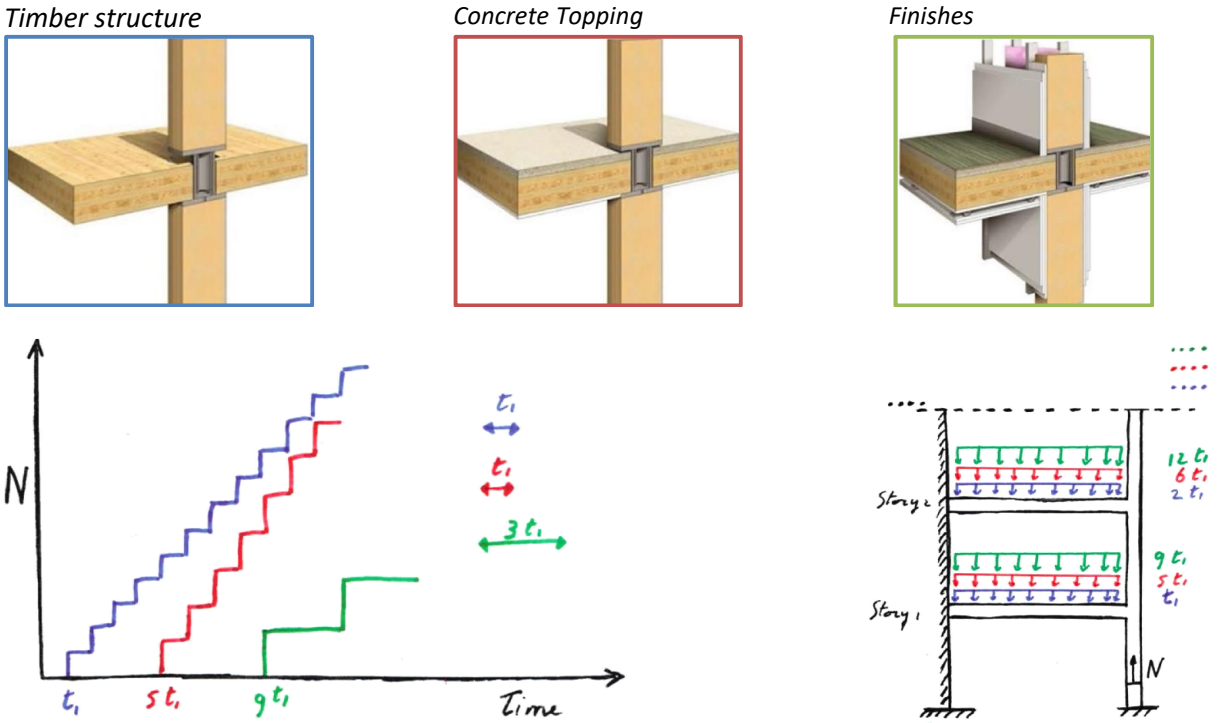

figure 5-1: Top: Building schedule overview of Brock Commons (Pilon, et al., 2017). Modelled load increments in the building process.

5.2 Staged construction analysis

In a traditional analysis where the construction sequence is not considered, it is assumed that the whole structure is placed before any load is applied, including self-weight. The consequence is that the structure will deform as a whole at one moment in time.

In a staged construction analysis the elastic, shrinkage and creep deformations are calculated in every stage before the next stage is built. First, the building method should be determined regarding the adaption of column lengths during construction. The columns can have a fixed length, which can be the case in prefabricated structures, or an adaptive length, which might be the case when columns or connections are poured in-situ and the scaffolding is aligned with the design datum reference lines each time a floor is built

(Park, Choi, & Park, 2013; Fintel, Ghosh, & Iyengar, 1987). The principle difference between both building methods are shown in figure 5-2.

With fixed length columns, storeys are simply stacked without column lengths being adapted if there is not consciously made use of correction methods. Deformations that occur before slab installation should be taken in consideration in the analysis.

With adaptive length columns, the DVS deformations that occur before slab installation are automatically corrected due to the levelling of the formwork and scaffolding. These pre-slab installation deformations do not have to be considered in the analysis (Kim & Shin, 2011).

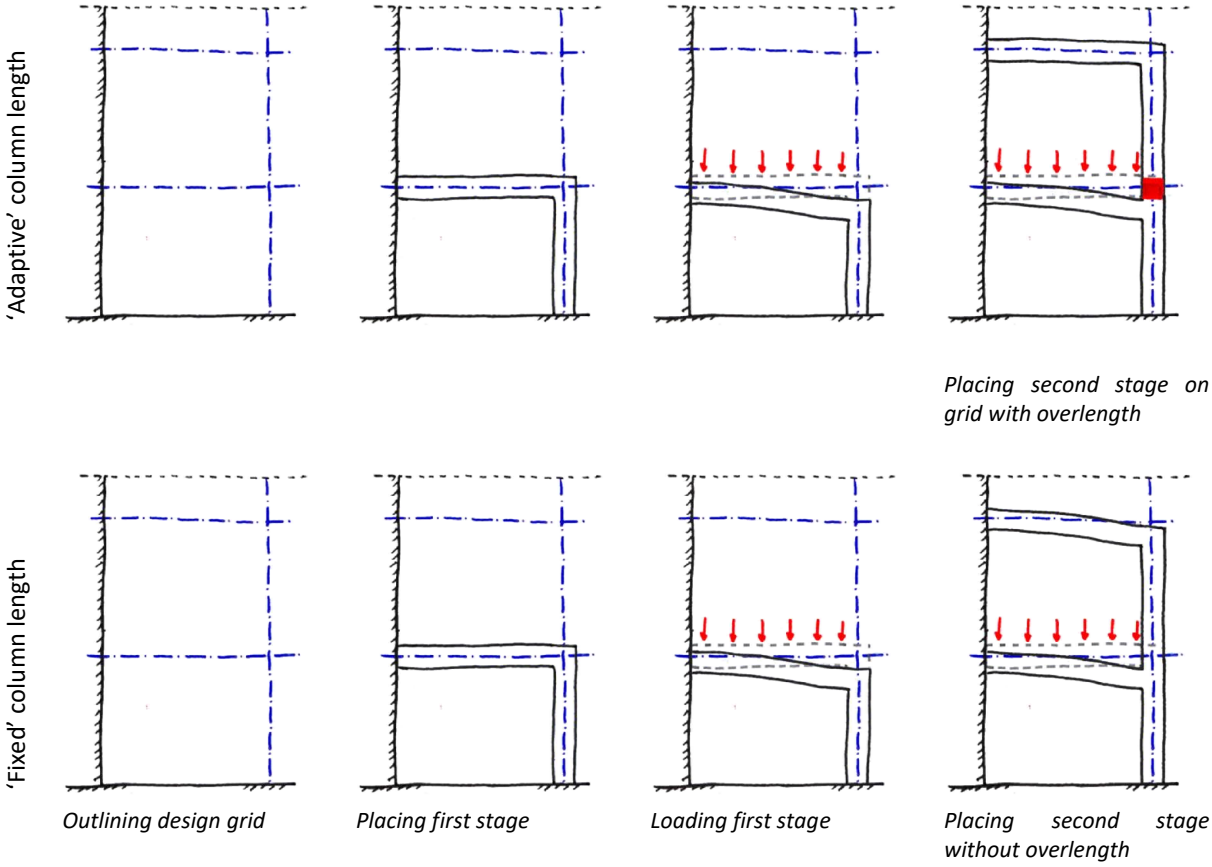

figure 5-2: Levelling of pre-slab installation deformations.

For an explanation of how the over-length is theoretically develops over the building height in case of a staged construction analysis with adaptive column lengths due to levelling, a simplified example is drafted in which the following is assumed:

- All load cases are applied at once for every building stage, the induced axial force in the column from every floor is the same.
- Deformations are only due to elastic strains.
- The column design properties are constant over the building height.
- Redistribution of forces through the floor slabs or beams is neglected.
- A DVS deformation in a certain stage is based on the following expression: $\Delta L_e = \frac{P \cdot L}{E \cdot A}$ with AE: Column stiffness, L: Column length, P: Applied force on the column.

With every stage (floor) that is being built a load P is applied on the column. With every stage built the length of the column L is linearly increasing. When the column stiffness over the building height is assumed as being

constant, only L will increase linear when going up the building. This means that ΔL_e and by that the correction due to levelling, is increasing linear when going up the building (Computers and Structures, Inc (CSI), 2017). At the same time the elastic strain in the column and by that the shortening of the column per individual floor is highest the base of the building. Both the elastic deformation (blue) per floor column δL and the correction (red) per floor are conceptually shown in the left graph of figure 5-3. The deformations of the floor supports are the cumulative of the individual column shortening deformations. Both the floor support deformation due to elastic column shortening (blue) and correction (red) are conceptually shown in the right graph figure 5-3.

Because every stage has a certain duration, shrinkage and creep deformations will develop in the vertical load bearing structure within every stage. These time dependent deformations should superimposed with the elastic deformations and considered as pre-installation deformations for the next stage. This result in an over-length in the still to install vertical load bearing structure with respect to their original design length in which time dependent and elastic deformations are included (Samarakkody, 2016; Fintel, Ghosh, & Iyengar, 1987).

$$\Delta L_e = \frac{N \cdot L}{E \cdot A}$$

N: Axial column force
L: Column length
E: Young's modulus
A: Column cross section

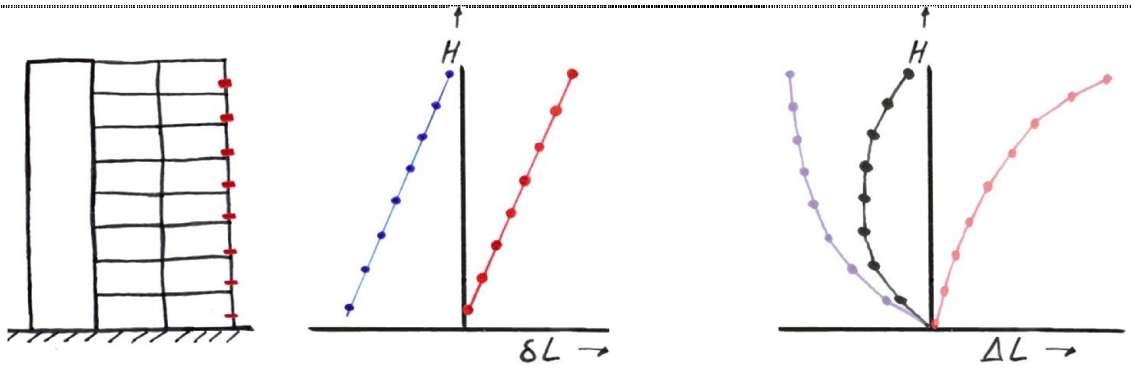

Blue = Individual elastic column shortening.

Red = Theoretical compensation.

Blue = Floor displacements due to individual elastic column shortening.

Red = Theoretical floor displacements due to compensation.

figure 5-3: Theoretical influence of levelling on the column deformations.

As shown in chapter 5.1 the load increments due to the building process can be much more complex. Some load cases are induced after floor slab installation, which means that the deformations due to these load cases are not compensated by levelling on that same floor. With a building sequence as is shown in the graph of figure 6-11 and with the presence of time effects, the staged construction analysis becomes too complex to execute by hand.

5.3 Compensation methods

When the differential vertical shortening is predicted, there is the possibility to compensate for it according several compensation techniques. According to (Park, Choi, & Park, 2013) there is no systematic approach that used widely in the area of compensating for differential vertical shortening. The absolute correction, uniform compensation and lumped compensation are several techniques that can be used. "To enhance the performance of the first three compensation techniques, the optimal compensation technique is presented in

the form of structural optimization" (Park, Choi, & Park, 2013). The principles of the optimization methods are explained in the following sub chapters.

5.3.1 Absolute correction

The absolute correction would exactly compensate the predicted differential shortenings in a high-rise building. It is an idealised correction method that would be very expensive because each column on each floor level would need a different compensation (Samarakkody, 2016). Due to time dependent deformations and deviations in the material response mechanism, an absolute correction can never be achieved in practice for every time moment in the service range of a building. Besides, the execution of the building structure is subjected to size deviations due to prefabrication of elements, outlining the structures grid and positioning elements. Size deviations are further discussed in chapter 0.

The concept of absolute compensation is shown in figure 5-4. It is a simplified diagram that only considers elastic deformation due to a mechanical load in the column that is represented by the blue line. It is assumed that the core has infinite axial stiffness and will not deform vertically. The column design properties are assumed to be the same over the height of the building. This would mean that in general the elastic strain increases from top to bottom of the building as the axial column stress increases from top to bottom. The compensation is represented in red, which is the exact opposite of the predicted column shortening. The right graph shows the support settlements for ever floor due to elastic deformations (blue) and compensation (red). The final result is shown in black which is zero on every floor because the floor displacements and compensation cancel each other out. The floor displacement graph is basically the integral of the individual column shortening graph.

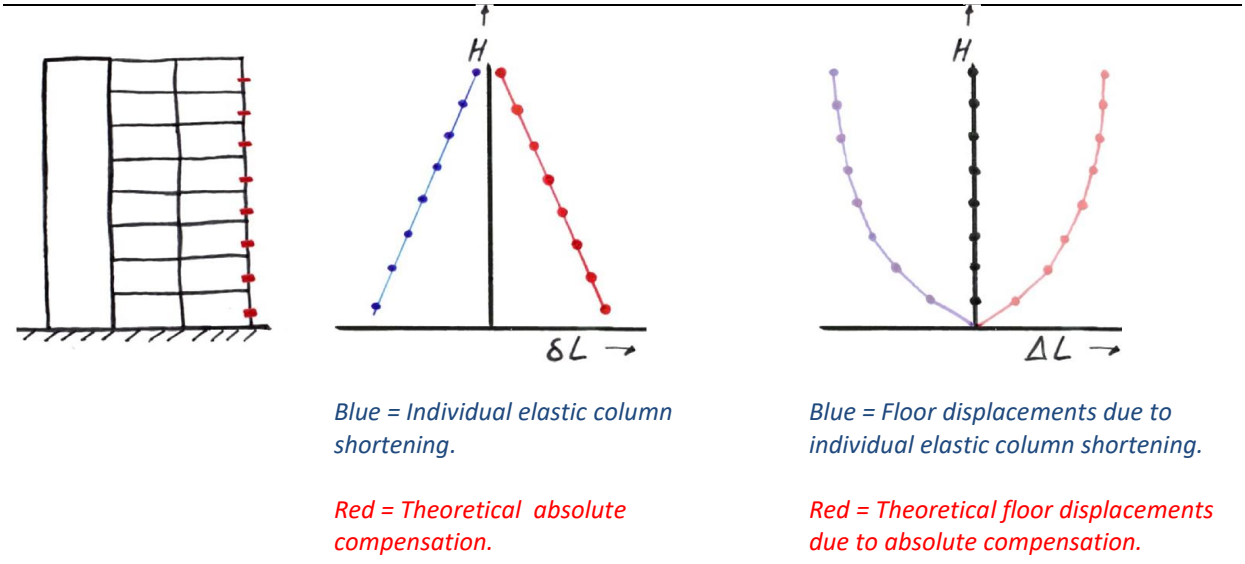

figure 5-4: Abstracted concept of absolute compensation. Blue: Deformations due to elastic strains. Red: Displacements due to absolute compensation.

5.3.2 Uniform compensation

In this form of compensation one correction value is applied on all the columns on each level. This compensation method decreases the maximum deviation value by vertical shortening, but will not eliminate the predicted differential shortening (Park, Choi, & Park, 2013). The concept of uniform compensation is abstractly shown in figure 5-5.

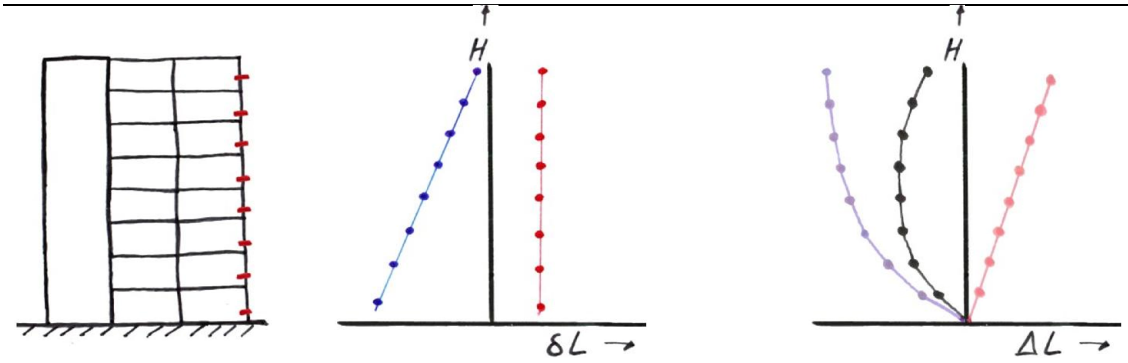

Blue = Individual elastic column shortening.

Red = Theoretical uniform compensation.

Blue = Floor displacements due to individual elastic column shortening.

Red = Theoretical floor displacements due to uniform compensation.

figure 5-5: Abstracted concept of uniform compensation. Blue: Deformations due to elastic strains. Red: Displacements due to absolute compensation.

5.3.3 Lumped compensation

"In the lumped compensation, the lengths of vertical members are increased at the lumped level by the amount of lumped correction for a few floors" (Park, Choi, & Park, 2013). On a local position in the building a correction is made by the use of shim plates. This method jacks up the part of the building above the location where the compensation is applied. The concept of lumped compensation is shown abstractly in figure 5-6.

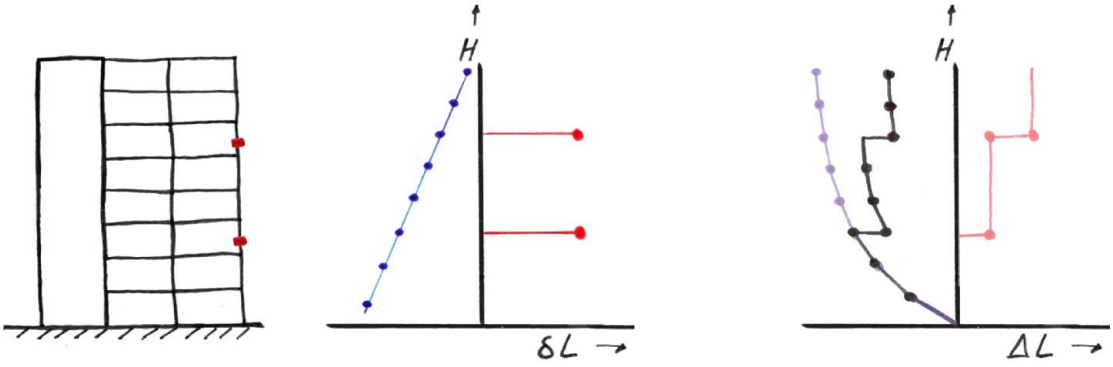

Blue = Individual elastic column shortening.

Red = Theoretical lumped compensation.

Blue = Floor displacements due to individual elastic column shortening.

Red = Theoretical floor displacements due to lumped compensation.

figure 5-6: Abstracted concept of lumped compensation. Blue: Deformations due to elastic strains. Red: Displacements due to absolute compensation.

6 Case study: Tallwood House at Brock Commons

A case study is conducted on the Tallwood house at Brock Commons in Vancouver. The first part will explain the structural design of the building with respect to the superstructure, detailing, the construction sequence and the dealing with differential vertical shortening (DVS) deformations by the designers. The second part is the own analysis on DVS deformations and the determination of the requirements on vertical deformations in the serviceability limit state.

6.1 Building description

Brock Commons is an 18 storey residential building for students of the British Colombia University in Vancouver, Canada. The height of the building is 53 meters and will provide housing for a total of 404 students. This case study will map the structural design using literature that is published by the involved engineers and designers of the building. The structural engineering was performed by Fast+Epp in cooperation with Acton Ostry Architects and Hermann Kaufmann Architekten (Fast, Gafner, Jackson, & Li, 2016).

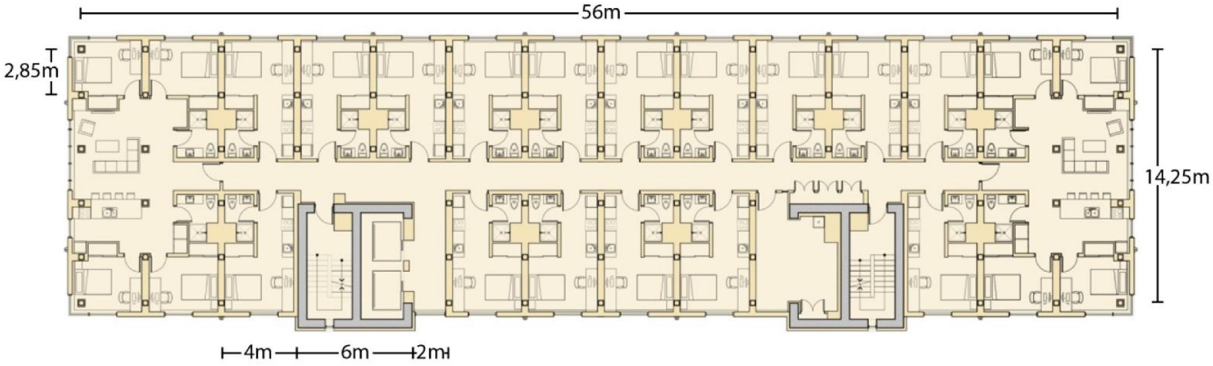

figure 6-1: Floor plan of Tallwood House Brock Commons (Pilon, Utimati, & Jin, 2016).

6.1.1 Superstructure

The 2nd to the 18th floor is made of 5-ply cross laminated timber floors with a concrete topping that are directly supported by timber columns. The mass timber pendulum structure is placed on a concrete platform structure and gains it stability from two concrete cores.

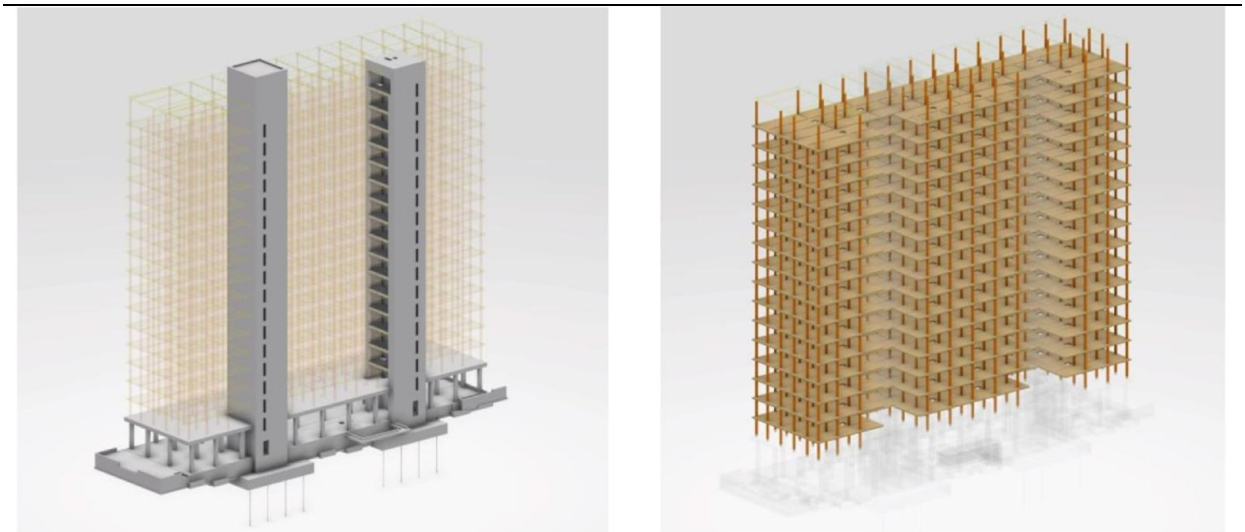

figure 6-2: Structural system Brock Commons (Fast, Gafner, Jackson, & Li, 2016).

The highly loaded columns from the 2nd to the 5th floor are made from parallel strand lumber (PSL). The columns from the 6th to the 18th floor are made from glue laminated timber (GLT). The cross sectional size of the timber columns is 265 x 265 mm from the 2nd to the 9th floor and is decreased to 265 x 215 mm for the timber columns on the 10th to the 18th floor. The timber column design is depicted in figure 6-10 and calculations are elaborated in appendix H.2 on page 169.

The cross laminated timber (CLT) floor has a thickness of 169mm on which a concrete topping is poured of 40 mm. *"The concrete topping was designed primarily for acoustic purposes, but was used for water- and fire-management measures as well"* (Pilon, et al., 2017). The laying pattern of the CLT floor slabs causes that the floor acts as a two-way slab diaphragm structure to direct lateral loads to the concrete cores. The floor is directly supported by the columns that are placed on a 2,85m x 4,0m grid size. The laminations of the CLT slabs are machine stress rated. The outer layers have a modulus of elasticity of $E_0 = 10.300$ Mpa and a bending stress capacity of 23,9 Mpa. The inner layers have a modulus of elasticity of $E_0 = 9.500$ Mpa and a bending strength of 11.8 Mpa (Fast, Gafner, Jackson, & Li, 2016). Whether or not these values are characteristic or design values is not further mentioned by the authors.

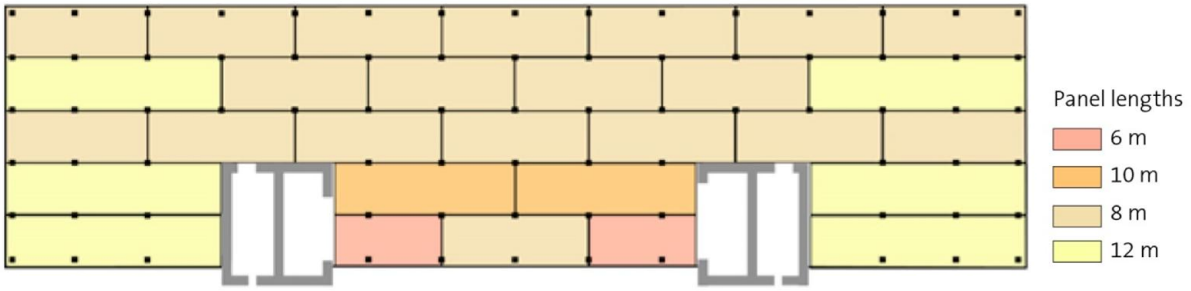

figure 6-3: Panelling plan of CLT floor slabs.

The vision of the structural design was to make a kit of parts that could be easily assembled with little labour on site. This enhanced the building speed and cost reduction. The light weight of the timber columns made it possible to lift them by crane in bundles to install and put them upright by hand. Only the perimeter columns were lifted by crane for safety reasons. The CLT panels came in four different sizes with a total of 29 panels per floor that are connected by a nailed or screwed plywood spline. By directly supporting the floors, the depth of the structural floor could be minimized and the service distribution was not obstructed by beams. Having no beams also means that the amount of construction elements is minimized, which saves crane picks and labour (Fast, Gafner, Jackson, & Li, 2016; Pilon, Utimati, & Jin, 2016).

6.1.2 Detailing

A steel end plate is connected to the column ends by glued in rods . To the steel end plate a structural hollow section is welded. The steel hollow section that is attached at the base of each column fits in the structural hollow section at the top of each column as shown in figure 6-4. The floor is supported at the top of each column and is bolted by four threaded rods pointing upwards on the upper column end plate. This detail causes that the gravity loads are directed to the next column through the steel node, so perpendicular to the grain loading of the floors slabs is avoided. The timber column itself has a length of 2532mm while the total floor to floor height is 2810mm when the steel node is included.

figure 6-4: Column detail (Pilon, et al., 2017; Pilon, Utimati, & Jin, 2016).

At the concrete core the CLT floor slab is picked up by a ledger angle that transfers vertical shear forces from the CLT slabs to the concrete core. At the corners of the concrete core, long drag straps are installed on the top of the CLT slabs to transfer diaphragm forces from the floor to the core to provide stability to the total structure.

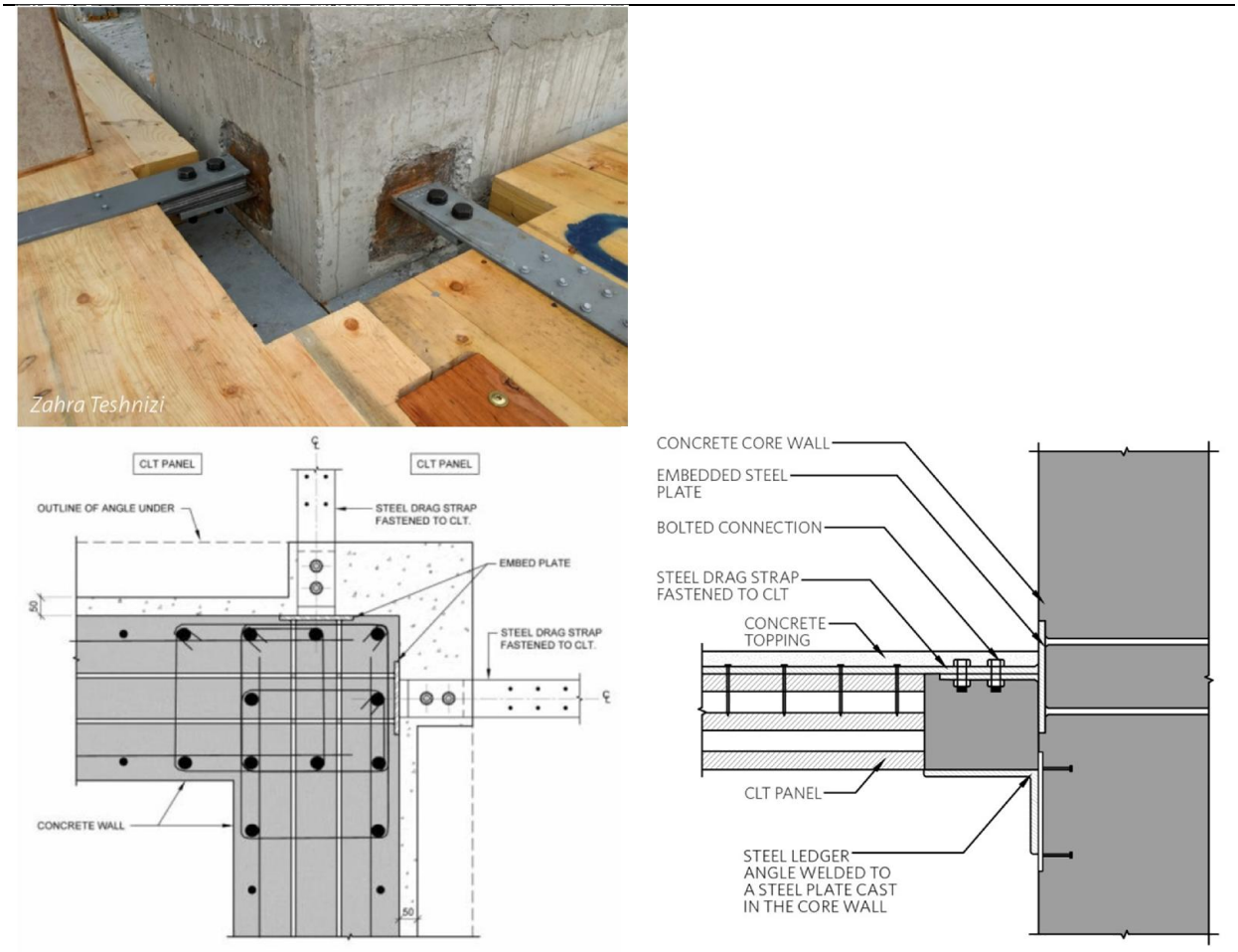

figure 6-5: Floor to core detail of angle ledger and drag straps (Pilon, et al., 2017; Pilon, Utimati, & Jin, 2016)

The ledger angle is installed at its theoretical design datum by welding it to the embeds that are installed in the cast-in-place core. The distance between the angle ledger and the elevator and door sills will variate due to tolerances of the cast in place core. These tolerances are accommodated by applying a slope in the concrete topping of the floor. Tolerances up to 24mm or a deviation of $\pm$12mm can be accommodated by this system. When dimension deviations exceed the slope limitations, the sills will be chipped down or grouted. The description of the core to floor detail is illustrated in figure 6-6.

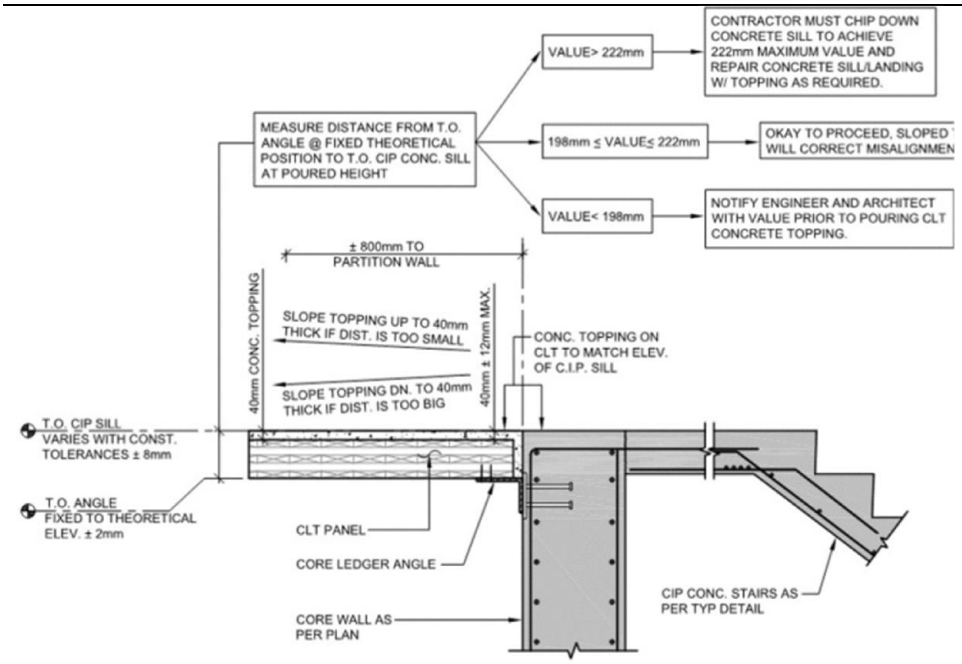

figure 6-6: Floor to core detail at door sill (Fast, Gafner, Jackson, & Li, 2016).

The timber pendulum structure gains its stability from the two concrete cores through diaphragm action of the CLT with concrete floor structure. Steel drag straps are mounted at the core corners to ensure that lateral loads are transferred to the concrete cores.

6.1.3 Building sequence

When looking at the time lapse movie from the construction of the Tall Wood House at Brock Commons, one can see that a floor is added every 4 days. The concrete topping comes approximately 5 floors behind the timber structure (naturally:wood, 2016). Finally the loads due to placement of finishing's like partition walls, ducts, installations and other fixed interiors are exerted on the structure.

6.1.4 Differential vertical shortening

The designers accounted for vertical column shortening of the timber columns, but considered vertical core shortening due to elastic and creep strains as negligible. The dead load from the floors on the cores is relatively small because of the large core wall dimensions for lateral stability reasons. The cores are also built prior to the timber structure, so it is expected that most vertical elastic and creep deformations already have taken place in the concrete before mounting the timber structure. Therefore these deformations are ignored by the engineers (Fast, Gafner, Jackson, & Li, 2016). Core shortening due to shrinkage are not mentioned.

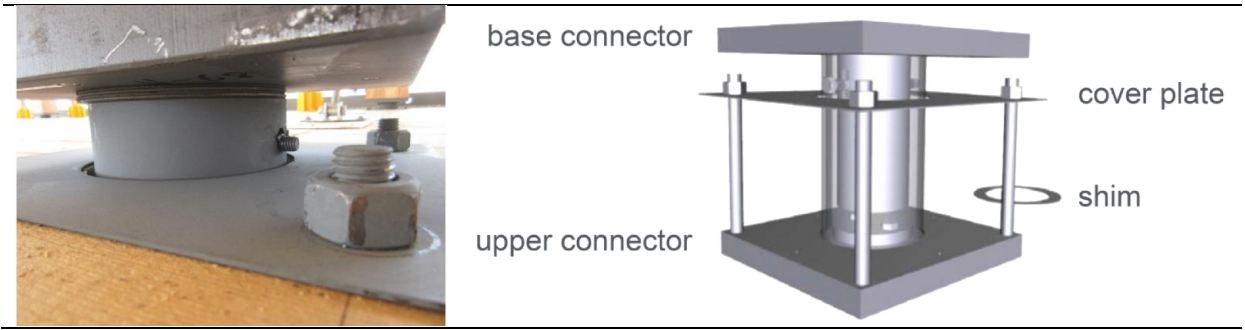

figure 6-7: Application of shim plates in column to column connection detail. Left: (R. Jackson, personal communication, September 13, 2017). Right: (Acton Ostry Architects, Inc., 2016)

The deformations due to the shortening of the columns is cumulative at the roof. The expected column shortening deformations by Fast+Epp are shown in figure 6-8. The figure shows a total deflection at the roof of 48mm, but the sum of all individual deflections is 45mm with a deviation of ±4mm. The predictions shown are the deflections when left unmitigated. To compensate for these effects the plan was to use five shim plates of 1.6mm are placed at the 7th, 11th and 15th level, so at each of these levels there is a compensation of 8mm and 24mm in total (Fast, Gafner, Jackson, & Li, 2016).

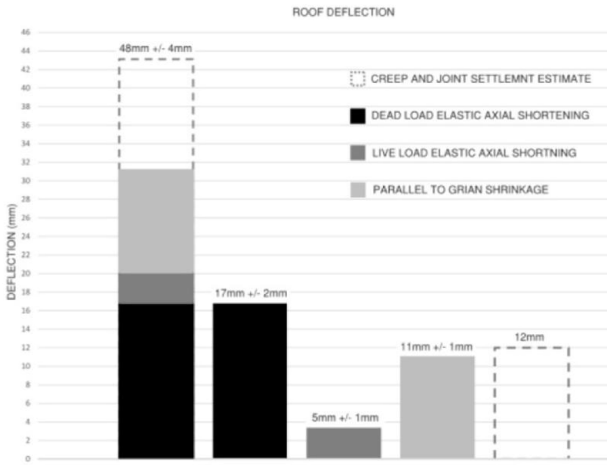

Creep and joint settlement estimate:	12mm
Dead load elastic axial shortening:	17mm +/- 2mm
Live load elastic axial shortening:	5 mm. +/- 1mm
Parallel to grain shrinkage:	11 mm. +/- 1mm

figure 6-8: Cumulative axial shortening at roof (Fast, Gafner, Jackson, & Li, 2016).

6.2 Model description

An analysis on differential vertical shortening of the original Brock Commons design will be conducted and compared to the results that are shown in figure 6-8. A model will be prepared in ETABS, which is an integrated software package for the analysis and design of building structures of 'Computers and Structures, Inc'.

ETABS is used to model the DVS-deformations because it is specialised in modelling building structures. The program allows the user to model the building process in a staged construction analysis. Also, the concrete strain model CEB-fip 2010 is already integrated in the software package. In addition, it also provides the ability to input customized elastic, shrinkage and creep strain models, which is necessary for the representation of the timber strain models that are elaborated in chapter 4.2.

The model is set up beginning from the following starting points:

- The building is considered as being located in The Netherlands. The Dutch standard will be used in the analysis.
- The building will be considered as a consequence class 3 building, because the building has more than 15 floors. According to the Eurocode and Dutch high-rise covenant buildings that are higher than 15 floors should categorized in CC3 (NTA 4614-1, 2012, p. 7; NEN-EN1991-1-7, 2015, p. 32)
- This analysis will use the material strain models that are elaborated in chapter 0.
- The loads that are applied are calculated according to the Eurocode (Appendix H.3).
- Next to a conventional static analysis, a staged construction analysis will be conducted without the use of the levelling effect, because it concerns a prefabricated structure.
- Compensations are applied after the analysis.

- Deformational results will be separated as much as possible in elastic, shrinkage and creep deformations. In the end, results should also be separated in pre- and post-deformations in order to assess the deformations against the serviceability limit state requirements that are based on Eurocode requirements and established in chapter 2.3.1. of this thesis.

- Only the upper structure above the concrete platform will be modelled. This platform structure is assumed as infinitely rigid. This implies that foundation settlements are not considered which is justified in chapter 2.3.1.

6.2.1 Geometry

Modelling the full structure for the analysis of differential vertical shortening is presumed to be unnecessary. To minimize modelling and calculation time, the model only consists out of half of the building in which one concrete core with adjacent columns is modelled as is shown in figure 6-9. On column on the far right side (column 8) additional point loads will be modelled that represent the cut off distributed floor loads which are carried by this column.

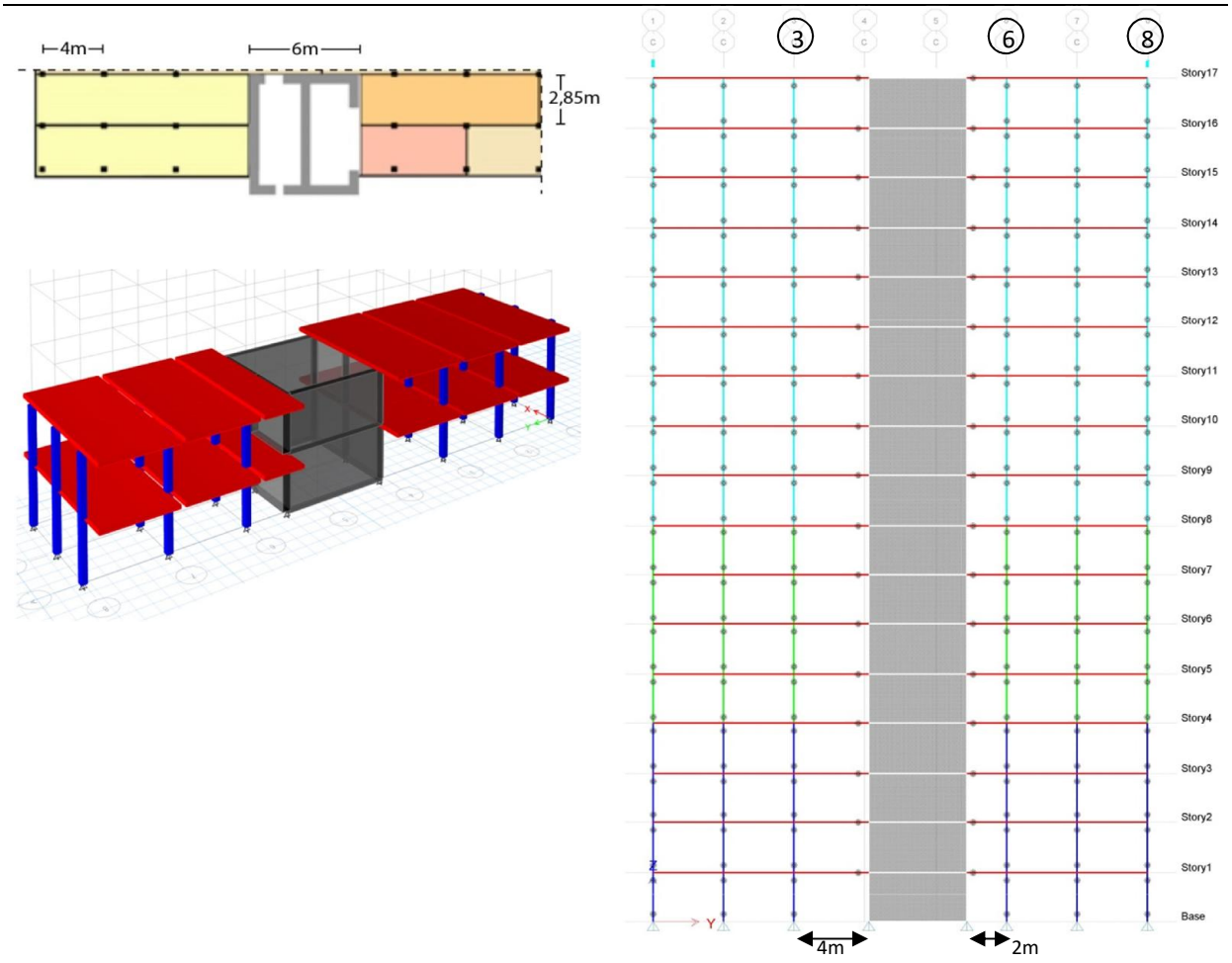

figure 6-9: Plan view, 3D view of the first two stories and elevation view of the mechanical wire frame of the ETABS model.

6.2.2 elements

The column is modelled in two parts. One short part of 278mm in length, with a round steel tube HSS 127x13 cross section assigned to it, resembles the steel node. The longer part of 2532mm has the timber material and cross section as shown in figure 6-10 assigned to it.

The floor slabs are modelled as one way spanning continuous horizontal elements. The cross section of these elements is designed with a corresponding stiffness as the CLT slabs. The floors are attached to the core by a hinged connection.

The core wall is 450mm thick and modelled with the concrete strength class C40/50.

GL24h			
Bending	$f_{m,k}$	24	N/mm^2
Tension parallel	$f_{t,0,k}$	16,5	N/mm^2
Tension perp	$f_{t,90,k}$	0,5	N/mm^2
Compression parallel	$f_{t,0,k}$	24	N/mm^2
Compression perp	$f_{c,90,k}$	2,7	N/mm^2
Shear	$f_{v,k}$	2,5	N/mm^2
Parallel	$E_{0,mean}$	11600	N/mm^2
Perpendicular	$E_{90,mean}$	390	N/mm^2
Shear	G_{mean}	720	N/mm^2
Characteristic Density	ρ_k	380	kg/m^3
PSL 2.0E			
Bending	$f_{m,k}$	59	N/mm^2
Tension parallel	$f_{t,0,k}$	-	N/mm^2
Tension perp	$f_{t,90,k}$	0,9	N/mm^2
Compression parallel	$f_{c,0,k}$	32	N/mm^2
Compression perp	$f_{c,90,k}$	2,8	N/mm^2
Shear	$f_{v,k}$	2,5	N/mm^2
Parallel	$E_{0,mean}$	14300	N/mm^2
Perpendicular	$E_{90,mean}$	-	N/mm^2
Shear	G_{mean}	530	N/mm^2
Characteristic density	ρ_k	703	kg/m^3

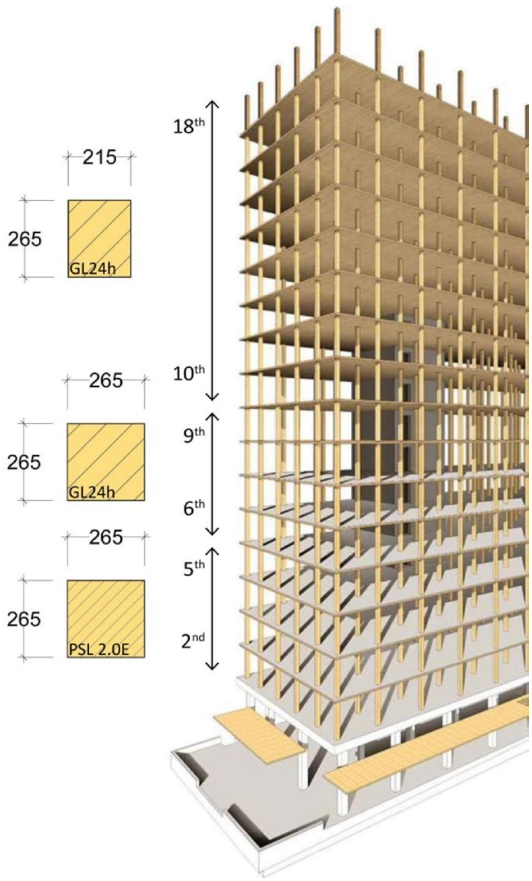

figure 6-10: Assumed material properties for the timber columns.

6.2.3 Load patterns

The characteristic floor loads that are used in the model can be found in appendix H.3. Three permanent load patterns for the floor loads are implemented in the model: The 'Timber structure', 'Concrete topping' and 'Finishes'. The 'Timber structure' load pattern represents the self-weight of the CLT slabs and columns. The 'concrete topping' load pattern represents the self-weight of the 40mm concrete topping layer. The 'Finishes' represents the mechanical systems, partition walls, floor finishings gypsum boards etcetera.

The core self-weight is not considered as the cores are build prior before the timber structure. Elastic deformations have already occurred before the angle ledgers are aligned and mounted on their position. Because the cores are build 2 months in advance, it is expected that most creep deformations due to the own weight of the core also have occurred by the time the timber structure is erected.

The induced floor live load is classified as a residential floor load. When calculating columns or walls in a building with more than two floors, the total induced floor loads may be reduced for the probability of simultaneity by the factor Ψ_0 except for two floors (NEN-EN 1991-1-1+C1/NB, 2011). The quasi-permanent part of the induced live load is determined by the factor Ψ_2.

Load pattern	**Floor surface load**		**Distributed line load** $(\cdot\, \mathbf{2,85}\boldsymbol{m})$	
Timber structure	0,77	kN/m^2	2,2	kN/m
Concrete topping	1,0	kN/m^2	2,85	kN/m
Finishes	1,23	kN/m^2	3,5	kN/m
Quasi -Live	$0{,}3 \cdot 1{,}75$	kN/m^2	1,5	kN/m

table 15: Load patterns used in the ETABS model.

Using the combination of the load patterns in table 15 results in the quasi-permanent load combination that is normally used for the long-term effects and the appearance of the structure (NEN-EN 1990, 2011, p. 48). The vertical short-term effects on the vertical load bearing structure are determined by applying the $\Psi_0 = 0{,}4$ factor on the live loads except for two floor in the building. This would be a variant on the characteristic load combination. This load combination is not considered further in the analysis as it increases the quasi live load only by 33%. The value of the total quasi-permanent load combination would only be increased by 5%.

$\sum_{j\geq 1} G_{k,j}\ "+"P"+"Q_{k,1}"+"Q_{k,2}"+"\sum_{j\geq 1} \Psi_{0,i} Q_{k,i}$	*(6.14b)*	*Characteristic load combination*
$\sum_{j\geq 1} G_{k,j}" + "P" + "\sum_{j\geq 1} \Psi_{2,i} Q_{k,i}$	*(6.16b)*	*Quasi permanent load combination*

table 16: Quasi permanent load combination and characteristic load combination (NEN-EN 1990, 2011, p. 48).

6.2.4 Staged Construction Loadcase

“Staged construction is a static modeling, analysis, and design application which enables the definition of a sequence of construction stages in which structural systems and load patterns are added or removed, and time-dependent behaviors are evaluated, including creep, shrinkage, aging (change in elastic modulus with age), and tendon relaxation” (Abell, 2012).

First one should determine if the building method is according to the ‘fixed column length’ or ‘adaptive column length’. An explanation on these two building methods is given in chapter 5.2 on page 83.

Adding the structure story by story per building stage in ETABS will result in an analysis that simulates the building sequence of a structure that uses the ‘adaptive column length’ building method. This is because ETABS ads the structure at the original intended design datum and provides an over length in the column, which causes that deformations that occur before the installation of a storey are automatically corrected. This principle is shown in figure 5-2 on page 84.

When a stage construction analysis with ‘fixed column length’ is desirable, a staged construction analysis can be conducted with a so-called ‘Ghost structure’. Adding a ‘Ghost structure’ in the first stage with zero to minimum stiffness and weight properties, ensures that the geometry of all elements is placed, and by that fixed from the first stage. Because of the zero stiffness properties the elements do not yet contribute to the structural stiffness. As a certain story is built in reality, the element properties for this story are changed in the model to the design properties and are loaded according to the load patterns that are active at that moment.

As the element properties are changed, the elements do contribute to the structural stiffness. The part of the structure that still has ‘ghost properties’ assigned to it will move along with the deformations that occur during the building process, but will not contribute to them due to the zero stiffness of the ghost structure.

The original design of Brock Commons makes use of prefabricated columns and uses ‘dry’ connections. Floor and column elements are simply stacked on top of the previous column. This ensures that the column length is fixed, except for locations where consciously compensation is applied with the use of shim plates. This compensation is not included in the analysis, but is applied afterwards on the analysis results. The building sequence is depicted in figure 6-12 for the first 12 stages. The total input for the staged construction load case in ETABS for the original Brock Commons design is elaborated in appendix H.4 on page 173.

A time lapse video of the Brock Commons building sequence shows that every 4 days a floor is added. When the fifth floor is added, the concrete topping on the first floor is poured and follows the same building speed as the timber structure (naturally:wood, 2016). For the ‘Finishes’ load pattern it is assumed that it takes 3 times as long for one floor and that this start approximately halfway erecting the timber structure. This is deduced from the construction overview in the top picture of figure 6-11. The structure is at its completion when the last ‘Finishes’ load pattern at the top floor is applied. 90 days after completion half of the ‘Quasi-Live’ load pattern is applied on all floors. After another 90 days the second half is applied on all floors. At this moment (180 days after completion) the building is fully occupied.

Brock Commons construction overview

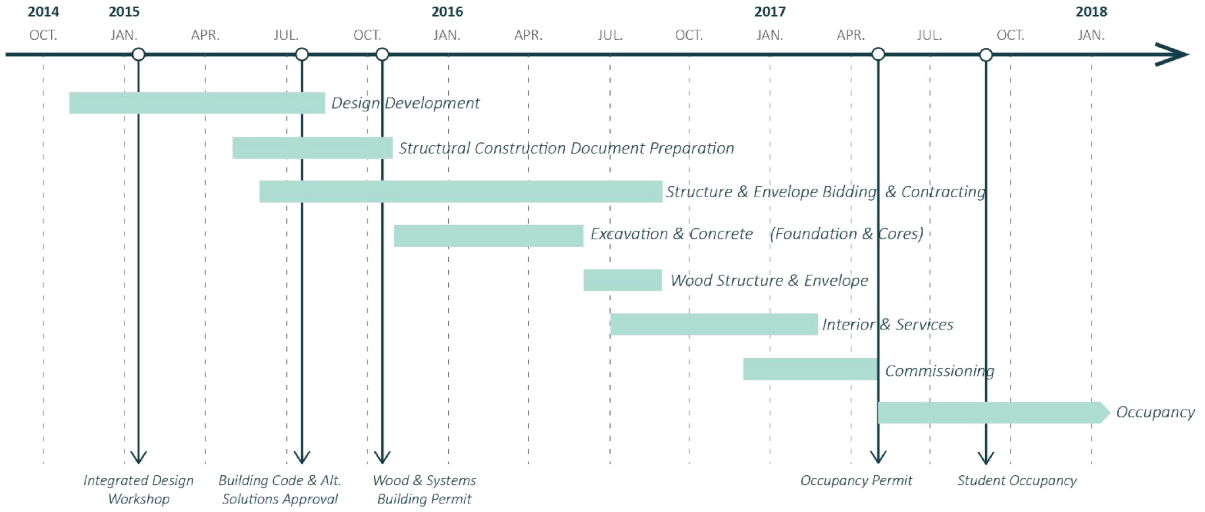

figure 6-11: Top: Building schedule overview of Brock Commons (Pilon, et al., 2017). Modelled load increments in the building process.

Load patterns:

Timber Structure (blue)

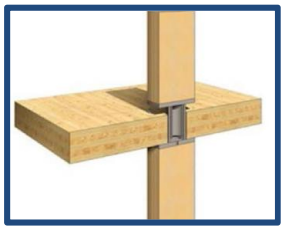

0,77 kN/m^2
2,2 kN/m

Concrete topping (red)

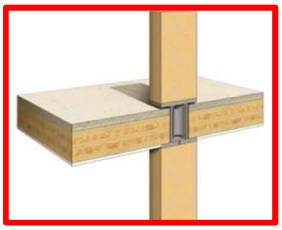

1,0 kN/m^2
2,85 kN/m

Finishes (green)

1,23 kN/m^2
3,5 kN/m

Stage0

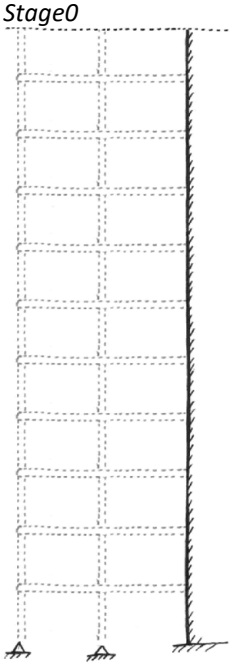

Stage1 (4days)

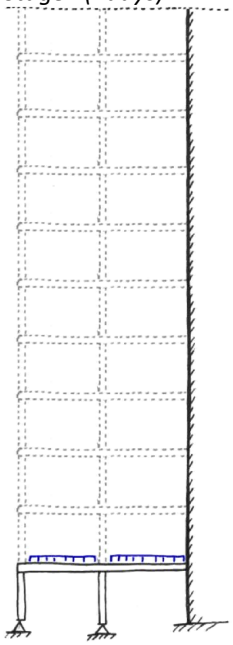

Stage2 (4days)

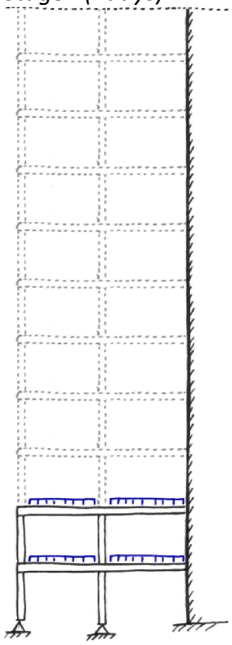

Stage3 (4days)

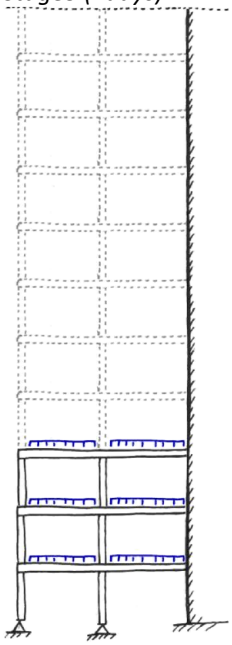

Stage4 (4days)

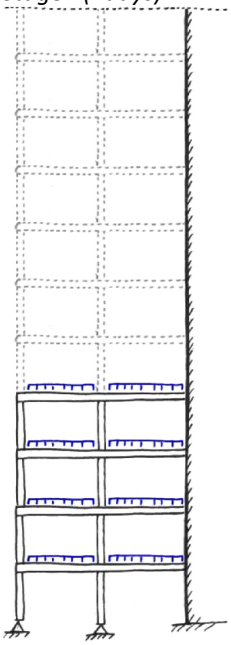

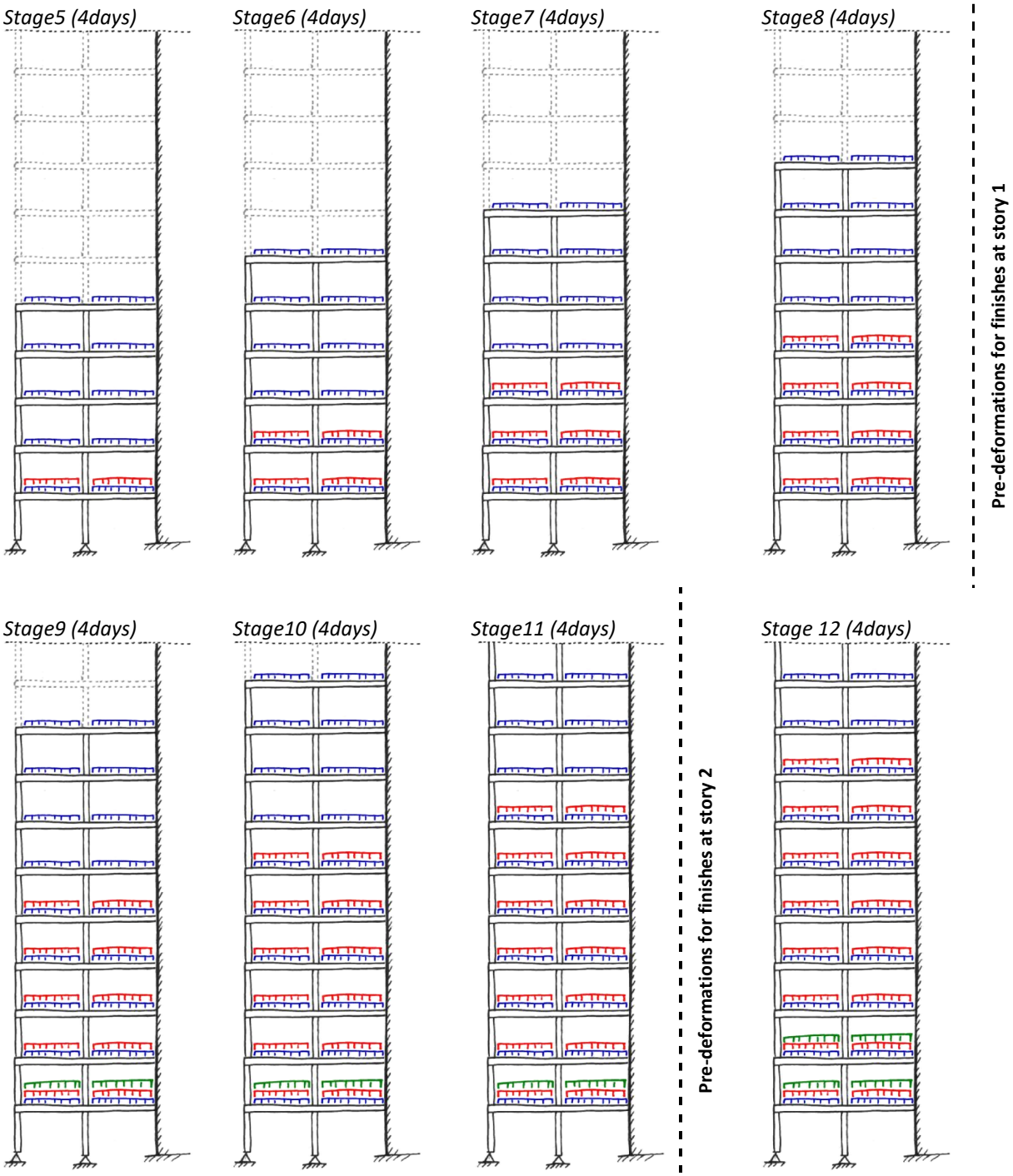

figure 6-12: Modelled building sequence of Brock Commons design (does not show deformations).

6.3 Model validation

The model that is presented in the previous chapter will be validated with analytical hand calculations with the use of Maple at several time moments in the building sequence loadcase. Time dependent deformations are not considered in the validation model.

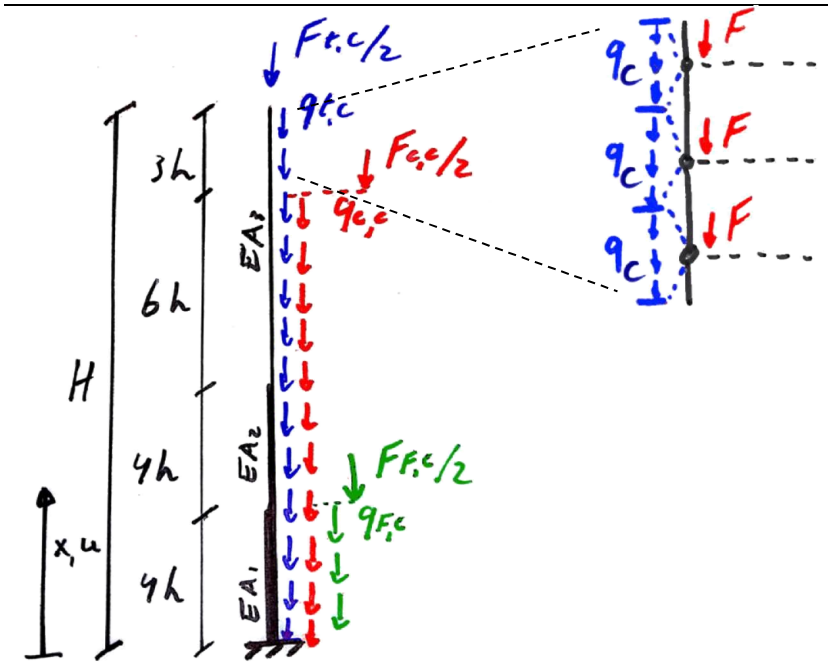

figure 6-13: Bar model that is solved with maple for stage 17.

A bar model is evaluated with the use of maple and compared to the ETABS model at stage4, stage8 and stage18. The bar is loaded according to the load patterns that are applied in the considered stages. The load patterns that are present per floor in stage 4, stage 8 and stage 18 are depicted in figure 6-14 and figure 6-15 together with the corresponding vertical deformation results. Stage 4 is also calculated by hand for validation of the simplified bar model in Maple. A more extensive elaboration for the model validation at the three considered stages is given in appendix H.5 starting from page 176.

Stage4		***Hand calculation***	***Maple***	***ETABS***
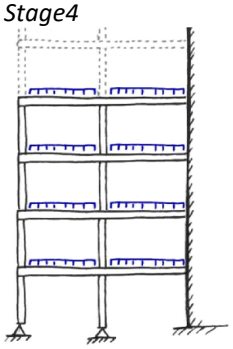	$\Delta L_4 =$	$-0{,}277mm$	$-0{,}277mm$	$-0{,}290mm$
	$\Delta L_3 =$	$-0{,}249mm$	$-0{,}249mm$	$-0{,}256m$
	$\Delta L_2 =$	$-0{,}194mm$	$-0{,}194mm$	$-0{,}197mm$
	$\Delta L_1 =$	$-0{,}110mm$	$-0{,}111mm$	$-0{,}112mm$

Stage8			***Maple***	***ETABS***
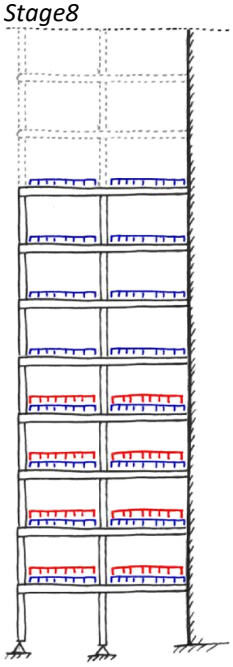	$\Delta L_8 =$		$-1{,}479mm$	$-1{,}485mm$
	$\Delta L_6 =$		$-1{,}376mm$	$-1{,}346mm$
	$\Delta L_4 =$		$-1{,}134mm$	$-1{,}091mm$
	$\Delta L_2 =$		$-0{,}694mm$	$-0{,}670mm$

figure 6-14: Comparison between hand calculations, Maple calculations and ETABS results for the applied loads in stage 4 and stage 8.

Stage18		***Maple***	***ETABS***
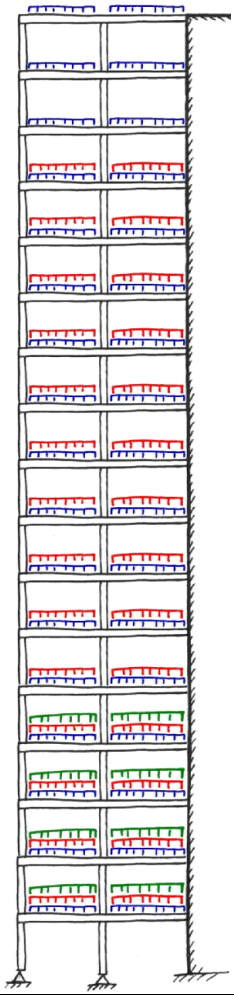	$\Delta L_{17} =$	$-10{,}137mm$	$-9{,}839mm$
	$\Delta L_{14} =$	$-9{,}883mm$	$-9{,}561mm$
	$\Delta L_{8} =$	$-7{,}072mm$	$-6{,}783mm$
	$\Delta L_{4} =$	$-3{,}971mm$	$-3{,}828mm$

figure 6-15: Comparison between Maple calculations and ETABS results for the applied load patterns in stage 18.

The results of the hand calculations are the same as the results from the maple model and by that the maple model is validated. The vertical deformation results of the ETABS model are slightly higher in stage 4 and stage 8 and slightly lower in stage 18. These differences can be attributed to the fact that the maple model does not consider load redistributions through the floors, because the floors are not modelled. Also the steel nodes are not modelled in the maple model, which can cause some small differences in the total column stiffness between both models.

The results of the maple model and the ETABS model are of the same order of magnitude. Differences can be explained because of simplifications in the maple model. For this reason it may be assumed that the ETABS model gives reliable results regarding vertical elastic deformations.

6.4 Analysis on differential vertical shortening

In this chapter an analysis is conducted on the deformations due to column shortenings of the column next to the core. On column stand 2 meters away from the core and the other stands 4 meters away from the core. This analysis is conducted to give a comparison with the column shortening deformations that are predicted by the engineers of the Brock Commons design. After that, the analysis is expanded by considering also the deformations due to vertical core shortening. Both the core and column vertical deformations should be analysed in order to obtain the differential vertical shortening (DVS) deformations. The building sequence is of importance to distinguish post- from total-DVS deformations. These deformations can be assessed against the

serviceability limit state (SLS) requirements that are established in chapter 2.3.1 on basis of Eurocode principles.

Analysis design

The serviceability limit state criteria for this case study are determined according to the criteria from chapter 2.3.1. The serviceability state criterium for the lateral drift of the building is used to determine the maximum vertical movement $u_{lateral} = 8mm$ according to the procedure in appendix G. This is dependent of the core width and the maximum angular rotation of the core. The resultant requirement for DVS deformations is shown in equation 15 for the 2 meter span and the 4 meter span at both sides of the core. It shows that the requirement is extended severely when considering a longer span.

figure 6-16: DVS analysis and serviceability state requirement.

The nonlinear staged construction loadcase makes it possible to generate deformation results at different moments during- and after the building process. For the analysis, the results are generated at the moment that the building is completed, that it is fully occupied, 1 year after occupation, 10 years after occupation and 50 years after occupation. Furthermore, pre- and post-deformations at each floor relative to the moment that the 'Finishes' load pattern is applied at that particular floor are distinguished. This means that the pre-deformations for every floor should be given at a different moment in time during the building process, namely the moment at which the 'Installations' load pattern is applied at that particular floor. The corresponding post-deformations are obtained by subtracting the pre-deformations from the total maximum deformations that are predicted in the service life of the building.

$$\Delta L_{post} = \Delta L_{total} - \Delta L_{pre}$$

2 meter span:

$u_{post-DVS} \leq \theta_{2+3} \cdot l - u_{lateral} = 6/1000 \cdot 2000 - 8 = 4mm$

$u_{total\ DVS} \leq \theta_{max} \cdot l - u_{lateral} = 8/1000 \cdot 2000 - 8 = 8mm$

4 meter span:

$u_{post-DVS} \leq \theta_{2+3} \cdot l - u_{lateral} = 6/1000 \cdot 4000 - 8 = 16mm$

$u_{total\ DVS} \leq \theta_{max} \cdot l - u_{lateral} = 8/1000 \cdot 4000 - 8 = 24mm$

equation 15: Serviceability limit state criteria according to chapter 2.4 for the case study.

Results

The total maximum column shortening that was predicted by the engineers (figure 6-8) is compared to the total maximum column shortening deformations ΔL_T that is found in this analysis with the ETABS model in figure 6-17. The deformations due to shortening of the core are not yet considered in the ETABS results to make them comparable with the results that are provided by the engineers. In the results that are obtained from the ETABS analysis it was not possible to distinguish the deformations due to shrinkage from the

deformations due to creep because one would affect the other. For this reason the creep and shrinkage deformations are taken together in the representation in figure 6-17.

The maximum value for the total column shortening is found at 50 years after occupation at the highest floor in the building. The column shortening deformation results of the top five floors from the analysis in ETABS are shown in figure 6-17. For column three, the values are higher than for column six. This is because column six is standing closer to the core, causing more load redistribution from the column to the core and that the floor surface that is being carried by this column is smaller.

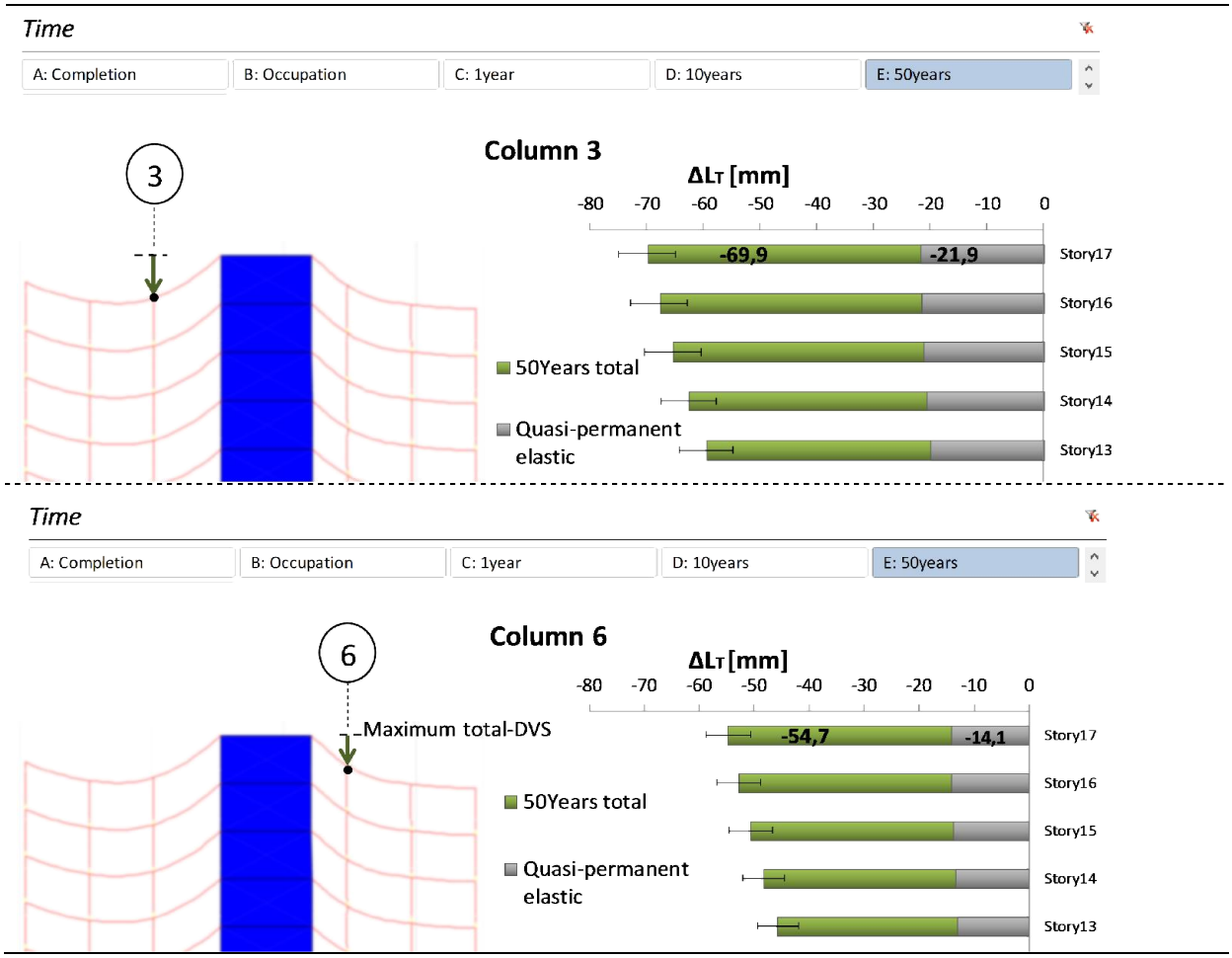

figure 6-17: Maximum column shortening deformations at the top of the building from the ETABS analysis (Fast, Gafner, Jackson, & Li, 2016).

The maximum column shortening deformations at the top floors are compared with the column shortening results that are provided by the engineers of Brock Commons. These original results are shown in figure 6-8 and adopted in figure 6-18. The results on vertical elastic deformations from the engineers are comparable to the vertical elastic deformation results in column three from the ETABS model. The time dependent deformations are much higher in the ETABS analysis with which can be attributed to the higher creep factor and higher amount of shrinkage that is determined in chapter 4.2.

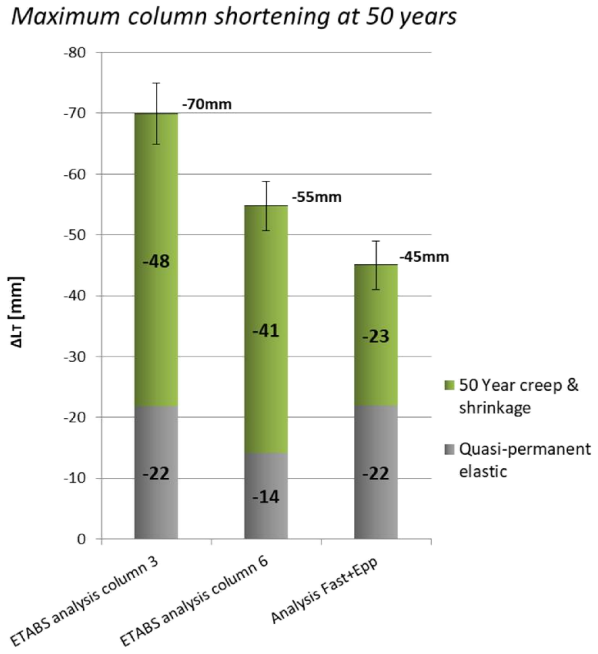

Two left bars are the maximum column shortening deformation values from figure 6-17. The right bar are the results that are provided by the engineers of Brock Commons from which the original results are shown in figure 6-8.

figure 6-18: Comparison of maximum column shortening deformation from the ETABS analysis with the column shortening deformation results provided by the engineers.

The differential vertical shortening (DVS) deformations between both column 3 and 6 and the core are shown in figure 6-19 at 50 years after occupation. In these results, also the deformations due to shortening in the concrete core are considered. Appendix H.6 shows a comprehensive view on the development of the DVS deformations between column 3 and the core floor supports and column 6 and the core floor supports at all considered time moments and floors. The serviceability limit state criteria that are determined in equation 15 for both columns and the corresponding spans are indicated on the background of the graph along with the DVS results. It shows that the requirements at the right of the core are a lot more stringent due to the shorter span at this side.

In the results shown in figure 6-19, no compensation measures are considered. The strategic plan in the original design was to apply 8mm compensation with the use of shim plates at the 7^{th}, 11^{th} and 15^{th} storey. The results where compensation is considered are shown at the 50year time moment in figure 6-20.

The graph shows the amount of compensation by showing the positive upward translation of 0 to 8, 16 or 24 mm that the floor support points experience, depending on the floor level. The amount of deformation is not affected, but only the total-DVS deformations that should be assessed to the SLS requirement are decreased and occur at lower floor levels. The post-DVS deformations are not affected.

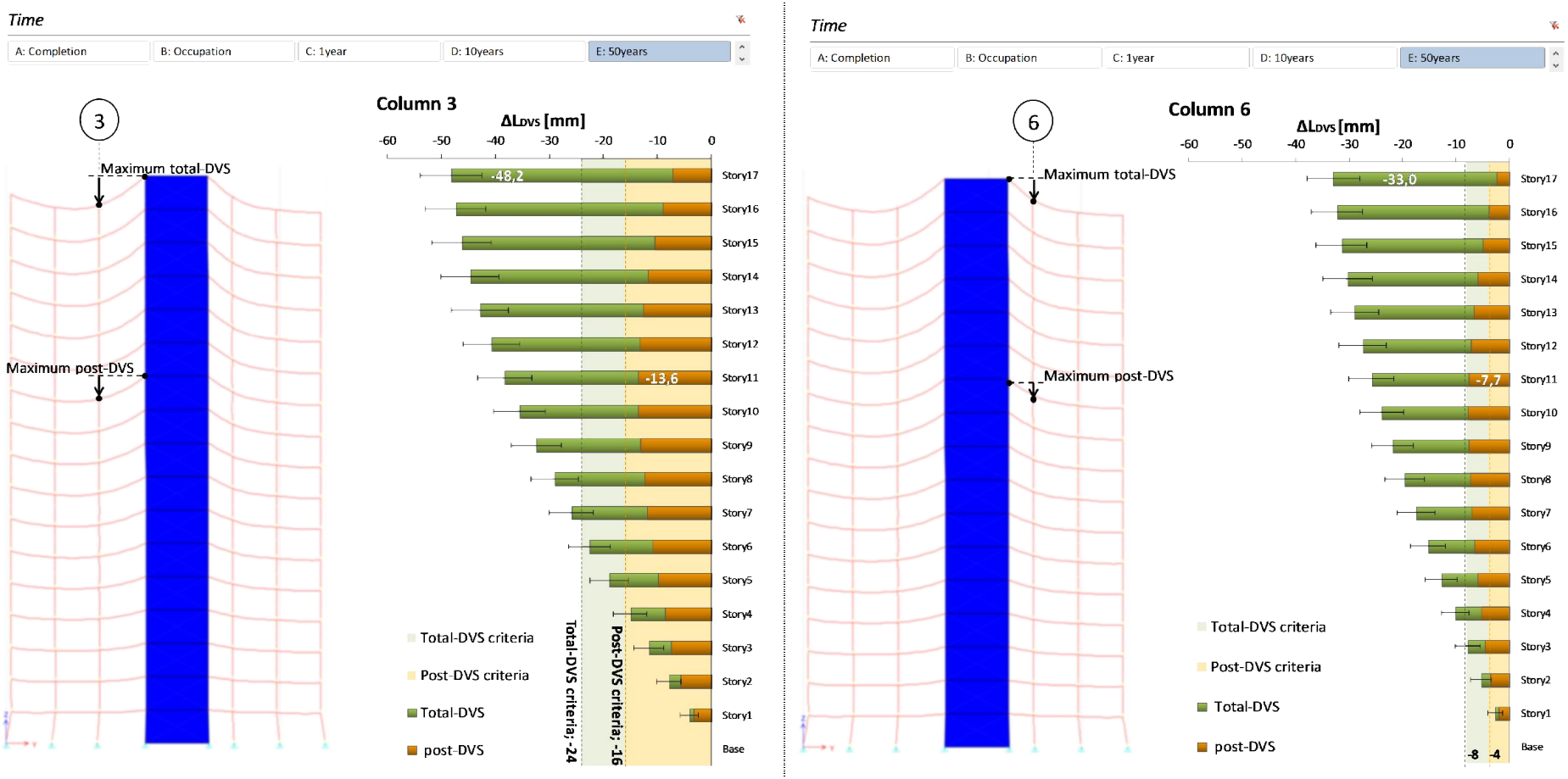

figure 6-19: The total- and post-DVS deformations at 50 years and the SLS criteria. Left: DVS deformations between column 3 and the core. Right: DVS deformations between column 6 and the core.

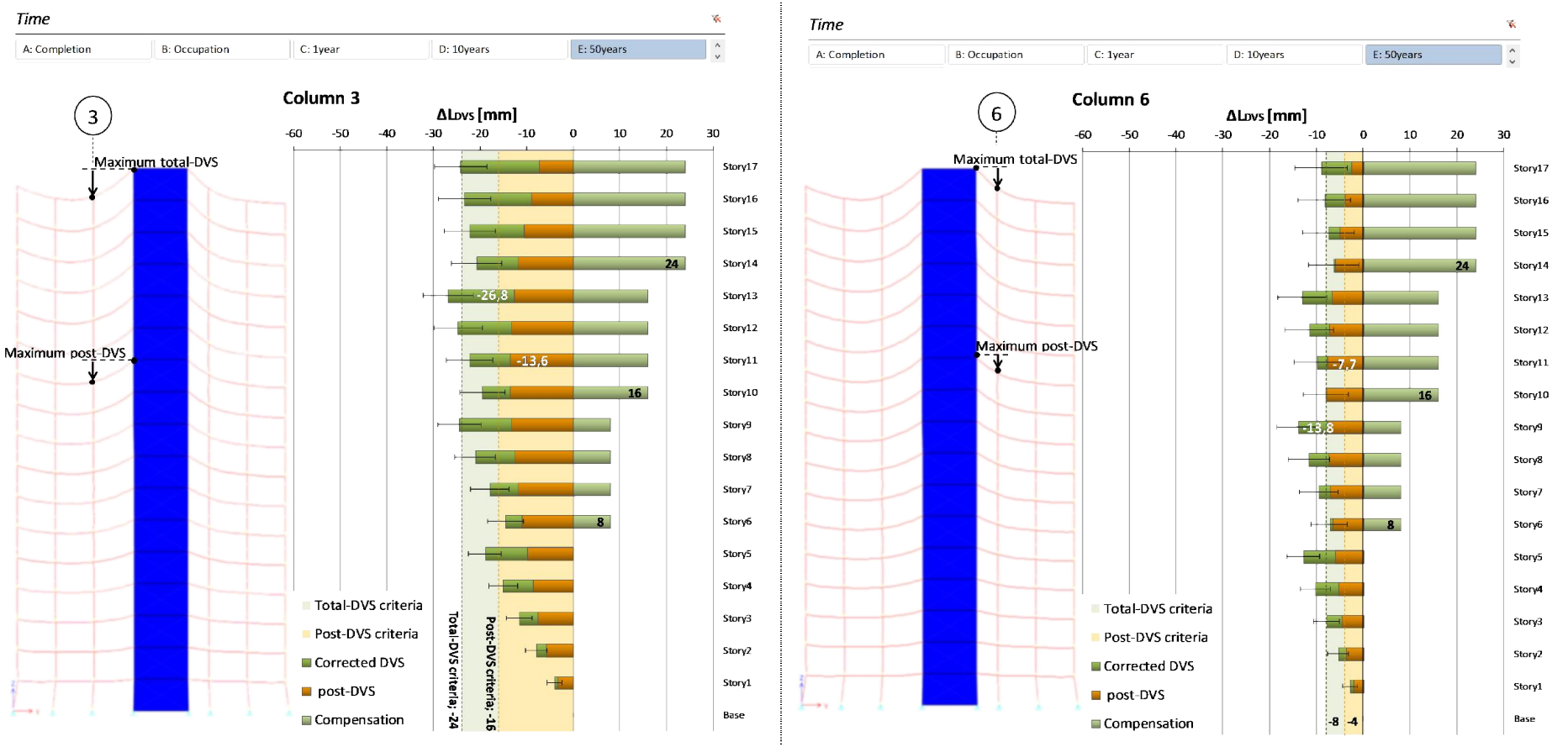

figure 6-20: The total- and post-DVS deformations at 50 years including compensation and the SLS criteria. Left: DVS deformations between column 3 and the core. Right: DVS deformations between column 6 and the core.

In figure 6-21 the DVS deformations between column 3 and the core are shown over the 50 year service life of the building. The graphs show that most of the post-DVS deformations occur within 1 year after occupation. After 1 year the DVS deformations stay nearly constant. The total-DVS deformations do even recover for the non-compensated analysis after one year. These maximum total-DVS deformations are measured at the top floor level. In the compensated analysis the total-DVS deformations starting from 0, are significantly lower. These results are measured at the 9th floor level as here the maximum occurs.

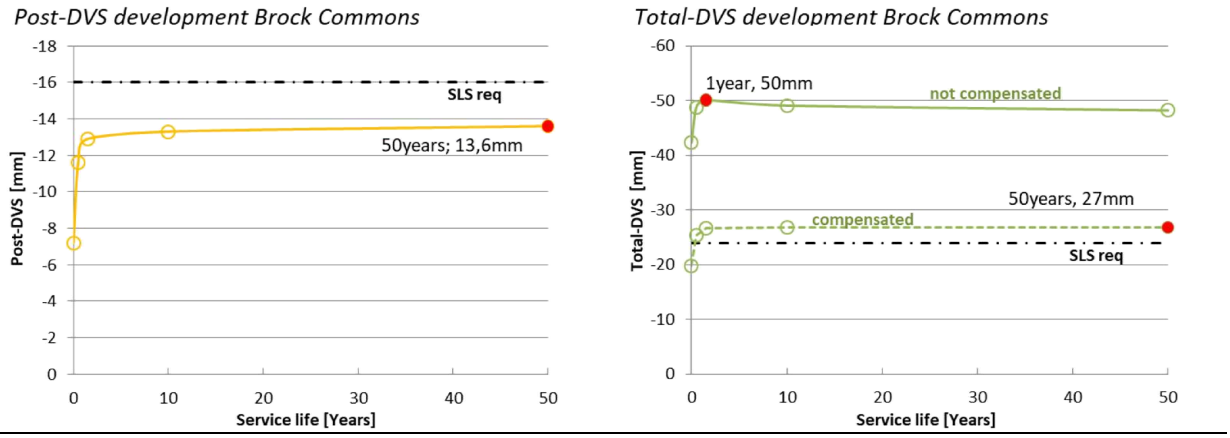

figure 6-21: Post- and total-DVS developments over the building service life.

Finally, the post-DVS deformations meet the SLS requirement but are not affected by the compensation. The total-DVS deformations do not comply with the SLS requirement for both the non-compensated and compensated analysis. However, the compensations causes a significant decrease on the total-DVS deformations.

Conclusions

The analysis regarding vertical deformations is first conducted by only considering the deformations due to column shortening and neglecting the deformations due to core shortening. The results are compared to the results that are provided by the structural engineers of the Brock Commons project. Firstly, the values do not represent the wanted DVS deformations as they ignore core shortening deformations due to shrinkage and only consider the deformations of the columns individually. Secondly, the deformations are subdivided in elastic and time dependent deformations, which is not a representation of the values that should be assessed to the established SLS requirements, namely the total- and post-DVS deformation criteria that is determined in chapter 2.3.1. But the ETABS results and the results from the engineers of Brock Commons are comparable and in the same order of magnitude regarding elastic deformations.

From the analysis in ETABS, the post-DVS deformations are distinguished from the total-DVS deformations. These values can be assessed against the SLS requirements that are depicted in figure 6-16. The values will be lower when compared to the values in figure 6-17, because core shortening is considered. However, the SLS requirement regarding DVS-deformations between column 6 and the core are very small, and because of that the SLS requirement cannot be met.

The compensation plan is applied on the DVS-results. It shows that the total-DVS deformations that should be assessed against the SLS requirement are reduced significantly, but do still not meet the SLS requirement. The post-DVS deformations are not affected.

From the results that are discussed previously, the following conclusions can be drawn:

- Only considering the column shortening and neglecting the core shortening gives results that are not representing DVS-deformations. Using these values will give an overestimation of the problem.

- The total DVS-deformations should be subdivided in total- and post-DVS deformation in order to asses them to the SLS-requirements.

- The span length between the core and the adjacent column has a considerable influence on the serviceability state requirement concerning DVS deformations. The short 2 meter span causes that the SLS requirement is unreachable for between column 6 and the core.

- The individual column shortening and core shortening increases in the course of time due to the time dependent deformations creep and shrinkage. However, the resultant DVS deformations can develop differently and can even decrease in the course of time. In this case, the total-DVS deformations do not further increase after one year.

- Compensation can be effective in decreasing the total-DVS deformations that should be assessed against the serviceability limit state requirement. However, post deformations will not be affected.

Discussion

In this case study analysis, the previously found information with regard to material strain models, SLS requirements, building sequence and compensation, is applied in a model in ETABS with a geometry that is based on the Brock Commons design.

The results that are generated in ETABS on the individual column shortening deformations differ with 25mm and 15mm for column 3 and column 6 respectively with the results that are provided by the engineers. However, this difference can be explained by the higher creep factor that is used compared to the building code. This higher value is found by the analysis of experimental studies that was conducted by other researchers. The amount of shrinkage in the own analysis can be higher due to a higher estimation of moisture content decrease in the timber elements. Whether or not this is an overestimation is difficult to capture as it is dependent on environmental conditions during manufacturing transport and construction.

7 Sensitivity/variable study on DVS deformations

In this chapter a sensitivity analysis will be conducted between the total- and post-DVS deformations as dependent variables and several other independent variables of the design and building process. The following independent variables will analysed:

- *Building height*
- *Relative column capacity*
- *Building speed*

These variables are considered as 'independent' input variables, but in reality the variety of these variables can be limited due to dependency on for instance: The building assignment, design process, building methods, site conditions etc.

The analysis is conducted by using a staged construction analysis in ETABS with fixed column length. Using a staged construction analysis gives the possibility to obtain the deformations at every floor at the time that the installation+finishing load case is applied on every floor. This gives an insight in pre- and post deformations regarding the technical and architectural systems. Just as in the case study analysis, the results will be retrieved at the moment of completion, at occupation, at 1year after occupation, at 10 years after occupation and 50 years after occupation. The values that are of interest are the maximum total- and maximum post-DVS deformations in the service life of the building.

7.1.1 Variation in building height

In this chapter the effect of increasing or decreasing the building height on differential vertical shortening is studied.

Research design

First, a column design is made for an increasing height of eight additional floors by lifting up the original design of Brock Commons and placing two times four floors underneath that prosecutes the discontinuity rhythm in column properties of the original column design. Secondly, the column properties will be designed based upon the principle that the column utilization should be comparable on the governing locations. Calculations on the redesign are elaborated in appendix I.2 on page 203. The column redesign for increasing the building with eight floors is shown in figure 7-1. From this redesign four height variants can be made next to the original Brock Commons design by removing one, three or four column type layers of four floors from the redesign.

In this study it is assumed that the core can provide enough stiffness for lateral stability for all height variants. Because the vertical deformations due to elastic and creep strains in the core are negligibly small, it is assumed that a redesign of the core for stiffness increase will not affect the vertical deformation of the core, because shrinkage would not be affected under the condition that the wall thickness, thus notional size would stay the same. The building sequence is kept the same for every variant, by keeping building speed and the time moment at which loadcases are applied relative to the start of building on every floor the same.

Goal	The goal of this variation is to research the effect of an increasing or decreasing building height on the differential vertical shortening.
Assumptions	The utilization of the columns will be the same as the original design: $\frac{N_{ed}}{N_{rd}} = Constant$ It is assumed that buckling is not a governing factor, because the column cross section will increase, the column length will stay constant and the stress relative to strength will stay constant. The performance of the lateral stability system will be the same as the original design: $\frac{\delta_{EI}}{H/500} = Constant$ The building sequence schedule is kept the same for every height variant.

table 17: Goals and assumptions for the building height variant.

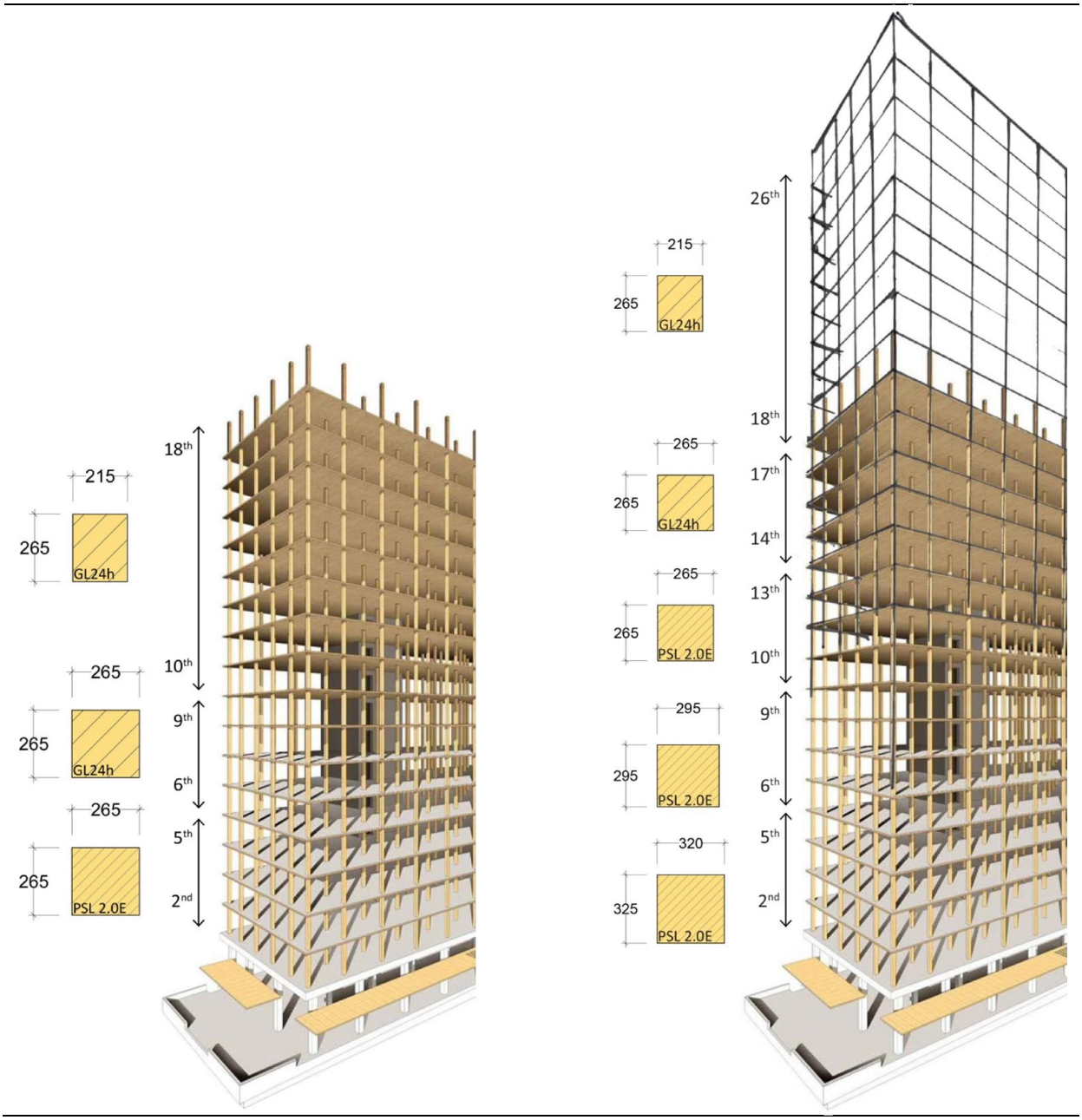

figure 7-1:Original column design (left) and the column design of the height variant.

Results and analysis

The results of the maximum total-DVS and maximum post-DVS between the core and column 3 regarding the height level in the building, are retrieved from the ETABS model for all analysed time moments and are presented in figure 7-2. The graphs show the results for every height variation and the starting point which is retrieved from the original design in the case study analysis and indicated by 0. Next to the results, the SLS criteria for the total-DVS and post-DVS as determined in the case study are shown in the graph.

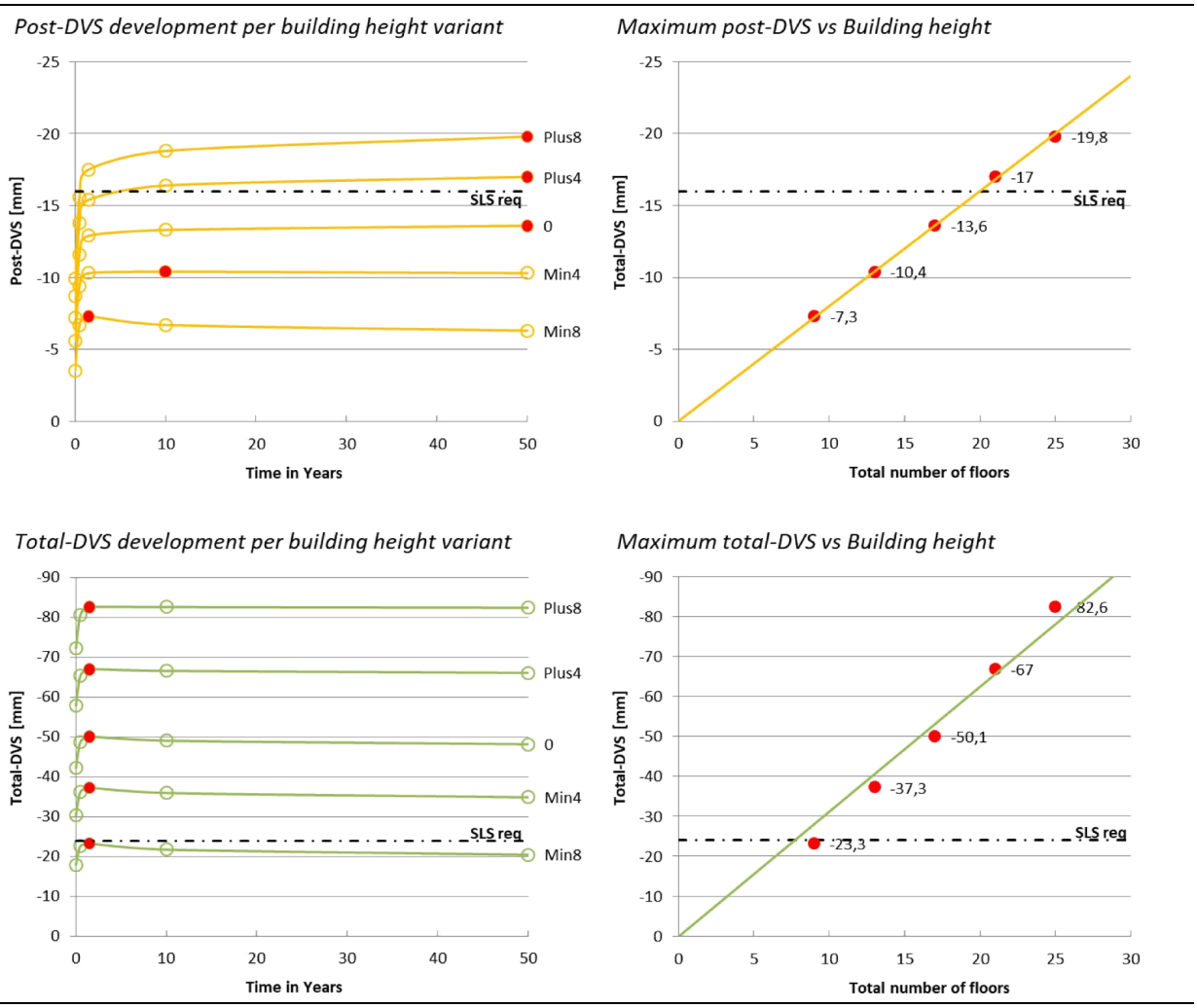

figure 7-2: Left: Total- and post-DVS deformations per variant over the service life, Right: Correlation between Maximum total- and post-DVS and the building height.

Most of the maximum total-DVS deformations and post-DVS deformations occur within 1 year after occupation. For the 'Plus4' and 'Plus8' variant, the post-DVS deformations increase slightly after this moment. The smaller variants show a small recovery on the total- and post-DVS deformations. The maximum values over the building service life are plotted in the right graphs of figure 7-2.

The right graph of figure 7-2 shows that there is a linear trend between the building height, expressed by the number of floors and the total- and post-DVS deformations. The total-DVS deformation results show some small deviations from this linear trend line.

Conclusions

From the results and the research design conditions that are used, the following conclusions can be drawn:

- Most of total- and post- DVS deformations occur within one year. For some cases it can even decrease after one year.

- The relation between the building height and the amount of maximum total- and post-DVS deformations that can occur in the sevice life of the building show a linear trend, provided that the column utilasition is kept as good as constant and the floor to floor height stays the same.

Discussion

In this chapter the relation between the post- and total-DVS deformations and the building height is studied with the original design of Brock Commons as a starting point. For valid results the column load bearing capacity is changed with the variation of building height in order to obtain a column utilisation that is as constant as possible between the variants. However, there is some inconsistency in the continuity of the column utilisation over the building height as is depicted in figure 7-3 which can have influence to some extent on the results.

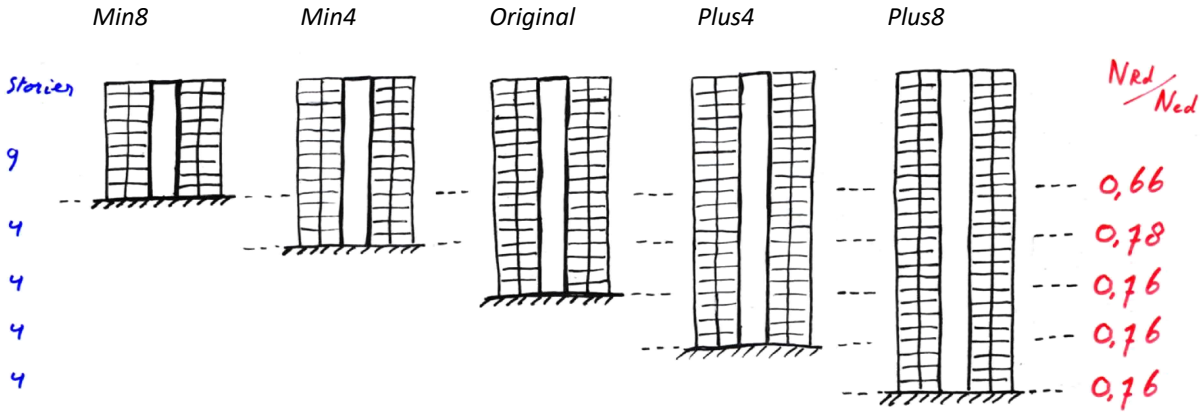

figure 7-3: Building height variants and the column utilisation.

Because the column utilisation for the top 9 stories is significantly lower with 0.66, the column utilisation on average over the total building height increases for the higher variants. This would mean that the column load bearing capacity relative to the axial column load is higher for the smaller variants. If the column utilisation would be more consistent between variants, it would be logical that the total-DVS deformations would be slightly higher for the lower variants relative to the higher variants which can lead to results that tend to have a more linear trend.

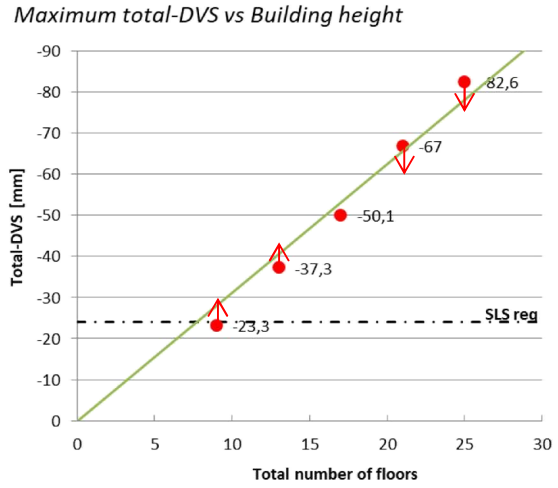

figure 7-4: Effect on results with a more consistent column utilisation.

Another possible reason for the small error between the measured points total-DVS points and the trend line can be the time moment at which the maxima are measured. For all variants the maxima occur at the moment of completion. But the moment of completion is for every variant different because the building process takes longer for the higher variants.

The linear trend that is found in this analysis can be of interest in the design process of similar high-rise structures, as it gives an insight in the effect of adding or removing floors in the preliminary design stage with

regard to DVS deformations. Altering the building height by increasing or decreasing the number of floors cannot be considered as an effective measures because it is not a variable that can be freely changed by the engineer. The number of floors and the building height is established early in the design process by the client and/or architect.

The line that is plotted with the results in the right graphs of figure 7-3 and figure 7-4 only show the trend of the results. The results and the function of this trend line are dependent on parameters of this particular case and may not or cannot be generalised and used for other projects or cases.

7.1.2 Column capacity

The redesign of the columns in chapter 7.1.1 is based on the column utilisation, which is the column load bearing capacity relative to the axial load in the ultimate limit state. In this variant the influence of column capacity on differential vertical shortening deformations will be explored. When loads are kept constant, the increase of column capacity will lead to a smaller column utilisation and vice versa.

Research design

In this variant, the 25 story design with timber columns, shown in figure 7-1 of chapter 7.1.1, is taken as a starting point. The column design is adapted by altering the column cross section, and by that the column load bearing capacity and stiffness in several steps with the scalar factors 0.8, 0.9, 1.1, 1.2, 1.3, 1.5 and 2.0 as shown in table 18. The column utilisation, which is a ratio of the axial column loads and axial column resistance follows with the change of column capacity, provided that the axial column loads will stay constant.

	Column cross section A [mm^2]							
	0.8	**0.9**	**1.0**	**1.1**	**1.2**	**1.3**	**1.5**	**2.0**
Floor 17-25	45580	51278	56975	62673	68370	74068	85463	113950
Floor 13-16	56180	63203	70225	77248	84270	91293	105338	140450
Floor 9-12	56180	63203	70225	77248	84270	91293	105338	140450
Floor 5-8	69620	78323	87025	95728	104430	113133	130538	174050
Floor 1-4	83200	93600	104000	114400	124800	135200	156000	208000
	Column utilisation (N_{ed}/N_{rd})							
	/0.8	**/0.9**	**/1.0**	**/1.1**	**/1.2**	**/1.3**	**/1.5**	**/2.0**
Floor 17-25	0,83	0,73	0,66	0,6	0,55	0,51	0,44	0,33
Floor 13-16	0,98	0,87	0,78	0,71	0,65	0,60	0,52	0,39
Floor 9-12	0,95	0,84	0,76	0,69	0,63	0,58	0,51	0,38
Floor 5-8	0,95	0,84	0,76	0,69	0,63	0,58	0,51	0,38
Floor 1-4	0,95	0,84	0,76	0,69	0,63	0,58	0,51	0,38

table 18: Altering of the column capacity and column utilisation.

Results

The results of the maximum total-DVS and maximum post-DVS between the core and column 3 regarding the column capacity of the columns are presented in figure 7-5.

For the variant with the 1.2 scalar factor the maximum post-DVS deformations stay constant from 1 year after occupation. The variants with a higher scalar factor show some recovery after 1 year and the variants with a lower scalar factor show an increase till 50 years with a decreasing rate. The total-DVS deformations show the same phenomena, but here the transition between recovery and ongoing increase lies at the scalar factor 1.0. The maximum values that occur within the 50 years building service life are plotted in the right graphs of figure 7-5.

With the maximum values in the building service life for every variant, the relation between the post- and total-DVS deformations and the relative column capacity can be shown in a plot (figure 7-5). The relation between both total- and post-DVS deformations and the relative column capacity can be well described by an exponential trend line.

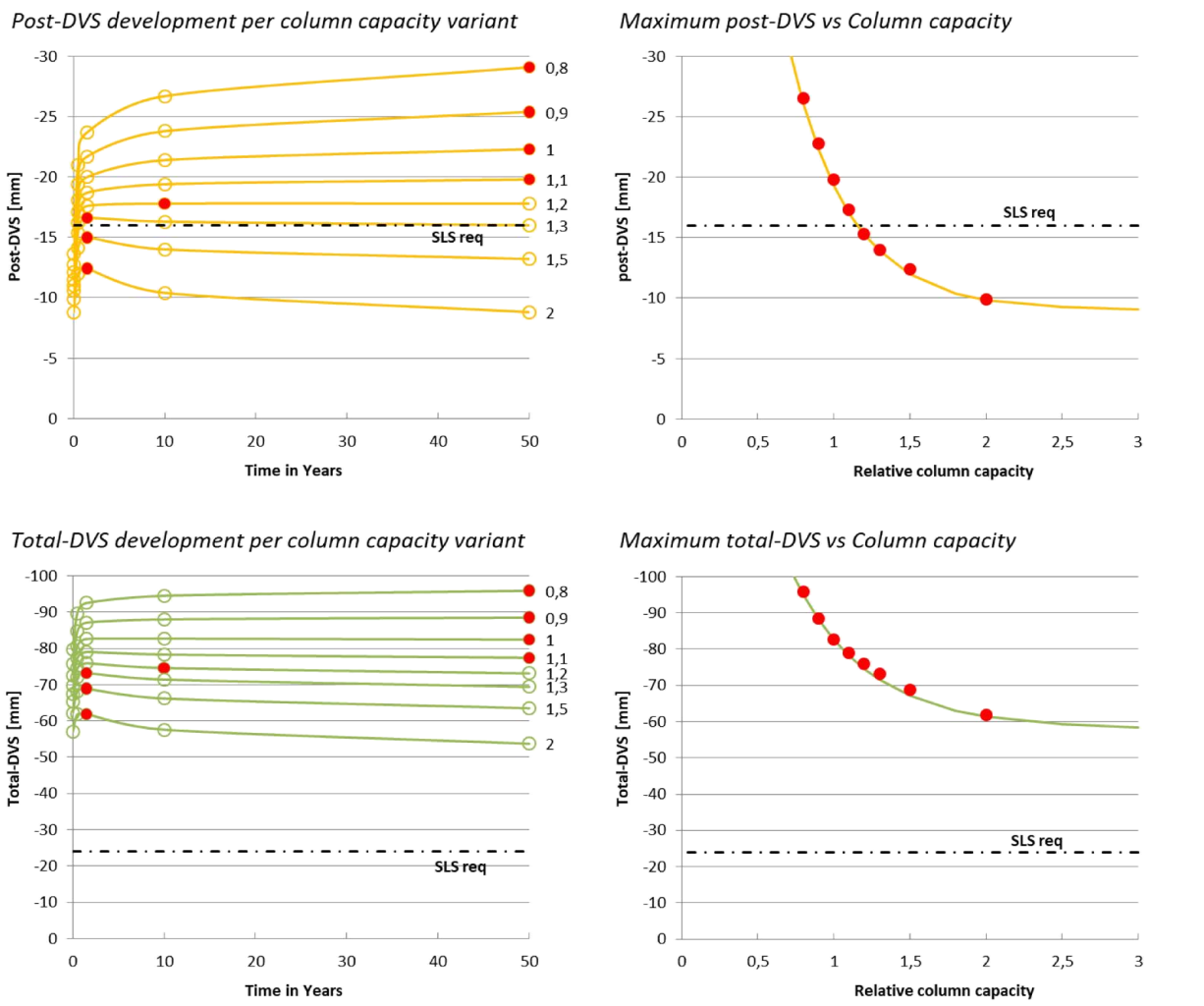

figure 7-5: Left: Total- and post-DVS deformations per variant over the service life, Right: Correlation between Maximum total- and post-DVS and the relative column capacity.

Conclusions

From the results that are presented in figure 7-5, the following conclusions can be drawn:

- The relation between the post- and total-DVS deformations and the relative column capacity can be described as a negative exponential relation, which implies that there is a limit for which post- and total-DVS deformations cannot be further decreased.

Discussion

The relation between the post- and total-DVS deformations and column load bearing capacity are studied in this chapter. Several variants are modelled in which only the column load bearing capacity is altered and all other variables in the model are kept constant.

The results, that show a negative exponential relation, can explained because the altered variable, the column cross section thus column stiffness, only has influence on the DVS deformations due to mechanical loading. These are the elastic and creep DVS deformations, but not the DVS deformations due to shrinkage. With the increase of the column stiffness EA to infinity, the elastic and creep DVS deformations tend to decrease with a decreasing rate to zero. The limit is determined by the DVS deformations due to shrinkage. Note, this is only the case when the elastic and creep deformation in the core are virtually nil.

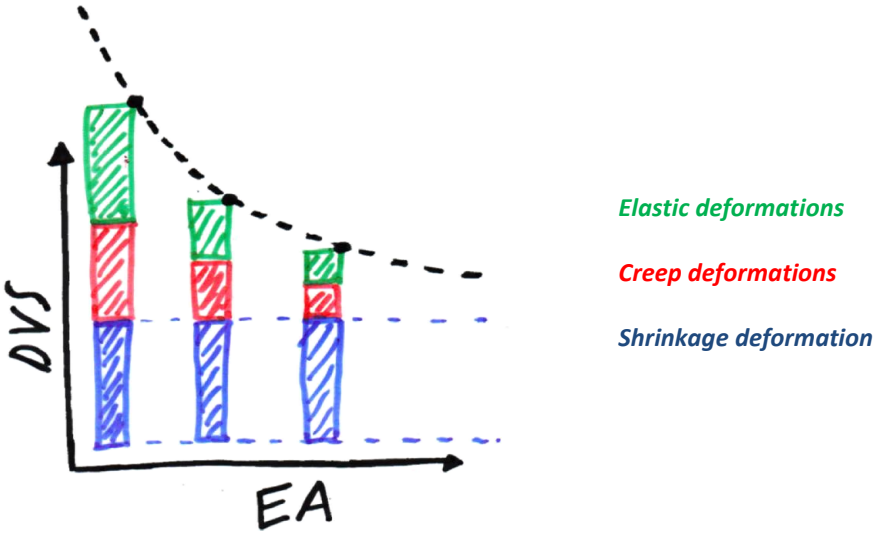

figure 7-6: Explanation of negative exponential correlation between DVS deformations and column load bearing capacity.

The results, shown in figure 7-5, and the explanation, that is depicted in figure 7-6, imply that altering the column cross section and by that the column stiffness, has more effect in decreasing the DVS deformations if these deformations emanate for the most part from elastic and creep deformations. This makes this measure less effective if shrinkage predominates the DVS deformations.

In the case of figure 7-5, the column cross section should be increased with more than a factor 1.3 to comply with the SLS requirements for post-DVS deformations. The question is whether this is desirable for economic, sustainability and architectural reasons. It would mean that the material use for the columns would increase with 30%.

The line that is plotted with the results in the right graphs of figure 7-5 only show the trend of the results. The results and the function of this trend line are dependent on parameters of this particular case and may not or cannot be generalised and used for other projects or cases.

7.1.3 Building speed

In this variable study, a regression analysis of the building speed of the 'Finishes' load pattern versus the differential vertical shortening (DVS) deformations will be conducted.

Research design

The time length of one building step for the 'Finishes' load pattern will be taken as the independent variable that will be altered in this analysis. The starting point of this variable will be according to the original building sequence. The principle of how the building sequence is modelled in ETABS is shown in figure 7-7. In this building sequence design, the time length of placing the full 'Finishes' load pattern is $3t_1$, with one building stage $t_1 = 4days$.

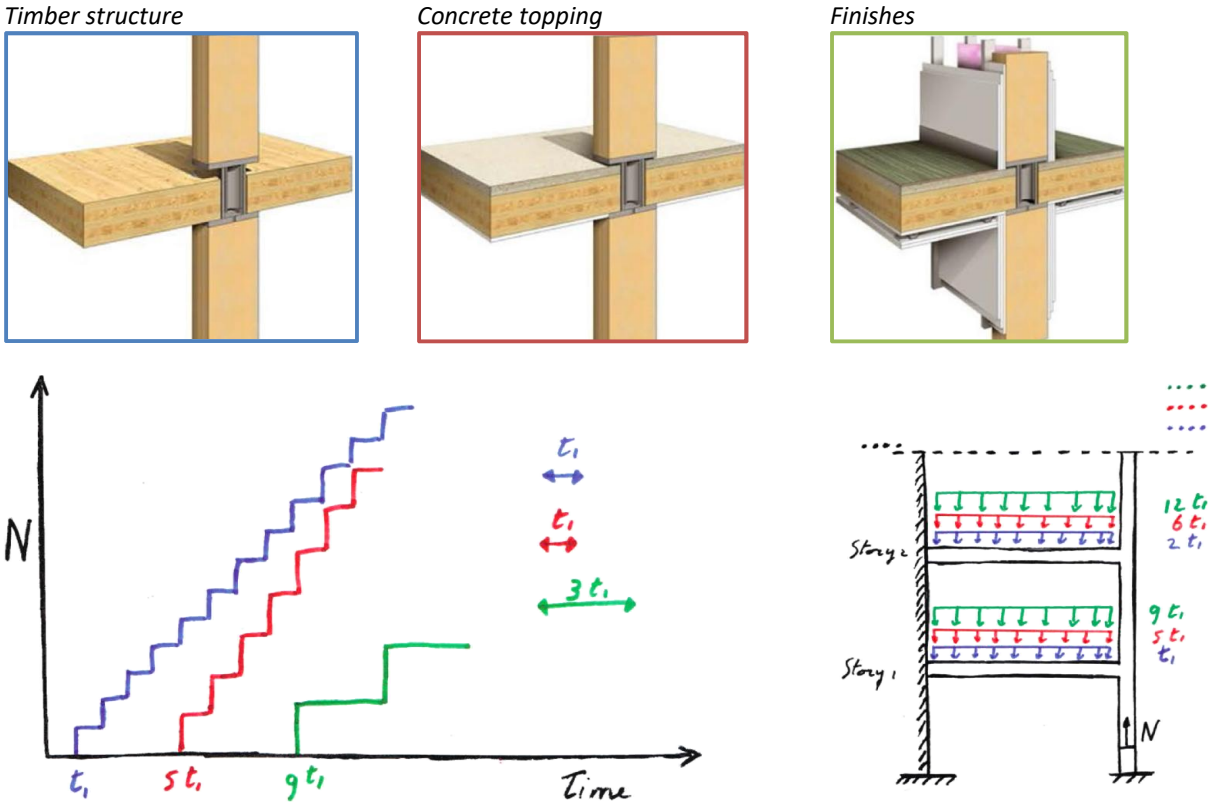

figure 7-7: Principle of building sequence model.

From the starting point of $3t_1$ (12 days), the time length of the placing or duration of the 'Finishes' load pattern will be altered. The start of the sequence of the 'Finishes' load pattern will stay constant at $9t_1$ as well as the start time and building duration of both the 'Timber structure' and 'Concrete topping' load pattern.

Building speed variation of Finishings+Installations load patern

1 building stage	*2 building stages*	*3 building stages*	*4 building stages*	*5 building stages*
$1t_1$	$2t_1$	$3t_1$	$4t_1$	$5t_1$
4days	8days	12days	16days	20days

table 19: Building speed variation of Finishings+Installations load patern.

Results

The results of the maximum total-DVS and maximum post-DVS between the core and column 3 regarding the building speed of the 'Finishes' load pattern, are retrieved from the ETABS model for all analysed time moments and are presented in figure 7-8.

Each building speed variant shows the same development of post-DVS deformations, but with a decreasing amplitude when the building duration of the 'Finishes' load pattern is increased. For the total-DVS deformations the difference in development or amplitude is negligible.

With the maximum values in the building service life for every variant, the relation between the post- and total-DVS deformations and the building duration of the 'Finishes' load pattern can be shown in a plot (figure 7-8). The post-DVS deformations decrease when the building duration is increased with a decreasing rate which can be described by a negative exponential relation. The total-DVS deformation only show a negligibly small variation from which no relation can be derived.

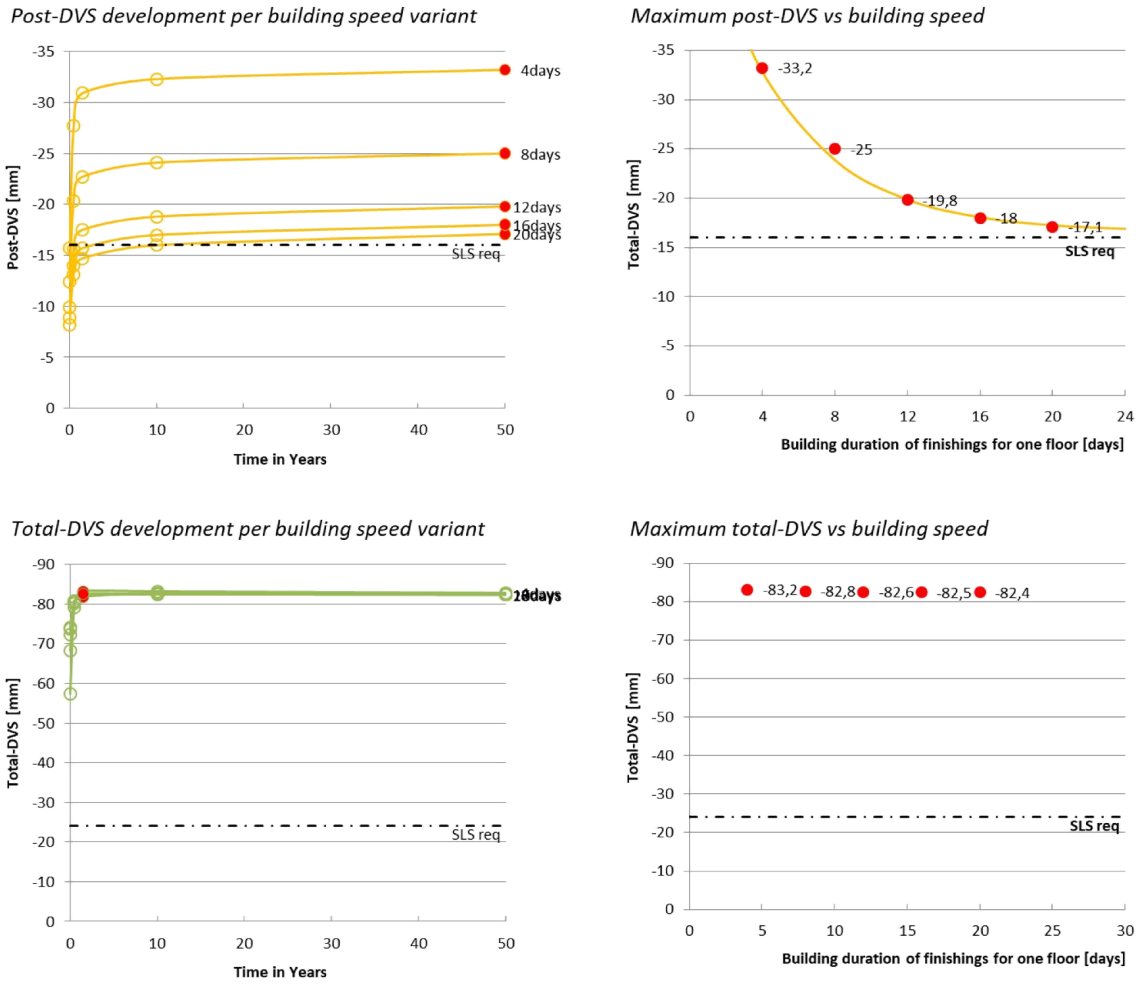

figure 7-8: Left: Total- and post-DVS deformations per variant over the service life, Right: Correlation between Maximum total- and post-DVS and the building speed of finishing elements.

Conclusions

- The relation between the post-DVS deformations and the duration of installing finishings can be described as a negative exponential, which implies that there is a limit for which post-DVS deformations cannot be further decreased.

- No relation is found between the total-DVS deformations and the duration of installing finishings.

Discussion

In this chapter, the relation between the post- and total-DVS deformations and the building speed of the finishings in a high-rise building is studied. All variables are fixed except the duration of one building step for the 'Finishes' load pattern.
The results show that only the post-deformations are significantly influenced by altering the building speed with regard to finishings. There is a minuscule influence on the total-DVS deformations. These can be explained because the total building process increases or decreases when altering the variable. This influences the moment at which the deformations are measured as the time at completion (zero point) is shifted in time.

The exponential relation and the associated limit can be explained by the fact that deformations due to the 'Timber structure' and 'concrete topping' load pattern will stop further increasing significantly from a certain time moment and deformations due to the 'Finishes' load pattern itself will only start developing when

finishings are actually placed in the structure. Planning the construction of finishes closer to the rough structural work will cause that post-DVS deformations have a greater share on the total-DVS deformations.

The variable/sensitivity analysis in this chapter only considered the duration of the 'Finishes' load pattern. The starting point for this load pattern at the first floor stayed the same. Likewise, for the starting point and duration for the 'Timber structure' and 'concrete topping' load pattern. Also the 'Timber structure' and 'concrete topping' load pattern can be influence by bringing the structural work of the timber structure and concrete topping further forward in the building process relative to the construction of finishes and installations. This could be beneficial with regard to the post-DVS deformations as it increases the time duration between both load patterns so that more time dependent deformation can occur before finishings are installed.

A perfect example where this measure is conducted, whether or not it is consciously done for bringing down post-DVS deformations, is the LifeCycle Tower One building in Dornbirn, Austria (Tahan, 2013). The concrete topping is prefabricated on the timber structure, which causes that the 'Concrete topping load case is brought forward by prefabricating the total floor on beforehand.

An example where the prefabrication is further increased is Hotel Jakarta in Amsterdam, The Netherlands. Room size modules are totally prefabricated with finishes and installations already placed in the module before the module is hoisted in its final position on site (Starink, 2017). This causes that all load patterns are placed at the same moment in time which makes all DVS deformations, post-DVS deformations. This would cause that more post-DVS deformations can be expected.

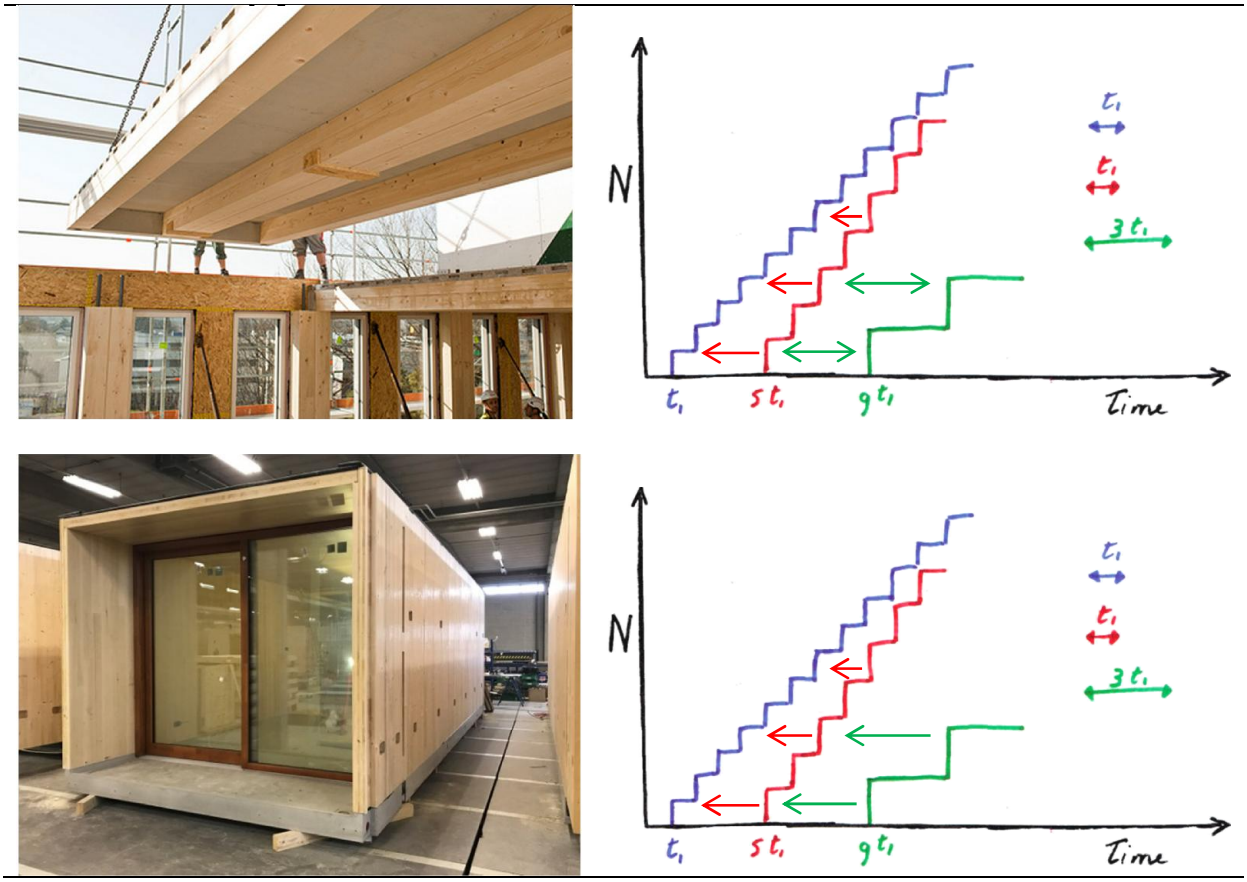

figure 7-9: Examples of prefabricated building systems Left: LCT One floor system (Tahan, 2013). Right: Hotel Jakarta module (Starink, 2017).

The line that is plotted with the results in the right graphs of figure 7-8 only show the trend of the results of this particular case. The results and the function of this trend line are dependent on parameters of this particular case and may not or cannot be generalised and used for other projects or cases.

7.2 Compensation variants

In this chapter the compensation strategy will be studied to determine in what way compensation can be effectively applied to fulfil the SLS requirement regarding total-DVS deformations.

The 'Plus8' variant of the previous chapter in which the column capacity will be increased with a factor 1,1 and the building speed of the finishings will be extended to 16 days will serve as a starting point. These measures together will ensure that the SLS requirements for post-DVS deformations of the left column are met. The right column is not further considered as the short span is causing that SLS requirements are unreachably low. The results of this variant are shown in figure 7-11 and will be used as a basis on which compensation strategies will be studied. Post-DVS deformations will not be visualized further in this chapter as those are not affected by compensation.

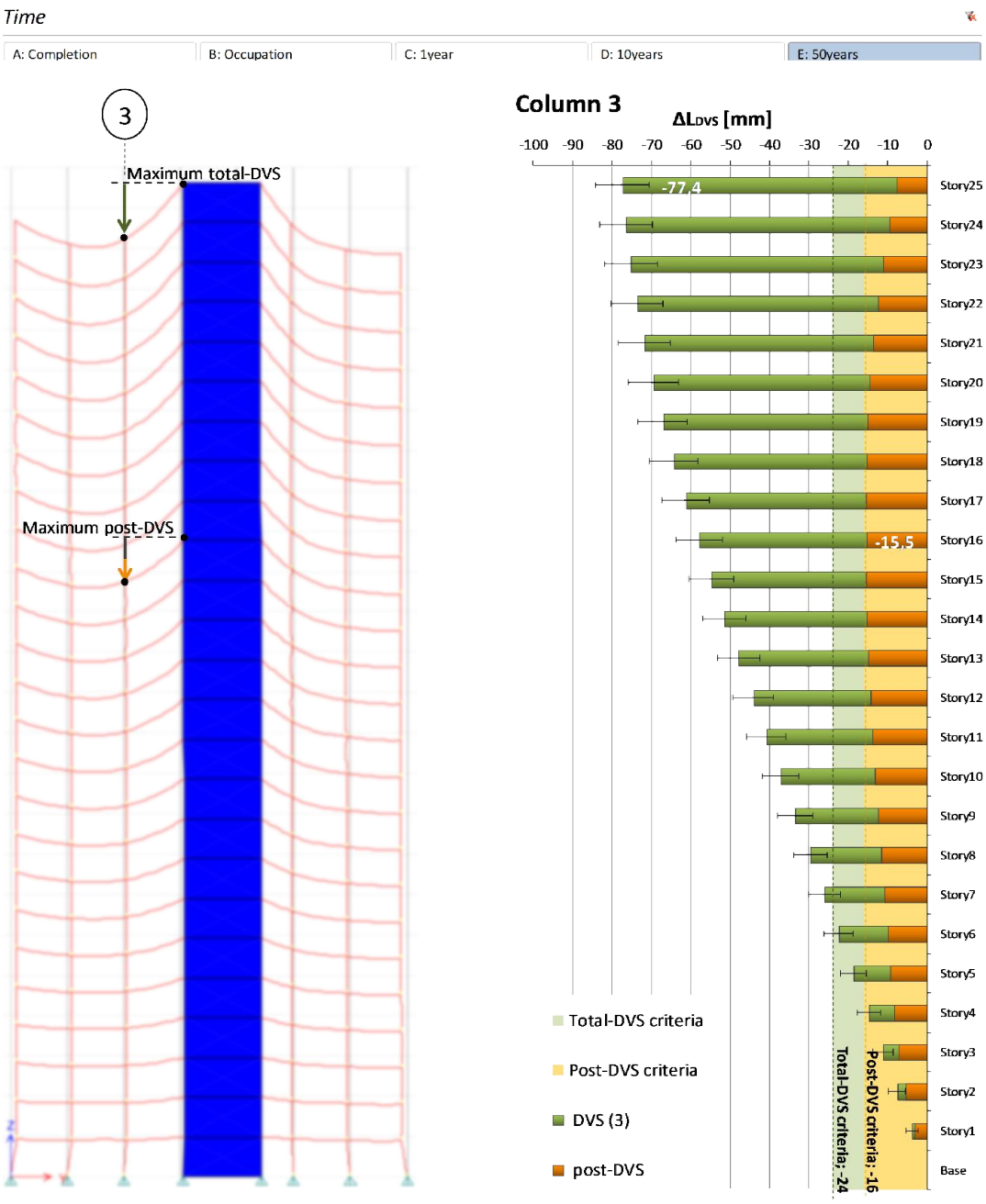

figure 7-10:DVS deformations between column 3 and the core at 50 years after occupation for the Plus8 variant with 1.1 column capacity and 16days duration of 'Finishes' load pattern. No compensation applied.

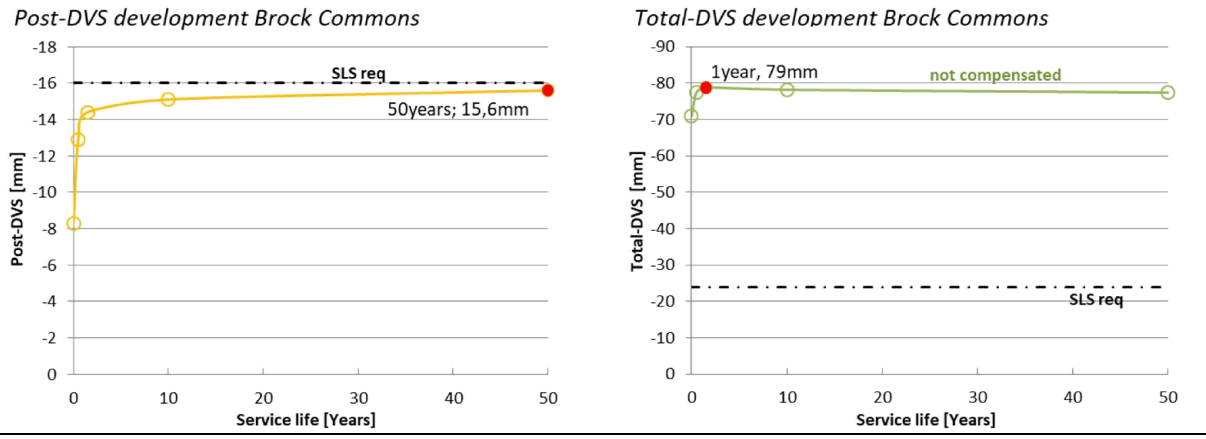

figure 7-11: Maximum results of total- and post-DVS deformations of optimised variant. Column capacity: 1,1; Building speed finishes: 16days/floor. No compensation applied.

The original compensation strategy of the Brock Commons design will be pursued on the 'Plus8' variant by applying 8mm of compensation not only on the 7th, 11th and 15th floor, but also on the 19th and 23rd floor. Finally, another compensation method will be proposed.

7.2.1 Original compensation strategy

The original compensation strategy of the Brock Commons design will be pursued for the 'Plus8' variant. This is done by applying compensation of 8mm at the 7th, 11th, 15th 19th and 23rd floor level.

Results

The results with the compensation included are shown in figure 7-12. From the results it can be noted that the total-DVS deformations still exceed the SLS requirements on most floors.

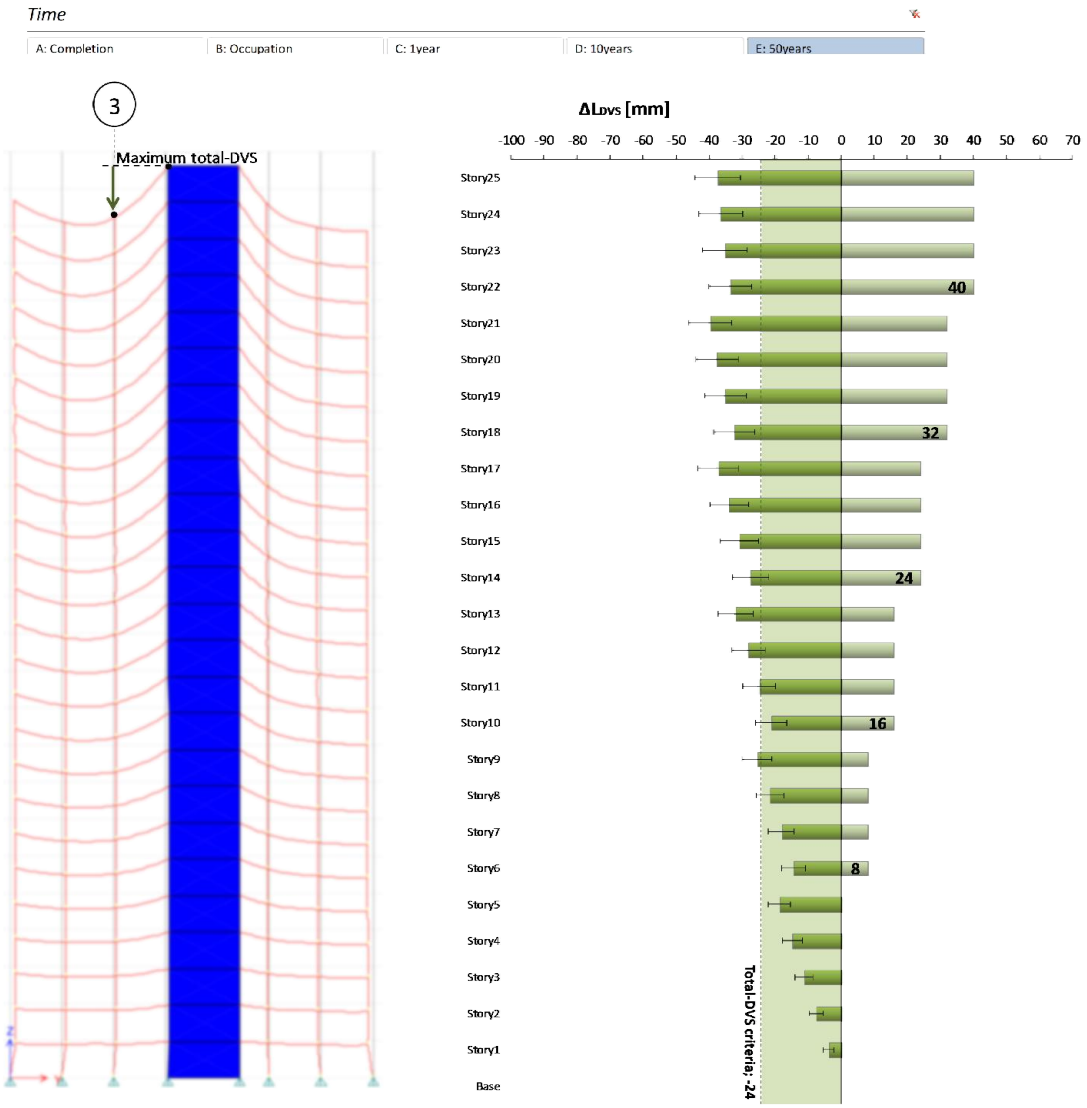

figure 7-12: Results of original compensation strategy applied on the 'Plus8' variant with column capacity 1.1 and duration of 'Finishes' of 16 days.

7.2.2 Proposed compensation strategy

A strategy will be proposed for compensating the total-DVS deformations in a more efficient manner. In this strategy it is not only desirable to fulfil the SLS requirement, but also to exploit the range of the SLS requirement as much as possible to minimize the locations of compensation.

Approach and results

The target is to keep the mean total-DVS deformations between 0 and the SLS requirement of -24mm.

In figure 7-13 it is shown how vertical lines are set on the multiples of the SLS requirement. At the floor where the total-DVS results exceed the SLS requirement a compensation is applied of the amount that is equal to the SLS requirement of 24mm by using shim plates. At the floor where the total-DVS deformations exceed twice the SLS requirement, again compensation of 24mm is applied. For the top part, 12mm shimming is applied. As the shimming at one location translates all floors above upward with the same amount, the total graph in figure 7-13 above the shimmed location will shift. The result of the total-DVS deformations and the amount of compensation are shown in the right picture of figure 7-13.

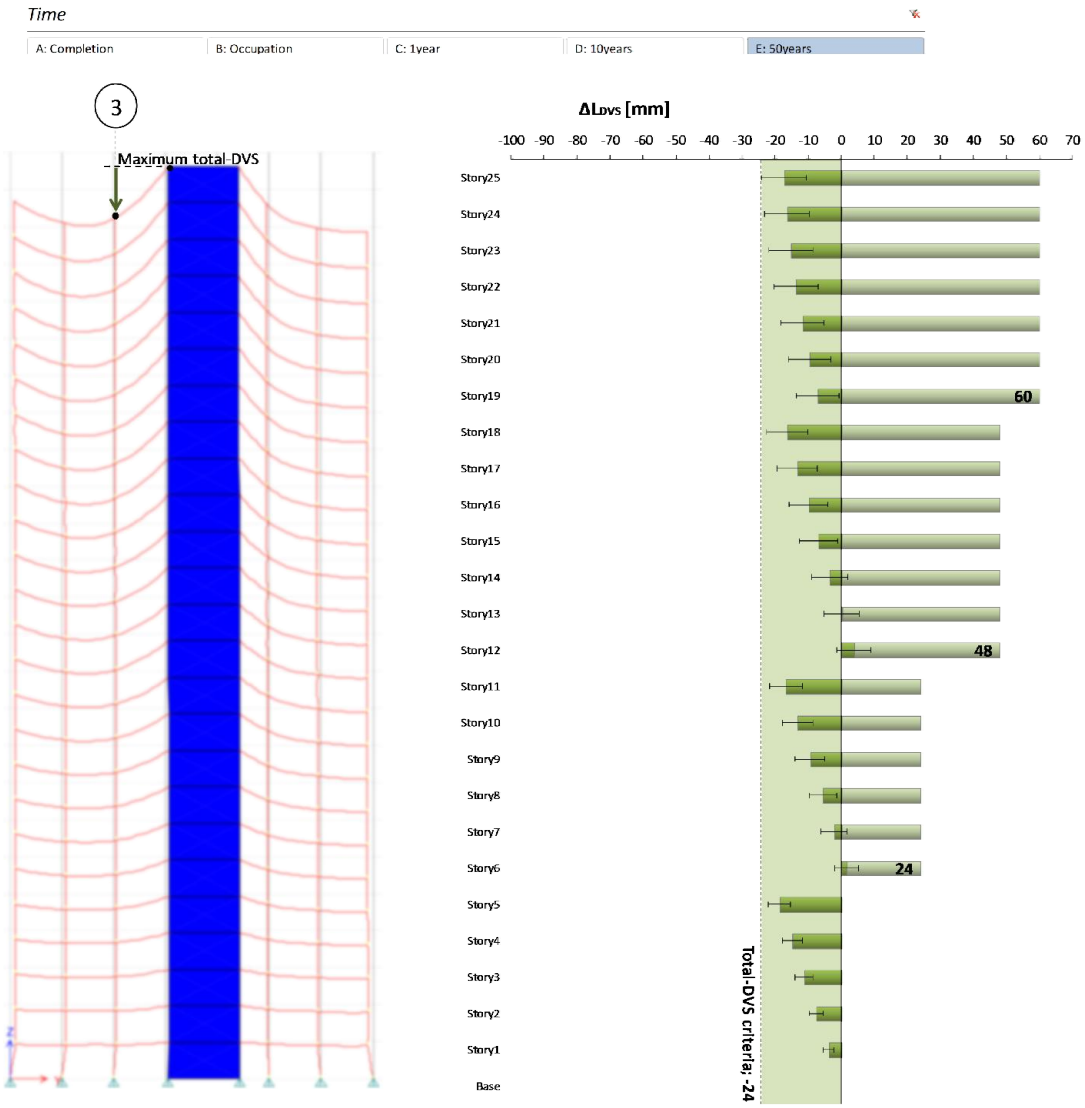

figure 7-13: Proposed compensation strategy by using the full criterium of 24 mm as a compensation amount.

When it is desired to also include the deviations that originate from material deviations, within the range of the SLS requirement, the 5th percentile is taken as the governing value.

Conclusion

The original strategy that was used in the Brock Commons design pursued in the 'Plus8' variant. The results show that this is not enough to comply with the SLS requirement. By setting out the range in which the total-DVS deformations are allowed to occur, the compensation can be applied more effectively. For this case only three locations are needed to apply compensation. The following conclusions are drawn from the compensations study.

- Compensation has effect on the total difference in vertical position between the floor supports. The vertical translational movement is not prevented. This means that post-DVS deformations cannot be influenced by compensation that is applied in the building process.

- With the determined criteria regarding DVS deformations, a compensation strategy can be drafted much more effectively.

8 Conclusions and recommendations

8.1 Introduction

In this research differential vertical shortening is studied by use of the following main research question:

"What are effective measures which can be applied in the design and construction phase to mitigate the differential vertical shortening during the service life of high-rise buildings that uses a timber gravitational load bearing system with stabilizing concrete cores?''

The following sub questions where formulated to come to an answer step by step.

"What are the criteria on which differential vertical shortening deformations in the building structure should be assessed in order to guarantee the quality and the functional performance of the building during its service life?"

"How can differential vertical shortening deformations be quantified for a timber-concrete high-rise structure?"

"What is the response mechanism of axially loaded concrete load bearing elements and axially loaded timber load bearing elements on external influences?"

"What factors in the design and construction phase have influence on the magnitude of differential vertical shortening?"

This chapter will give an answer on the formulated sub questions and main research question. It will also provide the restrictions of this research and recommendations for further research

8.2 Conclusions

When criteria for DVS deformations are determined, it should be known where DVS deformations can have a negative effect on secondary building elements. Proper detailing is allows some deformation capacity in the interaction between the main load bearing structure and the secondary building elements.

To perform an accurate analysis on DVS deformations, post-DVS deformations that can affect secondary building elements should be distinguished from the total-DVS deformations. The criteria on post-DVS deformations should ensure that secondary building elements are not negatively affected or damaged. The criteria on total-DVS deformations should ensure that the appearance and quality of the structure is preserved. Both criteria have the purpose to ensure a certain building quality and level of comfort for the building users.
The determination of the total- and post-DVS deformation criteria is project dependent, but Eurocode principles on vertical deformations that are based on the span to vertical deformation ratio can be used for the determination of these criteria.

For the quantification of DVS deformations, the CEB-fip 2010 model can be used in order to predict elastic, shrinkage and creep strains in concrete. The timber elastic strains can be predicted by the strength class system that is provided by Eurocode 5.

Using the Eurocode creep factor of 0,6 for timber in climate class 1 over a 50 year service life, may provide an underestimation of the creep deformations. The analysis of experimental results shows that a creep factor between 0,61 and 1,33 with a mean of 0,97 is more likely to occur at 50 years in the service life.

The mean shrinkage coefficient for parallel to the grain shrinkage in small spruce specimens is determined on $0{,}011\%/\%\Delta MC$. The variance in the 90-percent confidence interval is determined at $\pm 99\%$.

A staged construction analysis can be used to predict the total- and post-DVS deformations. This analysis makes it possible to predict the pre-DVS deformations just before finishings are installed in the structure. From the pre- and total-DVS deformations, the post-DVS deformations can be determined.

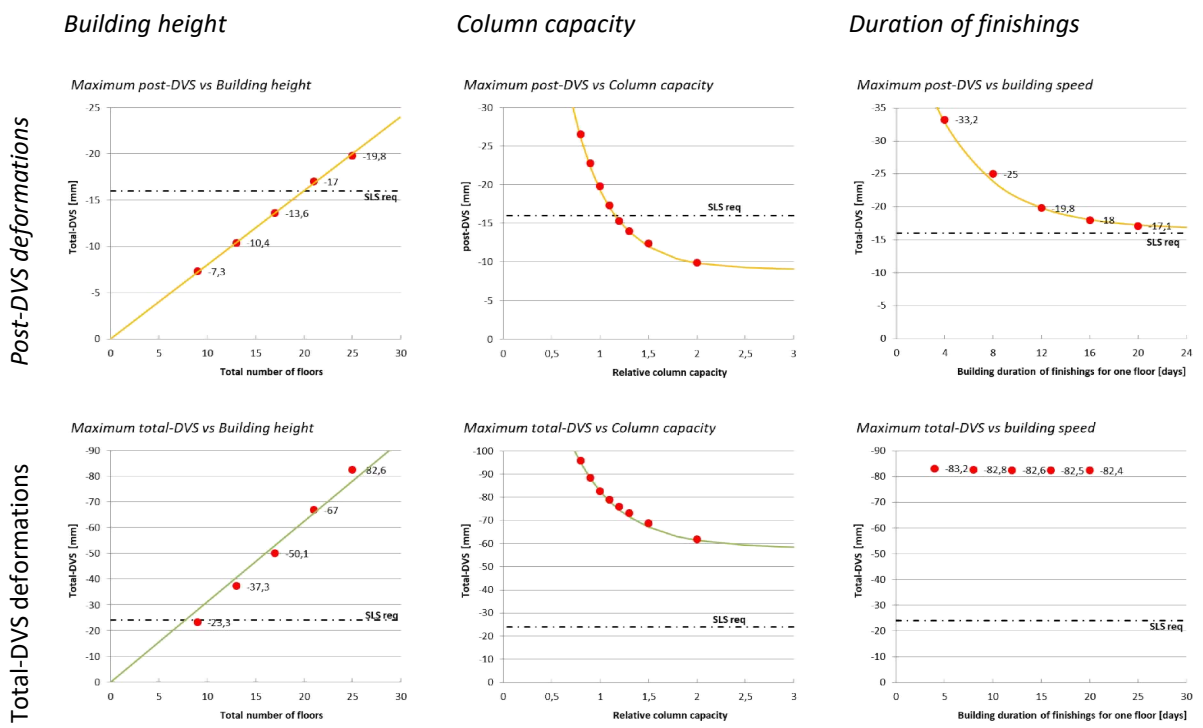

figure 8-1: Relations between the DVS-deformations and several altered variables.

A recap on the relation between the total- and post-DVS deformations and the altered variables in this research is shown in figure 8-1. The following statements can be drawn from these relations:

- Both the total- and post-DVS deformations show a linear trend with the increase of the building height, provided that the column utilisation is kept constant and the floor to floor height stays the same.

- The relation between the post- and total-DVS deformations and the relative column capacity can be described as a negative exponential relation, which implies that there is a limit for which post- and total-DVS deformations cannot be further decreased.

- The relation between the post-DVS deformations and the duration of installing finishings can be described as a negative exponential, which implies that there is a limit for which post-DVS deformations cannot be further decreased.

- No relation is found between the total-DVS deformations and the duration of installing finishings.

From all previous pronunciations the main research question can be answered:

"What are effective measures which can be applied in the design and construction phase to control the differential vertical shortening during the service life of high-rise buildings that uses a timber gravitational load bearing system with stabilizing concrete cores?''

- *Increasing the column cross section can be an effective measure to decrease post- and total-DVS deformations due to elastic and creep strains. The effectiveness decreases with the increase of the column cross section because shrinkage strains are not affected.*

- *Post-DVS deformations can be decreased by postponing the building process of secondary structural elements in the construction schedule. The effectiveness decreases with increasing building duration because DVS-deformations due to loads of the finishes itself are not affected. Total-DVS deformations are not affected.*

- *Compensation has effect on the total difference in vertical position between the floor supports. The vertical translational movement is not prevented. This means that post-DVS deformations cannot be influenced by compensation.*

8.3 Restrictions and recommendations

This research is universally applicable for cases using similar building systems, even though the research was conducted for a specific case.

The method that is used in this research to determine the SLS criteria is generalizable. However, the values of the criteria are project specific. These criteria should be determined in agreement with the client and other actors in a design project.

The predicted shrinkage strain in the timber columns is based on a predicted moisture content decrease in the timber columns from the moment these elements are installed in the building. The moisture content in structural timber is highly dependent on the environmental conditions in which it is situated and is therefore site specific and dependent on conditions during transport and construction. The predicted timber moisture content development in this research should therefore be treated as indicative.

The insight that is provided by the relations that are found is universally applicable for buildings that make use of comparable building systems. One must be aware that the results are based on a particular structural system, in which a core provides the lateral stability and the columns do not contribute substantially to the lateral stability, but are mostly utilized for gravitational loads. Other building systems, such as an outrigger structure, tube in tube structure or bundled tube structures are not considered in this research. This would be an interesting topic for the extensive research on differential vertical shortening in high-rise structures.

Increasing or decreasing the building height is not considered as an effective measure because it is not a variable that can be freely altered by the engineer. The relation that is found does provide in an insight for knowing what might happen if the building height is changed due to changes in the design specification of a high-rise building.

Only the differential vertical shortening deformations of the upper structure are considered in this research. Foundation settlements are left out of consideration, but may have a considerable effect. However, foundation settlements may be treated as independent from the differential vertical shortening deformations.

9 Bibliography

Abdul-Wahab, H., Taylor, G., Price, W., & Pope, D. (1998). Measurement and modelling of long-term creep in glued laminated timber beams used in structural building frames. *The Structural Engineer, Volume 76/No 14*, 271-281.

Abell, M. (2012, June 5). *Staged Construction*. Opgeroepen op Oktober 25, 2017, van CSI Knowledge Base: https://wiki.csiamerica.com/pages/viewpage.action?pageId=9536112&navigatingVersions=true

Acton Ostry Architects, Inc. (2016, May 12). a Tale of Tall Wood, Brock Commons Student Residence, University of British Columbia. Acton Ostry Architects, inc.

AEneas. (2012). Autogenen krimp. *Betoniek, vakblad over technologie en uitvoering van beton*.

Akatherm BV. (2017). *Akatherm: Kunstof leidingsystemen*. Opgeroepen op Juli 5, 2017, van http://www.akatherm.nl/nl/cat/bouw/gebouwriolering/gebouwriolering-pvc-grijs/fittingen/bocht-0-180-flexibel/s+t+g+c+a

Andriamitantsoa, L. (1995). STEP lecture A19: Creep. In H. Blass, P. Aune, & B. Choo, *Timber Engineering step 1: Basis of design, material properties, structural components and joints.* Almere: Centrum Hout.

Aratake, S., Morita, H., & Arima, T. (2011). Bending creep of glued laminated timber (glulam) using sugi (Cryptomeria japonica) laminae with extremely low Young's modulus for the inner layers. *J Wood Sci 57*, 267-275.

Baker, W., Korista, D., Novak, L., Pawlikowski, J., & Young, B. (2007). Creep and Shrinkage and the Design of Supertall Buildings—A Case Study: The Burj Dubai Tower. *ACI Special Publications 246*, 127.

Bazant, Z. (1989). *Mathematical Modelling of Creep and Shrinkage of Concrete.* John Wiley and Sons.

Bažant, Z. (2001). Prediction of concrete creep and shrinkage: past, present and future. *Nuclear Engineering and design*, 27-38.

Bengtsson, C. (2001). Variation of moisture induced movements in Norway spruce (Picea abies. *Springer Verlag/EDP Sciences 58 (5)*, 568-581.

BetonPrisma. (1996). Temperatuur en Sterkte. *Betoniek*, 10-18.

Boonekamp, H., & Meischke, J. (1979). Efficiënter bouwen door betere maatcontrole. *Cement XXXl*, 387-399.

Braam, C., & Lagendijk, P. (2011). *Constructieleer: Gewapend Beton.* Boxtel: Aeneas, Cement&BetonCentrum.

Brandner, R. (2013). *Stochastic system actions and effects in engineered timber products and structures.* Graz: Verlag der Technischen Universität Graz.

Buchanan, A. H. (1990). Bending Strength of Lumber. *Journal of Structural Engineering, Vol. 116, No. 5*, 1213-1229.

CEB-fib. (2012). *Model Code 2010: Final draft, Volume1.* Switzerland: International Federation for Structural Concrete (fib).

Choi, S., Kim, Y., Kim, J., & Park, H. (2013). Field Monitoring of Column Shortenings in a High-Rise Building during Construction. *Sensors, 13*, 14321-14338.

Colling, F. (1995). Glued laminated timber - Production and strength classes. In H. Blass, P. Aune, & B. Choo, *Timber Engineering: step1.* Almere: Centrum Hout.

Computers and Structures, Inc (CSI). (2017). *''Watch & Learn'' series: Vertical Displacements in Tall Buildings*. Opgeroepen op 6 24, 2017, van CSI Computers & Structures, Inc.: https://www.csiamerica.com/products/etabs/watch-and-learn

CTBUH. (2017, June). *Tall Buildings in Numbers, Tall Timber: A Global Audit*. Opgeroepen op August 25, 2017, van Council on Tall Buildings and Urban Habitat: http://www.ctbuh.org/Publications/CTBUHJournal/InNumbers/TBINTimber/tabid/7530/language/en-US/Default.aspx

Dietsch, P., Gamper, A., Merk, M., & Winter, S. (2015). Monitoring building climate and timber moisture gradient in large-span timber structures. *Journal of Civil Structural Health Monitoring, 5(2)*, 153-165.

Fast, P., Gafner, B., Jackson, R., & Li, J. (2016). *Case Study: An 18 storey tall timber hybrid student residence at the University of British Columbia, Vancouver.* Vienna: World Conference on Timber Engineering.

Fintel, M., Ghosh, S., & Iyengar, H. (1987). *Column Shortening in Tall Structures - Prediction and Compensation.* Portland Cement Association.

Franke, B., Franke, S., Schiere, M., & Müller, A. (2016). Moisture diffusion in wood - Experimental and numerical investigations. *World Conference on Timber Engineering.* Vienna.

Freedman, D., Pisani, R., & Purves, R. (2007). *Statistics: Fourth Edition.* London: W. W. Norton & Company, Inc.

fvb ffc constructiv. (2000). *De sanitair installateur: Leidingen in koper.* Brussel: Fonds voor Vakopleiding in de Bouwnijverheid.

Geberit. (2004). *Geberit Sovent: The innovative soil and waste drainage system.* Rapperswil: Geberit.

Gerhards, C. (1980). *Effects of Moisture Content and Temperature on the Mechanical Properties of Wood: An Analysis of immediate Effects.* Blacksburg: U.S. Department of Agriculture.

Glos, P. (1995). STEP lecture A6: Strength grading. In H. Blass, P. Aue, B. Choo, R. Görlacher, Griffiths, B. Hilson, et al., *Timber Engineering: step 1.* Almere: Centrum Hout.

Gowda, C., Kortesmaa, M., & Ranta-Maunus, A. (1996). *Long term creep tests on timber beams on heated and non-heated environments.* ESPOO: Technical Research Centre of Finland (VTT).

Groot, H. d. (2016, August 14). *HoHo Wien Oostenrijk*. Opgeroepen op August 18, 2017, van Het Houtblad: http://www.houtblad.nl/Projecten/HoHo_Wien

Gryc, V., Vavrcík, P., & Horácek. (2007). Variability in swelling of spruce (Picea abies [L.] Karst.) wood with the presence of compression wood. *Journal of forest science, 53*, 243-252.

Hasslacher Norica Timber. (2016). *Glue Laminated Timber BSH.* Sachsenburg: Hasslacher Norica Timber.

Hoffmeyer, P. (1993). Non-linear creep caused by slip plane formation. *Wood Science and Technology*(Volume 27, Number 5), 321-335.

Hoffmeyer, P. (1995). STEP lecture A4: Wood as a building material. In H. Blass, P. Aue, B. Choo, R. Görlacher, Griffiths, B. Hilson, et al., *Timber Engineering: step 1.* Almere: Centrum Hout.

Hoffmeyer, P., & Davidson, R. (1989). Mechano-sorptive creep mechanism of wood in compression and bending. *Wood Science and Technology*, 215-227.

Holzer, S. M., Loferski, J. R., & Dillard, D. A. (1989). A Review of Creep in Wood: Concepts Relevant to Develop Long-Term Behavior Predictions for Wood Structures. *Wood and Fiber Science*, 376-392.

Hoof, P. (1986). *Maatbeheersing in de bouw: een ontwikkeling van uitzetmethoden.* Eindhoven: Technische Universiteit Eindhoven.

Hráský, J., & Král, P. (2010). *Analysis of selected Mechanical Properties of Construction Wood KVH and Parallam 2.0E.* Brno.

Illston, J., Dinwoodie, J., & Smith, A. (1979). *Concrete, Timber and Metals, the nature and behaviour of structural materials.* Wokingham: Van Nostrand Reinhold Ltd.

Johansson, M. (2003). Prediction of bow and crook in timber studs based on variation in longitudinal shrinkage. *Wood and Fiber Science 35(3)*, 445-455.

Kim, H., & Shin, S. (2011). The Twelfth East Asia-Pacific Conference on Structural Engineering and Construction. *Column Shortening Analysis with Lumped Construction Sequence* (pp. 1791-1798). Elsevier.

Kim, H.-S. (2013). Effect of horizontal members on column shortening in reinforced concrete building structures. *The Structural Design of Tall and Special Buildings 22*, 440-453.

Knaack, U., Klein, T., Bilow, M., & Auer, T. (2014). *Façades: Principles of construction, second edition.* Basel: Birkhäuser Verlag GmbH.

Lam, F., & Prion, H. (2003). Engineered Wood Products for Structural Purposes. In S. Thelandersson, & H. Larsen, *Timber Engineering* (pp. 81-102). West Sussex: John Wiley & Sons Ltd.

Matar, S. S., & Faschan, W. J. (2017). A Structural Engineer's Approach to Differential Vertical Shortening in Tall Buildings. *International Journal of High-Rise Buildings, Vol 6, No 1.*, 73-82.

Morlier, P., & Palka, L. (1994). Basic knowledge. In P. Morlier, *Rilem Report 8: Creep in Timber Structures* (pp. 9-39). London: E & F Spon.

MOUS Systems B.V. (2004). *MOUS Systeem - Hoogte*. Opgeroepen op 5 17, 2017, van MOUS Systems: http://www.moussystems.nl/nl/systemen/msh.html

naturally:wood. (2016, 9 13). *Brock Commons Time Lapse - UBC Tall wood Building*. Opgehaald van Youtube: https://www.youtube.com/watch?v=GHtdnY_gnmE

NEN 2881. (1990). *Maattoleranties voor de bouw: Begripsomschrijving en algemene regels.* Delft: Nederlands Normalisatie-Instituut.

NEN 2887. (1990). *Maximaal toelaatbare maatafwijkingen voor het uitzettten op de bouwplaats.* Delft: Nederlands Normalisate-Instituut.

NEN 2888. (1990). *Maximaal toelaatbare maatafwijkingen voor het stellen van draagconstructies van gebouwen.* Delft: Nederlands Normalisatie-Instituut.

NEN 2889. (1990). *Betonelementen: Maximaal toelaatbare maatafwijkingen.* Delft: Nederlands Normalisatie-Instituut.

NEN-EN 14080. (2013). *Timber structures - Glued laminated timber and glued solid timber - Requirements.* Delft: Nederlands Normalisatie-instituut.

NEN-EN 14358. (2016). *Timber structures - Calculation and verification of characteristic values.* Delft: Koninklijk Nederlands Normalisatie-instituut.

NEN-EN 1990. (2011). *Eurocode 0: Basis of structural design.* Delft: Nederlands Normalisatie-instituut.

NEN-EN 1990-1-1/NB. (2011). *Nationale bijlage bij: Eurocode: Grondslagen van het constructief ontwerp.* Nederlands Normalisatie-instituut.

NEN-EN 1991-1-1+C1/NB. (2011). *Nationale bijlage bij NEN-EN 1991-1-1+C1:Eurocode 1: Belastingen op constructies – Deel 1-1: Algemene belastingen - Volumieke gewichten, eigen gewicht en opgelegde belastingen voor gebouwen.* Delft: Nederlands Normalisatie-instituut.

NEN-EN 1992-1-1. (2011). *Ontwerp en berekening van betonconstructies - Deel 1-1: Algemene regels en regels voor gebouwen.* Nederlands Normalisatie-instituut.

NEN-EN 1995-1-1. (2011). *Eurocode 5: Ontwerp en berekening van houtconstructies - Deel 1-1: Algemeen - Gemeenschappelijke regels en regels voor gebouwen.* Nederlands Normalisatie-instituut.

NEN-EN1991-1-7. (2015). *Eurocode1: Belastingen op constructies - Buitengewone belastingen: stootbelastingen en ontploffingen.* Delft: Nederlands Normalisatie-instituut.

NPR 3685. (1995). *Nederlandse praktijkrichtlijn: Maattoleranties voor de bouw: Instructies en voorbeelden voor de berekening.* Delft: Nederlands Normalisatie Instituut.

NSC. (2013, March 25). *Cladding Interfaces with Structure.* Opgeroepen op July 7, 2017, van NSC: newsteelconstruction: http://www.newsteelconstruction.com/wp/cladding-interfaces-with-structure/

NTA 4614-1. (2012). *Nederlandes Technische afspraak, NTA4614-1, Convenant hoogbouw - Deel 1: Algemeen.* Delft: Nederlands Normalisatie-instituut.

NTA 4614-6. (2012). *Convenant hoogbouw - Deel6: Gebouwgebonden installaties.* Delft: Nederlands Normalisatie-instituut.

Ormarsson, S., & Cown, D. (2005). Moisture-related distortion of timber boards of radiata pine: Comparison with Norway spruce. *Wood and Fiber Science, 37 (3)*, 424-436.

Park, H. (2003). Optimal compensation of differential column shortening in high-rise buildings. *The structural design of tall and special buildings*, 49-66.

Park, S., Choi, S., & Park, H. (2013). Moving average correction method for compensation of differential column shorteing in high-rise buildings. *The structural design of tall and special buildings 22*, 718-728.

Perstorper, M., Johansson, M., Kliger, R., & Johansson, G. (2001). Distortion of Norway spruce timber, part1: Variation of relevant wood properties. *Holz als Roh- und Werkstoff 59*, 94-103.

Pilon, A., Teshnizi, Z., Gilmore, L., Behar, D. L., Koleilet, S., Rimland, J., et al. (2017). *Construction of a Tall Wood Building, Brock Commons Tallwood House: Construction Overview.* University of British Colombia, Centre for Interactive Research on Sustainability.

Pilon, A., Utimati, A., & Jin, J. (2016, July). *Design and Preconstruction of a Tall Wood Building, Brock Commons Phase 1: Overview.* University of British Colombia.

Poot, M. (2013). *Tijdsafhankelijke vervormingen in betonnen hoogbouw: Metselwerkgevels op Nederlandse hoogbouw: Een gelukkige combinatie?* Delft: TU Delft, Faculteit Civiele Techniek & Geowetenschappen.

Ritter, M. A. (1990). *Timber Bridges: Design, Construction, Inspection, and Maintenance.* Washington, DC.: United States Department of Agriculture, Forest Service.

Ross, R. J. (2010). *Wood Handbook:Wood as an Engineering Material. Centennial ed. General technical report FPL ; GTR-190.* Madison: U.S. Dept. of Agriculture, Forest Service, Forest Products Laboratory.

Saint-Gobain Gyproc. (2011). *Wandenboek.* Vianen: Saint-Gobain Gyproc Nederland.

Samarakkody, D. (2016). *Differential Axial Shortening in high rise buildings with concrete filled tube columns.* Brisbane: Queensland university of Technology.

Serrano, E. (2009). *Documentation of the Limnologen Project: Overview and Summaries of Sub Project Results.* Växjö: Växjö University.

Sovent. (2005). *Design manual NO. 101/0 Sovent: Single Stack DWV System.* Walter Cornwall , LLC.

Starink, P. (2017, May 15). *Klimaatneutraal Hotel Jakarta.* Opgeroepen op August 1, 2017, van De wereld van de architect: https://www.architectuur.nl/nieuws/klimaatneutraal-hotel-jakarta-door-search-architecture-and-urban-planning/

Stichting Bouwresearch. (1982). *Maatbeheersing in de bouw.* Den Haag: Ten Hagen B.V.

Stora Enso. (sd). *CLT (Cross Laminated Timber).* Opgeroepen op September 6, 2017, van Stora Enso: http://assets.storaenso.com/se/buildingandliving/ProductServicesDocuments/CLT%20Imagebroschure%20[final%202016-04-22]%20-%20EN-WEB.pdf

Strähle Raum-systeme Gmbh. (sd). *Trennwand System 2300.* Strähle Raum-systeme Gmbh.

StructureCraft. (n.d.). *StructureCraft: Materials*. Retrieved 5 29, 2017, from StructureCraft: https://structurecraft.com/materials

Tahan, N. (2013). LCT One: Case Study of an Eight-Storey Timber Office Building. *STRUCTURE magazine*, 20-23.

Taylor-Foster, J. (2013, December 14). *C.F. Møller and DinnellJohansson's Wooden Skyscraper Wins International Competition.* Opgeroepen op August 18, 2017, van ArchDaily: http://www.archdaily.com/458202/c-f-moller-s-wooden-skyscraper-wins-international-competition

The University of British Columbia's Centre for Interative Research on Sustainabilty and Forestry and Innovation Management. (2017, March). Brock Commons Tallwood House: Project Overview Presentation. University of British Columbia.

Thelandersson, S. (1994). Variation of moisture content in timber structures. In M. P, *Creep in Timber Structures.* London: E & F Spon.

Toratti, T. (1992). *Creep of Timber Beams in a Variable Environment.* Helsinki: Helsinki University of Technology.

Van der Put, T. (1989). *Deformation and damage processes in wood.* Delft: Delft University Press.

Ventilatieshop.com B.V. (2012). *Ventilatieshop.com*. Opgeroepen op 07 03, 2017, van https://www.ventilatieshop.com

Vereniging Nederlandse Cementindustrie. (1990). Eigenschappen van beton (I). *Betoniek*, 1-8.

Verver, M., & Fraaij, A. (2004). *Materiaalkunde: Bouwkunde & Civiele Techniek. Derde druk.* Noordhoff Uitgevers.

Vincent, J. (2012). *Structural Biomaterials, Third Edition.* Princeton University Press.

Walraven, J., & Bigaj-van Vliet, A. (2016). Model Code in ontwikkeling. *Cement online*, 22-27.

Walraven, J., & Braam, C. (2015). *Prestressed Concrete.* Delft: Faculty of Civil Engineering and Geosciences, TU Delft.

WeatherOnline. (sd). *Rotterdam The Hague Airport, Relative Humidity*. Opgeroepen op September 6, 2017, van WeatherOnline: http://www.weatheronline.co.uk/weather/maps/city

Wikipedia. (2017, May 4). *Superposition principle*. Retrieved May 15, 2017, from Wikipedia: The Free Encyclopedia: https://en.wikipedia.org/wiki/Superposition_principle#References

Xiong Yu, Z., Su Xin, R., & Sabri, O. (2009). *Vertical Displacements in a Medium-rise Timber Building - Limnologen in Växjö, Sweden.* Växjo: Växjo University: School of Technology and Design, TD.

Young, R., & Lovell, P. (2011). *Introduction to Polymers, Third Edition.* Taylor & Francis Inc.

10 Appendices

A. Concrete material model CEB-fip 2010

A.1 Concrete shrinkage The shrinkage model as formulated in CEB-fip 2010 is elaborated.

A.2 Concrete creep The creep model as formulated in CEB-fip 2010 is elaborated.

A.1 Concrete shrinkage CEB-fip 2010 model

$$\varepsilon_{cs}(t,t_s) = \varepsilon_{cas}(t) + \varepsilon_{cds}(t,t_s)$$

$\varepsilon_{cas}(t)$: Autogenous shrinkage strain

$\varepsilon_{cds}(t,t_s)$: Drying shrinkage strain

equation 16: Shrinkage strain according to the CEB-fip 2010 model.

$$\varepsilon_{cds}(t,t_s) = \varepsilon_{cd,0}(f_{cm}) \cdot \beta_{RH}(RH) \cdot \beta_{ds}(t-t_s)$$

Drying shrinkage strain

$$\varepsilon_{cd,0} = \left((220 + 110 \cdot \alpha_{ds1}) \cdot e^{-\alpha_{ds2} \cdot f_{cm}}\right) \cdot 10^{-6}$$

Notional drying shrinkage coefficient.

$$\beta_{RH} = \begin{cases} 1{,}55 \cdot \left(1 - \left(\frac{RH}{100}\right)^3\right), & 40 \le RH < 99\% \cdot \beta_{s1} \\ 0{,}25 & RH \ge 99\% \cdot \beta_{s1} \end{cases}$$

Ambient relative humidity coefficient

$$\beta_{ds}(t-t_s) = \left(\frac{t-t_s}{0{,}035 \cdot h_0^2 + (t-t_s)}\right)^{0{,}5}$$

Drying shrinkage time development function.

$$h_0 = 2 \cdot \frac{Ac}{u}$$

Notional size of the concrete element.

$$\beta_{s1} = \left(\frac{35}{f_{cm}}\right)^{0{,}1} \le 1{,}0$$

$$\alpha_{ds1} = \begin{cases} 6 & Cement\ class\ S \\ 4 & Cement\ class\ N \\ 3 & Cement\ class\ R \end{cases}$$

$$\alpha_{ds2} = \begin{cases} 0{,}11 & Cement\ class\ S \\ 0{,}12 & Cement\ class\ N \\ 0{,}13 & Cement\ class\ R \end{cases}$$

equation 17: Drying shrinkage according to CEB-fip 2010.

$$\varepsilon_{ca}(t) = \varepsilon_{cas0}(f_{cm}) \cdot \beta_{as}(t)$$

Autogenous shrinkage strain.

$$\beta_{as}(t) = 1 - e^{-0{,}2 \cdot \sqrt{t}}$$

Autogenous shrinkage time development function.

$$\varepsilon_{cas0}(f_{cm}) = \alpha_{as} \cdot \left(\frac{f_{cm}/10}{6 + f_{cm}/10}\right)^{2{,}5} \cdot 10^{-6}$$

Notional autogenous shrinkage coefficient

$$\alpha_{as} = \begin{cases} 800 & Cement\ class\ S \\ 700 & Cement\ class\ N \\ 600 & Cement\ class\ R \end{cases}$$

equation 18: Autogenous shrinkage according to CEB-fip 2010.

A.2 Concrete creep CEB-fip 2010 model

$$\varphi(t,t_0) = \varphi_{bc}(t,t_0) + \varphi_{dc}(t,t_0)$$

$\varphi_{bc}(t,t_0)$: Basic creep coefficient

$\varphi_{dc}(t,t_0)$: Drying creep coefficient

equation 19: Creep coefficient according to the CEB-fip 2010 model.

$$\varphi_{bc}(t,t_0) = \beta_{bc}(f_{cm}) \cdot \beta_{bc}(t,t_0)$$

$$\beta_{bc}(f_{cm}) = \frac{1{,}8}{(f_{cm})^{0{,}7}}$$

$$\beta_{bc}(t,t_0) = \ln\left(\left(\frac{30}{t_0} + 0{,}035\right)^2 \cdot (t - t_0) + 1\right)$$

equation 20: Basic creep coefficient according to the CEB-fip 2010 model.

$$\varphi_{dc}(t,t_0) = \beta_{dc}(f_{cm}) \cdot \beta(RH) \cdot \beta_{dc}(t_0) \cdot \beta_{dc}(t,t_0)$$

$$\beta_{dc}(f_{cm}) = \frac{412}{(f_{cm})^{1{,}4}}$$

$$\beta(RH) = \frac{1 - \frac{RH}{100}}{\sqrt[3]{0{,}1 \cdot \frac{h_0}{100}}}$$

$$\beta_{dc}(t_0) = \frac{1}{0{,}1 + t_0^{0{,}2}}$$

$$\beta_{dc}(t,t_0) = \left(\frac{t - t_0}{\beta_h + (t - t_0)}\right)^{\gamma(t_0)}$$

$$\gamma(t_0) = \frac{1}{2{,}3 + \frac{3{,}5}{\sqrt{t_0}}}$$

$$\beta_h = \quad 1{,}5 \cdot h_0 + 250 \cdot \alpha_{f_{cm}} \leq 1500 \cdot \alpha_{f_{cm}}$$

$$a_{f_{cm}} = \left(\frac{35}{f_{cm}}\right)^{0{,}5}$$

equation 21: Drying creep coefficient according to the CEB-fip 2010 model.

B. Timber moisture content

B.1 Absorption analysis

In this chapter an experimental study is analysed to estimate the increase of the average moisture content of a structural member that is subjected to harsh outside conditions during transport and at the building site. The experimental study that is analysed, tested the moisture content distribution over the cross section of softwood glue laminated timber specimens as a function of loading duration (Franke, Franke, Schiere, & Müller, 2016).

Glue laminated timber blocks of 200x200x200mm were cut from one glue laminated timber member of 200x600x4000mm. All specimens were first conditioned to 12% moisture content at a temperature of 20 °C and relative humidity of 65%. When the equilibrium moisture content of 12% was reached over the whole cross section, the specimens were loaded with a 95% relative humidity for 12 months. “For the observation of the developing moisture content over the cross section, the test series were prepared in the three material axes: radial (R), tangential (T) and longitudinal (L)” (Franke, Franke, Schiere, & Müller, 2016). Gages were installed at a depth of 25, 45, 75 and 100mm to measure the moisture content.

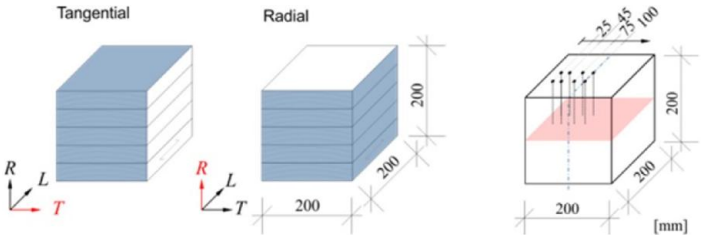

figure 10-1: Test specimen preparation. White: Open surface. Blue: Sealed surface (Franke, Franke, Schiere, & Müller, 2016).

The original results from the experiment are presented at the left of figure 10-3. These results are adopted with the use of Webplotdigitizer and Excel. The original results do not show the moisture content at the perimeter of the cross section, but in the adopted results this is assumed to be 24% as this is the equilibrium moisture content at a relative humidity of 95% and a temperature of 20°C according to the Wood Handbook (Ross, 2010, pp. 4-4). The moisture content curve is symmetrical, which is the reason why only half of the curve is shown. From the curve, the average moisture content for the whole cross section is determined which is indicated by the dotted lines. The average moisture content values can be plotted over time, which shows the development of the average moisture content over time (figure 10-2).

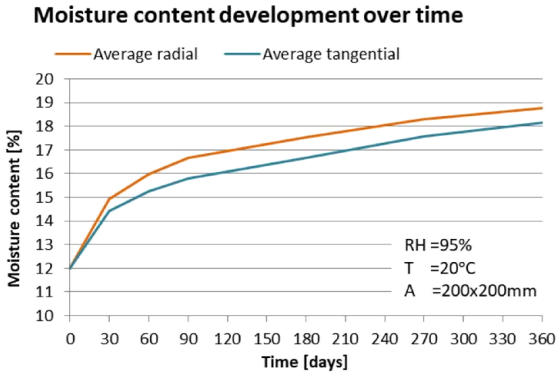

figure 10-2: Average moisture content development over time of a 200x200mm cross section, loaded with a RH of 95% and 20°C. Based on results of (Franke, Franke, Schiere, & Müller, 2016)

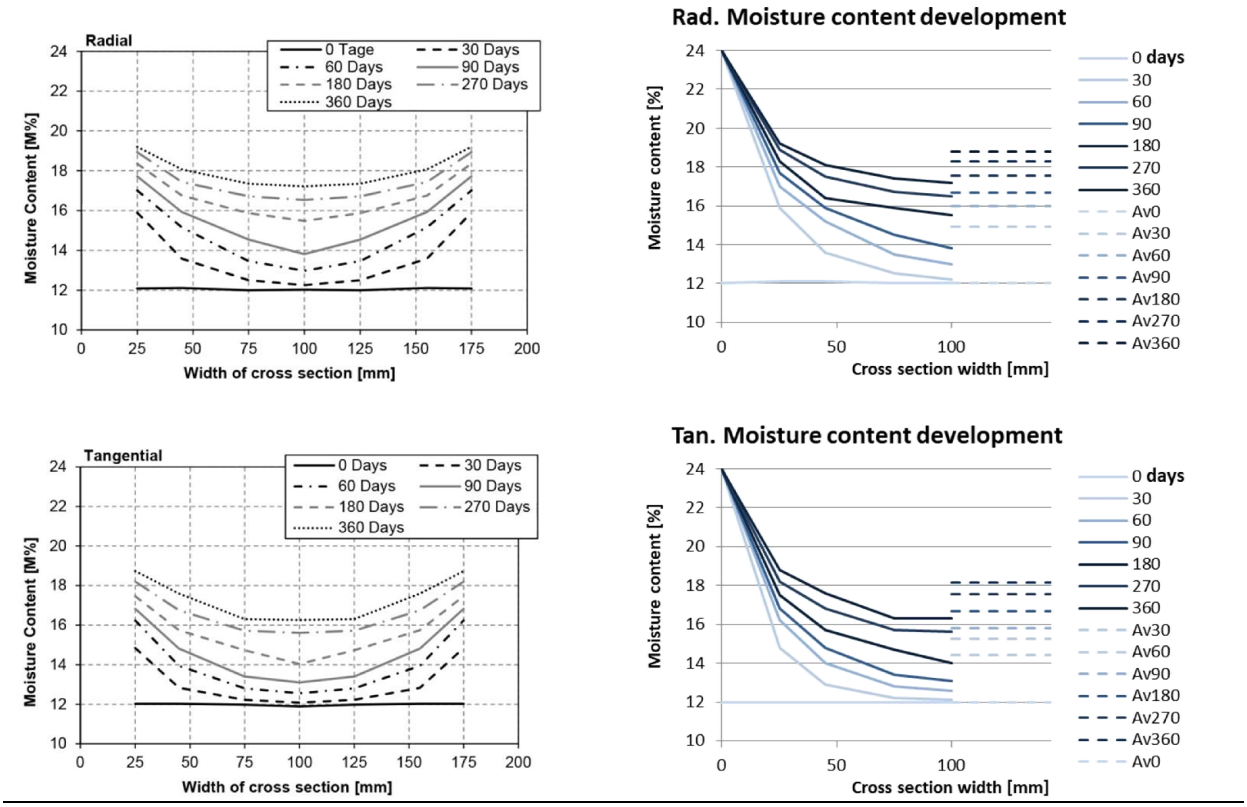

figure 10-3: Moisture content development results. Left: Original from source. Right: Adopted results with average moisture content (Franke, Franke, Schiere, & Müller, 2016).

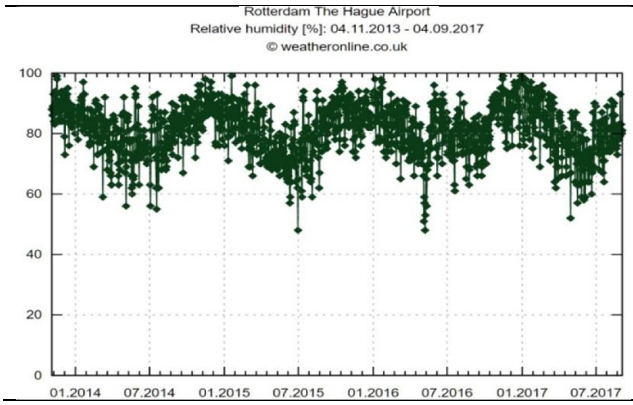

figure 10-4: Relative Humidity over the past 4 years at Rotterdam The Hague Airport. Retrieved from (WeatherOnline).

The plot of the average moisture content over time in figure 10-2 shows how fast the average moisture content of a specimen with a thickness of 200mm can increase, starting from 12%MC, subjected to a relative humidity of 95% and a temperature of 20°C when loaded in the radial and tangential axis. These conditions can be assumed as a good representation of a structural element coming from the factory at 12% moisture content and loaded to harsh outside weather conditions in the Netherlands (figure 10-4). This could be a CLT panel with a thickness of 200mm or a column with a cross section of 200x200mm with covered ends to prevent longitudinal diffusion.

The following assumptions can be made on basis of the experimental results of this analysis:

- When a structural member with a notional size of $h_0 = 200$, is subjected to outside conditions for not more than 30 days, a maximum moisture content increase can be expected of 3%. When the member is subjected to these conditions for not more than 60 days, a maximum moisture content increase of 4% can be expected.

B.2 Moisture content regression

After installation of timber structural elements the building structure will be closed by placing the façade elements. In further occupation, the relative humidity will decrease due to heating of the building, with a decrease of the average moisture content of the structure as a result.

In this chapter field measurements of the relative humidity and corresponding equilibrium moisture content of the Limnologen project in Växjo will be analysed to obtain an estimate of the moisture content regression in timber structural elements from the moment of installation to in service conditions.

figure 10-5: Limnologen at Växjo. Left: (Xiong Yu, Su Xin, & Sabri, 2009). Right: (Serrano, 2009).

The environmental conditions in terms of relative humidity and temperature were measured at the second and seventh floor. From this data the corresponding equilibrium moisture content was calculated by the authors. Because the average moisture content in the CLT will not immediately change with the change in relative humidity due to the slow process of water diffusion, a 30 day delay was used in the analysis of the authors (Xiong Yu, Su Xin, & Sabri, 2009, p. 14).

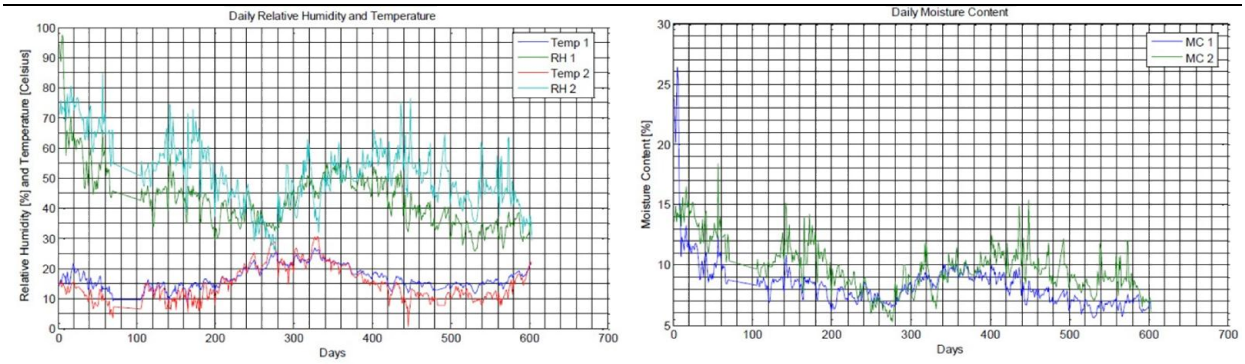

figure 10-6: Left: Measured temperature and Relative humidity an Limnologen. Right: Calculated equilibrium moisture content (Xiong Yu, Su Xin, & Sabri, 2009).

Because the water diffusion process takes time, and especially in larger structural elements, the high amplitudes of the average moisture content in the structure will mitigate as is also made clear in chapter 3.5.1 on page 58 of this thesis.

A trend curve is fitted over the calculated equilibrium moisture content graph with the upper moisture content value of 15% as a starting point (figure 10-7). This value is explained in chapter 4.2.3 on page 77 and appendix B.1. The moisture content will decrease to a lower moisture content value of 8% that is determined in chapter 4.2.3 on page 78.

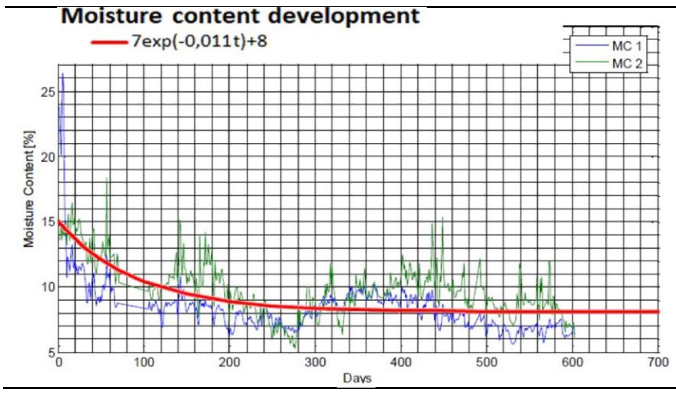

$$MC(t) = \Delta MC \cdot e^{-0{,}011 \cdot t} + MC_{lower}$$

$$\Delta MC = MC_{upper} - MC_{lower}$$

$$MC_{upper} = 15\%$$

$$MC_{lower} = 8\%$$

figure 10-7: Estimate of moisture content regression. Based on data of (Xiong Yu, Su Xin, & Sabri, 2009).

C. Timber longitudinal shrinkage experiments

In this chapter several experimental studies on longitudinal shrinkage in spruce timber are elaborated, compared and analysed to obtain an approximation of the mean longitudinal shrinkage coefficient α_l and its standard deviation in spruce timber.

All studied experiments showed a relatively high variation for the longitudinal shrinkage coefficient between small specimens from within one board or tree stem (Johansson, 2003; Gryc, Vavrcík, & Horácek, 2007; Bengtsson, 2001; Ormarsson & Cown, 2005).

C.1 Johansson

This study measured the distorted geometry of 12 Norway spruce studs (45x95x2500) with respect to bow and crook. After the bow and crook measurements the studs were sawn into a total of 3600 sticks (10x10x200mm). The longitudinal shrinkage of the sticks was obtained for a moisture content change of 17,6% to 7,8% from which the longitudinal shrinkage coefficient for every stick was calculated. The sticks were grouped into samples according to the studs from which they were obtained. The results showed a mean value with a certain standard deviation. "The longitudinal shrinkage coefficient varied considerably between studs but also within one stud" (Johansson, 2003, p. 450).

The numerical results of (Johansson, 2003) are adopted in excel and graphically shown in figure 10-8. In this figure one can see the high variability between the mean values of the studs, but also the high variability within one stud. In figure 10-9 all 12 samples are taken together as on sample. It shows the mean value and variance of all specimens together.

Stud number	Dim [mm]	n	Mean [%]	Std. Dev
110511	45 x 95	259	0,012	0,008
120632	45 x 95	274	0,007	0,004
131413	45 x 95	276	0,005	0,002
140632	45 x 95	272	0,011	0,006
140532	45 x 95	227	0,010	0,004
130551	45 x 95	247	0,007	0,003
1U1	45 x 120	391	0,014	0,008
4U1	45 x 120	359	0,012	0,010
6U2	45 x 120	338	0,008	0,006
7U1	45 x 120	344	0,026	0,023
4U2	45 x 120	298	0,010	0,011
12N	45 x 120	317	0,008	0,006

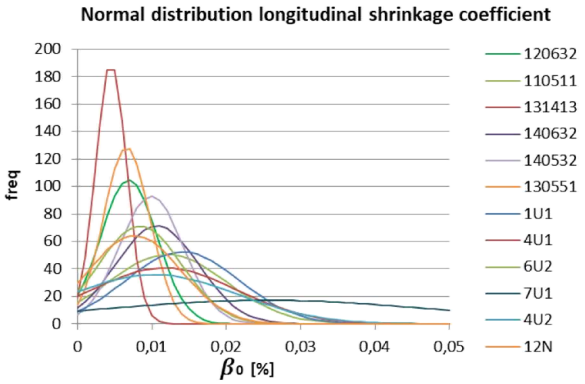

figure 10-8: Normal distribution for longitudinal shrinkage coefficient per stud. Data retrieved from (Johansson, 2003).

All samples are taken together in one large sample from which the normal distribution is shown in figure 10-9. The normal distribution of the total sample shows a high variance for small Norway spruce specimens.

Mean: *0,011*

Standard deviation: *0,011*

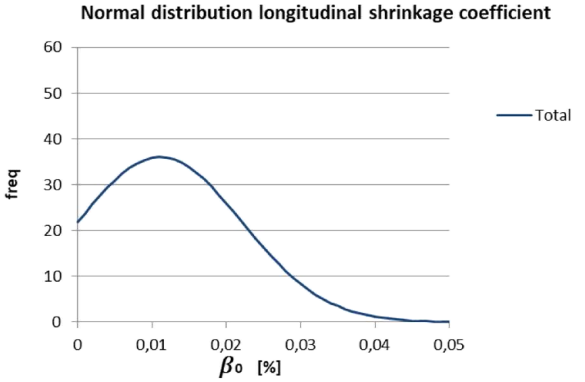

figure 10-9: Normal distribution of mean shrinkage coefficient. Based on data from (Johansson, 2003).

When plotting the normal distribution of the mean values that represent the shrinkage coefficient of a large specimen of 45x90x2500mm, the mean value will stay the same but the variance will decrease.

n=12

Mean: *0,011*

Standard deviation: *0,0052*

$$k_s(12) = \frac{6{,}8 \cdot 12 + 6}{3{,}7 \cdot 12 - 3} = 2{,}1$$

$\beta_{0,05}$: $\mu - k_s \cdot SD$ *0,001*

$\beta_{0,95}$: *0,021*

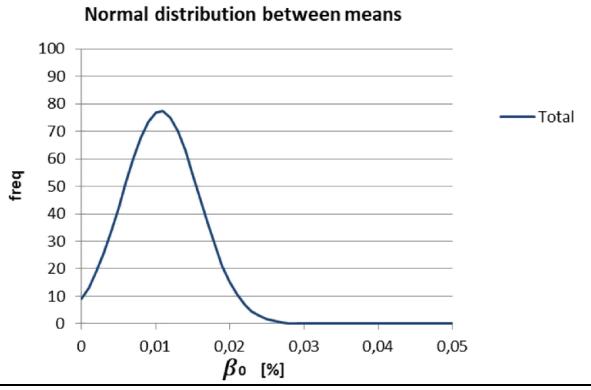

figure 10-10: Normal distribution between the studs.

C.2 Ormarsson & Cown

The goal of this research was to further develop a distortion model for radiate pine based on a previous research for Norway spruce. The model is based on data with respect to variation in the main material properties from pit to bark of radiate pine specimens. The specimens were retrieved from 50mm thick discs as is depicted together with the experimental data in figure 10-11 (Ormarsson & Cown, 2005).

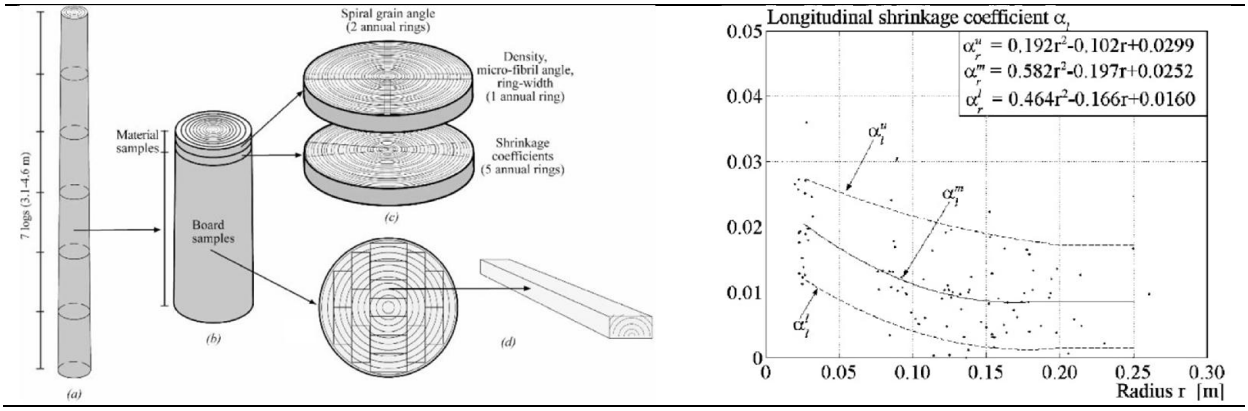

figure 10-11: Experimental procedure and presentation of longitudinal shrinkage coefficient data (Ormarsson & Cown, 2005).

For this research the material data is adopted in excel using 'webplotdigitizer'. The position from pit to bark is ignored, so the data represents the shrinkage coefficient and its variation for the whole tree stem. The data forms a sample of $n = 100$ specimens from which a normal distribution is plotted with a mean and standard deviation value according to figure 10-12.

Mean: *0,012*

Standard deviation: *0,0076*

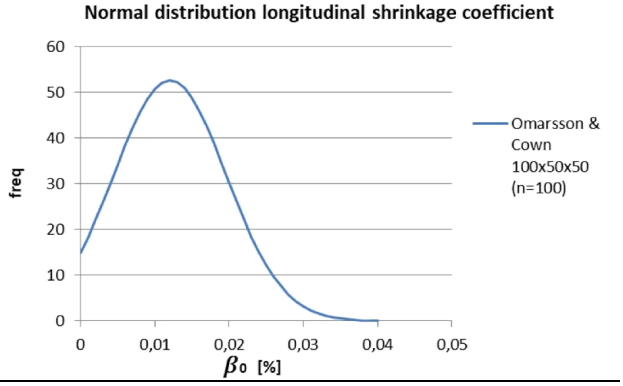

figure 10-12: Normal distribution of mean shrinkage coefficient. Based on data from (Ormarsson & Cown, 2005).

From figure 10-12 it can be concluded that there is a high variance for the longitudinal shrinkage coefficient within one tree. Just as in the experiment of Johansson in appendix C.1 the sample represents small specimens.

C.3 Bengtsson

This research studied the variability of moisture induced movements in Norway spruce (Picea abies) wood. The aim was to evaluate the shrinkage and swelling properties and how these properties are affected by the variability of the wood raw material. The research did not conduct tests on specifically clear specimens, but on a variability of specimens that represent the structural wood material. In total 987 specimens of 11x11x200mm were tested from 6 slow-grown and 6 fast-grown trees, which results in 12 separable samples (Bengtsson, 2001).

The results of the experiment are adopted in excel an presented in figure 10-13. The plots show the mean value and variance of the longitudinal shrinkage coefficient within every tree. The slow and fast grown trees are plotted in separated graphs. In figure 10-14 the total normal distribution is shown that takes all samples of the individual trees together.

From figure 10-13 it can be concluded that there is a high variation for the longitudinal shrinkage coefficient within the trees but also among the trees. From the total normal distribution of figure 10-14 it can be concluded that there is a high overall variation in the longitudinal shrinkage coefficient for small specimens (11x11x200) from Norway spruce wood.

Tree nr	Dim [mm]	n	Mean [%]	Std. Dev
f2	11x11x200	90	0,005	0,002
f22	11x11x200	90	0,006	0,002
f32	11x11x200	90	0,012	0,007
f4	11x11x200	45	0,013	0,002
f52	11x11x200	90	0,01	0,002
f62	11x11x200	89	0,009	0,002
s1	11x11x200	90	0,006	0,002
s12	11x11x200	90	0,006	0,002
s3	11x11x200	43	0,004	0,001
s42	11x11x200	90	0,006	0,002
s72	11x11x200	90	0,006	0,002
s82	11x11x200	90	0,005	0,003

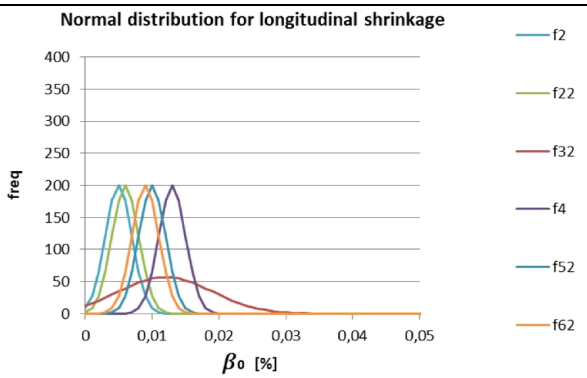

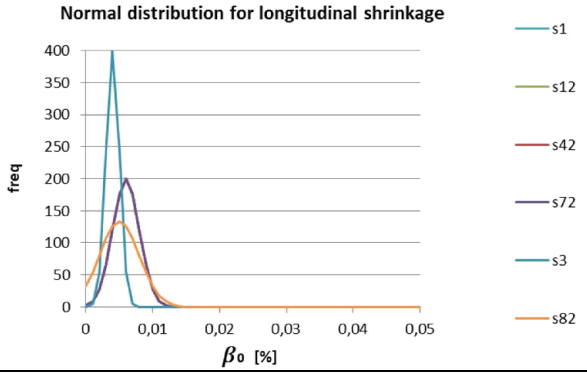

figure 10-13: Normal distribution for longitudinal shrinkage coefficient per tree. Data retrieved from (Bengtsson, 2001).

Mean: *0,0072*

Standard deviation: *0,0039*

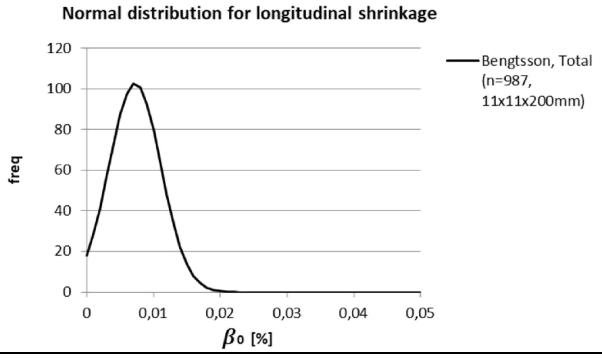

figure 10-14:Normal distribution longitudinal shrinkage coefficient. Based on data from (Bengtsson, 2001).

C.4 Gryc, Vavrcík, Horácek

This research conducted an experiment to study the variability in swelling and shrinkage in spruce with the presence of compression wood. A sample was selected from which it was presumed that there was a presence of compression wood, because the tree stem axis was deflected from the direction of gravitation. Several logs were cut out of one tree on several heights and subdivided in several zones according to figure 10-15. It is presumed by visual judgement that the CW and CW/CW zones contain compression wood (Gryc, Vavrcík, & Horácek, 2007).

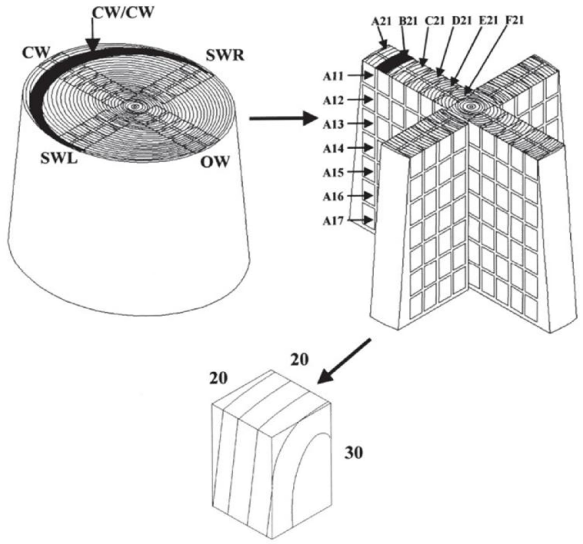

figure 10-15: Cutting pattern of specimens from the log (CW - compression wood, OW - opposite zone, SWL-SWR - Side zones) (Gryc, Vavrcík, & Horácek, 2007).

The mean value and standard deviation for each zone is presented by (Gryc, Vavrcík, & Horácek, 2007) and adopted for this research in excel. The normal distribution curve of each zone is shown in the top graph of figure 10-16 including the zones with compression wood. The lower graph of figure 10-16 represents the weighted average normal distribution of all zones together.

The total normal distribution takes the 5 samples of the different zones together as one sample that represents the whole tree stem cross section. The mean longitudinal shrinkage coefficient of the total sample is increased by the longitudinal shrinkage in the compressive zones of the tree stem. The higher longitudinal shrinkage value in compression wood is explained by because of the increased fibrillar angle in the S2 layer of the secondary cell wall (Gryc, Vavrcík, & Horácek, 2007).

When adopting the results for the longitudinal shrinkage coefficient of (Gryc, Vavrcík, & Horácek, 2007), one should question if these results are a good representation of the longitudinal shrinkage coefficient for structural timber. The presence of reaction wood is a characteristic that is adopted in the strength grading requirements, so excessive amounts of compression or reaction wood are not allowed in structural timber by the strength grading regulations (Glos, 1995). This is why the results of (Gryc, Vavrcík, & Horácek, 2007) overestimate the longitudinal shrinkage coefficient for structural timber. Even the non-compressive zones (OW, SWL and SWR) can contain higher amounts of reaction wood in comparison to normal structural timber, which makes a full comparison with normal wood impossible as is also stated by (Gryc, Vavrcík, & Horácek, 2007, p. 250).

Zone	n	Mean [%]	Std. Dev
OW	204	0,015	0,012
SWL	202	0,017	0,01
SWR	217	0,02	0,014
CW	297	0,022	0,017
CW/CW	133	0,031	0,018
Total	1053	0,0204	0,019

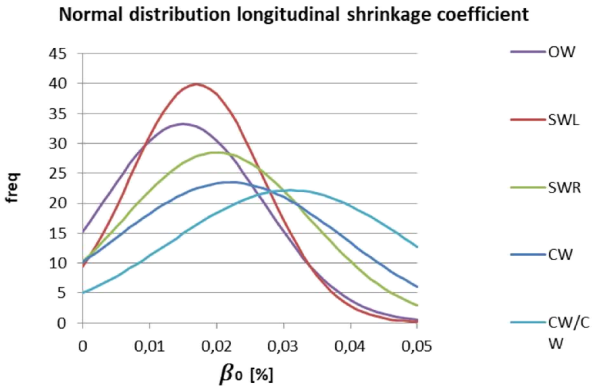

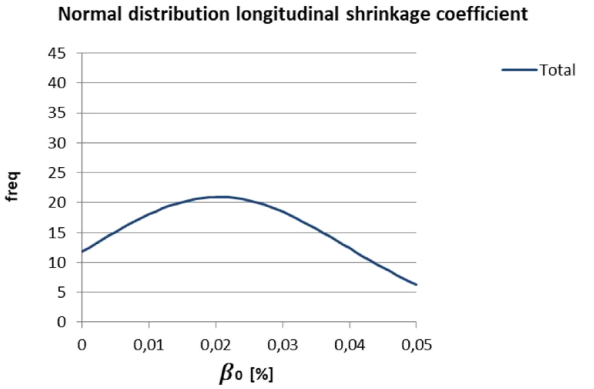

figure 10-16: Normal distribution for longitudinal shrinkage coefficient per zone and the weighted average normal distribution of OW, SWL and SWR. Data retrieved from (Gryc, Vavrcík, & Horácek, 2007).

C.5 Analysis

The results of each experimental study on the longitudinal shrinkage coefficient are adopted and elaborated in appendix C.1 to C.4. The statistical results of these experiments are plotted together in figure 10-17.

Gryc, Vavrcík and Horácek conducted their experiment on specimens that were retrieved from a tree that was presumed to have reaction wood. It is known that reaction wood causes considerable larger values for longitudinal shrinkage, which was also proved in the several experimental studies (Bengtsson, 2001; Gryc, Vavrcík, & Horácek, 2007; Perstorper, Johansson, Kliger, & Johansson, 2001). It can be assumed that the mean value of this experiment overestimates the longitudinal shrinkage coefficient. For this reason this result should not be adopted in the estimation of the longitudinal shrinkage coefficient.

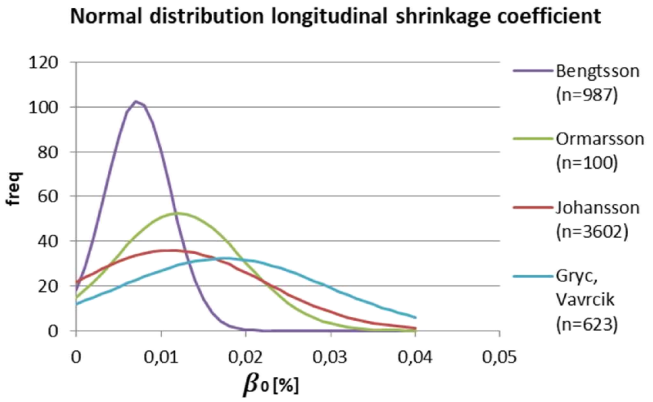

n: *4689*

$\beta_{0,mean}$*:* $0{,}01\%/\%\Delta MC$

Standard deviation: $0{,}0073$

$\beta_{0,05}$*:* *-0,003*

$\beta_{0,95}$*:* *0,027*

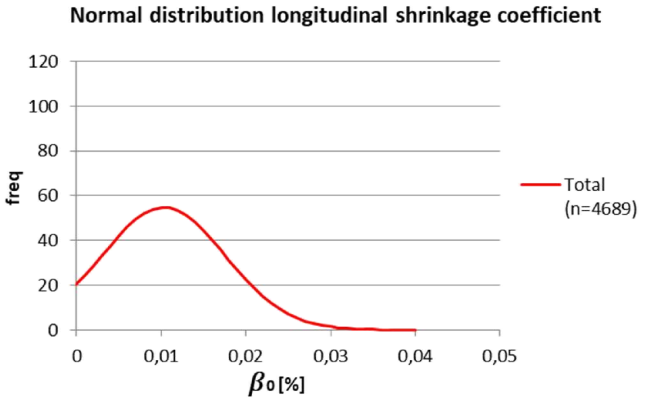

figure 10-17: Comparison between the normal distributions of the several experimental results on longitudinal shrinkage.

Conclusion and recommendations

The results of Bengtsson, Ormarsson and Cown and Johansson are taken together for a total estimation of the longitudinal shrinkage coefficient in small specimens for structural timber. The total normal distribution is shown in the bottom graph of figure 10-17.

The mean value of the shrinkage coefficient has a value of $0{,}01\%/\%\Delta MC$ and the 90 percent confidence interval ranges from *-0,003* till *0,027,* which is a variance of $\pm 145\%$. These values represent small specimens with the presence of material defects.

The mean value can be assumed to be a good estimator for the mean longitudinal shrinkage coefficient, but the variance can be incorrect when considering full size structural elements. 'In general, the smaller the cross section, the greater the variability' (Glos, 1995, p. 1). In small specimens local material defects can have a relative larger impact on the average piece properties and can cause a higher variation within the sample of small specimens. Additionally, the experiments that are elaborated showed the shrinkage variation in the cross section of the whole tree stem. This means that the samples are retrieved from a population that represents a large range of wood qualities. The variance that is retrieved from the different experiments and graphically shown in figure 10-17 is for these reasons assumed to overestimate the variance that is present in full size structural elements that are picked from on particular strength class. The results of figure 10-10 that are retrieved from the experiments of Johansson show the same mean value of $0{,}01\%/\%\Delta MC$. However, the standard deviation is smaller resulting in a variance of $\pm 99\%$ in the 90 percent confidence interval. These values represents a sample with a specimen size of 45x90x2500mm, which is a better representation of full sized structural elements.

From an engineering perspective it could be more interesting to retrieve samples from particular timber strength classes. The strength class system orders the quality of the whole wood population with respect to knots, grain deviations and other material defects. In the shrinkage experiments it is shown that an increase of these material defects increase the longitudinal shrinkage coefficient (Bengtsson, 2001; Perstorper, Johansson,

Kliger, & Johansson, 2001). This implies that, if samples are taken from particular strength classes, the longitudinal shrinkage coefficient can be determined more precisely per strength class with less variance.

D. Timber creep experiments

The goal of this chapter is to attain a quantitative approximation of the creep behaviour of timber structural elements that are situated in service lass 1 (indoor) conditions. Experimental data results of several independent creep experiments are compared to one another and analysed to gain insight in the mean creep development and standard deviation in timber structural elements (Gowda, Kortesmaa, & Ranta-Maunus, 1996; Abdul-Wahab, Taylor, Price, & Pope, 1998; Aratake, Morita, & Arima, 2011).

For this research the graphical results from the experimental research were analysed by 'webplotdigitizer' and were replotted in Excel. The data is used to plot a mean curve, its standard error and to determine the standard deviation of the samples. From the standard deviation and the sample size, the 5^{th} and 95^{th} percentile values can be determined according to the Dutch standard (NEN-EN 14358, 2016).

D.1 Gowda, Kortesmaa and Ranta-Maunus

This experimental research investigated the long-term creep behaviour of structural timber elements of various species and various engineering methods over a four year time period. The experiments were conducted in a sheltered climate with natural environmental conditions of Southern Finland. This research also conducted a creep experiment on glue laminated beams in a heated room environment. The specimens were all loaded in a four-point bending test (Gowda, Kortesmaa, & Ranta-Maunus, 1996). The specimens that were tested consisted of non-treated and treated or impregnated specimens. For this research only the non-treated specimens are considered. Specimen details are shown in table 20.

Experiment	Name	Load situation	Species	Climate class	Timber	Stress [N/mm2]	Number of specimens	bxh [mm]	L [mm]
Gowda, Kortesmaa, Ranta-Maunus	Pine 7.4	Four point bending	Pine	CL2	Sawn	7,4	2	50x150	5000
	Pine 7.1	Four point bending	Pine	CL2	Sawn	7,1	2	50x150	5000
	Spruce 7.1	Four point bending	Spruce	CL2	Sawn	7,1	2	50x150	5000
	Spruce 7.0	Four point bending	Spruce	CL2	Sawn	7	2	50x150	5000
	Spruce 2.2_1	Four point bending	Spruce	CL2	Sawn	2,2	2	50x100	5000
	Spruce 2.2_2	Four point bending	Spruce	CL2	Sawn	2,2	2	50x100	5000
	GLT 2.1_1	Four point bending	Spruce	CL2	GLT	2,1	2	90x180	6500
	GLT 2.1_2	Four point bending	Spruce	CL2	GLT	2,1	2	90x180	6500
	GH1_2	Four point bending	Spruce	CL1	GLT	2	1	90x270	9400
	GH4_2	Four point bending	Spruce	CL1	GLT	2	1	90x270	9400
	GH8_2	Four point bending	Spruce	CL1	GLT	2	1	90x270	9400
	GH5_2	Four point bending	Spruce	CL1	GLT	2	1	90x270	9400
	GH2_4	Four point bending	Spruce	CL1	GLT	4	1	90x270	9400
	GH3_4	Four point bending	Spruce	CL1	GLT	4	1	90x270	9400
	GH6_4	Four point bending	Spruce	CL1	GLT	4	1	90x270	9400
	GH7_4	Four point bending	Spruce	CL1	GLT	4	1	90x270	9400

table 20: Specimen details (Gowda, Kortesmaa, & Ranta-Maunus, 1996).

The results for the specimens in climate class 2 were given as the average of a couple. The results of the specimens in climate class 1 were given for each specimen individually. The data of the creep experiments are shown in figure 10-18. The data is ordered and grouped by climate class and stress level. In figure 10-19 a mean creep curve and its standard error is determined per climate class that is derived from the data in figure 10-18. The mean data is curve fitted and from the standard deviation and sample size a 90% confidence area is determined. Finally, the fitted trend curve is extrapolated in a 50 year time plot.

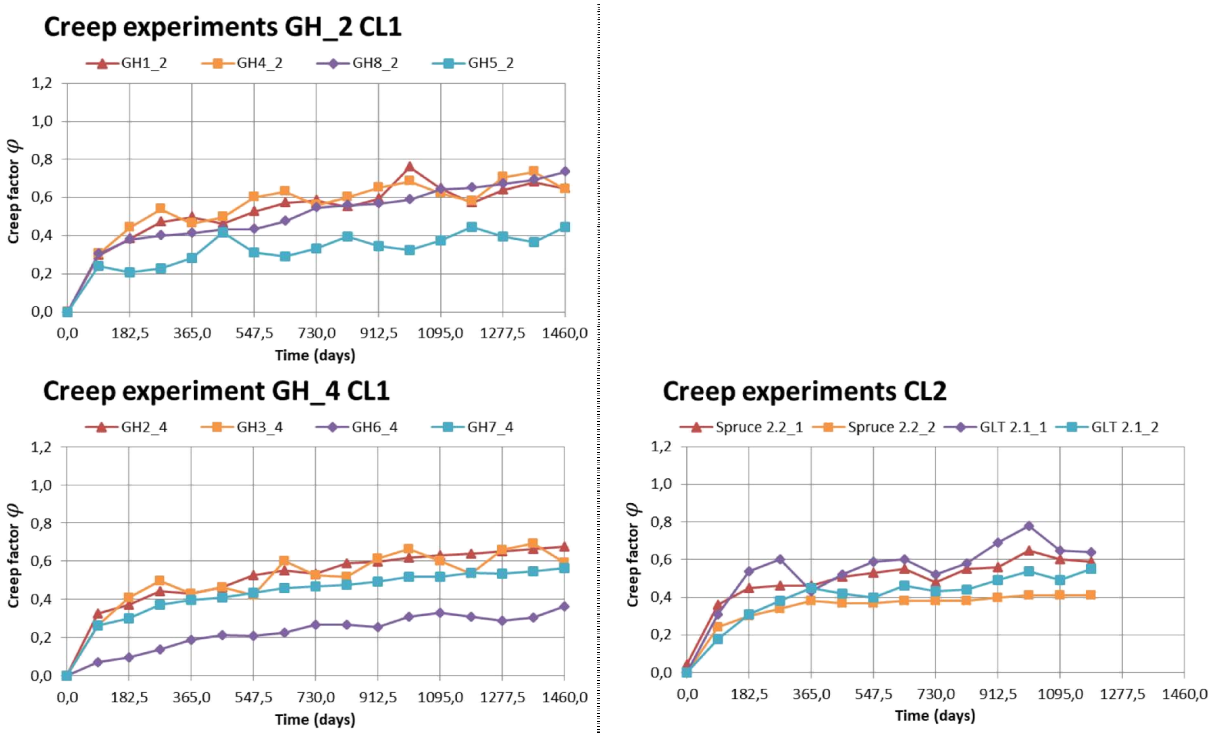

figure 10-18: Creep curves of experimental results of Ranta-Maunus, Kortesmaa and Gowda. Left: Climate class 1, Right: Climate class 2.

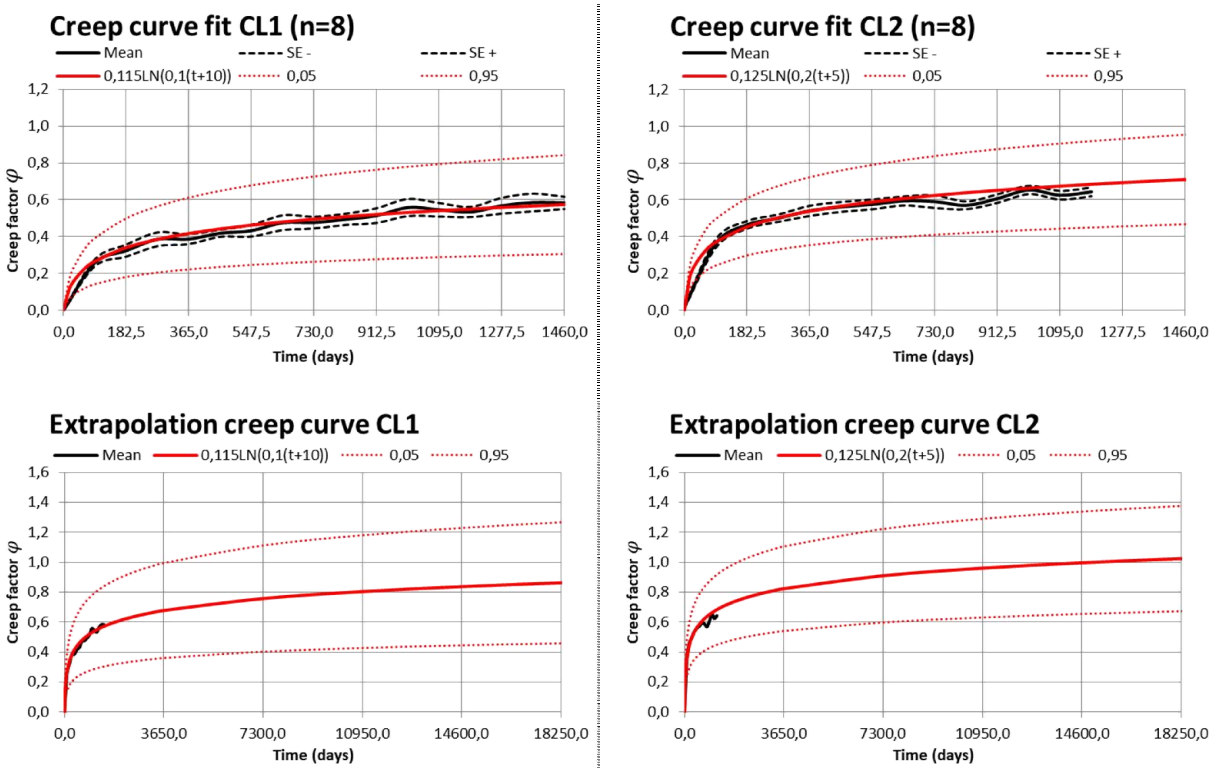

figure 10-19: Mean/average of experimental results with curve fit and extrapolation. Left: Climate class 1, Right: Climate class 2.

D.2 Abdul-Wahab, Taylor, Price and Pope

This experimental research investigated the long-term creep behaviour of glue laminated structural timber elements over an eight year time period. The experiment was conducted in constant, variable and outside environment conditions which is equivalent to climate class 1,2 and 3 respectively. This research also conducted a creep experiment on in situ beams in of existing structures. The specimens were all loaded in a four-point bending test. The specimens that were tested consisted of standard and highly loaded specimens, which corresponds to 7,5N/mm^2 and 11,75N/mm^2 respectively (Abdul-Wahab, Taylor, Price, & Pope, 1998). For this research only the standard loaded specimens in climate class 1 and 2 are considered.

Experiment	Name	Load situation	Species	Climate class	Timber	Stress [N/mm2]	Number of specimens	bxh [mm]	L [mm]
Abdul-Wahab	CMGSU	Four point bending	-	CL1	GLT	7,5	3	45x150	1800
	CLGSU	Four point bending		CL1	GLT	7,5	3	70x190	1800
	B2	In situ Church hall		CL1	GLT-Varnished		1	115x450	5000
	B3	In situ Church hall		CL1	GLT-Varnished		1	115x450	5000
	B8	In situ Church hall		CL1	GLT-Varnished		1	115x450	5000
	B12	In situ Church hall		CL1	GLT-Varnished		1	115x450	5000
	Beam3	In situ Moulescoomb		CL1	paired beam		1	130x270	4500
	Beam4	In situ Moulescoomb		CL1	paired beam		1	130x270	4500
	VLGSU	Four point bending		CL2	GLT-Varnished	7,5	3	70x190	1800
	VMGSU	Four point bending		CL2	GLT-Varnished	7,5	3	45x150	1800
	Beam1,2	Insitu Swimming pool		CL2	GLT-Varnished		2	140x405	6000
	Beam3,6,8	Insitu Swimming pool		CL2	GLT-Varnished		3	140x405	6000
	Beam4,5,7	Insitu Swimming pool		CL2	GLT-Varnished		3	140x405	6000

table 21: Specimen details (Abdul-Wahab, Taylor, Price, & Pope, 1998).

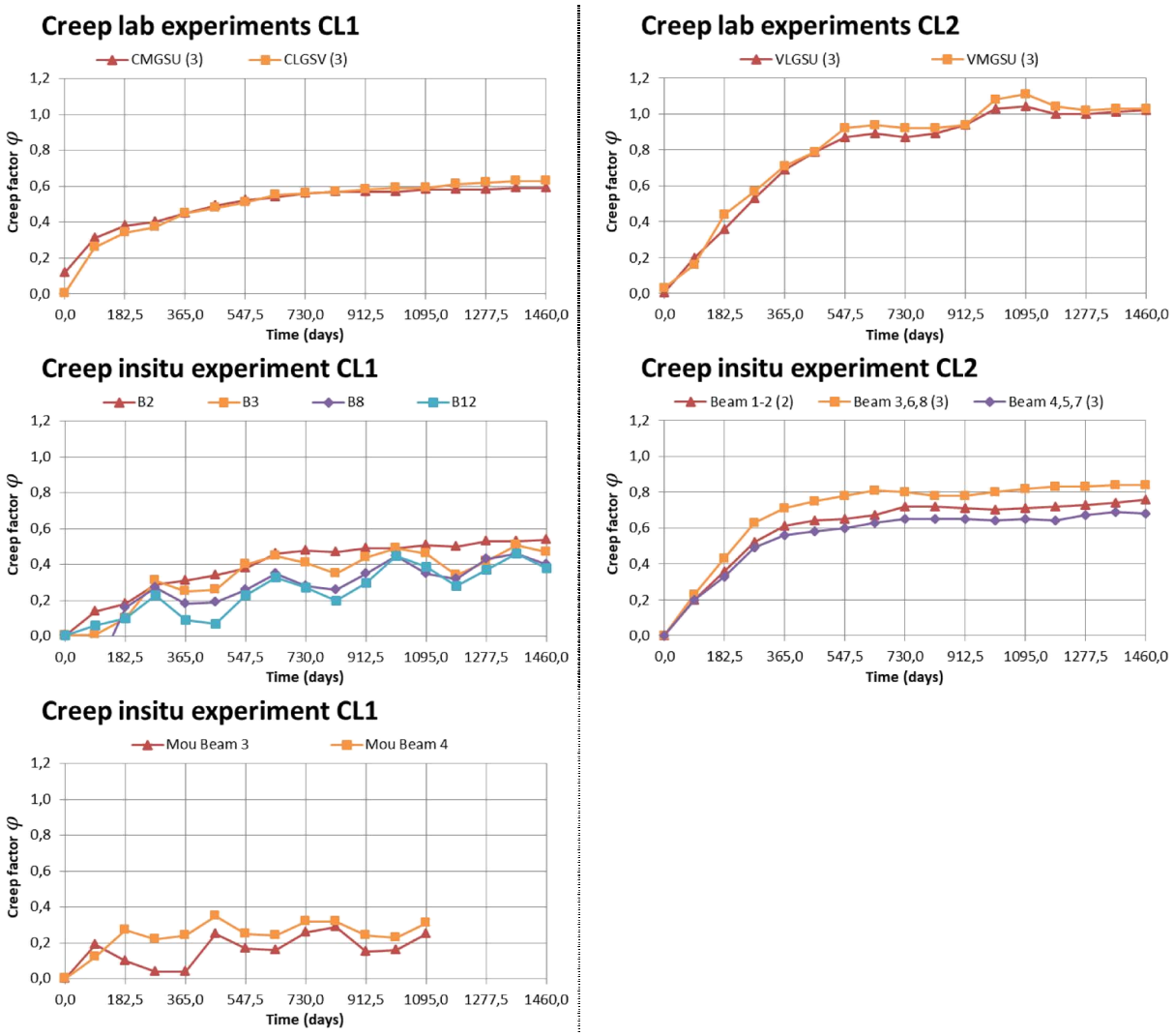

figure 10-20: Creep curves of experimental results of Abdul-Wahab. Left: Climate class 1, Right: Climate class 2.

The laboratory and in-situ results were given as the average of a group of 3 specimens. The data of the creep experiments are shown in figure 10-20. The data is ordered by climate class and lab or in-situ experiment. In figure 10-21 a mean creep curve with standard error is determined per climate class that is derived from the data in figure 10-20. The mean data is curve fitted and from the standard deviation and sample size a 90% confidence area is determined. Finally, the fitted trend curve is extrapolated in a 50 year time plot.

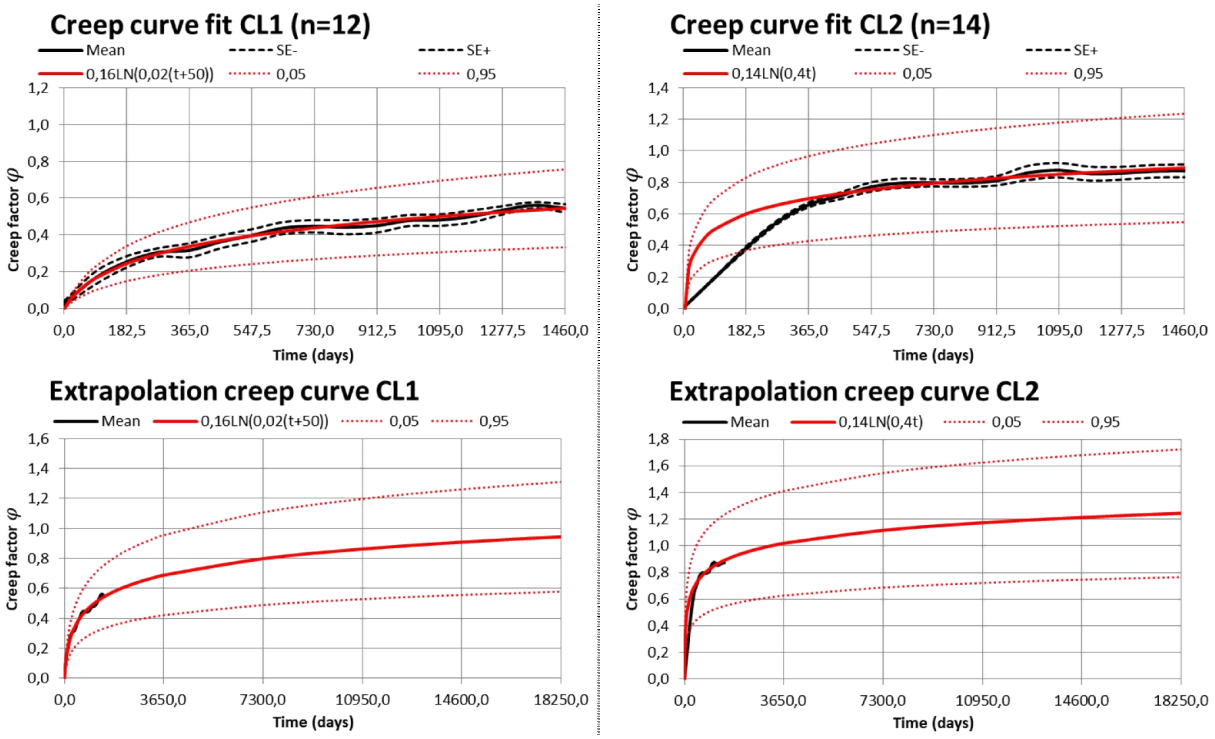

figure 10-21: Mean/average of experimental results with curve fit and extrapolation. Left: Climate class 1, Right: Climate class 2.

D.3 Aratake, Morita and Arima

This experimental research investigated the possibility to use sugi lumber with a very low Young's modulus as inner layers in glue laminated timber beams from the viewpoint of creep deformations. The outer laminae are made from Douglas-fir with much higher mechanical properties. The experiment was conducted in constant environment conditions which is equivalent to climate class 1. Eight specimens with different lamina setups were tested in a four-point bending test (Aratake, Morita, & Arima, 2011).

Experiment	Name	Load situation	Species	Climate class	Timber	Stress [N/mm2]	Number of specimens	bxh [mm]	L [mm]
Aratake, Morita, Arima	Hybrid L50	Four point bending	Sugi	CL1	GLT	10	1	105x210	3980
	Hybrid L30	Four point bending	Sugi	CL1	GLT	10	1	105x210	3980
	Sugi L50	Four point bending	Sugi	CL1	GLT	10	1	105x210	3980
	Sugi L30	Four point bending	Sugi	CL1	GLT	10	1	105x210	3980
	Sugi LH-L50	Four point bending	Sugi	CL1	GLT	10	1	105x210	3980
	Sugi LH-L30	Four point bending	Sugi	CL1	GLT	10	1	105x210	3980
	Sugi HL-L50	Four point bending	Sugi	CL1	GLT	10	1	105x210	3980
	Sugi HL-L30	Four point bending	Sugi	CL1	GLT	10	1	105x210	3980

table 22: Specimen details (Aratake, Morita, & Arima, 2011).

The data of the creep experiments that is obtained with 'webplotdigitizer' is shown in figure 10-22. The data is ordered by the symmetry of the cross section. In figure 10-23 a mean creep curve with standard error is determined per climate class that is derived from the data in figure 10-22. The mean data is curve fitted and from the standard deviation and sample size a 90% confidence area is determined. Finally, the fitted trend curve is extrapolated in a 50 year time plot.

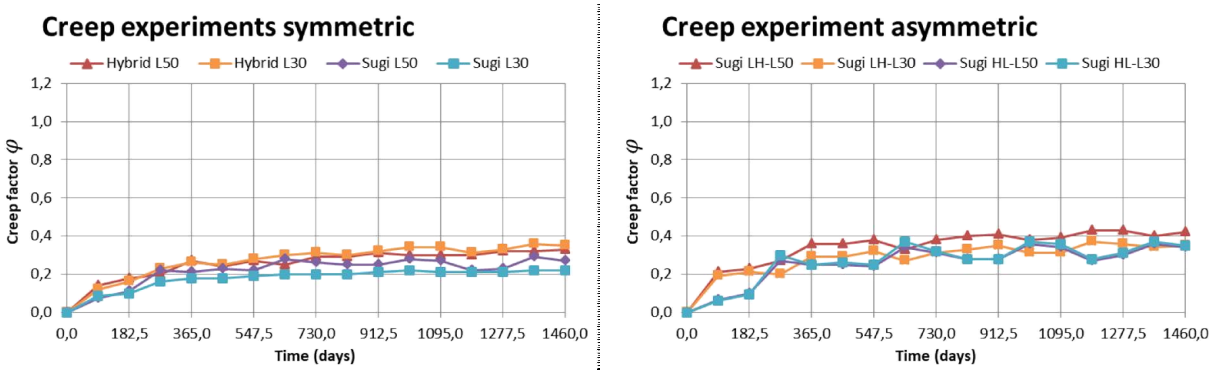

figure 10-22: Creep curves of experimental results of Aratake. Left: Symmetrical beam composition, Right: Asymmetrical beam composition.

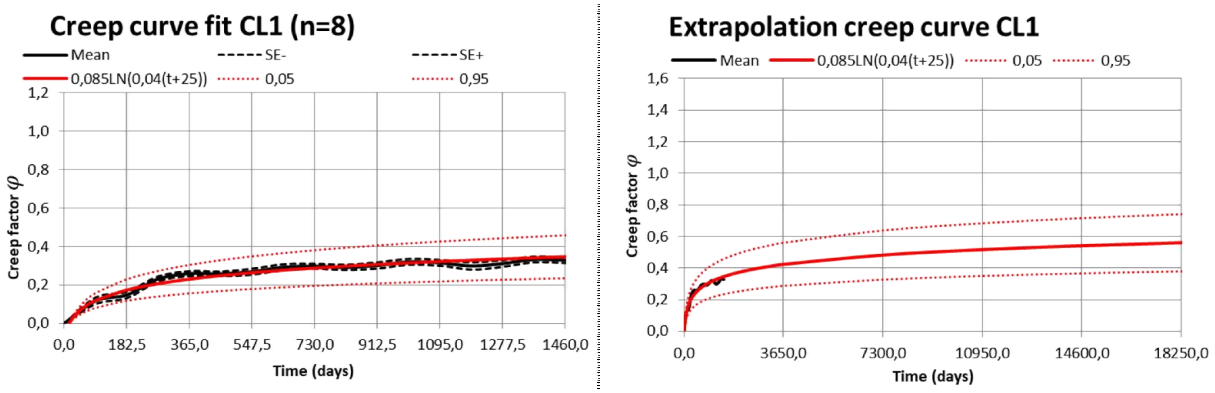

figure 10-23: Mean/average of experimental results with curve fit and extrapolation. Left: 4years, Right: 50year extrapolation.

D.4 Analysis

The results of each experimental research are elaborated and depicted in figure 10-18 till figure 10-23. In this evaluation each experiment is considered as a sample with a size of *n* specimens. The samples are compared to each other to verify what the resultant differences are and if the experiments are comparable to each other. Only the results of the specimens in climate class 1 are considered.

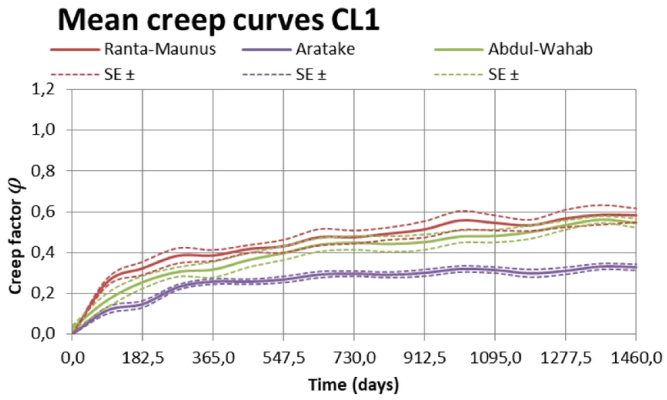

Standard Error: $SE = \frac{SD}{\sqrt{n}}$

Standard error for difference: $SE_{diff} = \sqrt{SE1^2 + SE2^2}$

z-statistic: $z = \frac{|\mu_1 - \mu_2|}{SE_{diff}}$

	Ranta-Maunus vs Aratake	Ranta-Maunus vs Abdul-Wahab	Abdul-Wahab vs Aratake
z-statistic	5,43	**0, 90**	5,48

figure 10-24: Mean creep curves for several experimental researches with their *Standard Error* and z-statistic between results.

The mean or average values of the three experiments are all subject to chance variability. The computed standard error *SE* must take this into account. The z-statistic can help in deciding if the difference in mean values of multiple samples is due to chance variability or due to differences in experimental conditions. The first would mean that the results of the multiple samples are comparable and the relatively small difference of mean values is due to chance variability, the latter would mean that the difference in mean values is too large for being explained by chance variability. Inconsistencies between experimental conditions such as sample qualities, wood species or environmental conditions are a more probable reason that explains the difference (Freedman, Pisani, & Purves, 2007). If the results of the experiments are comparable this would mean that the samples can be used in a single analysis. The advantage is that the sample size increases, so the mean value and confidence area can be determined more precisely.

The mean creep curves with their standard error of the three experiments are shown in figure 10-24. From the individual standard errors the *standard error for difference* can be found by using the square root law. The *z-statistic* can be determined by the difference between averages divided by the *standard error for differences.* A small z-statistic implies that the difference in sample mean values is relatively small compared to the standard errors of these samples which means that it can be likely that the difference is caused by chance variability

From figure 10-24 it can be concluded that the experiment of Ranta-maunus and Abdul-Wahab are comparable to one another and that it is likely that differences have occurred due to chance variability. The results of Aratake are very different when compared to the other two experiments. It is highly unlikely that this is only due to chance variability, so the results are incomparable.

The low creep factor results that were found in the experimental study of Aratake et al. can be explained by the use of Douglas fir with a high Young's modulus for the outer lamellas of the specimens. On the one hand, the outer lamellas are subjected to the highest stresses because the specimens are loaded by bending. On the other hand, the outer lamellas will be subjected to additional stresses because of the higher stiffness of these lamellas. For these reasons, the outer Douglas fir lamellas with a high Young's modulus provide most contribution to the experimental results. The other two experiments were conducted on spruce and pine specimens. The considerable difference can be due to the different use of wood species.

To finalize the evaluation of the creep experiments, the results of Ranta-Maunus and Abdul-Wahab are combined in one single analysis. The data of both experiments for the specimens that were categorized in climate class 1 are depicted in figure 10-25. From this data a new mean creep curve with standard error is determined and curve fitted. The 90% confidence interval is determined from the sample size and standard deviation according to the parametric calculation of the Dutch standard (NEN-EN 14358, 2016).

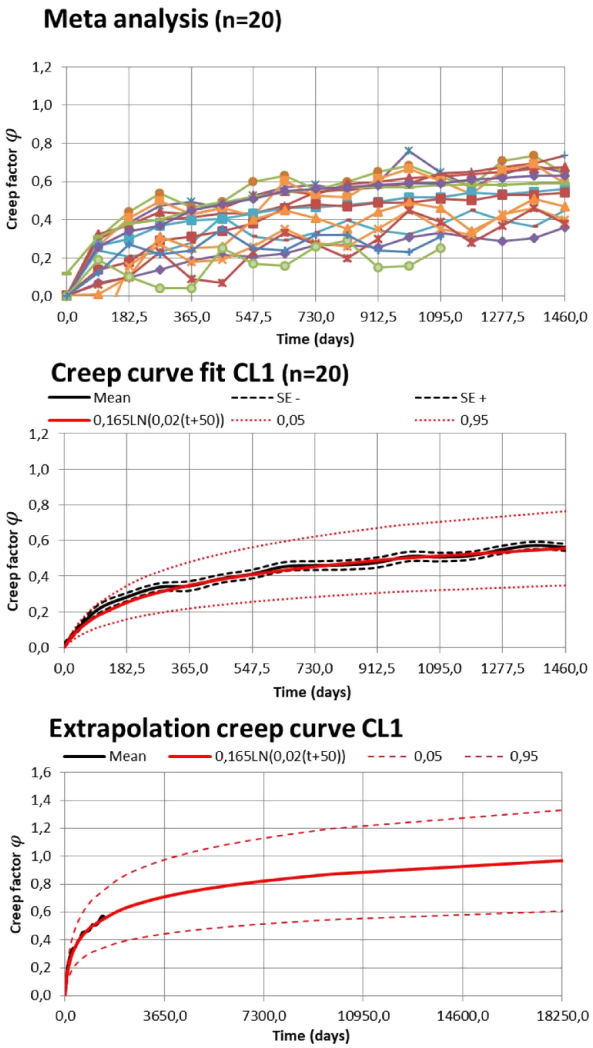

$$SD = 18{,}7\%$$

$$SE = \frac{1}{\sqrt{20}} \cdot 18{,}7 = 4{,}2\%$$

$$k_s(20) = \frac{6{,}8 \cdot 20 + 6}{3{,}7 \cdot 20 - 3} = 2{,}0$$

$$5^{th}\ perc. = \mu - k_s \cdot SD = 0{,}63\varphi(t)$$

$$95^{th}\ perc. = \mu + k_s \cdot SD = 1{,}37\varphi(t)$$

figure 10-25: Creep curve fit of meta-analysis.

Conclusions and recommendations

In this study the data of several creep experiments are elaborated and analysed. The data is ordered according to the climate class in which the specimens are situated. In figure 10-25 a meta-analysis is conducted for specimens that were situated in climate class 1.

Despite that the specimens are ordered to their climate class, there are still some inconsistencies in the test conditions among specimens and between the experiments. For instance stress level, element size and type of engineered timber varies. Additionally, the strength class from which the specimens are retrieved is not known. From the perspective of the engineer it could be interesting to know how the creep factor development is related to the strength class range that is available on the market. For future research to the creep development it can be useful to have more regulation on how the experiments should be conducted and data is presented to attain more consistency between sample data. This regulation can prescribe for instance the relative stress level, specimen size, climate conditions and test duration.

Despite the inconsistencies between creep experiments and the limited sample sizes, the analysis shows acceptable results with respect to the estimation of the creep development. The deviation in the 90% confidence interval is $\pm 37\%$ which is approximately in the same order of magnitude as the estimator of concrete creep which is $\pm 41\%$ (chapter 4.1.3). More test data should be generated in a regulated manner in order to gain more confidence in the creep behaviour of timber structural elements.

For the prediction of creep in structural timber elements that are situated in a climate class 1 environment, this research assumes that the predictive curve fitting function of figure 10-25 estimates proper results.

E. Load relative to resistance

This chapter shows what the maximum characteristic stresses can be relative to the characteristic and mean strength when a design satisfies the unity check in the ultimate limit state (ULS) according to the Eurocode. By knowing the maximum characteristic utilization of the material it can be decided whether or not to use linear elastic analysis when calculating deformations.

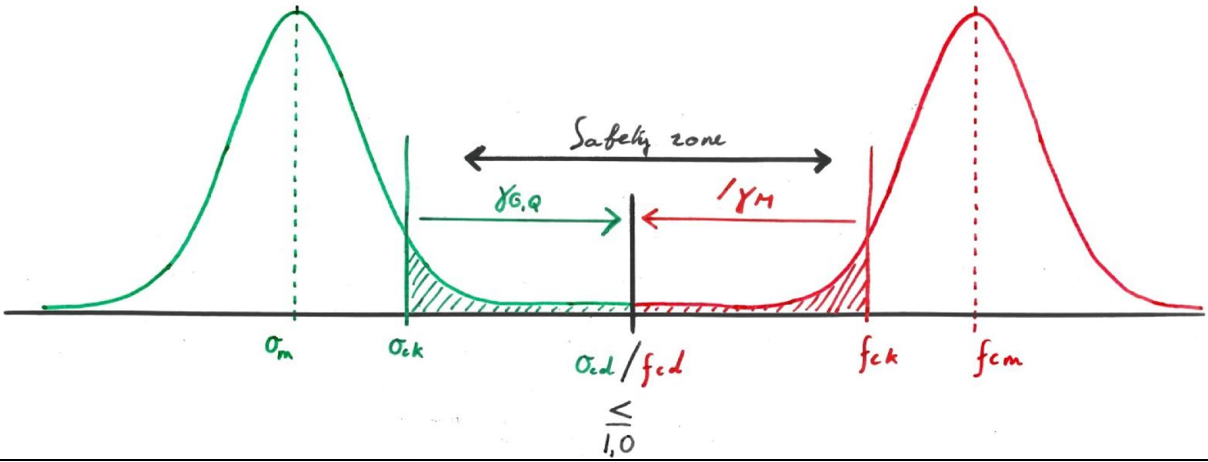

figure 10-26: Regulation of safety in the Ultimate limit state.

On the one hand, the estimated characteristic loads σ_{ck} on the design are multiplied by a safety factor which results in the design load σ_{cd}. The safety factor $\gamma_{G,Q}$ depends on the type of load (permanent (G) or variable (Q)) and the desired reliability of the design. The consequence class indicates the reliability of the design. Consequence class 1 (CC1) uses lower safety factors and includes structures with low consequences when failure occurs. These are for instance glass houses or barns. Buildings with high consequences at failure like large theatres or high-rise buildings are included in consequence class 3 that makes use of higher safety factors. The Eurocodes safety factors are given in figure 10-27.

On the other hand, the determined characteristic strength is reduced by a material factor γ_M from which the result provides a design strength f_{cd}. In timber design the characteristic strength is also reduced by a modification factor k_{mod} that takes into account the duration of load.

The safety factors, that are applied on the load, together with the material factors, that are applied on the strength, forms the safety zone that is depicted in figure 10-26. This safety zone has a minimum size because $\sigma_{cd} \leq f_{cd}$. The size of the safety zone determines the amount of actual characteristic stress σ_{ck} that is applied relative to the actual characteristic strength f_{ck} or mean strength f_{cm}.

When considering the design load in a pendulum column of a high-rise building in the ultimate limit state, the design strength should be assessed against the load combinations of equation 22. The Dutch national annex of the Eurocode also states that except for two floors the variable floor loads above the considered column can all be reduced by the φ_0 factor (NEN-EN 1991-1-1+C1/NB, 2011). When the amount of floors of a high-rise increases, the two floors that are not reduced by φ_0 will be less relevant. The second load combination with a higher factor for the permanent load can be assumed to be governing for a high-rise with more than 15 floors.

1. $\gamma_{G,1} \cdot G + \gamma_Q \cdot Q_1 + \gamma_Q \cdot \sum \varphi_0 \cdot Q_i$
2. $\gamma_{G,2} \cdot G + \gamma_Q \cdot \sum \varphi_0 \cdot Q_i$

equation 22: Governing loadcombinations for a pendulum column.

The load factors are shown in figure 10-27. The average load factor is dependent of the ratio between permanent and variable load. The graph shows the average load factor for the second load combination in equation 22. From the graph in figure 10-27 it can be concluded that the minimum average load factor $\gamma_{G,Q}$ is 1,5

	$\gamma_{G,1}$	$\gamma_{G,2}$	γ_Q
CC1	1,1	1,2	1,35
CC2	1,2	1,35	1,5
CC3	1,3	1,5	1,65

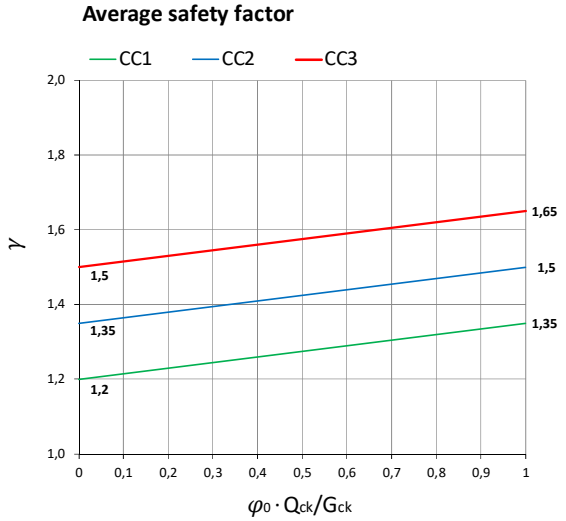

$$N_{ed} = \gamma_{G,2} \cdot G + \gamma_Q \cdot \varphi_0 \cdot Q$$

$$\gamma = \frac{\gamma_{G,2} \cdot G + \gamma_Q \cdot \varphi_0 \cdot Q}{G + \varphi_0 \cdot Q}$$

figure 10-27: Average load factor for the total load in ULS dependent on permanent variable load ratio.

Concrete:

$\gamma_{G,Q} = 1{,}5$

$\gamma_M = 1{,}5$

$$\sigma_{ck} \leq \frac{f_{ck}}{1{,}5 \cdot 1{,}5} = 0{,}44 f_{ck} \leq 0{,}4 f_{cm}$$

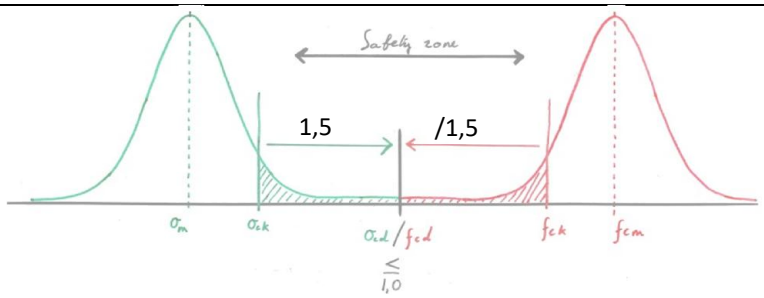

GLT – short-term:

$\gamma_{G,Q} = 1{,}5$

$\gamma_M = 1{,}25$

$k_{mod} = 0{,}9$

$$\sigma_{ck} \leq \frac{0{,}9 \cdot f_{ck}}{1{,}25 \cdot 1{,}5} = 0{,}48 f_{ck}$$

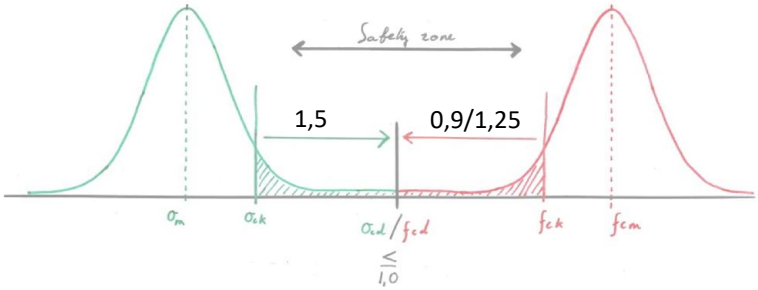

GLT – long-term:

$\gamma_{G,Q} = 1{,}5$

$\gamma_M = 1{,}25$

$k_{mod} = 0{,}9$

$$\sigma_{ck} \leq \frac{0{,}6 \cdot f_{ck}}{1{,}25 \cdot 1{,}5} = 0{,}32 f_{ck}$$

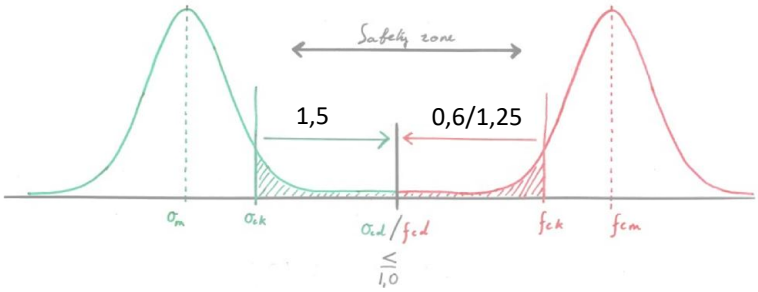

figure 10-28: characteristic stress relative to characteristic strength.

From figure 10-28 it can be concluded that the maximum characteristic stresses in both timber and concrete for a consequence class 3 building are sufficiently low when the ULS requirements are met.

- The stresses in concrete are well below 40% of the mean compressive strength and the material behaviour can be assumed to be linear viscoelastic. This means that a linear approach for the initial elastic deformations is valid and the creep deformations can be assumed to be stable and can be approximated linearly.

- The quasi permanent or long-term stresses in timber are well below 40% of the short-term characteristic strength and the material behaviour can be assumed to be linear viscoelastic. This means that a linear approach for the initial elastic deformations is valid and the creep deformations can be assumed to be stable and can be approximated linearly.

F. Dimensional deviations

In the analysis of differential vertical shortening, the shortening of vertical load bearing elements and the displacement of floor slabs is considered relative to the normative dimensions of the design. This implies that the analysis is theoretical relative to the intended ideal situation. Subsequent measuring of reality will result in descriptive dimensions that inevitably will deviate from the normative dimensions. This chapter will explain how size deviations should be dealt with and how tolerances should be used when executing a design according to the Dutch building codes. It will give insight in execution deviations so displacements that are caused by differential vertical shortening can be placed in the total perspective of size deviations.

To avoid excessive deviations, the Dutch building codes provide a size tolerance system in which rules are included for the determination, the indication and the examination of size tolerances (NEN 2881, 1990). The following definitions are explained for a better understanding of this chapter:

F.1 Positional tolerance T_e

For practical reasons it is of great importance to determine the size deviations and their probability of occurrence that originate from inaccuracies in manufacturing processes, outlining methods and adjusting methods. It is desired that in 98% of all cases, the deviations are within the predetermined tolerance area to assure quality (Stichting Bouwresearch, 1982; NEN 2881, 1990).

The sizes of a population can be graphically shown as a probability density function that belongs to a normal distribution with an average μ_v, that is in general the target size, and a standard deviation σ_v, for which a low value indicates a high precision of the building process (Hoof, 1986).

$\sigma_x{}'$: Standard deviation
x'''': Systematic deviation

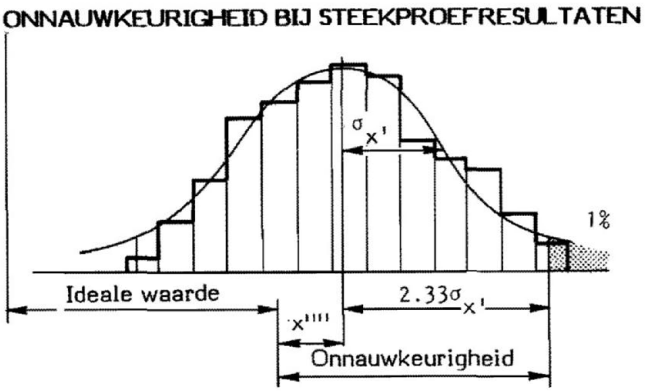

figure 10-29: Symmetrical 98% area of the manufacturing tolerances T_i (Hoof, 1986).

The total positional tolerance T_e consists of the manufacturing tolerance T_i, the outlining tolerance T_u and the adjustment tolerance T_s. All three deviation types can be considered as a stochastic variable and can be visualized as a normal distribution function as in figure 10-29. The prescribed tolerance covers the 98% inaccuracy area of this normal distribution.

T_i: Manufacturing tolerance to accommodate size deviations.

T_u: Outlining tolerance to accommodate for outlining errors.

T_s: Adjustment tolerance to accommodate space for adjustment.

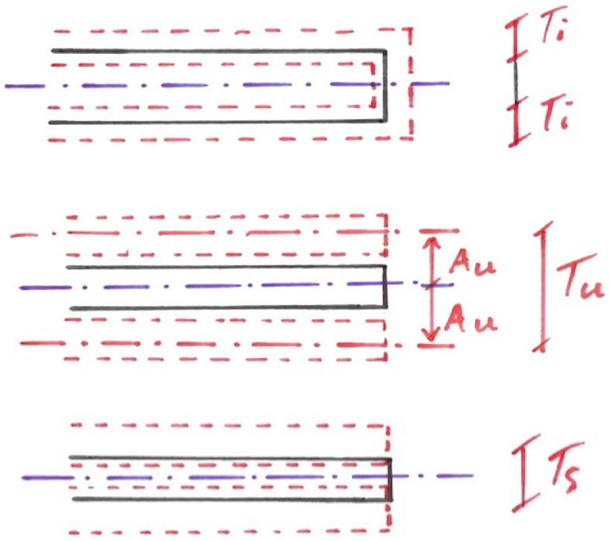

figure 10-30: Three types of tolerances that are incorporated in the positional tolerance. Aanpassen

The relation between the tolerances is analogue to the relation between the variance that are caused by manufacturing, outlining and adjusting, provided that for all tolerances the same 98% inaccuracy area is used and the different types of size deviations are independent of each other (Stichting Bouwresearch, 1982). The relation in equation 23 shows how the positional tolerance is determined from the three independent tolerance types from figure 10-30.

$$\sigma_e = \sqrt{\sigma_i^2 + \sigma_u^2 + \sigma_s^2} \qquad \text{so:} \qquad T_e = \sqrt{T_i^2 + T_u^2 + T_s^2}$$

equation 23: Tolerances analogue to the inaccuracy deviations.

F.2 Manufacturing tolerances T_i

The manufacturing tolerance (in Dutch: Vervaardigingstolerantie) is the tolerance which refers to shape and size deviations due to inaccuracies in the manufacturing process of a building element itself.
The manufacturing tolerance is defined as the symmetrical 98% probability area of the normal distribution of a series of sizes of the considered product. This means that statistically both the minimum and maximum boundary size will be exceeded by 1% of all individual sizes.

Manufacturing deviations can be caused by coincidental or by systematic effects in the production process (Boonekamp & Meischke, 1979; Hoof, 1986).
Systematic deviations are deviations that come back in each individual produced product within a production series. These inaccuracies are caused by for instance the setting of machinery, zero point errors in measuring equipment or deflections of a mould during casting. The systematic inaccuracies cause that the average production size of a series deviates from the target size which would cause a shift of μ_v in figure 10-29 for that one particular production series that is considered.
The standard deviation is caused by inaccuracies in the consistency of the production process and are coincidental.

The Dutch building codes provide maxima for the manufacturing deviations for concrete building elements that are allowed. The maximum allowable height deviations for concrete columns and concrete walls are given in table 23. Vertical manufacturing tolerances that are in general of frequent occurrence for concrete elements are given in (Boonekamp & Meischke, 1979) and are explicated in table 23.

	Maximum allowable tolerance	Boonekamp & Meischke
Column length	±11 mm	±10 mm
Wall height	±8 mm	±10 mm
Floor thickness	±12 mm	±6 mm

table 23: Maximum allowable vertical size deviations for concrete elements (NEN 2889, 1990).

Size deviations in machined timber elements turn out to be smaller than prefabricated concrete elements. The assured tolerances of several suppliers of engineered timber products are elaborated in table 24.

	Withagen houtproducten	De Groot Vroomshoop	Nordlam
Column length	±2 mm		±3 mm
Wall height		±5 mm	±3 mm
Floor thickness			±1 mm

table 24: Size deviations from several engineered timber manufacturers.

It can be concluded that manufacturing tolerances for timber structural elements can be kept much smaller due to a more precise manufacturing process. The manufacturing tolerance on length of a structural element can be assumed to be ±3 mm for timber and ±10 mm for concrete. These are the size deviations when the product comes out of the factory when moisture content is kept stable.

F.3 Outlining tolerances T_u

The outlining tolerance (in Dutch: Uitzettolerantie) is the tolerance that refers to deviations that occur when preparing the reference lines of the structure. The reference line is the marked line on a building structure or building element relevant to which other building parts are set (Stichting Bouwresearch, 1982).
The maximum allowable size deviation for distances when setting out reference lines on the construction site and the maximum allowable angular deviation relative to the design reference line is determined by the Dutch codes according to figure 10-31.

$$A = \sqrt{16 + 2 \cdot \frac{L}{1000}}$$

$$T = 2 \cdot \sqrt{16 + 2 \cdot \frac{L}{1000}}$$

$$A_\alpha = \tan(\alpha) = \frac{A}{L} = \frac{1}{L} \cdot \sqrt{16 + 2 \cdot \frac{L}{1000}}$$

$$T_\alpha = 2 \cdot \tan(\alpha) = \frac{2A}{L} = \frac{2}{L} \cdot \sqrt{16 + 2 \cdot \frac{L}{1000}}$$

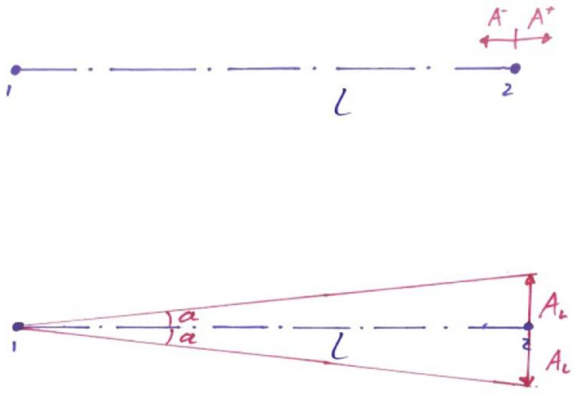

figure 10-31: Maximum allowable outline deviations (NEN 2887, 1990).

The setting of reference lines starts on the ground floor in the horizontal plane and are the result of reference base points. The location of these lines is chosen in such a way that there is no interference with structural elements on that floor and the floors above when the reference lines are plumbed up. This means that they are offset of the structural gridlines. The plumbing up is usually carried out with the MOUS system in small floor apertures according to figure 10-32. A minimum of two points is necessary with a biggest possible distance between the points for a precise plumbing up. This system ensures that the reference points and lines on above floors are set in the horizontal plane (MOUS Systems B.V., 2004; Hoof, 1986).

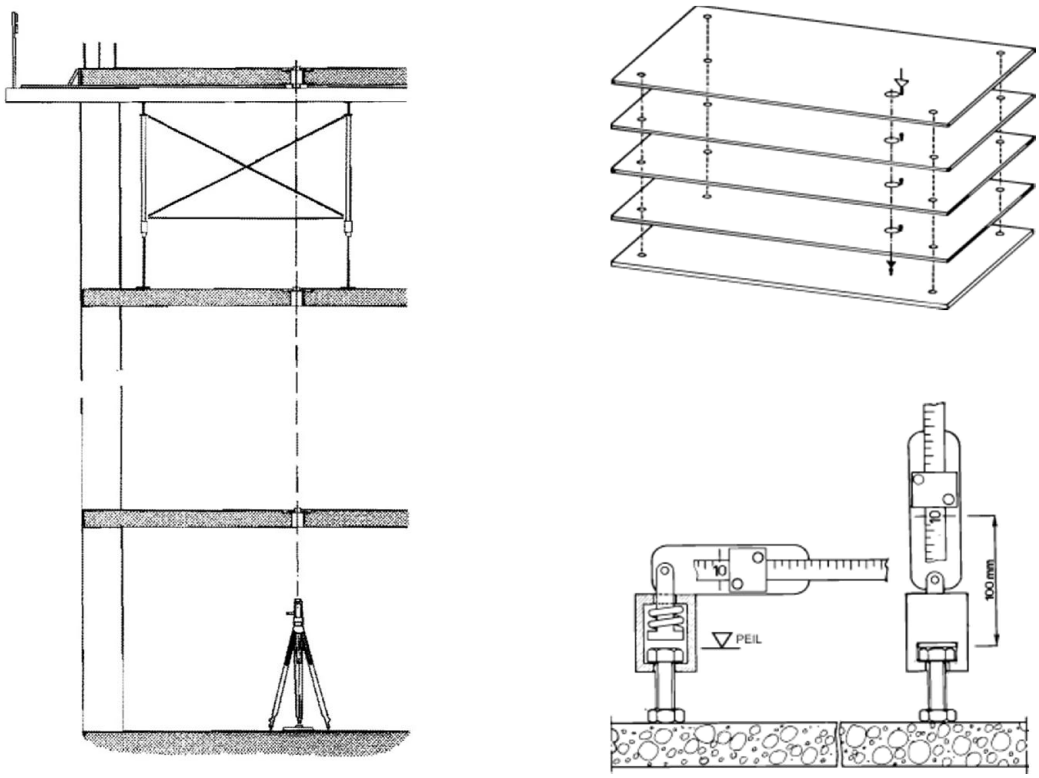

figure 10-32: Plumbing up of master reference points through apertures in floors (Hoof, 1986; MOUS Systems B.V., 2004).

In the vertical direction, the reference points and lines can be set by a measuring tape clamp that is passed through apertures and fixed to a bolt on ground floor that indicates the height level (figure 10-32). In this way every floor level is set relative to the ground floor level. This method is unsuitable for high-rise structures, because temperature and tension force in the measuring tape can cause cumulative size deviations on long distances (+/- 4mm over 40meter length). If a floor on 40 meters high can deviate with +/- 4mm, the distance between two floor on this height can deviate in the same inaccuracy area with $\sqrt{4^2 + 4^2} = 5{,}7mm$. Because finishing elements like façades or partition walls mostly need to fit between two floors, it is not desirable that the floor to floor distance can grow when the building gets higher. A more accurate technique is to measure from floor level to floor level with a ruler (+/- 1mm). This ensures that deviations between two floors will not grow with the building height. The deviation of a floor relative to the ground floor can grow with the building height with $\sqrt{n \cdot 1^2}$ where n are the number of floors. This is not much of a problem because it is very unlikely that other building elements need to fit between for instance the 40th floor and the ground floor (MOUS Systems B.V., 2004).

When looking at the vertical outlining deviations from the perspective of differential vertical shortening, the exact deviations relative to the ground floor are not of great interest. The major interest is what the outlining difference can be between a floor support at the concrete core of the building and a column support for that same floor in vertical direction for which the allowable maximum is described by the Eurocode and is depicted in the bottom picture of figure 10-31.

F.4 Adjustment tolerances T_s

The adjusting tolerance (in Dutch: steltolerantie) is the difference between the minimum and maximum allowable adjusting size deviation relative to the reference line. The Dutch building code provides maximum allowable adjusting deviations for several building element typologies. For load bearing elements like columns and walls the maximum allowable vertical adjusting deviation is 5mm, which means a maximum allowable adjusting tolerance in the vertical direction of 10mm (NEN 2888, 1990).

F.5 Deviations and deformations

Size deviations can be considered as the changes in shape and size of a building element relative to its target size that occur before assembly. The changes in shape and size that occur after assembly can be considered as deformations.
The size deviations are partly caused by the technology of the building process and can be partly physical. The physical part can be for instance the shrinkage process in prefabricated concrete elements or deformations that occur in prestressed concrete elements before assembling them in the structure. These deformations can be covered by giving the building element an over length.
The deformations are physical and can be caused by climate conditions, material properties and mechanical loads. On the one hand the main load bearing structure will be susceptive to these deformations and on the other hand the secondary structure like façades and partition walls will be also susceptive to deformations. Problems can occur when deformations in both are unequal to each other and no proper provision has been made. Next to the positional tolerance that covers size deviations, the Dutch building code mentions the expected size enlargement b^+ or reduction b^- of a junction to provide room for deformations (NPR 3685, 1995).

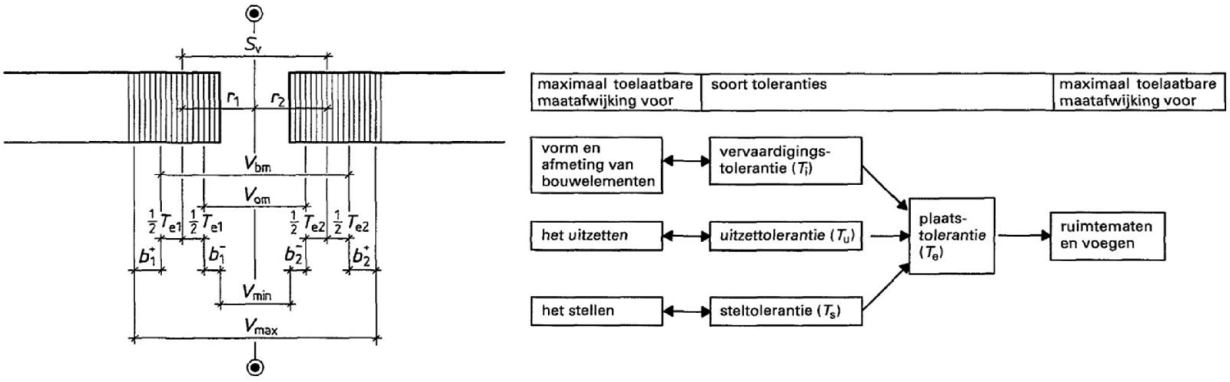

figure 10-33: Relation between tolerances and allowable size deviations according to Dutch building codes (NPR 3685, 1995).

When the size of a junction is determined, first the lower boundary size V_{min} of the junction should be determined. This is minimal size of the junction during use. The amount of joint reduction b^- due to elastic, shrinkage and creep settlements of the load bearing structure and thermal expansion and deflection of the façade should be determined to acquire the lower boundary size of the junction at the time of assembly V_{om}. When the tolerances are known, the upper boundary size at the time of assembly V_{bm} can be determined. Finally, the junction size can increase due to thermal shrinkage of façade elements, which determines the upper boundary size of the junction during use. How all these size definitions are related to the target size S_v is shown in figure 10-33. Of all different aspects that are mentioned to determine the joint size, the quantity of b^- and b^+ determine the amount of movement in the joint during the service life.

The strain in joint material should be within certain limits to avoid damage of the joint material. The deformation limit is in general 5% - 25% and depends on the joint material used. The maximum strain that will occur in a joint is given by equation 24 (Stichting Bouwresearch, 1982). From this equation the minimum junction size at assembly V_{om} can be determined. This is only the case when a junction makes use of a joint seal that has a maximum deformation capacity.

$$\varepsilon_j = \frac{b^- + b^+}{V_{om}} \leq \varepsilon_{j,max}$$

equation 24: Strain of joint material.

F.6 Discussion

When the design of a junction is defined the minimum junction size V_{om} at the moment of assembly is determined by the deformations that are expected after assembly and the minimum junction size V_{min} which is desired when all deformations have occurred. When a joint sealant is used in for instance a horizontal dilatation in a brick façade, the minimum junction size is determined by the deformation capacity of the sealant. Because a sealant can only deform for 25% maximum, the lower boundary size of the junction at the time of assembly V_{om} has to be 4 times the expected deformation.

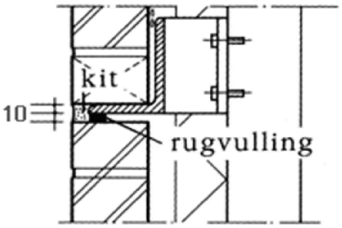

Baksteen wordt koud op het hoekstaal gemetseld

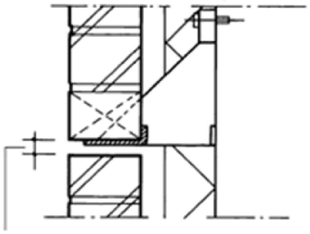

Standaard voegwijdte

positional tolerance, that is needed to cover size deviations, determines upper and lowe

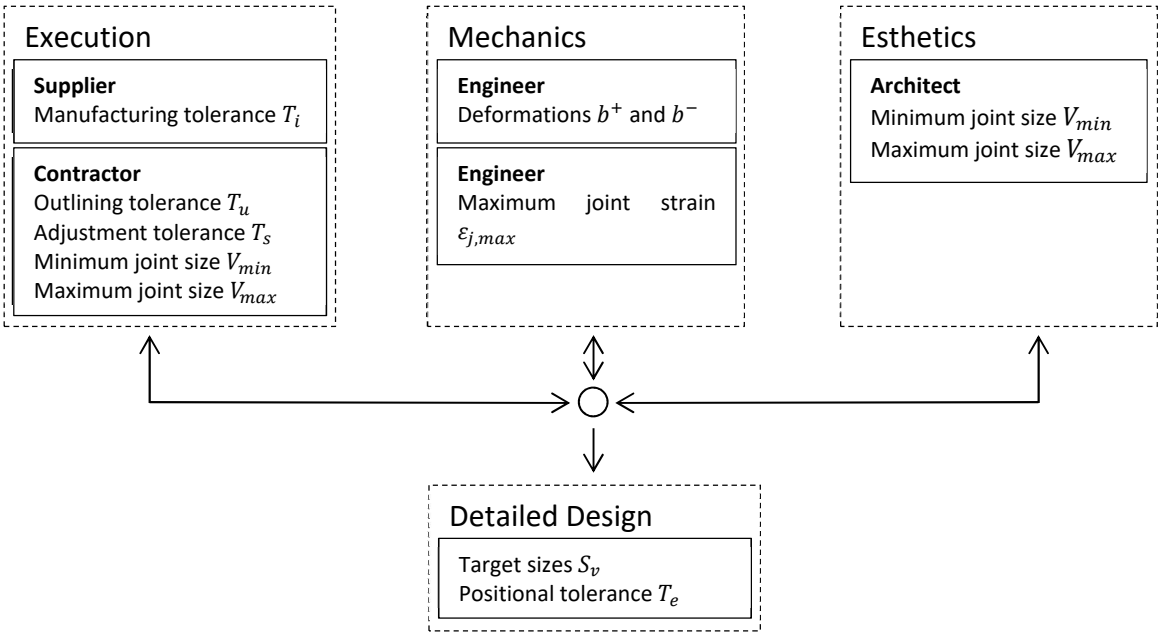

figure 10-34: Translation and adaption of figure 10-33.

G. Determination of Differential vertical shortening limit

The Eurocode requirement for the lateral displacement for the total building with more than one floor states the following:

$$u_h(H) \leq \frac{H}{500}$$

From this requirement, the maximum allowable rotation of the concrete core can be determined. Together with the core width the maximum vertical displacement of the floor support can be determined.

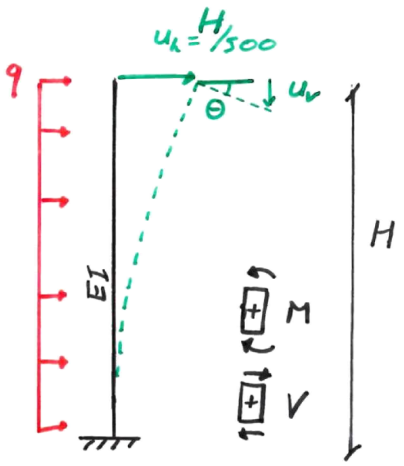

$$u_h(x) = \left(-\frac{1}{EI}\right) \cdot (-q)$$

$$u_h'(x) = \left(-\frac{1}{EI}\right) \cdot (-qx + C_1)$$

$$u_h''(x) = \left(-\frac{1}{EI}\right) \cdot \left(-\frac{qx^2}{2} + C_1 x + C_2\right)$$

$$u_h'(x) = \left(-\frac{1}{EI}\right) \cdot \left(-\frac{qx^3}{6} + \frac{C_1 x^2}{2} + C_2 x + C_3\right)$$

$$u_h(x) = \left(-\frac{1}{EI}\right) \cdot \left(-\frac{qx^4}{24} + \frac{C_1 x^3}{6} + \frac{C_2 x^2}{2} + C_3 x + C_4\right)$$

(1) Solving the constants with the boundary conditions:

$u_h(0) = 0 \qquad -EIu_h'''(H) = 0 \quad (V)$

$u_h'(0) = 0 \qquad -EIu_h''(H) = 0 \quad (M)$

$$C_1 = qH, \quad C_2 = \frac{qH^2}{2}, \quad C_3 = 0, \quad C_4 = 0$$

(2) Solving the corresponding maximum rotation by the horizontal drift limit:

$$u_h(H) = \frac{H}{500}$$

$$u_h'(H) = 0{,}00267$$

(3) Find the maximum vertical deformation due to horizontal drift by using the maximum rotation and core width:

$$u_v = u_h'(H) \cdot \left(\frac{b}{2}\right)$$

equation 25: Calculation of the maximum vertical floor support deformation due to lateral displacement.

H. Brock Commons original design

This appendix represents a quantitative analysis of the structural design of the Brock Commons building according to the Eurocode.

H.1 Core design

The core dimensions as depicted in table 25 are based on drawings.

Assumed core properties

H	$= 53$	m
b	$= 6$	m
h	$= 6{,}5$	m
t	$= 450$	mm
	C45/55	
f_{cm}	$= 53$	N/mm^2
f_{ck}	$= 45$	N/mm^2
E_{cm}	$= 36000$	N/mm^2
$E_{c,eff}$	$= 25000$	N/mm^2

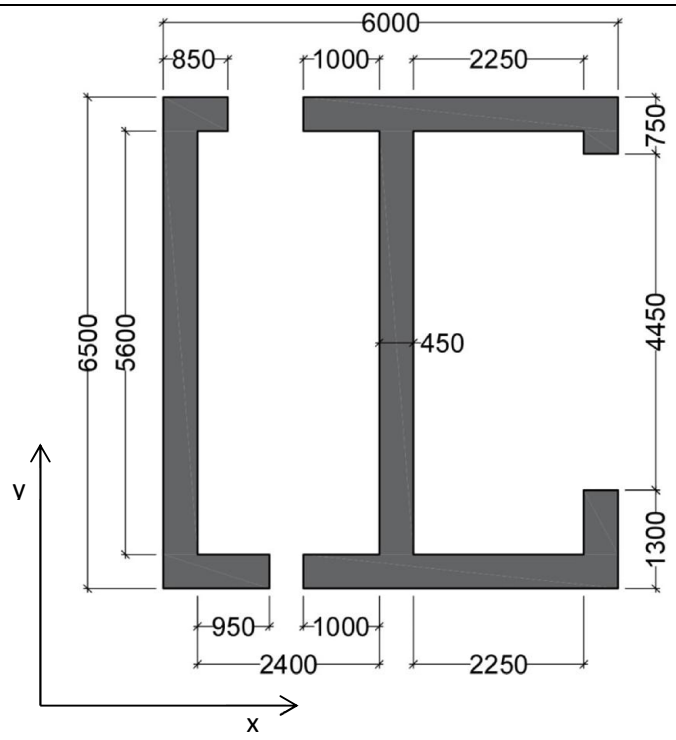

Windloads

$q_{w,ch}$	$= 1{,}7$	kN/m^2
$q_{w,y}$	$= 57 \cdot 1{,}5 \cdot 1{,}7$	
	$= 144$	kN/m
$q_{w,x}$	$= 16 \cdot 1{,}5 \cdot 1{,}7$	
	$= 41$	kN/m

Moment of inertia

The moments of inertia are determined for the depicted cross section with Bitmap Cross Sectional Analyser:

$I_{c,y} = 61{,}6 \cdot 10^{12}$ mm^4

$I_{c,x} = 37{,}6 \cdot 10^{12}$ mm^4

Deflection in y-direction

The building has two mirrored cores that provide the lateral stability, so the moment of inertia is multiplied by a factor 2:

$$\delta_{EI,y} = \frac{q_{w,y} \cdot H^4}{8 \cdot E_{c,eff} \cdot 2 \cdot I_{c,y}} = 46{,}1 \text{ mm} < \frac{H}{500} = 106\ mm$$

Unity check

$$UC = \frac{\delta_{EI,y} \cdot 500}{H} = 0{,}435$$

The deflection calculation does not consider deflections that are caused by rotations at the foundation due to settlements so the low unity check is certainly not an over capacity.

Deflection in x-direction

The building has two mirrored cores that provide the lateral stability, so the moment of inertia is multiplied by a factor 2:

$$\delta_{EI,x} = \frac{q_{w,x} \cdot H^4}{8 \cdot E_{c,eff} \cdot 2 \cdot I_{c,x}} = 21{,}5 \text{ mm} < \frac{H}{500} = 106\ mm$$

Unity check

$$UC = \frac{\delta_{EI,x} \cdot 500}{H} = 0{,}203$$

table 25: Original concrete core properties.

H.2 Column design

The columns are grouped in 265 x 265 mm columns for the 2nd to the 9th floor and 265 x 215 mm columns for the 10th to the 18th floor. The columns from the 2nd to the 5th floor are made of PSL (Parallel Strand Lumber). The columns from the 6th to the 18th floor are executed in GLT (Glue Laminated Timber).
The calculation considers the columns on the 2nd, 6th and the 10th floor as governing because these are the most highly loaded columns within their column group.

Column geometry

Floor 10 to 18

H_{10}	$= 2532$	mm
b_{10}	$= 265$	mm
h_{10}	$= 215$	mm
A_{10}	$= 56975$	mm^2

Floor 2 to 9

H_2	$= 2532$	mm
b_2	$= 265$	mm
h_2	$= 265$	mm
A_2	$= 70225$	mm^2

Material properties

GL24h

$f_{c,0,k}$	$= 24$	N/mm^2
$E_{0,mean}$	$= 11600$	N/mm^2
γ_M	$= 1{,}25$	

PSL 2.0E

$f_{c,0,k}$	$= 32$	N/mm^2
$E_{0,mean}$	$= 14300$	N/mm^2
γ_M	$= 1{,}25$	

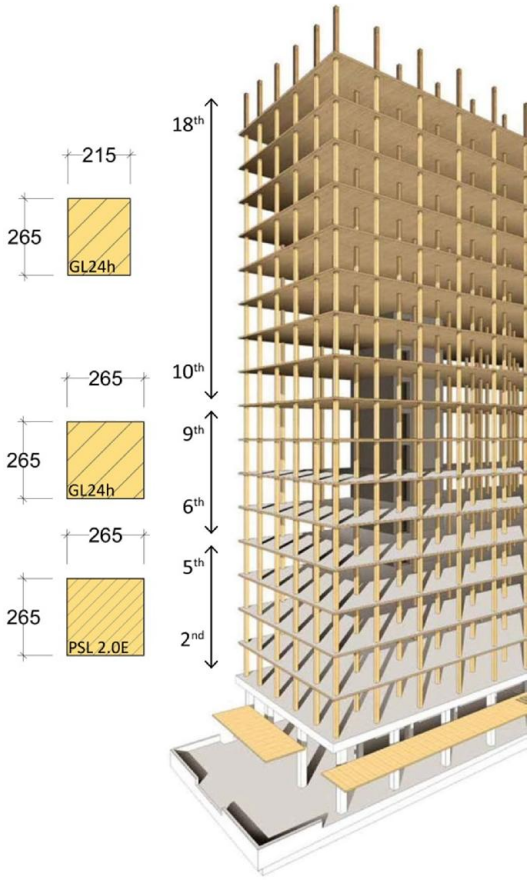

table 26: Original column dimensions with assumed material properties of the Tallwood House, Brock Commons.

Axial column loads

A_f	$= 4 \times 2{,}85$	$= 11{,}4$ m²
$q_{G,f}$		$= 3$ kN/m²
$q_{Q,f}$		$= 1{,}75$ kN/m²

Characteristic column load:

$G_{k,f}$	$= 34{,}2$ kN
$Q_{k,f}$	$= 19{,}95$ kN

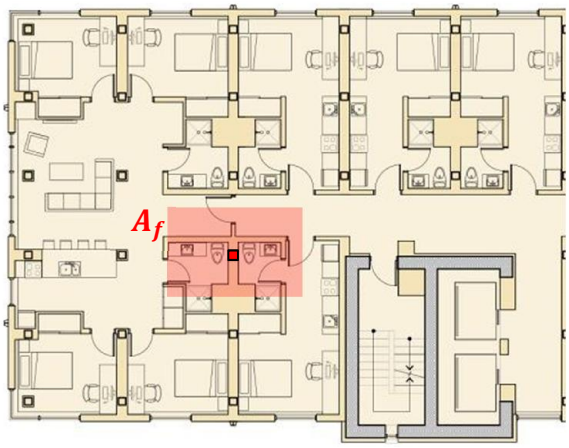

Load combinations (ULS)

1. (Vgl.6.10a) $\gamma_G \cdot G_{k,n} + \gamma_Q \cdot (Q_{k,17-18} + \varphi_0 \cdot Q_{k,n-16})$	(short-term)
$N_{ed,10}$	$= \mathbf{580}$ **kN**
$N_{ed,6}$	$= \mathbf{83\ 8}$ **kN**
$N_{ed,2}$	$= \mathbf{1096}$ **kN**

2. (Vgl.6.10b) $\gamma_G \cdot G_k + \gamma_Q \cdot \varphi_0 \cdot Q_k$	(medium-term)
$N_{ed,10}$	$= \mathbf{558}$ **kN**
$N_{ed,6}$	$= \mathbf{789}$ **kN**
$N_{ed,2}$	$= \mathbf{1019}$ **kN**

3. $\gamma_G \cdot G_k$	(permanent)
$N_{ed,10}$	$= \mathbf{462}$ **kN**
$N_{ed,6}$	$= \mathbf{667}$ **kN**
$N_{ed,2}$	$= \mathbf{872}$ **kN**

Load combinations (SLS)

1. $G_{k,n} + \varphi_2 \cdot Q_{k,n}$	(quasi-permanent)
$N_{ed,10}$	$= 362$ kN
$N_{ed,6}$	$= 522$ kN
$N_{ed,2}$	$= 683$ kN

2. $G_{k,n} + (Q_{k,17-18} + \varphi_0 \cdot Q_{k,n-16})$	(characteristic)
$N_{ed,10}$	$= 404$ kN
$N_{ed,6}$	$= 572$ kN
$N_{ed,2}$	$= 741$ kN

table 27: Axial loads and load combinations for the governing columns on the 2nd , 6th and 10th floor.

Axial design resistance (ULS)

		Short-term ($k_{mod} = 0{,}8$)	*Medium-term ($k_{mod} = 0{,}65$)*	*Long-term ($k_{mod} = 0{,}5$)*
$N_{rd,10}$	$= k_{mod} \cdot A_{10} \cdot \frac{f_{c,0,k}}{\gamma_M}$	$= 875$ kN	$= 711$ kN	$= 547$ kN
$N_{rd,6}$	$= k_{mod} \cdot A_{6} \cdot \frac{f_{c,0,k}}{\gamma_M}$	$= 1079$ kN	$= 876$ kN	$= 674$ kN
$N_{rd,2}$	$= k_{mod} \cdot A_{2} \cdot \frac{f_{c,0,k}}{\gamma_M}$	$= 1438$ kN	$= 1167$ kN	$= 899$ kN

Unity check

		Short-term ($k_{mod} = 0{,}8$)	*Medium-term ($k_{mod} = 0{,}65$)*	*Long-term (k_{mod}=0,5)*
Column 10:	$\frac{N_{ed,10}}{N_{rd,10}}$	$= 0{,}66$	$= 0{,}73$	$= 0{,}84$
Column 6:	$\frac{N_{ed,6}}{N_{rd,6}}$	$= 0{,}78$	$= 0{,}86$	$= 0{,}99$
Column 2:	$\frac{N_{ed,2}}{N_{rd,2}}$	$= 0{,}76$	$= 0{,}84$	$= 0{,}97$

table 28: Axial design resistance and Unity check for the governing columns on the 2nd , 6th and 10th floor.

H.3 Partial factors and loads

	γ_G *Partial factors for permanent loads*		γ_Q *Partial factors for*	γ_Q *Partial factors for*
	Favourable	*Unfavourable*	*predominant variable loads*	*simultaneous variable loads*
Vgl. 6.10a	1,5	0,9	$1{,}65 \cdot \varphi_0$	$1{,}65 \cdot \varphi_0$
Vgl. 6.10b	1,3	0,9	1,65	$1{,}65 \cdot \varphi_0$

table 29: Partial factors for a consequence class 3 building (NEN-EN 1990-1-1/NB, 2011, p. 11).

Permanent load patterns							
Building element/material			Density		Dimensions	Characteristic load	
Floor							
	Timber structure	$\boldsymbol{q_{t,f}}$	450	kg/m³	169mm	0,77	kN/m²
	Concrete topping	$\boldsymbol{q_{c,f}}$	2500	kg/m³	40mm	1	kN/m²
	Finishings	$\boldsymbol{q_{F,f}}$				1,23	kN/m²
	Total	$\boldsymbol{q_{G,f}}$				3	kN/m²
Core							
	Reinforced concrete		2500	kg/m³	350mm x 24m (at openings)	210	kN/m
					350mm x 30m (at closed part)	262,5	kN/m
	Average					236,25	kN/m

table 30: Permanent loads on Tallwood House at Brock Commons.

Variable load patterns						
					Characteristic load	
Floor						
	Residential	$\boldsymbol{q_{Q,f}}$			1,75	kN/m²
			φ_0	0,4		
			φ_1	0,5		
			φ_2	0,3		
Wind						
	53 meters	$\boldsymbol{q_w}$			1,7	kN/m²
			φ_0	0,5		
			φ_2	0,3		

table 31: Variable loads on Tallwood House at Brock Commons.

Load cases for column calculations

ULS		**SLS**	
1. $\gamma_G \cdot G_{k,n} + \gamma_Q \cdot \varphi_0 \cdot Q_{k,n}$	(Short-term)	1. $G_{k,n} + Q_{k,n}$	(Short-term)
2. $\gamma_G \cdot G_{k,n} + \gamma_Q \cdot Q_{k,n}$	(Short-term)	2. $G_{k,n} + \varphi_2 \cdot Q_{k,n}$	(Quasi-permanent)
3. $\gamma_G \cdot G_{k,n}$	(Permanent)		

table 32: Load combinations for column calculations.

H.4 Staged construction loadcase

Stage	*Duration*	*Activity*	*Element*	*Load pattern or element name*
Stage 1	4days	Add structure	All (60days age)	
		Change sections	All columns and floors	Ghost
			Columns 1	PSL265
			Floors 1	CLT
		Load objects	Story 1	Timber structure
Stage 2	4days	Change sections	Columns 2	PSL265
			Floors 2	CLT
		Load objects	Story 2	Timber structure
Stage 3	4days	Change sections	Columns 3	PSL265
			Floors 3	CLT
		Load objects	Story 3	Timber structure
Stage 4	4days	Change sections	Columns 4	PSL265
			Floors 4	CLT
		Load objects	Story 4	Timber structure
Stage 5	4days	Change sections	Columns 5	GLT265
			Floors 5	CLT
		Load objects	Story 1	Concrete topping
			Story 5	Timber Structure
Stage 6	4days	Change sections	Columns 6	GLT265
			Floors 6	CLT
		Load objects	Story 2	Concrete topping
			Story 6	Timber Structure
Stage 7	4days	Change sections	Columns 7	GLT265
			Floors 7	CLT
		Load objects	Story 3	Concrete topping
			Story 7	Timber Structure
Stage 8	4days	Change sections	Columns 8	GLT265
			Floors 8	CLT
		Load objects	Story 4	Concrete topping
			Story 8	Timber Structure
Pre-deformations for finishes at story 1				
Stage 9	4days	Change sections	Columns 9	GLT215
			Floors 9	CLT
		Load objects	Story1	Finishes
			Story 5	Concrete topping
			Story 9	Timber Structure
Stage 10	4days	Change sections	Columns 10	GLT215
			Floors 10	CLT
		Load objects	Story 6	Concrete topping
			Story 10	Timber Structure

Stage 11	4days	Change sections	Columns 11 Floors 11	GLT215 CLT
		Load objects	Story 7 Story 11	Concrete topping Timber Structure
Pre-deformations for finishes at story 2				
Stage 12	4days	Change sections	Columns 12 Floors 12	GLT215 CLT
		Load objects	Story2 Story 8 Story 12	Finishes Concrete topping Timber Structure
Stage 13	4days	Change sections	Columns 13 Floors 13	GLT215 CLT
		Load objects	Story 9 Story 13	Concrete topping Timber Structure
Stage 14	4days	Change sections	Columns 14 Floors 14	GLT215 CLT
		Load objects	Story 10 Story 14	Concrete topping Timber Structure
Pre-deformations for finishes at story 3				
Stage 15	4days	Change sections	Columns 15 Floors 15	GLT215 CLT
		Load objects	Story3 Story 11 Story 15	Finishes Concrete topping Timber Structure
Stage 16	4days	Change sections	Columns 16 Floors 16	GLT215 CLT
		Load objects	Story 12 Story 16	Concrete topping Timber Structure
Stage 17	4days	Change sections	Columns 17 Floors 17	GLT215 CLT
		Load objects	Story 13 Story 17	Concrete topping Timber Structure
Pre-deformations for finishes at story 4				
Stage 18	4days	Load objects	Story 4 Story 14	Finishes Concrete topping
Stage 19	4days	Load objects	Story 15	Concrete topping
Stage 20	4days	Load objects	Story 16	Concrete topping
Pre-deformations for finishes at story 5				
Stage 21	12days	Load objects	Story 5 Story 17	Finishes Concrete topping
Pre-deformations for finishes at story 6				
Stage 22	12days	Load objects	Story 6	Finishes
Pre-deformations for finishes at story 7				
Stage 23	12days	Load objects	Story 7	Finishes
Pre-deformations for finishes at story 8				

Stage 24	12days	Load objects	Story 8	Finishes
Pre-deformations for finishes at story 9				
Stage 25	12days	Load objects	Story 9	Finishes
Pre-deformations for finishes at story 10				
Stage 26	12days	Load objects	Story 10	Finishes
Pre-deformations for finishes at story 11				
Stage 27	12days	Load objects	Story 11	Finishes
Pre-deformations for finishes at story 12				
Stage 28	12days	Load objects	Story 12	Finishes
Pre-deformations for finishes at story 13				
Stage 29	12days	Load objects	Story 13	Finishes
Pre-deformations for finishes at story 14				
Stage 30	12days	Load objects	Story 14	Finishes
Pre-deformations for finishes at story 15				
Stage 31	12days	Load objects	Story 15	Finishes
Pre-deformations for finishes at story 16				
Stage 32	12days	Load objects	Story 16	Finishes
Pre-deformations for finishes at story 17				
Stage 33	12days	Load objects	Story 17	Finishes
Deformations at completion				
Stage 34	90days	-	-	-
Stage 35	90days	Load objects	All Stories	0,5 Quasi-Live
Stage 36	0days	Load objects	All Stories	0,5 Quasi-Live
Deformations at occupation				
Stage 37	365days	-	-	-
Deformations at 1 year after occupation				
Stage 38	3285days	-	-	-
Deformations at 10 years after occupation				
Stage 38	1460days	-	-	-
Deformations at 50 years after occupation				

table 33: Staged construction loadcase.

H.5 Model validation

The deformations of column 3, which is the first column left of the core, will be elaborated in a simplified bar model for the validation of the ETABS model. The bar will be modelled with a discontinuous stiffness EA according to the original column design of Brock Commons. The point loads on the total column from the floor load patterns will be modelled as a distributed load $q_c = F_c/h$ over the total column. The load F_c that is transferred to column 3 is equivalent to the distributed floor load over an approximately 4,5meter span according to figure 10-35 that is present in the considered stage. The column point load F_c is composed of $F_{t,c}$, $F_{c,c}$ and $F_{F,c}$ that originate from the distributed floor load patterns *'Timber structure', 'Concrete topping'* and *'Finishes'* respectively.

Bar model

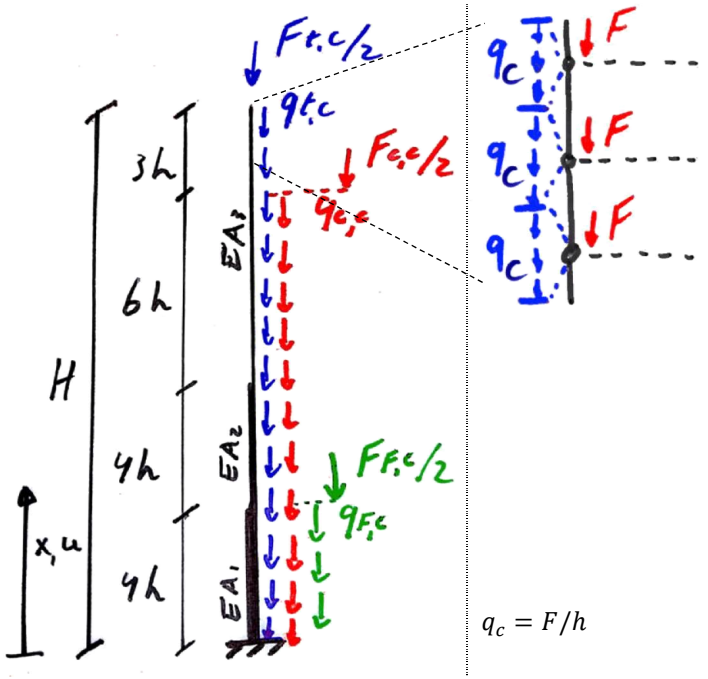

$q_c = F/h$

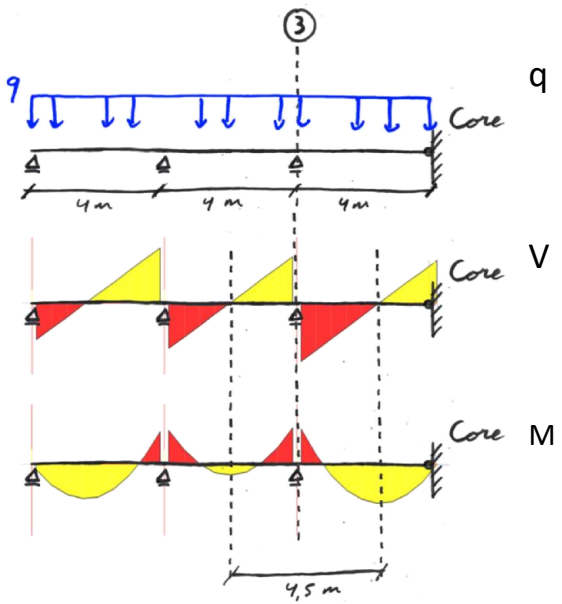

$F_c = 4{,}5 \cdot q_f$

Determination of F_c and q_c

H	$= 17 \cdot h$	
h	$= 2810mm$	
$F_{t,c}$	$= 4{,}5 \cdot 2{,}2$	$= 9{,}9\ kN$
$F_{c,c}$	$= 4{,}5 \cdot 2{,}85$	$= 12{,}8\ kN$
$F_{F,c}$	$= 4{,}5 \cdot 3{,}5$	$= 15{,}8\ kN$
$q_{t,c}$	$= F_{t,c}/h$	$= 3{,}52\ kN/m$
$q_{c,c}$	$= F_{c,c}/h$	$= 4{,}56\ kN/m$
$q_{F,c}$	$= F_{F,c}/h$	$= 5{,}62\ kN/m$

figure 10-35: Basic simplified bar-model. Distribution of floor load over the columns and core. Represented by the shear and bending moment graph.

Stage4

Hand calculation

The model in stage 4 is simplified to a bar with a constant stiffness EA_1 that is equal to the column stiffness for the first 4floors of the original Brock Commons design. The distributed floor load only consists of the *'Timber structure'* load pattern. This will be simplified to a point load applied on the vertical bar that represents the column. The floor to floor height is 2810mm. For this problem, the axial force, the axial elastic strain and the deformations for every floor support due to the axial strain will be calculated.

$h = 2810 \; mm$

$F = F_t = -9{,}9 \cdot 10^3 \; N$

$EA_1 = 1004{,}3 \cdot 10^6 \; N$

Active load patterns

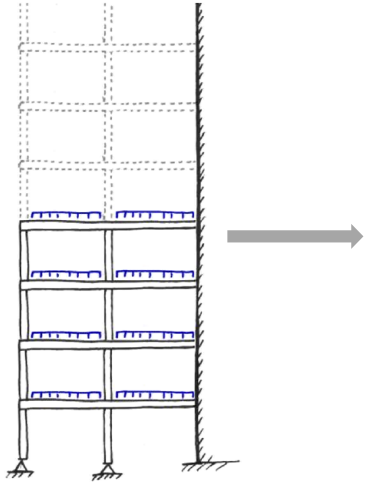

$q_{t,f} = 2{,}2 \; kN/m$

Model

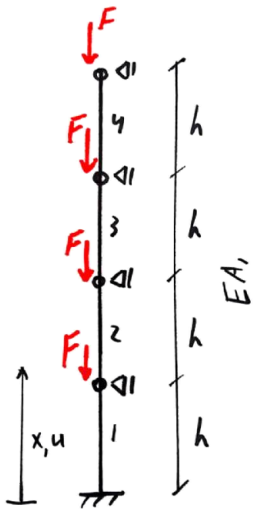

Axial Force

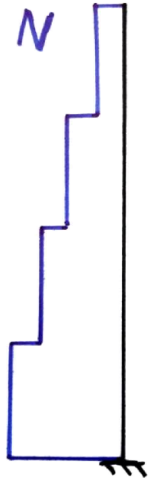

$N_4 = F = -9{,}9 \cdot 10^3 \; N$

$N_3 = 2F = -19{,}8 \cdot 10^3 \; N$

$N_2 = 3F = -29{,}7 \cdot 10^3 \; N$

$N_1 = 4F = -39{,}6 \cdot 10^3 \; N$

Axial strain

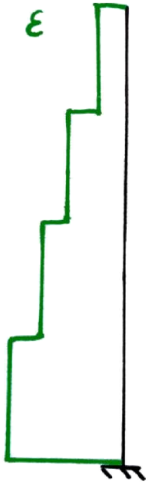

$\varepsilon_4 = \frac{N_4}{EA_1} = -0{,}986 \cdot 10^{-5}$

$\varepsilon_3 = \frac{N_3}{EA_1} = -1{,}972 \cdot 10^{-5}$

$\varepsilon_2 = \frac{N_2}{EA_1} = -2{,}958 \cdot 10^{-5}$

$\varepsilon_1 = \frac{N_1}{EA_1} = -3{,}944 \cdot 10^{-5}$

Floor support deformations

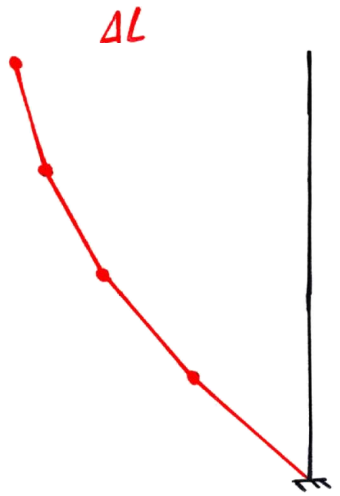

$\Delta L_4 = \frac{\varepsilon_1+\varepsilon_2+\varepsilon_3+\varepsilon_4}{h} = -0{,}277mm$

$\Delta L_3 = \frac{\varepsilon_1+\varepsilon_2+\varepsilon_3}{h} = -0{,}249mm$

$\Delta L_2 = \frac{\varepsilon_1+\varepsilon_2}{h} = -0{,}194mm$

$\Delta L_1 = \frac{\varepsilon_1}{h} = -0{,}110mm$

figure 10-36: Hand calculation for stage 4.

Maple

In the maple model, the pointloads $F_{t,c}$ will be modelled as a distributed load $q_{t,c}$ along the column. The pointload will be smeared out with $F_{t,c}/2$ upwards and downwards over the column. This results in the boundary condition of $N_1 = F_{t,c}/2$ at the the very top of the column.

Active load patterns

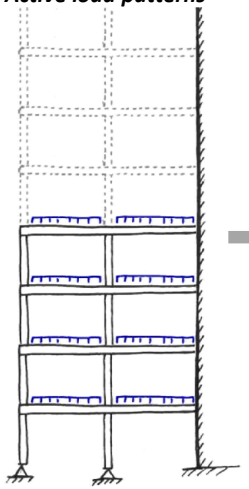

$q_{t,f} = 2,2\ kN/m$

Model

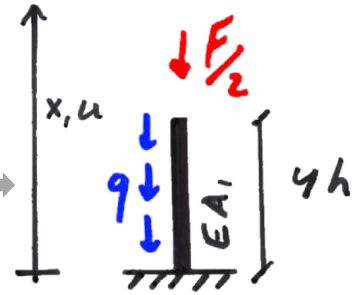

$F_{t,c} = -9{,}9 \cdot 10^3 \quad N$

$q_{t,c} = \frac{F_{t,c}}{h} = -3{,}52 \quad kN/m$

General solution:

$EA_1 \cdot \frac{d^2u_1}{dx^2} = -q$

$EA_1 \cdot \frac{du_1}{dx} = -q \cdot x + C_1 = N_1$

$EA_1 \cdot u_1(x) = \frac{-q \cdot x^2}{2} + C_1 \cdot x + C2$

Boundary conditions:

$u_1(0) = 0$

$N_1(4h) = F_{t,c}/2$

Constants are solved with maple:

$C_1 = -\frac{27}{608660}, \quad C_2 = 0$

Deformation results:

$u(4h) = -0{,}277$

$u(3h) = -0{,}249$

$u(2h) = -0{,}194$

$u(1h) = -0{,}111$

figure 10-37: Maple calculation results for stage4.

Maple document:

$h := 2810 : H := 4 \cdot h : a := 4 \cdot h : F\_t := -9900 : q\_t := \frac{F\_t}{h} : EA1 := 70230 \cdot 14300 :$

(1)

Equations:

$u1 := \frac{-q\_t \cdot x^2}{2\,EA1} + C1 \cdot x + C2$

$$\frac{3}{1710334600}\,x^2 + C1\,x + C2 \qquad \textbf{(1.1)}$$

$N1 := EA1 \cdot diff(u1, x);$

$$\frac{990}{281}\,x + 1004289000\,C1 \qquad \textbf{(1.2)}$$

Boundary conditios

> $x := 0;$

$$x := 0 \qquad \textbf{(2.1)}$$

> $eq1 := u1 = 0;$

$$eq1 := C2 = 0 \qquad \textbf{(2.2)}$$

> $x := H;$

$$x := 11240 \qquad \textbf{(2.3)}$$

> $eq2 := N1 = \frac{F\_t}{2};$

$$eq2 := 39600 + 1004289000\,C1 = -4950 \qquad \textbf{(2.4)}$$

> $solution := solve(\{eq1, eq2\}, \{C1, C2\});$

$$solution := \left\{C1 = -\frac{27}{608660},\ C2 = 0\right\} \qquad \textbf{(2)}$$

> $assign(solution);$

> $x := 'x';$

> $x := 1 \cdot h$

$$x := 2810 \qquad \textbf{(3)}$$

> $x := 1 \cdot h; evalf(u1); x := 2 \cdot h; evalf(u1); x := 3 \cdot h; evalf(u1); x := 4 \cdot h; evalf(u1);$

$x := 2810$
-0.1108007755
$x := 5620$
-0.1939013571
$x := 8430$
-0.2493017448
$x := 11240$
-0.2770019387 **(4)**

> $x := 'x';$

$$x := x \qquad \textbf{(5)}$$

> $with(plots) :$

> $F := plot(u1, x = 0..a, y = -10..0, labels = ["DeltaL", "H"], title = "DVS-deformations", style = line) :$

> $tf := plottools:-transform((x, y) \rightarrow [y, x]) :$

> $tf(F) :$

> $display(\{tf(F)\});$

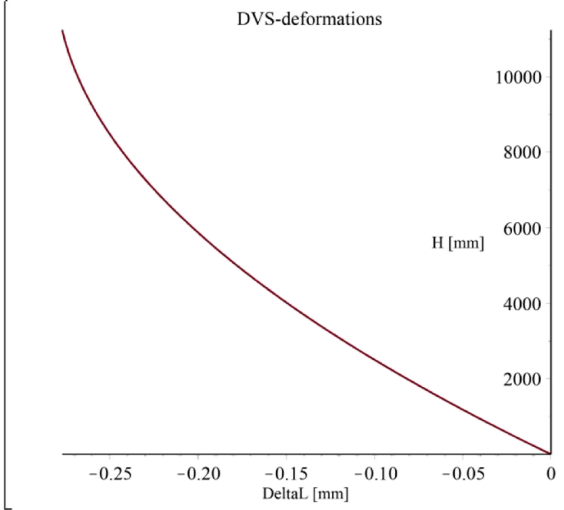

figure 10-38: Maple document stage 4.

ETABS model results

Beding moments

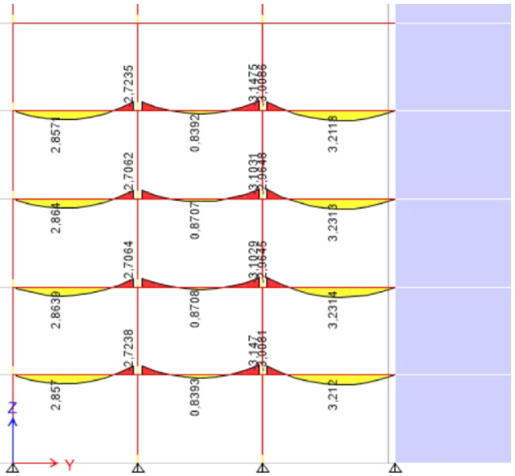

Deformations (scaled 200x)

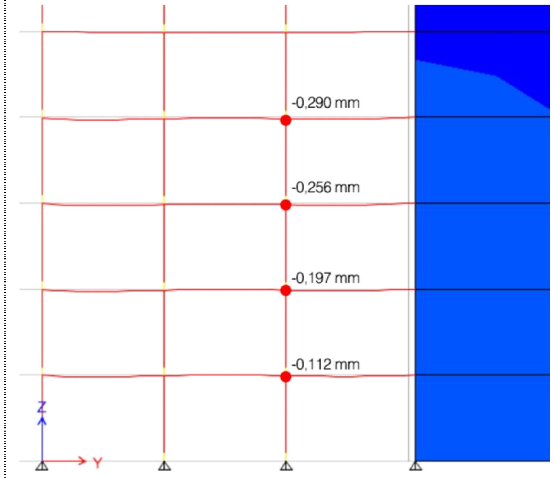

figure 10-39: ETABS model results for stage 4.

The Maple model matches with the hand calculations and is by that validated. The ETABS model shows similar values for the column deformations. Small deviations can occur due to force redistribution or a small difference in the length of the distributed floor load.

Stage4		***Hand calculation***	***Maple***	***ETABS***
	$\Delta L_4 =$	$-0{,}277mm$	$-0{,}277mm$	$-0{,}290mm$
	$\Delta L_3 =$	$-0{,}249mm$	$-0{,}249mm$	$-0{,}256m$
	$\Delta L_2 =$	$-0{,}194mm$	$-0{,}194mm$	$-0{,}197mm$
	$\Delta L_1 =$	$-0{,}110mm$	$-0{,}111mm$	$-0{,}112mm$

table 34: Hand calculations vs Maple vs ETABS results for stage4.

Stage8

Maple

In the maple model, the pointloads $F_{t,c}$ will be modelled as a distributed load $q_{t,c}$ along the column. The pointload will be smeared out with $F_{t,c}/2$ upwards and downwards over the column. This results in the boundary condition of $N_1 = F_{t,c}/2$ at the the very top of the column.

Active load patterns

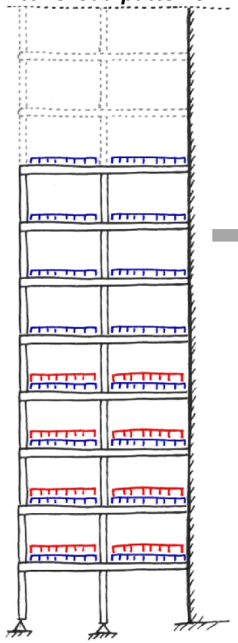

$q_{t,f} = 2,2\ kN/m$

$q_{c,f} = 2,85\ kN/m$

Model

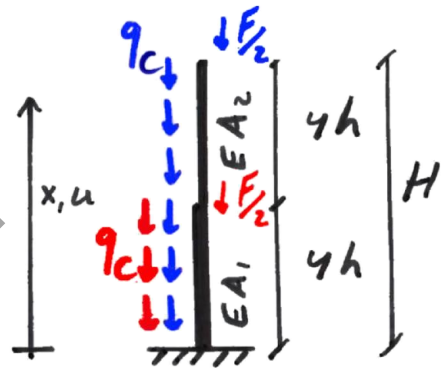

$F_{t,c} = -9{,}9 \cdot 10^3 \quad N$

$F_{c,c} = -12{,}8 \cdot 10^3 \quad N$

$q_{t,c} = \frac{F_{t,c}}{h} = -3{,}52\ kN/m$

$q_{c,c} = \frac{F_{c,c}}{h} = -4{,}56\ kN/m`$

General solution:

$EA_2 \cdot \frac{d^2u_2}{dx^2} = -q_{t,c}$

$EA_2 \cdot \frac{du_2}{dx} = -q_{t,c} \cdot x + C_3 = N_2$

$EA_2 \cdot u_2(x) = \frac{-q_{t,c} \cdot x^2}{2} + C_3 \cdot x + C_4$

$EA_1 \cdot \frac{d^2u_1}{dx^2} = -(q_{t,c} + q_{c,c})$

$EA_1 \cdot \frac{du_1}{dx} = -(q_{t,c} + q_{c,c}) \cdot x + C_1 = N_1$

$EA_1 \cdot u_1(x) = \frac{-(q_{t,c}+q_{c,c}) \cdot x^2}{2} + C_1 \cdot x + C_2$

Boundary/matching conditions:

$N_1(4h) = F_{t,c}/2$

$u_1(4h) = u_2(4h)$

$N_1(4h) = N_2(4h)$

$u_1(0) = 0$

figure 10-40: Maple calculation results for stage 8.

Constants are solved with maple:		***Deformation results:***		
C_1	$= -\frac{783}{5356208}$	$u(8h)$	$= -1{,}479$	mm
C_2	$= 0$	$u(6h)$	$= -1{,}376$	mm
C_3	$= -\frac{561}{5384300}$	$u(4h)$	$= -1{,}134$	mm
C_4	$= -\frac{18393417}{76995490}$	$u(2h)$	$= -0{,}694$	mm

table 35: Maple model results for stage 8.

Maple document:

$$h := 2810 : H := 8 \cdot h : a := 4 \cdot h : F\_c := -12825 : F\_t := -9900 : q\_c := \frac{F\_c}{h} : q\_t := \frac{F\_t}{h} : EA1 := 70230 \cdot 14300 : EA2 := 70230 \cdot 11500 : \quad (1)$$

Equations:

$$u1 := \frac{-(q\_c + q\_t) \cdot x^2}{2\, EA1} + C1 \cdot x + C2$$

$$\frac{303}{75254722400} x^2 + C1\, x + C2 \quad (1.1)$$

$$u2 := \frac{-q\_t \cdot x^2}{2\, EA2} + C3 \cdot x + C4$$

$$\frac{33}{15129883000} x^2 + C3\, x + C4 \quad (1.2)$$

$$N1 := EA1 \cdot diff(u1, x); N2 := EA2 \cdot diff(u2, x);$$

$$\frac{4545}{562} x + 1004289000\, C1$$

$$\frac{990}{281} x + 807645000\, C3 \quad (1.3)$$

Boundary conditios

$$> x := 0;$$

$$x := 0 \quad (2.1)$$

$$> eq1 := u1 = 0;$$

$$eq1 := C2 = 0 \quad (2.2)$$

$$> x := a;$$

$$x := 11240 \quad (2.3)$$

$$> eq2 := u1 = u2;$$

$$eq2 := \frac{170286}{334763} + 11240\, C1 + C2 = \frac{74184}{269215} + 11240\, C3 + C4 \quad (2.4)$$

$$> eq3 := N1 = N2 + \frac{F\_t + F\_c}{2};$$

$$eq3 := 90900 + 1004289000\, C1 = \frac{56475}{2} + 807645000\, C3 \quad (2.5)$$

$$> x := H;$$

$$x := 22480 \quad (2.6)$$

$$> eq4 := N2 = \frac{F\_t}{2};$$

$$eq4 := 79200 + 807645000\, C3 = -4950 \quad (2.7)$$

$$> solution := solve(\{eq1, eq2, eq3, eq4\}, \{C1, C2, C3, C4\});$$

$$solution := \left\{C1 = -\frac{783}{5356208}, C2 = 0, C3 = -\frac{561}{5384300}, C4 = -\frac{18393417}{76995490}\right\} \quad (2)$$

$$> assign(solution);$$

$$> x := 'x';$$

$$> x := 2 \cdot h; evalf(u1); x := 4 \cdot h; evalf(u1); x := 6 \cdot h; evalf(u2); x := 8 \cdot h; evalf(u2);$$

$$x := 5620$$
$$-0.6943934963$$
$$x := 11240$$
$$-1.134448849$$
$$x := 16860$$
$$-1.375560971$$
$$x := 22480$$
$$-1.478894738 \quad (3)$$

$$> x := 'x';$$

$$x := x \quad (4)$$

```
> with(plots) :
> F := plot(u1, x = 0 ..a, y = -10 ..0, labels = ["DeltaL", "H"], title = "DVS-deformations", style
    = line) :
> G := plot(u2, x = a ..H, y = -10 ..0, labels = ["DeltaL", "H"], title = "DVS-deformations", style
    = line) :
> tf := plottools:-transform( (x, y) → [y, x]) :
> tf(F) :
> tf(G) :
> display( {tf(F), tf(G)}, labels = ["DeltaL [mm]", "H [mm]"]);
```

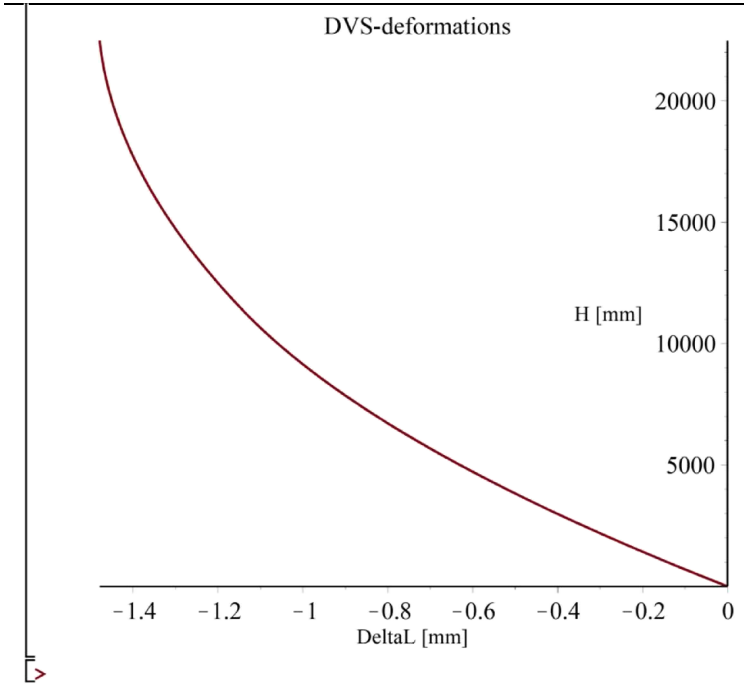

figure 10-41: Maple document stage 8.

ETABS model results

Beding moments

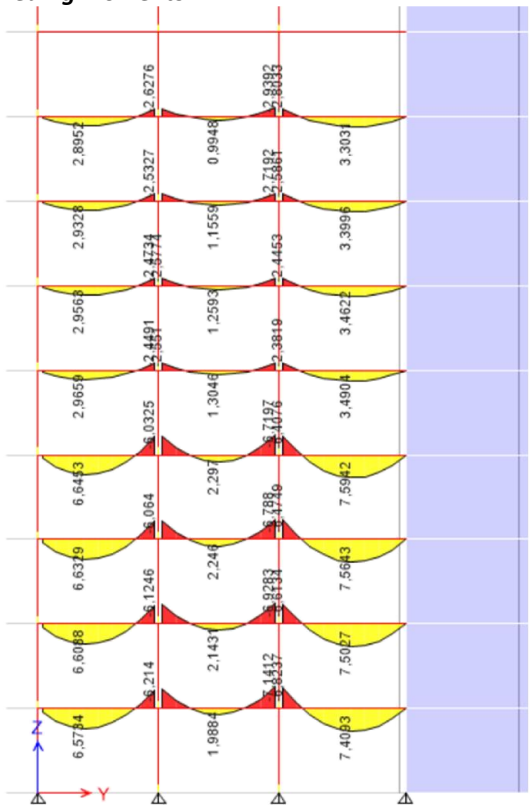

Scaled 200x

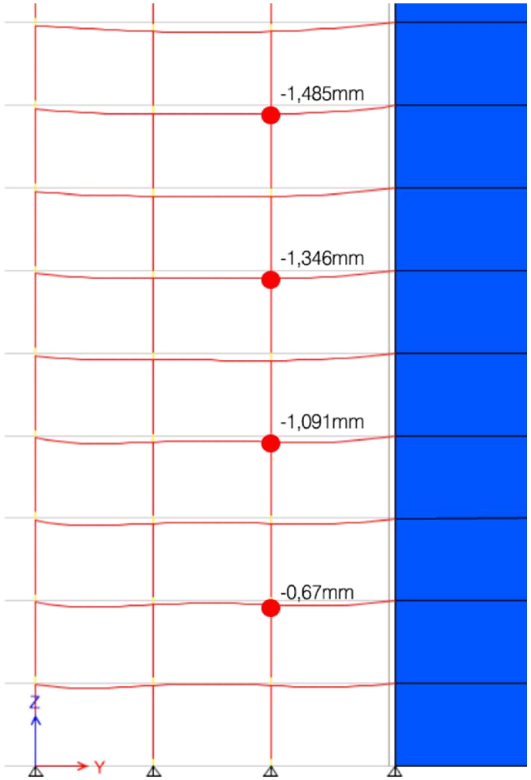

figure 10-42: ETABS results for stage 8.

Stage8		***Maple***	***ETABS***
	$\Delta L_4 =$	$-1{,}479mm$	$-1{,}485mm$
	$\Delta L_3 =$	$-1{,}376mm$	$-1{,}346mm$
	$\Delta L_2 =$	$-1{,}134mm$	$-1{,}091mm$
	$\Delta L_1 =$	$-0{,}694mm$	$-0{,}670mm$

table 36: Maple vs ETABS results for stage 8.

Stage18

Active load patterns

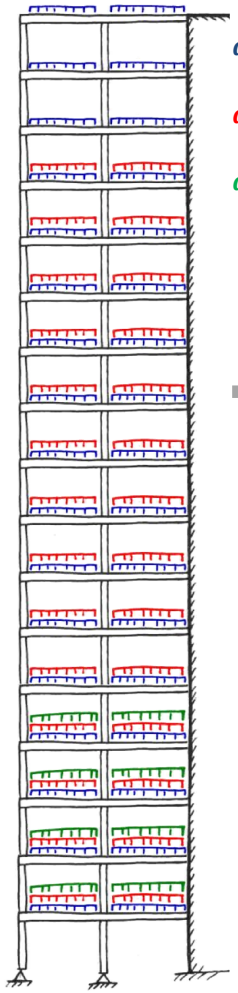

$q_{t,f} = 2,2\ kN/m$

$q_{c,f} = 2,85\ kN/m$

$q_{F,f} = 3,5\ kN/m$

Maple model

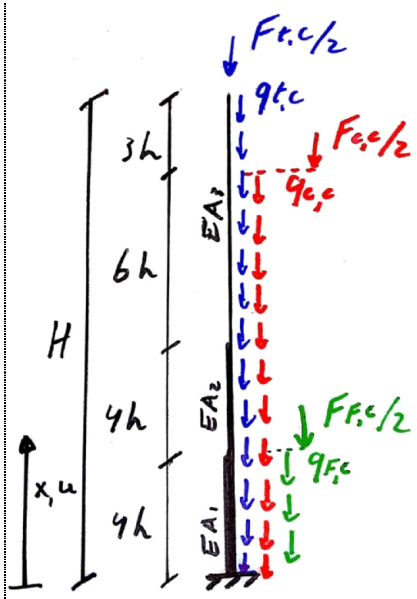

$h = 2810\ mm$

Column loads:

$F_{t,c} = -9,9 \cdot 10^3\ N$

$q_{t,c} = \frac{F}{h} = -3,52\ kN/m$

$F_{c,c} = -12,8 \cdot 10^3\ N$

$q_{c,c} = \frac{F}{h} = -4,56\ kN/m$

$F_{F,c} = -16,4 \cdot 10^3\ N$

$q_{c,c} = \frac{F}{h} = -5,85\ kN/m$

General solution (4domains):

$EA_3 \cdot \frac{d^2u_4}{dx^2} = -q_{t,c}$

$EA_3 \cdot \frac{du_4}{dx} = -q_{t,c} \cdot x + C_7 = N_4$

$EA_3 \cdot u_4(x) = \frac{-q_{t,c} \cdot x^2}{2} + C_7 \cdot x + C_8$

$EA_3 \cdot \frac{d^2u_3}{dx^2} = -(q_{t,c} + q_{c,c})$

$EA_3 \cdot \frac{du_3}{dx} = -(q_{t,c} + q_{c,c}) \cdot x + C_5 = N_3$

$EA_3 \cdot u_3(x) = \frac{-(q_{t,c}+q_{c,c}) \cdot x^2}{2} + C_5 \cdot x + C_6$

$EA_2 \cdot \frac{d^2u_2}{dx^2} = -(q_{t,c} + q_{c,c})$

$EA_2 \cdot \frac{du_2}{dx} = -(q_{t,c} + q_{c,c}) \cdot x + C_3 = N_2$

$EA_2 \cdot u_2(x) = \frac{-(q_{t,c}+q_{c,c}) \cdot x^2}{2} + C_3 \cdot x + C_4$

$EA_1 \cdot \frac{d^2u_1}{dx^2} = -(q_{t,c} + q_{c,c} + q_{F,c})$

$EA_1 \cdot \frac{du_1}{dx} = -(q_{t,c} + q_{c,c} + q_{F,c}) \cdot x + C_1 = N_1$

$EA_1 \cdot u_1(x) = \frac{-(q_{t,c}+q_{c,c}+q_{F,c}) \cdot x^2}{2} + C_1 \cdot x + C_2$

Boundary/Matching conditions:

At $x = H$:

$N_4(H) = \frac{F_{t,c}}{2}$

At $x = 14h$:

$u_3(14h) = u_4(14h)$

$N_3(14h) = N_4(14h) + \frac{F_{c,c}}{2}$

At $x = 8h$:

$u_2(8h) = u_3(8h)$

$N_2(8h) = N_3(8h)$

At $x = 4h$:

$u_1(4h) = u_2(4h)$

$N_1(4h) = N_2(4h) + \frac{F_{F,c}}{2}$

At $x = 0$:

$u_1(0) = 0$

figure 10-43: Maple model for stage18.

Constants are solved with maple:

$C_1 = -\frac{1}{2678}$

$C_2 = 0$

$C_3 = -\frac{96}{215372}$

$C_4 = -\frac{4575}{11549}$

$C_5 = -\frac{2874}{5242160}$

$C_6 = -\frac{1276}{598}$

$C_7 = -\frac{9}{34040}$

$C_8 = -\frac{8715}{2393}$

Deformation results:

$u_4(H)$	$= -10{,}137$	mm
$u_3(14h)$	$= -9{,}883$	mm
$u_2(8h)$	$= -7{,}072$	mm
$u_1(4h)$	$= -3{,}971$	mm

table 37: Maple model results for stage 18.

Maple document:

$h := 2810 : H := 17 \cdot h : a := 4 \cdot h : b := 8 \cdot h : c := 14 \cdot h : F\_t := -9900 : F\_c := -12825 : F\_F := -16400 : q\_t := \frac{F\_t}{h} : q\_c := \frac{F\_c}{h} : q\_F := \frac{F\_F}{h} : EA1 := 70230 \cdot 14300 : EA2 := 70230 \cdot 11500 : EA3 := 56980 \cdot 11500 :$ **(1)**

Equations:

> $u1 := \frac{-(q\_t + q\_c + q\_F) \cdot x^2}{2\, EA1} + C1 \cdot x + C2$

$$u1 := \frac{313}{45152833440} x^2 + C1\, x + C2 \quad \textbf{(1.1)}$$

> $u2 := \frac{-(q\_t + q\_c) \cdot x^2}{2\, EA2} + C3 \cdot x + C4$

$$u2 := \frac{303}{60519532000} x^2 + C3\, x + C4 \quad \textbf{(1.2)}$$

> $u3 := \frac{-(q\_t + q\_c) \cdot x^2}{2\, EA3} + C5 \cdot x + C6$

$$u3 := \frac{909}{147304696000} x^2 + C5\, x + C6 \quad \textbf{(1.3)}$$

> $u4 := \frac{-q\_t \cdot x^2}{2\, EA3} + C7 \cdot x + C8$

$$u4 := \frac{9}{3347834000} x^2 + C7\, x + C8 \quad \textbf{(1.4)}$$

(1.5)

$N1 := EA1 \cdot diff(u1, x); N2 := EA2 \cdot diff(u2, x); N3 := EA3 \cdot diff(u3, x); N4 := EA3 \cdot diff(u4, x);$

$$\frac{7825}{562} x + 1004289000\, C1$$

$$\frac{4545}{562} x + 807645000\, C3$$

$$\frac{4545}{562} x + 655270000\, C5$$

$$\frac{990}{281} x + 655270000\, C7 \quad \textbf{(1.6)}$$

Boundary conditios

> $x := 0;$

$$x := 0 \quad \textbf{(2.1)}$$

> $eq1 := u1 = 0;$

$$eq1 := C2 = 0 \quad \textbf{(2.2)}$$

> $x := a;$

$$x := 11240 \quad \textbf{(2.3)}$$

> $eq2 := u1 = u2;$

$$eq2 := \frac{879530}{1004289} + 11240\, C1 + C2 = \frac{170286}{269215} + 11240\, C3 + C4 \quad \textbf{(2.4)}$$

> $eq3 := N1 = N2 + \frac{F\_F}{2};$

$$eq3 := 156500 + 1004289000\, C1 = 82700 + 807645000\, C3 \quad \textbf{(2.5)}$$

> $x := b;$

$$x := 22480 \quad \textbf{(2.6)}$$

> $eq4 := u2 = u3;$

$$eq4 := \frac{681144}{269215} + 22480\, C3 + C4 = \frac{1021716}{327635} + 22480\, C5 + C6 \quad \textbf{(2.7)}$$

> $eq5 := N2 = N3;$

$$eq5 := 181800 + 807645000\, C3 = 181800 + 655270000\, C5 \quad \textbf{(2.8)}$$

> $x := c;$

$$x := 39340 \quad \textbf{(2.9)}$$

> $eq6 := u3 = u4;$

$$eq6 := \frac{1788003}{187220} + 39340\, C5 + C6 = \frac{17703}{4255} + 39340\, C7 + C8 \quad \textbf{(2.10)}$$

> $eq7 := N3 = N4 + \frac{F\_c}{2};$

$$eq7 := 318150 + 655270000\, C5 = \frac{264375}{2} + 655270000\, C7 \quad \textbf{(2.11)}$$

> $x := H;$

$$x := 47770 \quad \textbf{(2.12)}$$

>

> $eq8 := N4 = \frac{F\_t}{2};$

$$eq8 := 168300 + 655270000\, C7 = -4950 \quad \textbf{(2.13)}$$

>

> $solution := solve(\{eq1, eq2, eq3, eq4, eq5, eq6, eq7, eq8\}, \{C1, C2, C3, C4, C5, C6, C7, C8\});$

$$solution := \left\{C1 = -\frac{11547}{26781040}, C2 = 0, C3 = -\frac{9579}{21537200}, C4 = \frac{45750734}{115493235}, C5 = -\frac{28737}{52421600}, C6 = \frac{127594309837}{59825495730}, C7 = -\frac{9}{34040}, C8 = -\frac{871530359087}{239301982920}\right\} \quad \textbf{(2)}$$

> $assign(solution);$

```
> x :='x';
                                  x := x                                  (3)

> x := H; evalf(u4); x := 14·h; evalf(u3); x := 8·h; evalf(u2); x := 4·h; evalf(u1);
                                  x := 47770
                                 -10.13746991
                                  x := 39340
                                 -9.882744373
                                  x := 22480
                                 -7.072079685
                                  x := 11240
                                 -3.970501021                             (4)

> x :='x':
> with(plots) :
> B := plot(u1, x = 0..a, y = -10..0, labels = ["DeltaL", "H"], title = "DVS-deformations", style
      = line) :
> E := plot(u2, x = a..b, y = -10..0, labels = ["DeltaL", "H"], title = "DVS-deformations", style
      = line) :
> F := plot(u3, x = b..c, y = -10..0, labels = ["DeltaL", "H"], title = "DVS-deformations", style
      = line) :
> G := plot(u4, x = c..H, y = -10..0, labels = ["DeltaL", "H"], title = "DVS-deformations", style
      = line) :
> tf := plottools:-transform((x, y) → [y, x]) :
> tf(B) : tf(E) : tf(F) : tf(G) :

> display({tf(B), tf(E), tf(F), tf(G)});
```

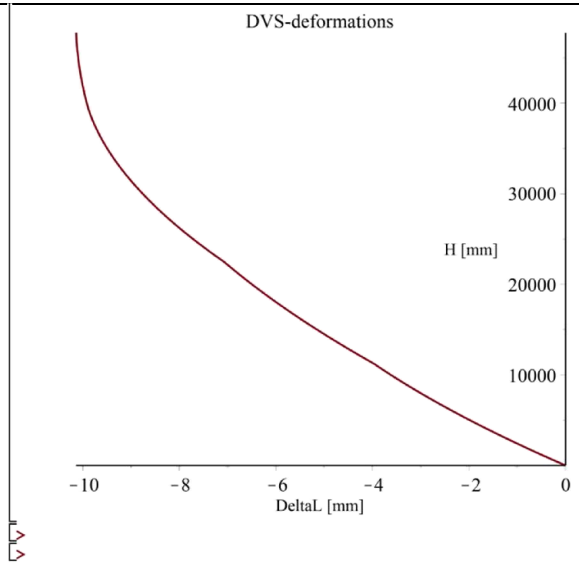

figure 10-44: Maple document stage 18.

ETABS model results

Beding moments

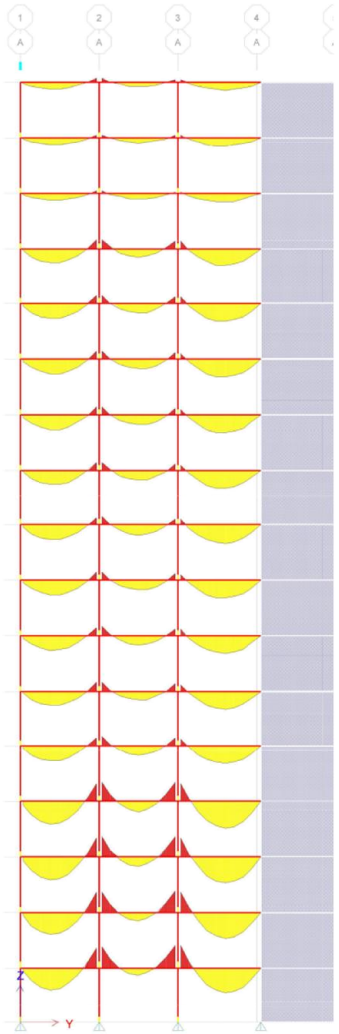

Scaled 200x

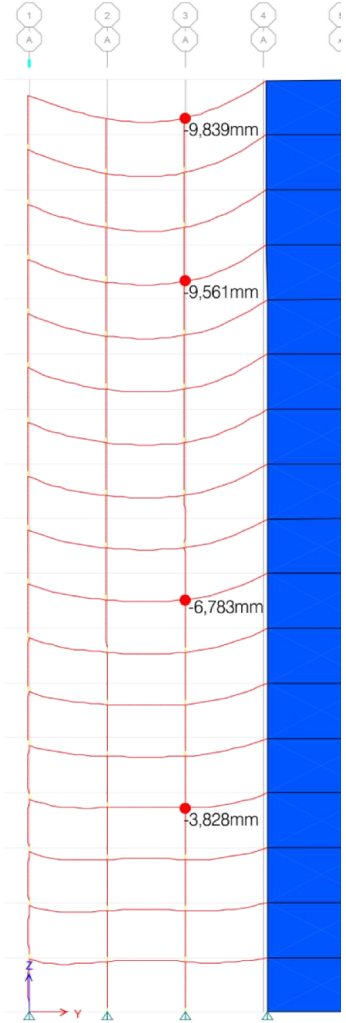

figure 10-45: ETABS results for stage 18.

Stage18		***Maple***	***ETABS***
	$\Delta L_4 =$	$-10{,}137mm$	$-9{,}839mm$
	$\Delta L_3 =$	$-9{,}883mm$	$-9{,}561mm$
	$\Delta L_2 =$	$-7{,}072mm$	$-6{,}783mm$
	$\Delta L_1 =$	$-3{,}971mm$	$-3{,}828mm$

table 38: Maple vs ETABS results for stage 18.

H.6 DVS deformation results

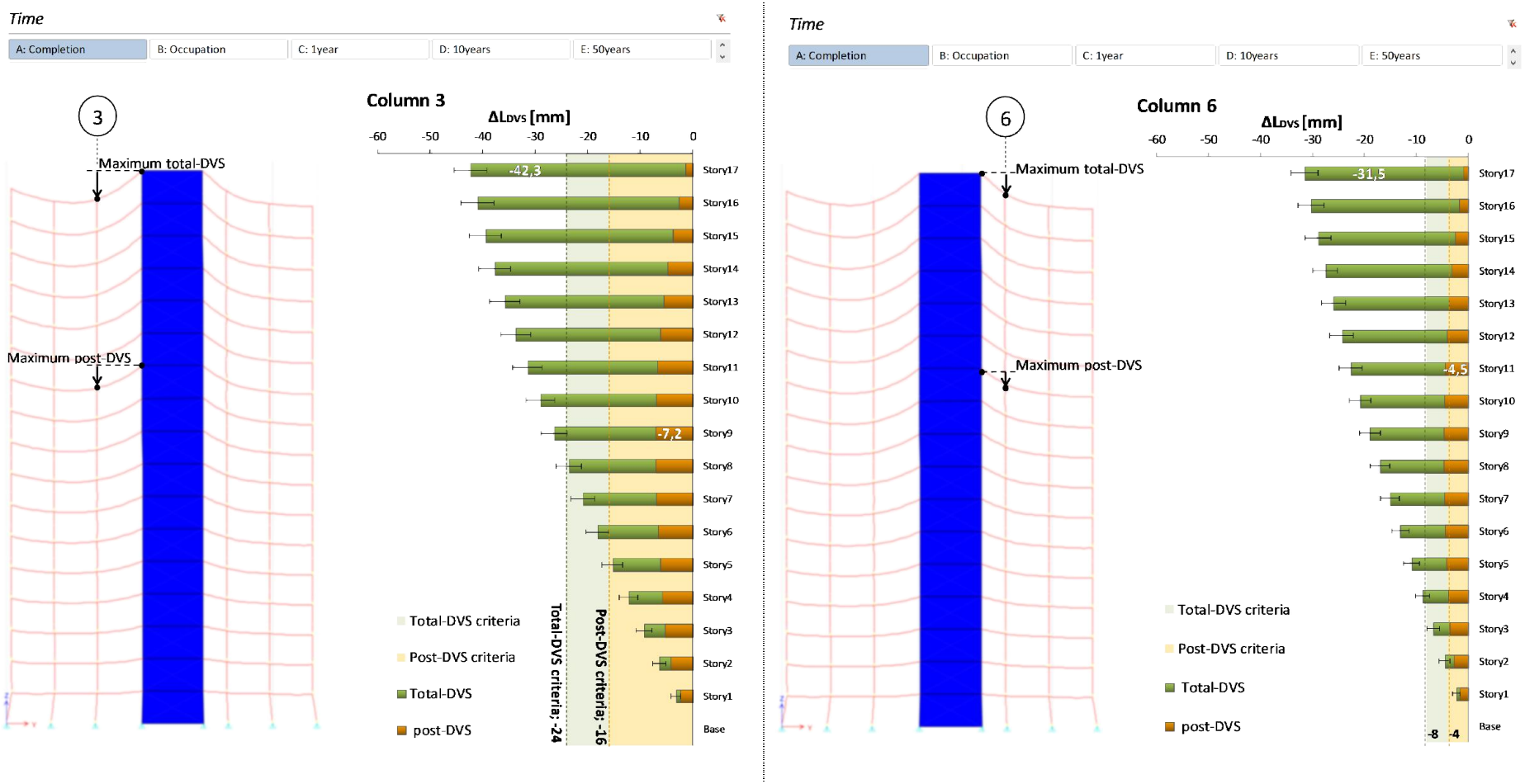

figure 10-46: Total-DVS deformations (green) and post-DVS deformations (orange) for the original Brock Commons design at completion of the structure.

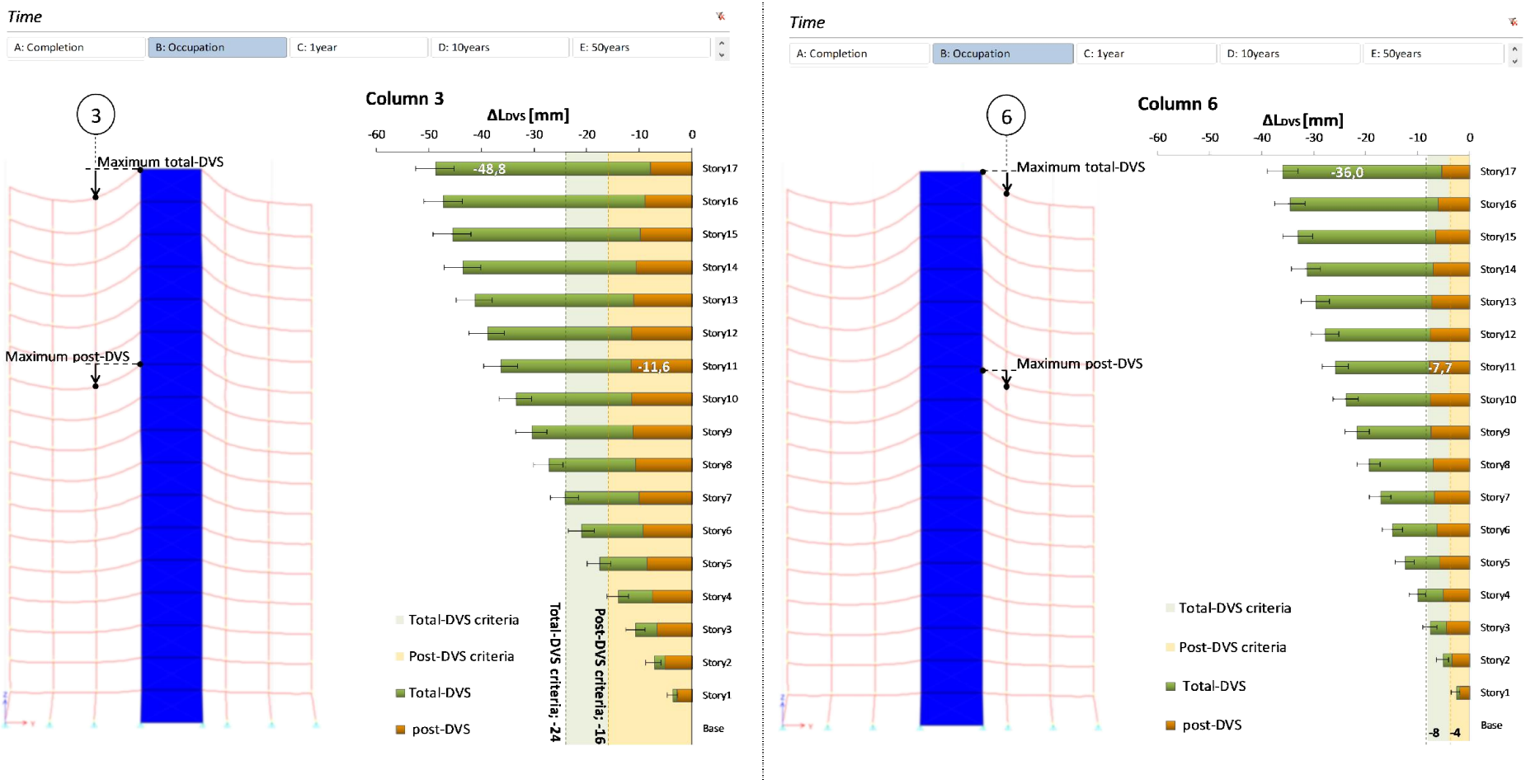

figure 10-47: Total-DVS deformations (green) and post-DVS deformations (orange) for the original Brock Commons design at occupation of the building.

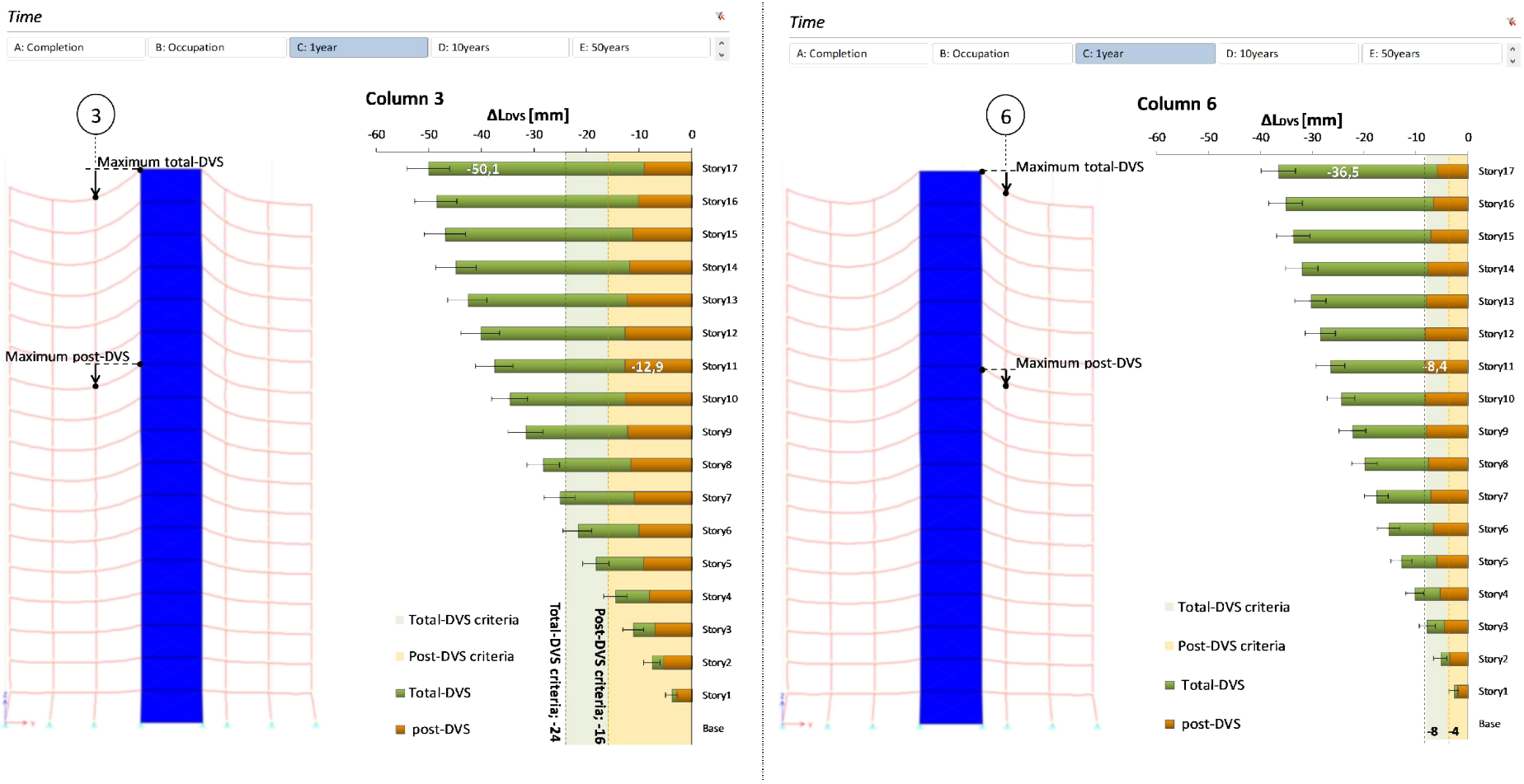

figure 10-48: Total-DVS deformations (green) and post-DVS deformations (orange) for the original Brock Commons design at 1year after occupation of the building.

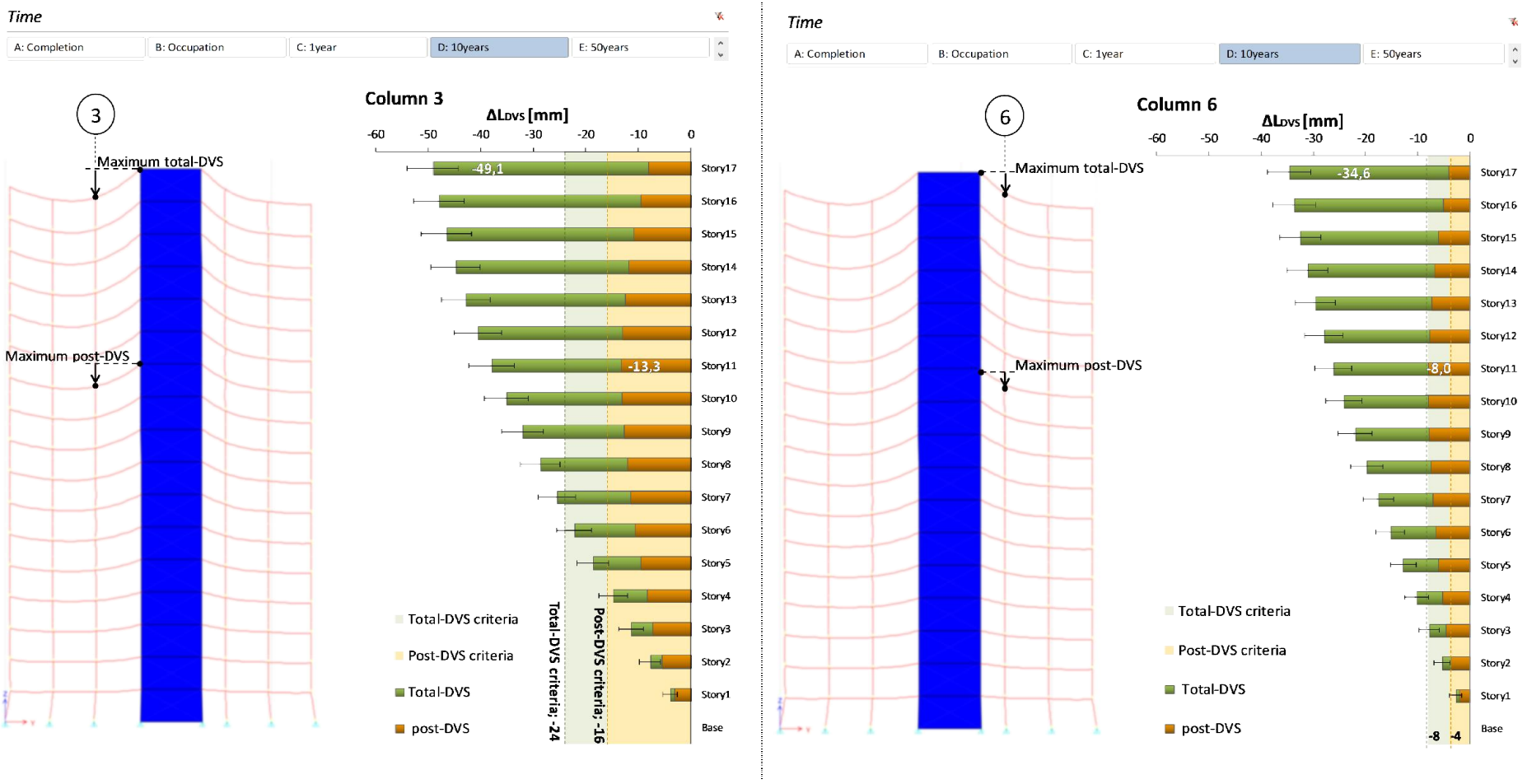

figure 10-49: Total-DVS deformations (green) and post-DVS deformations (orange) for the original Brock Commons design at 10 years after occupation of the building.

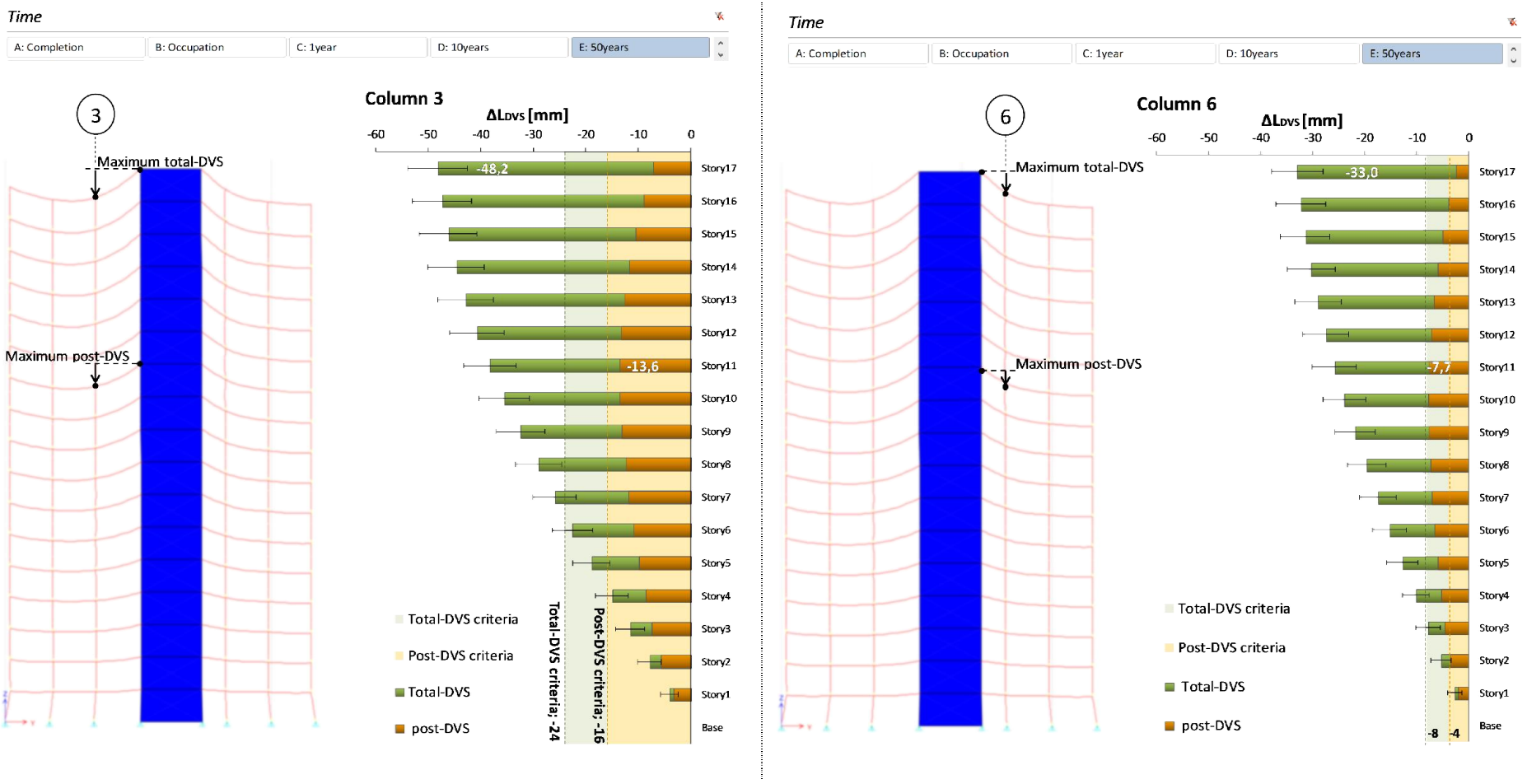

figure 10-50: Total-DVS deformations (green) and post-DVS deformations (orange) for the original Brock Commons design at 50years after occupation of the building.

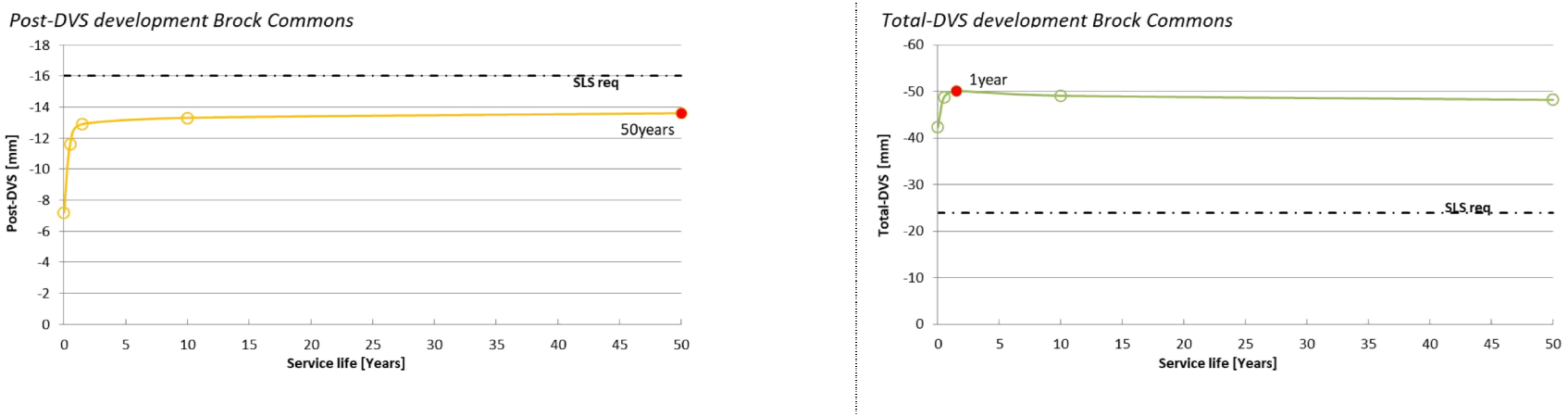

figure 10-51: The development of the maximum post-DVS deformations (left) and the maximum total-DVS deformations (right) of the original Brock Commons design over the service life of the building

H.7 Parallam strength properties

This appendix will explicate the used characteristic strength values that are used for the parallel strand lumber. The characteristic strength values are based on an analysis of an experimental study to Parallam 2.0E by Jaroslav Hrásky and Pavel Král (Hrásky & Král, 2010).
A normal distribution of the compression strength and the Young's modulus parallel to the grain is given in table 39. The 5% value is given in table 40.

n = 20	Compression strength $f_{c,0}$ [N/mm^2]	Modulus of Elasticity parallel $E_{\backslash\backslash}$ [N/mm^2]
Sample mean value μ	49,25	14302
Standard deviation σ	8,8825	3393

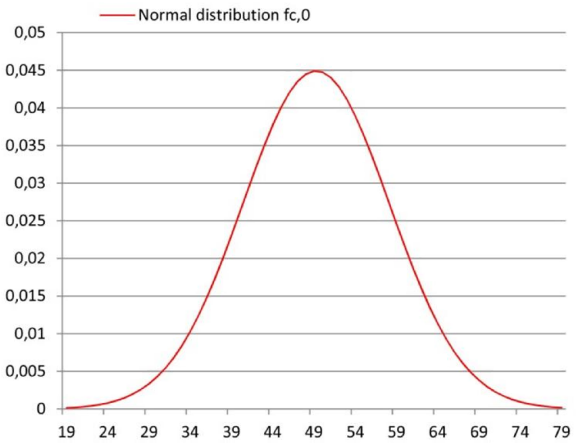

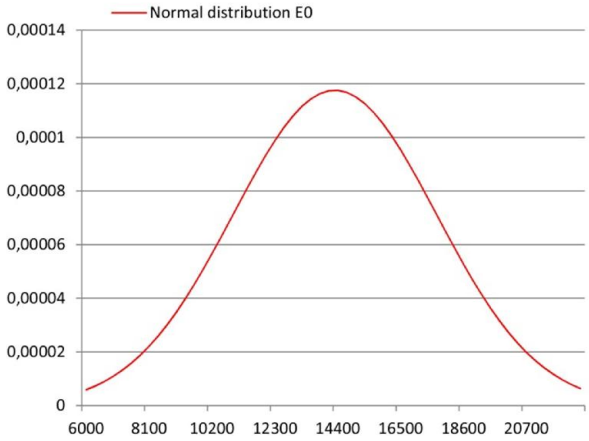

table 39: Normal distribution of compression strength and the Young's modulus parallel to grain for PSL 2.0E.

The characteristic value $f_{c,0,k}$ for the compression strength parameter modelled as a stochastic variable is defined as the 5th-percentile in the distribution function for $f_{c,0}$. For stiffness properties, the characteristic mean value shall be taken as the sample mean value μ.

$f_{c,0,k} = \mu - k_s \cdot \sigma$ $E_{mean} = \mu$

The characteristic value of the compression strength paramater or resistance shall be determined at a confidence level of $\alpha = 75\%$. According to the Eurocode the following simplified expression for k_s may be used to determine the 5th –percentile with a confidence level of $\alpha = 75\%$ (NEN-EN 14358, 2016, p. 6):

$k_s(n) = \frac{6{,}5n + 6}{3{,}7n - 3} = 1{,}92$ $k_s(n) = 1{,}65$

5-percentile value $f_{c,0,k}$	32,2	N/mm^2	5-percentile value $E_{0.05}$	8700	N/mm^2

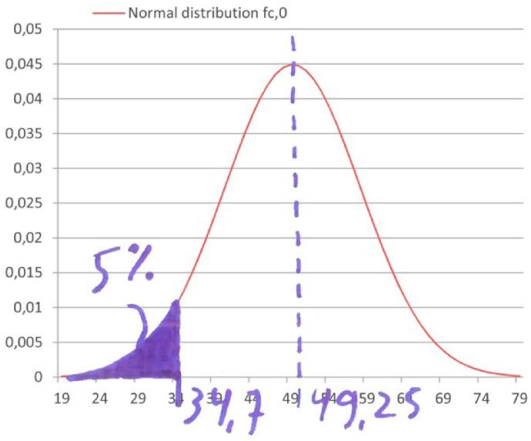

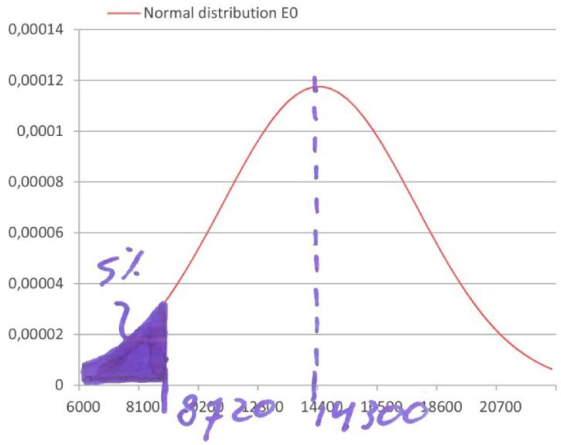

table 40: The 5% value of the normal distributions. **Aanpassen**

I. Height variant

The height variant scales up the building vertically to give insight in the problem of differential vertical shortening for an increase in floors and building height. In this appendix the following calculations are explicated:

D.1 Core design	The redesign and resizing of the core according to the utilization of the original design.
D.2 Column design	The redesign and resizing of columns according to the utilization of the original design.

I.1 Core design

Assumed core properties

H	$= 76$	m
b	=?	m
h	=?	m
t	$= 450$	mm
	C45/55	
f_{cm}	$= 53$	N/mm^2
f_{ck}	$= 45$	N/mm^2
E_{cm}	$= 36000$	N/mm^2
$E_{c,eff}$	$= 25000$	N/mm^2

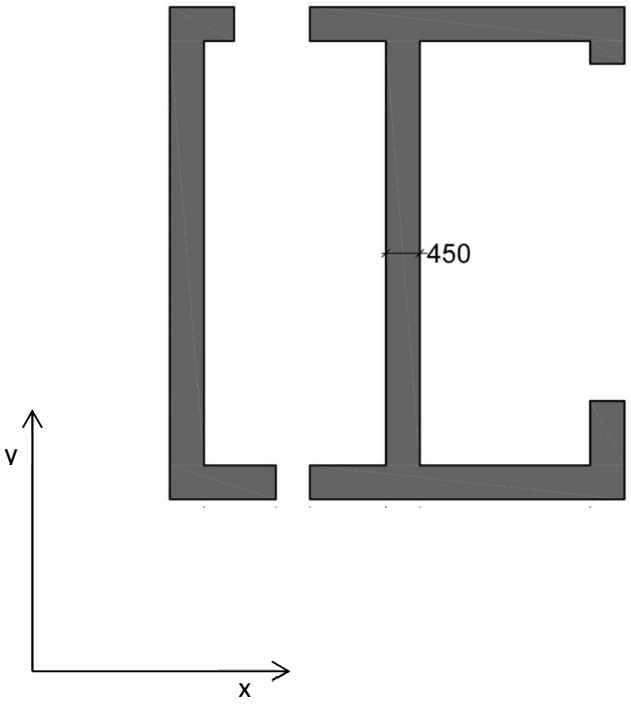

Windloads

$q_{w,ch}$	$= 1{,}7$	kN/m^2
$q_{w,y}$	$= 57 \cdot 1{,}5 \cdot 1{,}7$	
	$= 144$	kN/m
$q_{w,x}$	$= 16 \cdot 1{,}5 \cdot 1{,}7$	
	$= 41$	kN/m

Deflection in y-direction

The building has two mirrored cores that provide the lateral stability, so the moment of inertia is multiplied by a factor 2:

$$UC = \frac{\delta_{EI,y} \cdot 500}{H} = 0{,}435 \qquad \delta_{EI,y} = \frac{q_{w,y} \cdot H^4}{8 \cdot E_{c,eff} \cdot 2 \cdot I_{c,y}}$$

Substitution

$$UC = \frac{q_{w,y} \cdot H^3 \cdot 500}{8 \cdot E_{c,eff} \cdot 2 \cdot I_{c,y}} = 0{,}435$$

To keep a constant Unity check relative to the original design of 53 meters high, the moment of inertia of the 76 meter high variant should be increased with the height increase to the power three:

$$I_{c,y,76} = \left(\frac{H_{76}}{H_{53}}\right)^3 \cdot I_{c,y,53} \qquad \left(\frac{H_{76}}{H_{53}}\right)^3 = \left(\frac{76}{53}\right)^3 = 2{,}95$$

$$= 2{,}95 \cdot 61{,}6 \cdot 10^{12} = 181{,}6 \cdot 10^{12} \quad \text{mm}^4$$

By scaling up the core in both direction with a factor 1,32 this stiffness increase can be achieved:

$$I_{c,y,76} = 2{,}95 \cdot \frac{1}{12} \cdot b_{53} \cdot (h_{53})^3$$

$$= \frac{1}{12} \cdot 1{,}32 \cdot b_{53} \cdot (1{,}32 \cdot h_{53})^3$$

figure 10-52: The effect of the icreasing height on the core dimensions.

I.2 Column design

In the height variant, a comparable utilization of the columns with the original design is desired to get fair results on the column shortening and deformations.

Column geometry

Floor 18 to 26 (GL24h)

H_{18}	$= 2532$	mm
b_{18}	$= 215$	mm
h_{18}	$= 265$	mm
A_{18}	$= 56975\,\text{mm}^2$	

Floor 14 to 17 (GL24h)

H_{10}	$= 2532$	mm
b_{10}	$= 265$	mm
h_{10}	$= 265$	mm
A_{10}	$= 70225\,\text{mm}^2$	

Floor 10 to 13 (PSL2.0E)

H_{10}	$= 2532$	mm
b_{10}	$= 265$	mm
h_{10}	$= 265$	mm
A_{10}	$= 70225\,\text{mm}^2$	

Floor 6 to 9 (PSL2.0E)

H_6	$= 2532$	mm
b_6	$= 295$	mm
h_6	$= 295$	mm
A_6	$= 87025$	mm^2

Floor 2 to 5 (PSL2.0E)

H_2	$= 2532$	mm
b_2	$= 320$	mm
h_2	$= 325$	mm
A_2	$= 104000$	mm^2

Material properties

GL24h

$f_{c,0,k}$	$= 24$	N/mm^2
$E_{0,mean}$	$= 11600$	N/mm^2
γ_M	$= 1{,}25$	

PSL 2.0E

$f_{c,0,k}$	$= 32$	N/mm^2
$E_{0,mean}$	$= 14300$	N/mm^2
γ_M	$= 1{,}25$	

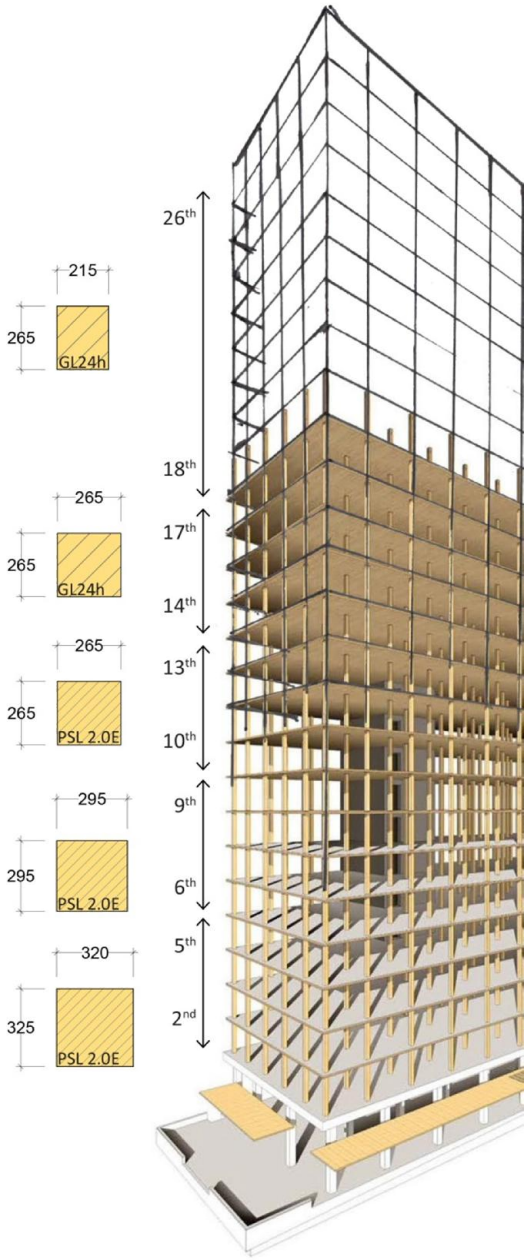

table 41: Timber column dimensions for the height variant.

Axial column loads

A_f	$= 4 \times 2{,}85$	$= 11{,}4$ m²
$q_{G,f}$		$= 3$ kN/m²
$q_{Q,f}$		$= 1{,}75$ kN/m²

Characteristic column load:

$G_{k,f}$	$= 34{,}2$ kN
$Q_{k,f}$	$= 19{,}95$ kN

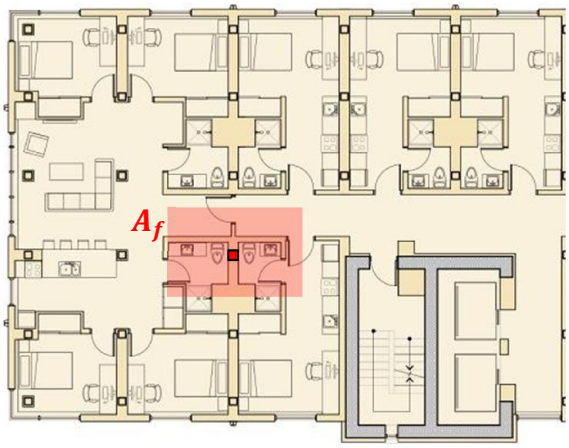

Load combinations (ULS)

4. (Vgl.6.10a) $\gamma_G \cdot G_{k,n} + \gamma_Q \cdot (Q_{k,17-18} + \varphi_0 \cdot Q_{k,n-16})$	(short-term)
$N_{ed,18}$	$= \mathbf{580}$ kN
$N_{ed,14}$	$= \mathbf{83\ 8}$ kN
$N_{ed,10}$	$= \mathbf{1096}$ kN
$N_{ed,6}$	$= \mathbf{13\ 54}$ kN
$N_{ed,2}$	$= \mathbf{1612}$ kN

5. (Vgl.6.10b) $\gamma_G \cdot G_k + \gamma_Q \cdot \varphi_0 \cdot Q_k$	(medium-term)
$N_{ed,18}$	$= \mathbf{558}$ kN
$N_{ed,14}$	$= \mathbf{789}$ kN
$N_{ed,10}$	$= \mathbf{1019}$ kN
$N_{ed,6}$	$= \mathbf{1250}$ kN
$N_{ed,2}$	$= \mathbf{1480}$ kN

6. $\gamma_G \cdot G_k$	(permanent)
$N_{ed,18}$	$= \mathbf{462}$ kN
$N_{ed,14}$	$= \mathbf{667}$ kN
$N_{ed,10}$	$= \mathbf{872}$ kN
$N_{ed,6}$	$= \mathbf{1077}$ kN
$N_{ed,2}$	$= \mathbf{1283}$ kN

Load combinations (SLS)

3. $G_{k,n} + \varphi_2 \cdot Q_{k,n}$	(quasi-permanent)
$N_{ed,18}$	$= 362$ kN
$N_{ed,14}$	$= 522$ kN
$N_{ed,10}$	$= 683$ kN
$N_{ed,6}$	$= 844$ kN
$N_{ed,2}$	$= 1005$ kN

4. $G_{k,n} + (Q_{k,17-18} + \varphi_0 \cdot Q_{k,n-16})$	(characteristic)
$N_{ed,18}$	$= 404$ kN
$N_{ed,14}$	$= 572$ kN
$N_{ed,10}$	$= 741$ kN
$N_{ed,6}$	$= 910$ kN
$N_{ed,2}$	$= 1078$ kN

table 42: Axial loads and load combinations for the governing columns on the 2nd , 6th, 10th, 14th and 18th floor.

Axial design resistance (ULS)

		Short-term ($k_{mod} = 0{,}8$)	*Medium-term ($k_{mod} = 0{,}65$)*	*Long-term ($k_{mod} = 0{,}5$)*
$N_{rd,18}$	$= k_{mod} \cdot A_{18} \cdot \frac{f_{c,0,k}}{\gamma_M}$	$= 875$ kN	$= 711$ kN	$= 547$ kN
$N_{rd,14}$	$= k_{mod} \cdot A_{14} \cdot \frac{f_{c,0,k}}{\gamma_M}$	$= 1079$ kN	$= 876$ kN	$= 674$ kN
$N_{rd,10}$	$= k_{mod} \cdot A_{10} \cdot \frac{f_{c,0,k}}{\gamma_M}$	$= 1438$ kN	$= 1167$ kN	$= 899$ kN
$N_{rd,6}$	$= k_{mod} \cdot A_{6} \cdot \frac{f_{c,0,k}}{\gamma_M}$	$= 1782$ kN	$= 1448$ kN	$= 1114$ kN
$N_{rd,2}$	$= k_{mod} \cdot A_{2} \cdot \frac{f_{c,0,k}}{\gamma_M}$	$= 2130$ kN	$= 1731$ kN	$= 1331$ kN

Unity check

		Short-term ($k_{mod} = 0{,}8$)	*Medium-term ($k_{mod} = 0{,}65$)*	*Long-term (k_{mod}=0,5)*
Column 18:	$\frac{N_{ed,10}}{N_{rd,10}}$	$= 0{,}66$	$= 0{,}73$	$= 0{,}84$
Column 14:	$\frac{N_{ed,10}}{N_{rd,10}}$	$= 0{,}78$	$= 0{,}86$	$= 0{,}99$
Column 10:	$\frac{N_{ed,10}}{N_{rd,10}}$	$= 0{,}76$	$= 0{,}84$	$= 0{,}97$
Column 6:	$\frac{N_{ed,6}}{N_{rd,6}}$	$= 0{,}76$	$= 0{,}86$	$= 0{,}97$
Column 2:	$\frac{N_{ed,2}}{N_{rd,2}}$	$= 0{,}76$	$= 0{,}85$	$= 0{,}96$

table 43: Axial design resistance and Unity check for the governing columns on the 2nd , 6th, 10th, 14th and 18th floor.